



PREDICTION OF WATER DROPLET BEHAVIOUR DURING FIRE EXTINGUISHMENT

KATERINA NYANKINA



*A thesis submitted in fulfillment of the requirements for the degree of
Doctor of Philosophy*

School of the Built Environment
VICTORIA UNIVERSITY
Melbourne, Australia
2003

FTS THESIS
628.9252 NYA
30001008249551
Nyankina, Katerina
Prediction of water droplet
behaviour during fire
extinguishment

ACKNOWLEDGEMENTS

I would like to thank my family and friends for supporting me. I also wish to express my gratitude to my friend, Dr Suzana Klopovic, for her encouragement and belief in me.

ABSTRACT

Sprinklers have been used in fire suppression for about 100 years. Even though their design has changed from simple perforated pipes to sophisticated automatic systems of mist and sprinkler nozzles, still they play the same role – they dramatically reduce death and injuries due to fire, as well as property loss. This reduction occurs due to sprinklers' capability either to extinguish the fire or to control it, usually until the arrival of the fire brigade. As an agent, water has become the most widely used fire suppressant due to its highly effective thermal properties and availability. Specifically, water mist sprays are becoming increasingly popular as total flooding agents, substituting hazardous gaseous suppressants, such as Halon. Commonly used as a fire engineering tool for predicting fire growth and hot gas movement in a compartment, are zone models. Even though the performance of fire sprinklers or mist sprays is predicted by some of these models, the analysis is very limited. This analysis is usually based only on a known water flow rate, compartment area and calculated spray activation time, with no consideration given to what actually happens to the water droplets within a fire environment, or how the droplets' characteristics affect fire suppression.

The principal objective of this research is to develop a more refined model of the interaction of water sprays and fires. Such a model, based on the physics of the flow of droplets through a hot layer has been formulated and it allows a detailed analysis of thermal performance of sprays in fire. The model predicts heat transfer rates between water droplets and solid combustibles. The model accounts for:

1. Spray characteristics, such as
 - droplet size and size distribution
 - the instantaneous velocities of droplets
 - spray discharge angle
 - spray mass flow rate
 - droplet initial temperature
2. External conditions affecting on spray thermal performance, such as
 - location of fire source relatively to spray nozzle
 - surrounding gas temperature and velocity
 - solid combustibles' temperature and material

The developed model has been integrated with a validated one-zone fire growth model and the results compared with full-scale fire extinguishment experiments. The comparison has been based on the overall gas room temperature change for two types of fire and water spray applications: 1) direct water impact on top of the surface of solid fuel due to early (pre-flashover) activation of conventional sprinklers, and 2) gas cooling by mist sprays during the post-flashover stage of liquid pool fire.

The experimental and computational results make possible a comparison in terms of: 1) minimum water flux needed for extinguishment due to direct water impact, and 2) immediate gas temperature drop as a function of droplet diameters and water mass flow rates for mist application at post-flashover fire. The results of comparison are promising and have shown that the temperature drop in rooms versus spray characteristics is in a close agreement with experiments for both pre-flashover and post-flashover fires.

The effect of heat-transfer between water sprays and hot gases during direct water impact has not been measured separately yet within the overall fire extinguishment process. Therefore, the prediction of gas cooling in pre-flashover fires without the consideration of water impact on solid combustibles was used only for comparative analysis of the effectiveness of different sprays. This prediction showed that gas cooling by the conventional large droplet sprays was particularly effective and does not lead to fire suppression or control, while mist sprays can control fires and prevent flashover.

In the modern performance based approach to building and fire codes, the design solution, which is expected to meet pre-established fire protection objectives due to specified performance levels of protection systems, can be based purely on fire modelling if the methods and results are accepted by the authorities. Consequently, methods of obtaining design solutions are viewed by the fire protection community as a way to reduce expenses on large projects. Therefore, this work focuses on a computer zone model which can then be applied to the evaluation of sprinkler/mist nozzles performance in a fire environment.

Table of Contents

Acknowledgements	ii
Abstract	iii
Table of Contents	iv
1 INTRODUCTION	1
1.1 USE OF WATER AS A FIRE SUPPRESSANT	5
1.2 PERFORMANCE OF WATER BASED SYSTEM	7
1.3 THE NEED FOR THIS PROJECT	9
2 LITERATURE REVIEW	10
2.1 PARAMETERS GOVERNING THE PERFORMANCE OF WATER BASED SYSTEMS	10
2.1.1 SPRAY DISCHARGE PROPERTIES	12
2.1.2 MECHANISMS OF FIRE EXTINGUISHMENT	14
2.1.2.1 Gas cooling	15
2.1.2.2 Fuel coverage	17
2.2 CRITERIA FOR FIRE EXTINGUISHMENT	17
2.3 MODELLING OF THE INTERACTION BETWEEN FIRE AND SPRINKLERS	20
2.3.1 DROPLET MODELS	20
2.3.2 NUMERICAL MODELS OF FIRE ENVIRONMENT	22
2.3.2.1 Zone models	22
2.3.2.2 Field Models	24
3 DROPLET DYNAMICS	27
3.1 INTRODUCTION	27
3.2 BACKGROUND	27
3.2.1 BASIC EQUATIONS	30
3.3 DYNAMICS: RESULTS AND DISCUSSION	32
3.3.1 DROPLET TRAJECTORIES IN TERMS OF RELATIVE FIRE-SPRINKLER LOCATION	32
3.3.2 DROPLET VELOCITIES AND RESIDENCE TIMES	35

3.3.3	EFFECT OF GAS VELOCITY PROFILES: MODELLING FIRE INDUCED GAS FLOW	39
3.3.4	COMPARISON WITH DATA AVAILABLE IN THE LITERATURE	45
3.4	NUMERICAL EVALUATION OF THE EFFECT OF MOMENTUM COUPLING BETWEEN WATER SPRAY AND GAS FLOW	50
3.4.1	CHANNEL FLOW	51
3.4.2	TWO-PHASE FLOW: GAS AND WATER DROPLETS INTERACTION.	52
3.5	CONCLUSIONS	56
4	DROPLET HEAT TRANSFER: GAS COOLING	58
4.1	INTRODUCTION	58
4.2	BASIC EQUATIONS	58
4.2.1	THE MODEL OF DROPLET-GAS FLOW	59
4.2.2	DROPLET-GAS FLOW EQUATIONS	62
4.2.3	DROPLET HEAT ABSORPTION TERM, ΔQ	65
4.2.4	HEAT TRANSFER COEFFICIENT	68
4.2.5	LOCAL HUMIDITY ASSUMPTION	69
4.3	WATER SPRAYS	70
4.3.1	MODEL VALIDATION	70
4.3.2	SENSITIVITY ANALYSIS	72
4.3.2.1	Droplet residence times and spray surface area	74
4.3.2.2	Droplet initial angles	76
4.3.2.3	Mean droplet diameter	79
4.3.2.4	Initial gas temperature	80
4.3.3	RESULTS AND DISCUSSIONS	81
4.3.3.1	Prediction of optimal droplet parameters	81
4.3.3.2	Stability of Hot Layer after Sprinkler Activation	85
4.3.4	CONCLUSIONS – SPRINKLER SPRAYS AND SENSITIVITY ANALYSIS	91
4.4	MIST SPRAYS	92
4.4.1	BACKGROUND	92
4.4.2	RESULTS AND DISCUSSION	93
4.4.2.1	Single droplets	93
4.4.2.2	Sprays	99
4.4.2.3	Heat absorption distribution within the spray occupied space	106

4.4.3 CONCLUSIONS - MIST SPRAYS	107
5 SURFACE COOLING	108
5.1 INTRODUCTION	108
5.1.1 FIRE EXTINGUISHMENT DUE TO FUEL COOLING WITH WATER	108
5.1.2 BASIC SURFACE COOLING	109
5.2 MECHANISMS OF SURFACE COOLING	111
5.2.1 PHYSICAL MODEL	111
5.3 QUANTITATIVE DESCRIPTION OF SPRAY COOLING	115
5.3.1 WETTED AREA	115
5.3.2 SURFACE HEAT FLUX	117
5.4 FUEL BEHAVIOUR: UNSTEADY CONDUCTION	121
5.5 RESULTS AND DISCUSSION	123
5.5.1 BEFORE WATER APPLICATION	123
5.5.2 AFTER WATER APPLICATION	128
5.5.2.1 Critical water flux	130
5.6 CONCLUSIONS	133
6 INTEGRATION OF SPRAY COOLING MODEL WITH NRCC-VUT ZONE MODEL	134
6.1 INTRODUCTION	134
6.2 MODELLING OF SPRINKLER IMPACT ON FIRE: ZONE MODEL AND SPRINKLER SUBMODEL	136
6.2.1 ZONE MODEL	139
6.2.2 SPRINKLER SUBMODEL	148
6.3 EXPERIMENTAL CONDITIONS FOR THE SPRINKLER TESTS	153
6.4 RESULTS AND DISCUSSION	155
6.4.1 NON-SPRINKLERED FIRE	155
6.4.2 SPRINKLERED FIRE: GAS COOLING	156
6.4.3 SPRINKLERED FIRE: FUEL COVERAGE. PREDICTION AND COMPARISON WITH EXPERIMENTS	162
6.5 WATER MIST IN SUPPRESSION OF PRE-FLASHOVER AND POST-FLASHOVER FIRES	165
6.5.1 PRE-FLASHOVER FIRE SUPPRESSION	165
6.5.2 POST-FLASHOVER FIRE SUPPRESSION	167

6.6 CONCLUSIONS	171
7 CONCLUSIONS	173
8 SUGGESTIONS FOR FUTURE WORK	178
8.1 EXPANDING THE PRESENT SUB-MODEL	178
8.1.1 EXTEND THE EXISTING DROPLET SUBMODEL	178
8.1.2 EXPAND THE FIRE ZONE MODEL	179
8.1.3 USE THE EXISTING COMBINED MODEL TO STUDY THE EFFECTS OF EXTERNAL FACTORS	180
8.1.4 DESIGN AND CONDUCT THE FIRE EXPERIMENTS USING MISTS FOR EXTINGUISHMENT TO VERIFY THE ACCURACY OF GAS COOLING PREDICTION AND VALIDITY OF THE COMBINED ZONE MODEL	180
8.2 NEW FIELD OF RESEARCH	181
REFERENCES	182
APPENDICES	193

List of Figures

Figure 1.1. Classification of mist sprays in terms of their cumulative volume distribution [5]	6
Figure 3.1. Three cases of gas flow relative to fire sprinkler location. Gas velocity distribution is assumed to be uniform in all cases. Gas velocity magnitude is taken as 2m/s with an initial droplet velocity, V_0 , of - 5m/s.....	33
F	Error! Bookmark not defined.
Figure 3.5. Droplet residence times as a function of initial discharge angles. The residence time corresponds to either a vertical distance of 1m or when the droplets (only the 0.3mm diameter ones) strike the ceiling. (a) 0.3mm droplet spray; (b) 0.7mm droplet spray.	35
Figure 3.7. Droplet residence times for different mean droplet diameters: 1- 1.5mm; 2 – 1mm; 3 – 0.7mm; 4 – 0.5mm; 5 – 0.3mm. Location 1 is chosen due to its common use in the literature. Horizontal gas velocity is constant, 2 m/s; layer depth is 1m and droplet initial velocity is 5m/s.	36
Figure 3.5. Comparison of mist spray droplet residence times in upward and downward discharge directions. The spray is represented by 0.3mm droplets discharged under 10 initial angles from 0 to 90°. The uniform updraft velocity is 2m/s.....	37
Figure 3.6 Droplet vertical trajectories for different diameters for zero gas velocity. Droplet diameters are listed next to corresponding curves. Initial conditions are the same for all droplets, consisting of 7m/s droplet initial velocity and 45° discharge angle.	38
Figure 3.7. Droplet vertical trajectories as a function of vertical velocities (a) and time (b) in the uniform updraft gas velocity of 2m/s. The droplet diameters are as listed. Location 3 is chosen as the most critical case. Initial conditions for droplets are the same as in Figure 3.6.	39
Figure 3.8. Trajectories of 0.7mm droplets in fire plumes modelled by Gaussian and uniform gas velocity distributions. The Gaussian distribution is for 0.2 and 0.5MW fires. The uniform distribution is modelled by 3.5m/s gas velocity.	42
Figure 3.9. Residence times as a function of initial discharge angle for the same conditions as those given in Figure 3.8.....	43
Figure 3.10. Residence times of 0.3mm droplets in uniform and triangular gas velocity profiles (a), and trajectories of 0.3mm droplets in uniform and triangular gas velocity profiles (b). The triangular profile has its minimum, i.e. the zero gas velocity, at $Y=-1.0m$ from the ceiling, that is the bottom of the hot layer. The maxima are at the ceiling, $Y = 0m$, and at $Y=-2m$ (entraining flow).	44
Figure 3.11. Actual Delivered Density in the 1 st area (ADD1) and 2 nd area (ADD2). Comparison between prediction and experiments: a (ESFR-A sprinkler) and b (ESFR-B sprinkler). 1 st column – ADD1; 2 nd column – ADD2.....	48
Figure 3.12. Actual Delivered Density in the 1 st area (ADD1) and 2 nd area (ADD2). Comparison between ADD in terms of spray representation by different angle and diameter distributions. Angle distribution modelled by power law (p is a power value). Diameter distribution either corresponds to Nam's	

distribution or given by one mean droplet diameter. a (ESFR-A sprinkler) and b (ESFR-B sprinkler). 1 st column – ADD1; 2 nd column – ADD2	49
Figure 3.13. Comparison of the water flux distribution obtained from the present model with the experimental data of Chan [86] given in [46]. Two different water flow rates are used in the calculations, as indicated. Chan's experimental data for two ESFR-A sprinklers are given by symbols. Calculations correspond to droplet distribution (lines with symbols) and mean droplet diameter (single lines), both discharged at 25 initial angles. Sprinkler height = 2.69m from the floor.....	50
Figure 4.1. Flow chart of gas-droplet flow computational scheme (reproduced from [59]).	60
Figure 4.3. Steady droplet-gas system: fire induced hot gas flow cooled by spray	63
Figure 4.3. Trajectories (lines) and temperatures (shown near the lines in °C) of droplets with initial diameters of 0.74 mm, 1 mm and 1.38 mm. Comparison between Crowe et al's [59] (sphere-symbols and numbers in brackets) and present calculations (solid lines). Initial droplet temperature is 60°C, and velocity is 2 m/s. Gas initial velocity is 2m/s, initial relative humidity is 30% and temperature is 20°C.	71
Figure 4.4. Schematic shows the water spray (thick dotted lines) activated in a moving hot layer. The hot layer divided into sub-layers shown by the faint dotted lines.....	73
Figure 4.5. Ratio of the evaporation rate to total mass flow rate of the spray (a) and spray heat absorption rates (b) for different mean droplet diameters for five initial gas temperatures. Initial gas temperatures are given on the curves. Location 1 is chosen due to its common use. The initial droplet discharge angle is 45°.	80
Figure 4.22. Droplet trajectories of 0.3 mm unconfined spray discharged with 10 m/s initial velocity in steady 400°C gas environment.....	105
Figure 4.23. Heat absorption rate (kW) distribution along the ceiling (I) and across the hot layer (J) inside 400°C gas environment.....	106
Figure 5.1. Regimes of heat transfer in a thin liquid layer due to droplets deposited on a hot surface of temperature $T_{surf,0}$. T_{sat} is the saturation temperature under atmospheric conditions ($T_{sat} = 100^\circ\text{C}$ for water). q_0 is the heat flux corresponding to the beginning of boiling, LT is Leidenfrost point (around 200°C for water on metal plates [123, 128]). q_{max} is the maximum heat flux corresponding to the occurrence of film or Leidenfrost boiling, and q_{min} is the minimum heat flux corresponding to transition from film boiling back to nucleate boiling.....	111
Figure 5.2 Time of evaporation of a droplet of 0.0465 cm ³ volume as a function of surface temperature [123, p.375].	113
Figure 5.4. Medium fire heat flux history	122
Figure 5.5. Temperature profile history in a PU slab across the non-dimensional depth x/R ($R=0.1\text{m}$). Each curve corresponds to a different time starting at 5 s with a time step 100 s.....	123
Figure 5.7. Time-temperature curves recorded during a flashover fire by 4 k-type thermocouples imbedded in a PU-slab [111]. Each curve corresponds to a different depth inside the PU-slab. The predicted surface temperature is given as a solid thick line.....	125

<i>Figure 6.12. Sensitivity of gas room temperature to spray characteristics during gas cooling by water sprays. Droplet diameter used in calculations corresponds: a) 0.2mm; b) 0.3mm; c) 0.5mm. Water flow rates are shown at the legends. Gas was assumed to be steady and droplet initial velocity was 1m/s in all calculations.....</i>	164
<i>Figure 6.13. Prediction of post flashover fire suppression with spray of different droplet diameters. Gas temperature histories in RFO (2.4x3.5x2.4 m³) with (curves 2, 3, 4) and without (curve 1) sprinkler intervention. Droplet diameters correspond: 2- 0.3 mm; 3 – 0.35 mm, 4- 0.5 mm – 0.25 mm. Water flow rate in all cases - 80 l/min (1.3 kg/s).....</i>	167
<i>Figure 6.14. Prediction of post flashover fire suppression with sprays of different discharge rates and uniform 0.3 mm droplet diameter. The discharge rates are: 1 – 1.3, 2- 1, 3 – 0.7 and 4 - 0.5 kg/s.....</i>	167
<i>Figure 6.15. Comparison of the predicted in the present work post-flashover fire suppression (a) with suppression experiments of Tuomissaari [13] in full scale fire (b). The figure (b) is taken</i>	168

List of Tables

<i>Table 2.1. Parameters governing the suppression performance of water spray systems.....</i>	11
<i>Table 4.1. Residence times (s) for 0.8m distance (or until droplets hit the ceiling) for different droplet diameters, initial droplet velocity of 5m/s, droplet initial angle of 68°. Gas velocity is 2m/s.....</i>	75
<i>Table 4.2. The total surface areas calculated as for water sprays represented by single-size droplets (first five rows) and by droplet distribution (the last row). The droplets' residence times are shown in the second column for each diameter. Water mass flow rate is 1.84kg/s, gas and droplet velocities are the same as in Table 4.1.....</i>	76
<i>Table 4.3. Convective heat absorption rate, kW, of the sprays, represented by one diameter (0.7mm) and one initial angle taken to the vertical. The residence times are calculated for Locations 1 and 3. Water mass flow rate, gas velocity and initial temperature are the same as in Tables 4.1 and 4.2.</i>	77
<i>Table 4.4. Calculated total spray interface area (m^2) for many-droplet (250 trajectories) and one-droplet (one trajectory) sprays.</i>	77
<i>Table 4.5. Comparison of the convective heat absorption rate (kW) between sprinklers represented by one diameter (0.7mm) and by different numbers of trajectories in the range -90-0-90°. Water mass flow rate, gas velocity and initial temperature are the same as in Tables 4.1 and 4.2.</i>	78
<i>Table 4.6. Convective heat absorption rate, kW, of the sprays, characterized by one diameter and one angle of 68°. Water mass flow rate, gas velocity and initial temperature are the same as in Tables 4.1 and 4.2. 79</i>	79
<i>Table 5.1 The single droplet evaporation characteristics obtained from Figure 5.3.....</i>	114
<i>Table 6.1. The values of the best fit coefficients and time decay constant for the approximation given by Equation (6.35) for the curves plotted in</i>	

Nomenclature

A	area (droplets, opening, etc)
B_M	Spalding or mass transfer number
B	Buoyancy
Bi	Biot number
$b_{\Delta T}$	plume radial distance at which the temperature rise equals half of the centerline temperature rise
C_d	drag coefficient
C_p	specific heat at constant pressure
d	droplet diameter
D	initial diameter of fire source; hot layer depth
\mathbf{D}	drag force
F_d	droplet projected area
f	fraction of radiation absorbed by each droplet
$f_j(d_i)$	mass fraction of non-evaporated droplets in total discharge
Fo	Fourier number
G	mass flow rate
Gr	Grashoff number
h	convective heat transfer coefficient
h_D	mass transfer coefficient
H_o	height of the opening
H	enthalpy
H_D	hot layer depth
k	thermal conductivity, absorption coefficient
L	characteristic length, latent heat of vaporization
Le	Lewis number
N	total number of droplets in water spray
N	droplet number flow rate
Nu	Nusselt number
m	mass

m_{ev}	evaporation rate
p_{sat}	vapour partial pressure at saturation temperature
p_∞	vapour partial pressure at ambient temperature
Pr	Prandtl number
q	heat flux
δQ	heat transfer rate in specified control volume
R	gas constant, radius, rate
Re	Reynolds number
Sc	Schmidt number
Sh	Sherwood number
St	Stokes number
T	temperature
Q_c	total convective heat release rate
t	time
\mathbf{u}, \mathbf{U}	gas velocity vector
\mathbf{v}, \mathbf{V}	droplet velocity vector
We	Weber number
x	specific humidity
X (x,y,z)	Cartesian coordinate
Y	concentration

Greek symbols

α	thermal diffusivity
γ	any variable
ϵ	emissivity
ϕ	fuel-to-air ratio
μ	viscosity, burning efficiency
ν	kinematic viscosity (μ / ρ)
θ	angle
ρ_∞	ambient gas density

ρ	density
σ	surface tension between liquid and gas, Stephan Boltzman constant
τ_d	droplet residence time

Subscripts

a	ambient air
abs	absorption
c	convective
d	droplet
ev	evaporative
g, G	gas
l	liquid
mix	gas-vapour mixture
rad	radiation
s	surface
sat	saturation
v	vapour
w	water, wall

1 INTRODUCTION

Water is widely used as an agent in fire suppression systems. Due to its relatively high specific heat capacity and latent heat of evaporation, water can effectively extract heat, contributing to extinguishment by cooling the fire. In addition to the thermal properties of water, the way it is delivered on the fuel and the resulting interaction with the fire, are equally important in its use as a fire suppressant. Water is usually dispersed into fine droplets and delivered to fire affected areas as a liquid spray either by sprinklers or specially designed mist nozzles. Consequently, the behaviour of water sprays and droplets determines whether or not water-based systems are effective in fire suppression. The extinguishing action of sprays involves several mechanisms, such as gas and flame cooling, fuel cooling and wetting, oxygen displacement with vapour (steam), and shielding against fire radiation. Understanding the contribution of each mechanism in fire suppression allows the prediction of spray performance in a given fire/sprinkler scenario. To deduce such an understanding, a thorough analysis is presented in this dissertation of water droplet behaviour in fire. This analysis has been used in the prediction of spray performance for a given fire scenario. The prediction is based on a combined zonal fire and spray cooling model, the outcome of which is a compact engineering tool. Another novelty of this research is in its detailed review of related phenomena, old and new, as thoroughly as possible. To present the specific objectives of this work, a brief description of the content of each chapter is given.

In Chapter 2 the general literature review is presented with a focus on sprinkler-fire interaction and sprinkler/nozzle properties relevant to this phenomenon. The first two sections of Chapter 2 are related to parameters that govern the performance of water sprays, mechanisms and criteria of extinguishment. The last section gives a brief description of the theoretical approaches used to model fire-spray interaction. To give a concise picture of fire-spray interaction, the reviewed publications are grouped in terms of different spray and fire properties affecting sprinkler/nozzle performance. While Chapter 2 is mostly to classify the existing research in fire-sprinkler interaction into areas of investigation, each of the

following chapters has its own critical review of the relevant literature showing the need for the work presented in that chapter.

In fire-spray interaction, heat, mass and momentum transfer between individual droplets and hot gases are interrelated. These processes should be studied together in order to correctly evaluate sprinkler performance in fire. Amongst practicing fire safety engineers, the traditional method of evaluating sprinkler performance is based on empirical area/density curves without any calculations, except for those related to the water piping system. This approach allows one to identify the water demand, i.e. the volume flow rate of water (or water pressure) needed for suppression the fires for compartments of given area and predetermined fire hazard level. Neither fire location within the compartment nor mechanisms of fire suppression by water and droplet characteristics are considered. This review has highlighted that very few other works exist in the literature which provide more complete physical models. A feature of the present study, on the other hand, is that a more complete physical model of fire suppression has been developed, in terms of spray properties and droplet behaviour, while keeping engineering simplicity.

In Chapter 3, spray dynamics is studied in terms of an individual droplet's motion in gas flow. Droplet trajectories and velocities are calculated by solving numerically the droplet motion equations in the presence of gravitational and drag forces. Droplet trajectories and velocities are then plotted explicitly for two classes of water sprays, coarse and fine, activated in a zone-type fire environment. A significant contribution in Chapter 3 is the classification of spray behaviour in terms of three relative fire-spray nozzle locations. These locations are related to the zones in fire environment. One of the new outcomes from Chapter 3 is that the information on droplet movement history is used to calculate the spray drag-to-buoyancy ratio distribution across the hot gas layer. Previously, such a ratio, which is used as a hot layer lowering criterion, was typically calculated as an overall value for the whole spray. In addition, the droplet residence time is presented as a key dynamic factor affecting the spray thermal performance, and it is calculated as a function of droplet diameter and discharge angle. Furthermore, comparisons are presented between this zonal approach and the present CFD (computational fluid dynamics) results in terms of droplet

dynamics. The effect of two-way coupling and gas turbulence is examined on droplet dynamics in gas flow.

Having established the motion of droplets, heat transfer equations are solved for a droplets-gas system in Chapter 4, where droplet motion and evaporation are taken into account. The computational algorithm is given in a clear, step-by-step form of solving the simultaneous equations, and is easy to use for engineering calculations related to spray heat transfer while passing through a layer of hot gas. This algorithm allows the prediction of spray heat absorption and evaporation rates as functions of initial gas parameters, such as temperature, moisture content and velocity. It can be used as a subroutine for calculating droplet heat and mass source/sink terms in combination with available fire codes. In addition, the algorithm has some features, such as sprinkler location, for example, that have been designed specifically to allow for integration with zone type fire models.

Prior to prediction of fire extinguishment, a detailed sensitivity analysis is presented for different gas and spray initial parameters. The results are divided in two parts. Part one deals with the behaviour of standard sprays under relatively low (pre-flashover) gas temperatures with negligible rates of droplet evaporation. Part two deals with the behaviour of mist sprays exposed to high (post-flashover) gas temperatures with droplet evaporation, up to full droplet disappearance. One of the important findings in Chapter 4 is the prediction of the optimal droplet diameter based on combined droplet heat transfer and motion. In the past, the existence of such a diameter had been assumed, but no model was presented towards prediction. Another contribution reported in this chapter relates to the prediction of mist performance. Even though different researchers have collected experimental data, water mist behaviour has not been generalised mathematically to the extent given in Chapter 4. Another new contribution reported in Chapter 4 is the evaluation of spatial distribution of spray's heat absorption rate within the volume embraced by this spray. This assessment has been carried at in order to evaluate how close the spatial distribution is to the assumption of uniform sink in zone models.

While gas cooling leads only to control of the fire, direct water application on top of solid combustibles makes possible full fire extinguishment. In Chapter 5, numerical predictions and experimental observations are given for the development of fuel temperature during the water impact. The model is based on the explicit solution of one-dimensional transient conduction equations, and therefore, a simple engineering approach is followed. The mechanisms of heat transfer due to droplets' impingement on a hot solid fuel surface are also described in detail. These mechanisms are classified in terms of non-boiling and two possible boiling regimes. The effects of the magnitude of the surface overheat (i.e. temperature rise above the water boiling point) and the properties used to establish each particular regime are studied first in connection with fuel cooling. Subsequently, fuel surface temperature histories, are presented as functions of external radiation from fire and cooling due to water coverage. The model allows estimation of minimal water flux needed for extinguishment as a function of external radiative heat flux.

In order to predict the performance level of water sprays in fire suppression, an existing zone model is used in Chapter 6 to simulate compartment fires. The availability of the source code and full scale experimental data used for the model validation, rendered NRCC-VUT FGM (National Research Council of Canada Fire Growth Model) a highly suitable zone model for this purposes. The significant contribution in Chapter 6 is that the spray cooling model developed in Chapters 3, 4 and 5 were incorporated as an additional sub-model, called SHAR (Spray Heat Absorption Rate), into the basic zone model. This addition has proved the ability to present fire development both before and after activation of the water/mist spray. As a result, sprinkler (or mist nozzle) performance can be evaluated in terms of fire control or extinguishment. Consequently, the combined effect of both spray and compartment parameters on a fire can be predicted. Thus, such parameters such as droplet diameter, water flow rate, room size, openings and the stage of fire development are taken into account.

In Chapter 7, the conclusions of the thesis are summarised. In addition, three appendices are included. A summary of the zone models with the list of input and output parameters of each is given in Appendix A as an extension of the general literature review given in

Chapter 2. Prior to the CFD results utilised in Chapter 3, two-dimensional calculations were carried out using stationary turbulent channel flow. The purpose of this exercise was to evaluate grid independence/refinement and model evaluation. These results are presented in Appendix B. In Appendix C, a sample input data file is given for the integrated NRCC-VUT FGM.

1.1 USE OF WATER AS A FIRE SUPPRESSANT

In the 1950's, the importance of being able to suppress fires using water sprays was recognised, and major mechanisms of extinguishment were established [1]. Since the 1970's, water has been widely considered to be an alternative to hazardous gaseous fire suppression agents, such as Halon 1301. Water is now recognised as the main extinguishing agent used by fire services in active fire protection [2, 3, 4].

In this work, water sprays are classified into sprays produced by standard sprinklers and those produced by water mist nozzles [5]. Standard sprinklers are usually ceiling mounted, and they are automatically activated by the fire. Water mist nozzles, on the other hand, are more flexible in use. A nozzle can be at a fixed position or attached to a fire hose. Standard sprinklers and mist nozzles have various applications and different performance requirements due to the ranges of droplet sizes produced by them. However, the same model of fire-droplets interaction can be used for both types of sprays.

According to NFPA (National Fire Protection Association) [5], water sprays are divided into three categories based on droplet size distribution. This distribution is illustrated in Figure 1.1, which has been reproduced from [5]. In Figure 1.1, representative cumulative percent volume (CPV) is plotted versus diameter distribution for Class 1, 2 and 3 mist sprays.

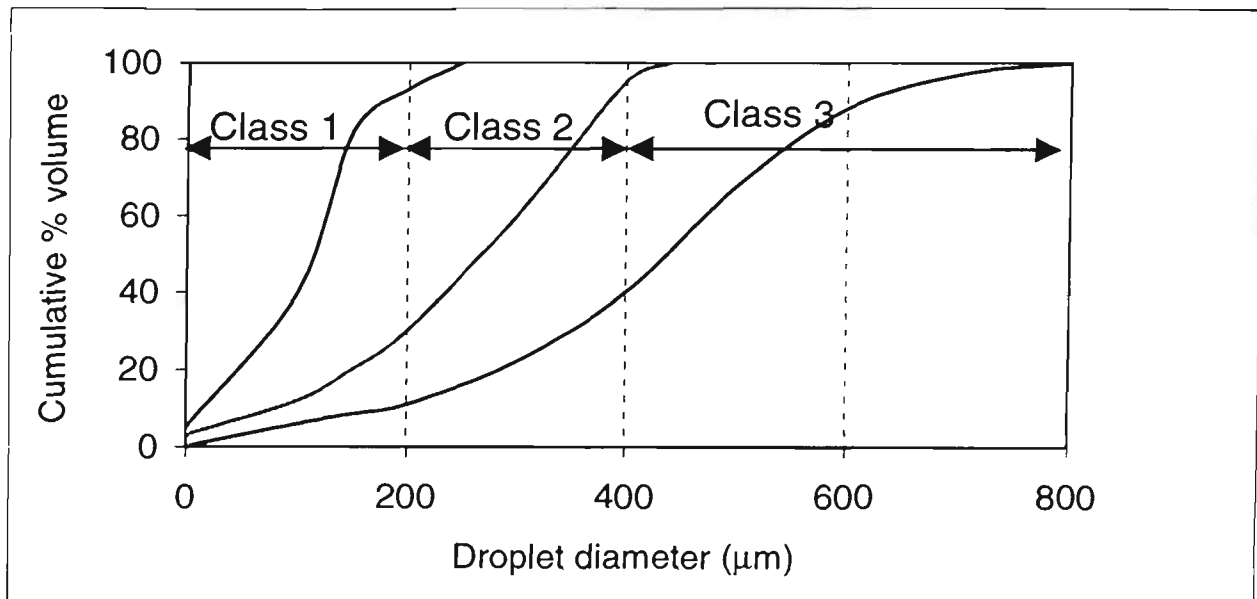


Figure 1.1. Classification of mist sprays in terms of their cumulative volume distribution [5].

According to this classification, Class 1 mist sprays are those with droplet diameters less than 200 μm for 90% of the droplets by volume. Such fine sprays are usually produced by twin-fluid nozzles under high pressure, and they are used in scenarios where fuel wetting is not critical to performance, such as in liquid fuel fires. Class 2 contains droplet diameters of 200 to 400 μm for 90% of the volume. For Class 2, 10% of the droplets have diameters less than 200 μm . Such sprays can be generated by low or intermediate pressure nozzles. These sprays produce considerable surface wetting [5], and therefore, they can be used in fires involving solid combustibles. For Class 3, 90% of the droplets are in the range of 400 to 1000 μm . This type of mist spray can be produced by sprinklers [5]. In this work, mainly, Class 2 and Class 3 sprays are studied as the characteristic sprays of mist and sprinkler systems, respectively.

In most practical cases, water distribution is provided by an automatic sprinkler (or mist) system which is designed to be activated by the fire, so as to ensure rapid suppression with minimum property damage [6]. In such systems, only those sprinkler discharge heads, which are thermally affected by the fire, will be operated. Thus, a sprinkler has to be evaluated in terms of two functions [6]. First, it must detect a fire, and secondly, it must

provide an adequate water supply to control or extinguish it. Each of these functions can be studied separately. In this dissertation, the second of these two issues, namely, the adequacy of water supply, is examined.

1.2 PERFORMANCE OF WATER BASED SYSTEM

Sprinkler performance as determined by Bouchar [7], involves a pass/fail consideration of whether a sprinkler system has successfully controlled or prevented the spread of fire, or extinguished it, in terms of pre-established life safety and property loss criteria. However, there is no precise assessment of the direct hazard to humans of exposure to fire conditions or the property loss criteria. In the impact assessment of sprinklers, completed in the residence sprinkler program of John Hopkins University [7], it was estimated that a properly installed and maintained sprinkler system could reduce death and injuries due to fire by up to 90%, and reduce property loss by 86%. Following NFIRS (National Fire Incident Reporting System, USA) data, given by Solomon [8], the reduction of residence fire deaths is estimated to be between 56-73% for buildings with sprinklers. On the other hand, the reduction of property damage, based on insurance company data, ranges from 1.5:1 to 10.5:1 for sprinklered versus unsprinklered compartments [8]. This reduction occurs due to a sprinkler's capability to alter the development of critical levels of smoke density, toxic gases, or temperatures, and either to extinguish the fire or to control it, until the arrival of the fire brigade.

Even though sprinkler protection capabilities are high, the level of life safety should be increased towards 100%, and property losses should be minimised. Property losses are rather high in many cases due to either delayed activation or excess water discharge causing damage. A poorly designed water mist system may be a potential cause of additional losses. For example, as reported from FMRC (Factory Mutual Research Corporation, MA, USA) [9], rapid cooling in suppression of combustion turbine fires by water spray (thermal shock) often results in turbine blade damage. There are also cases where installation of a water mist system does not help to suppress fire, or it may even enhance it [10]. As shown experimentally [9, 11], most cases of oil fires can not typically be extinguished by

sprinklers or water sprays. In the NFPA Fire Protection Handbook [5], the difficulty of extinguishment is related to “small” fires, while the ease is assigned to “large” fires. However, quantitatively, fire sizes are not defined. Even though there is some theoretical explanation of this phenomenon in the literature [5,9,10], it still needs to be quantified and predicted. The understanding and prediction of water spray system failure may open new horizons in the design and improvement of water spray systems.

Recent experimental and theoretical works had shown that water mist sprays may have broader application as a total flooding agent and substitute of Halon in fire suppression [12]. For example, in the case of suppression of gas or liquid pool fires, when direct water impact to the base of fire is ineffective, there is a need for water mist systems. However, as noticed by different researchers [12, 13], the complex relationship between mist spray parameters and the extinguishing capacity of such sprays at different fire scenarios has not been thoroughly investigated or completely understood yet. For a proper sprinkler system and for the selection of its working parameters, water droplet interaction with different fire scenarios must be understood. This understanding must extend from relatively simple fire cases to more sophisticated scenarios.

In modern performance based approaches to building and fire codes, the design solution, which is supposed to meet the pre-established fire protection objectives due to specified performance level of protection systems, can be based purely on fire modelling if the methods and results are accepted by the authorities. Such ways of obtaining design solutions is viewed by the fire protection community as a way to reduce expenses on large projects. Therefore, this work focuses on computer zone models which then can be applied to the evaluation of sprinkler/mist nozzles performance in fire environment.

1.3 THE NEED FOR THIS PROJECT

Reliable performance parameters are not clearly defined for mist and in some cases, sprinkler systems, in fire. This deficiency is the reason for the need to develop an accurate numerical code to model water droplet interaction with a fire environment. After validation with appropriate experimental data, such a numerical tool can be made available for fire safety engineers for the generation of reliable performance parameters. Therefore, the overall objective here is to numerically predict water droplets' behaviour during fire in order to contribute to the understanding of water extinguishing mechanisms for different applications.

The advantage of using a computer model instead of experimental simulations has been outlined by Galea [14]. Most experimental programs study a certain mist or sprinkler system for a specific fire scenario. In addition, full-scale tests are expensive, and the variety of building designs such as tall atria buildings, or the interior of an aircraft cabin, adds to cost and complexity. Extrapolating results from scaled models, on the other hand, can be unreliable, because of the absence of the reliable scaling rules [15]. Instead of relying only on investigations of fire accidents or new experimental fire simulations, a computer simulation can offer a different approach to the study of fire phenomena, which is cheaper and allows for more flexibility during application. For a numerical model to be reliable, extensive validation is necessary against experimental data. As explained in the next section, there are a number of experimental results available from the literature for this purpose. Additional information has also been obtained in this project from the full-scale experiments of the Centre for Environmental Safety and Risk Engineering (CESARE) at the Fiskville Experimental Building-Fire Facility, for the purpose of validation.

2 LITERATURE REVIEW

The literature review is presented with a focus on sprinkler-fire interaction and sprinkler properties relevant to this phenomenon. The first section is related to the water spray performance in a fire environment, and it summarises the governing parameters of a sprinkler system. The second section gives a brief description of the theoretical approaches used to model the fire environment and the mechanisms of fire extinguishment by water sprays. Both of these sections include the uncertainties in the modelling of fire suppression. The third and last section deals with the modelling of the interaction between water droplets and fire using the governing parameters defined in the first two sections of the Literature Review. The conclusions of each of these three sections are summarised in the last paragraph of each section.

2.1 PARAMETERS GOVERNING THE PERFORMANCE OF WATER BASED SYSTEMS

In order to reasonably predict the suppression performance of a water based system, Mawhinney and Hadjisophocleous [16] indicate that the fire scenario parameters and spray properties must be considered. A fire scenario is defined by the nature and configuration of fuel, rate of growth, room size and geometry, while water discharge rate and droplet size distribution contribute to spray characteristics. The governing fire parameters and different spray system characteristics that have to be correlated, are listed in Table 2.1, which is adopted from Table 1 from [16]. References have been added to the original table to show the workers on different parameters. A new parameter, fire dynamics, marked with an asterisk has also been added due to its importance.

Table 2.1. Parameters governing the suppression performance of water spray systems.

PARAMETER	PHYSICAL PRINCIPLES, DESIGN VARIABLES
I. Fire Scenario	
Fire dynamics *	<ol style="list-style-type: none"> Time dependent combustion energy release process (Bishop <i>et al.</i>[17]; Cooper [18]; Hadjisophocleous <i>et al.</i>[4] Sousa <i>et al.</i>[3]). Fire phase at the beginning of sprinkler activation (Cooper [18], Wighus [19]).
Fire safety objectives	<ol style="list-style-type: none"> Extinguish fire within a defined period of time. Control fire, prevent flashover; limit growth and spread, control temperature (Hinkley [20]; Hill <i>et al.</i>[21]; Hoffman and Galea [22], Jones and Nolan [23]).
Fuel types	<ol style="list-style-type: none"> Liquid fuels in pool fires (Rasbash <i>et al.</i>[24]; Kung[25]; Hadjisophocleous <i>et al.</i>[4]); spray fires (McCaffrey[26]); spill fires Solid fuels (Yao[27,28], Yang <i>et al.</i>[29]) Gas phase fuels (Downie and Gogos [30]; Ingason and Olsson [31]). Configuration of fuel (Rasbash <i>et al.</i>[24]), shielding (Yang <i>et al.</i>[29]).
Extinguishing mechanisms	<ol style="list-style-type: none"> Cooling flame and fuel; oxygen reduction; vapour dilution; (Kung[25], Chow [32]; Downie and Gogos [30]); radiation attenuation (Stephenson and Coward[33]; Lage and Rangel [34]; Log [35]); fuel wetting. Contrary effects: turbulence (Morgan [36]; Mawhinney <i>et al.</i>[37]; Hinkley [20]; Hoffman and Galea [22]), “flare - ups” (Rasbash <i>et al.</i>[24]).
Enclosure effects	<ol style="list-style-type: none"> Compartment ventilation (Morgan[36]; Hinkley[20]; Chow and Fong [38]; Chow [39] (ceiling vent); Hoffman and Galea [22] (doorway); Hadjisophocleous <i>et al.</i> [4] (forced air injection through duct); Ingason and Olsson [31] (experimental work with ceiling vents)). Compartment dimensions (Bill and Ural [9], Wighus [19]).
II. Water sprinkler system properties	
Spray characteristics	<ol style="list-style-type: none"> Droplet size distribution (Morgan[36]; Yao and Kalekar [40]; Gardiner [41], Wighus [42], Hadjisophocleous <i>et al.</i>[4]; Novozhilov <i>et al.</i>[43], Pietrzak <i>et al.</i>[44]). Flux density distribution (Harvie <i>et al.</i> [45], Nam [46]). Spray momentum (velocity distribution) (Nam [46]). Spray cone or linear generation [5].
Methods of drop generation	<ol style="list-style-type: none"> Spray characteristics, constant or variable. Efficiency. Reliability (Nash and Young [6]).
Details of application	<ol style="list-style-type: none"> Full compartment (total flooding for water mist) (Jones and Nolan [23], Tuomissaari [13]). Zoned or local application (Pietrzak <i>et al.</i>[47,48], Hinkley [20]). Obstructions (Hadjisophocleous <i>et al.</i>[4]); Nozzle spacing (Hinkley [20]). Intermittent or sustained discharge.
Method of fire detection and system activation (influence of the size of fire at activation; degree of penetration, etc.)	<ol style="list-style-type: none"> Automatic nozzles (individually thermally actuated nozzle groups: Yao [27,28]). Separate detection system: fire signature; analog thermal detection. Manual release (Salzberg <i>et al.</i>[49], Pietrzak <i>et al.</i>[44,47,48], Tuomissaari [13].).

2.1.1 Spray Discharge Properties

The main parameter that governs water droplet interaction with a fire is the water sprinkler or mist nozzle. Sprinkler/nozzle system performance can be determined indirectly in terms of pre-established life safety and property loss criteria [7]. In such an assessment, the effectiveness of a sprinkler/nozzle depends on how adequately its discharge characteristics were chosen for a given fire scenario. To understand sprinkler/nozzle performance, the values of mean droplet diameter or droplet size distribution, water mass flux density distribution, the angle of water discharge and initial droplet momentum must be considered in investigating spray behaviour. In order to explain how effective these parameters are, the operation principles of standard residence sprinklers need to be considered.

The bulk of water as discharged from an orifice first impinges on a deflector plate that is located beneath the nozzle. Water then spreads to form a sheet, and after contact with the deflector, it is projected outward. The outward motion results in instabilities that cause the water sheet to disintegrate and break-up into drops. The distance in which water break-up occurs is a function of pressure, bulk water velocity and deflector configuration. In general, drops are formed few centimeters downstream from the deflector [40]. There is information in the literature about methods of calculating this distance, such as in Paji and Galustov [50, p.75]. To investigate sprinkler interaction with a hot gas layer, or more specifically, within a thin moving ceiling jet, this value is vital.

As outlined by Gardiner [41], Morgan [36], and Stephenson and Coward [33], there is insufficient information about the initial velocity vectors of water droplets. Chow and Shek [51] obtained experimental values of the mean droplet velocities, by a photographic method for a limited number of pressure and droplet diameters for conventional and spray pendant sprinklers. From a theoretical point of view, the determination of initial droplet velocities is complicated because of the lack of understanding of jet or film breaking processes.

Droplet behaviour and suppression results depend on initial droplet angles [49, 43]. In most calculations, initial velocity directions are taken arbitrarily. Morgan [36] and Chow

[32] used only a horizontal initial direction, and Pietrzak and Johanson [48], and Yao and Kalelkar [40] considered only a vertical velocity component. As a more realistic approach, Hadjisophocleous *et al.* [4] and Nyankina *et al.* [52] used the random distribution of initial directions of droplet velocities within a given sprinkler discharge angle.

One of the most important characteristics of sprinkler systems is the delivered density (DD) on the area covered by a group of sprinklers. This characteristic is calculated as the total water discharge rate divided by the covered by spray floor area, usually with the assumption of uniform flux density distribution from one sprinkler [8, 27, 28]. The investigation in solid fuel fire suppression by Harvie *et al.* [45] outlines the possible errors associated with the non-uniformity of real sprinkler discharge. The characteristics of non-uniform discharge were obtained by Chow and Shek [51], where a detailed experiment was carried out on the water flux density distribution from residential sprinklers as a function of the radial distance and sprinkler orientation angle. Two types of distribution patterns were identified for conventional type pendant sprinklers: a filled cone (type 1) and a cone with a hollow central part (type 2). However, the effects of the different distributions on fire suppression were not studied. The experimental study of the ESFR (Early Suppression Fast Response) residence sprinklers [46] showed that sprinklers of the similar type, but produced by different manufacturers, may provide different DD distributions, and probably as a result, would have slightly different performances in fire suppression.

Droplet diameter distributions for a standard sprinkler at a limited number of operating pressures, were measured by a freezing method by Yao and Kalelkar [40]. These distributions are usually described in the literature by the Rosin-Rammler distribution function [44, 47, 48, 50, 51, 53] with several empirical parameters and constants. The measurements of Yao and Kalelkar further confirm the use of this distribution. The main parameter of this distribution is the volumetric mean droplet diameter. For standard sprinklers of similar geometry, this diameter is proportional to the 2/3 power of the orifice diameter and the minus 1/3 power of the nozzle pressure [25, 42, 51]. This dependence relates to the standard sprinklers of the FMRC (Factory Mutual Research Corporation, USA), and must be corrected when applied to other sprinkler products [8]. The importance

of using droplet size distribution, rather than one representative diameter, was generally explained in [5], specifically underlined by Log [35] in connection with radiation attenuation, and by Novozhilov *et al.* [43] in connection with fire cooling by water mist sprays.

In the review summarised above, the works on the spray discharge characteristics are given. As indicated, these properties are studied in the absence of a fire, and they can be used as the initial parameters in any sprinkler calculation. This part of the review also indicates a void in the literature regarding the effect of these sprinkler parameters on extinguishment.

2.1.2 Mechanisms of fire extinguishment

The mechanisms of extinguishment are listed by Mawhinney *et al.*[1] with reference to the early works published in 1955 to 1960, such as that of Rasbash *et al.*[24]. The major mechanisms were identified as follows:

- ◆ heat extraction, or cooling [5]
- ◆ oxygen displacement, or as explained by Grant and Drysdale [2], addition of a gas to dilute the air feeding the flame and reducing the oxygen partial pressure (in the case of droplet evaporation, water vapour has the same effect)
- ◆ blocking of radiant heat [35]

All three of these mechanisms are governed by the same complex processes of heat-mass transfer between droplets and fire environment. In addition to these three, a fourth mechanism, namely, fuel coverage must be considered in studying fire extinguishments [46]. All of these mechanisms are involved to some degree in every extinguishment. Due to the difficulty of direct measurements during fire, only a few works identify the extent to which these mechanisms participate individually in extinguishment. For this reason, the mechanisms of extinguishments are separated into two groups in this thesis:

- Gas cooling (including convection, oxygen displacement due to evaporation, radiation attenuation)
- Fuel coverage (including physical coverage and evaporation).

Selected works of these two mechanisms of fire extinguishment are given below.

2.1.2.1 Gas cooling

The *cooling mechanism* of extinguishment is provided by water droplets in two different ways in accordance with their sizes. Large droplets of high momentum penetrate the fire plume to act on the burning surface, or wet and cool the surrounding combustible materials and floor that are subjected to direct exposure to fire. Small droplets cool the hot gases spreading radially and prevent an excessive number of sprinklers from operating [20, 40]. Heat absorption due to droplet evaporation causing substantial gas cooling becomes an essential mechanism for mist sprays due to the large interface of heat exchange created by small droplets. Hence, cooling and *oxygen depletion* mechanisms of extinguishment act together. Therefore, mechanisms of extinguishment are conditionally divided into two groups in this study:

- *gas cooling* (includes convective cooling and oxygen displacement due to droplet evaporation, and blockage of radiant heat)
- fuel coverage (includes *cooling of fire base* due to direct impact of droplets, surface wetting)

Chow [32] theoretically estimated the effect of evaporation cooling and found that there was essentially no evaporation for droplets with diameters greater than 0.5 mm. Downie and Gogos [30] experimentally studied gas cooling and oxygen displacement by 250 μm mist sprays. The changes in gas temperature and oxygen concentration were measured within a buoyant diffusion flame in a natural gas (methane) enclosure fire. They observed that both gas cooling and oxygen displacement was insignificant. This was attributed to the droplets' physical deflection from the fire plume, rather than to insufficient cooling or evaporation. Computational results of Chow (1989), Downie and Gogos [30], Morgan [36], Hinkley [20] and Bill and Ural [9] confirmed experimentally that oxygen displacement mechanism does not play a dominant role in the extinguishment of compartment fires. On the other hand, Kung [25], Wighus [42] and Rasbash *et al.* [24] established experimentally that the most effective and probable extinguishing occurred when droplets were supplied either in the combustion zone or in a hot gas layer. They also determined that a

combination of oxygen depletion by production of steam, and cooling by the evaporation of water, resulted in extinguishment. In the recent work of Bill and Ural [9], it is suggested that mist sprays can be used in fire suppression as total flooding agents with much better success in comparison with gaseous flooding systems, since mists are much less affected by fire shielding or location, as well as by ventilation.

The range of mole fraction of steam necessary for extinguishment by water mists of droplet diameters from 150 - 300 μm , was specified by Kung [25] and Rasbash *et al.*[24]. to be no less than 30% and no more than 40% of this range. These figures were obtained from single small and large scale experiments, respectively, in Kung's and Rasbash *et al.*'s works. The CFD results of Sousa *et al.* [3] and Hadjisophocleous *et al.* [4] for a similar range of droplet diameters were not verified against these experiments.

The contribution of *radiation attenuation* by water droplets was identified as an insignificant source of reduction of thermal feedback to burning and unburned fuel surfaces [1]. Downie and Gogos [30] showed that the radiation attenuation effect of water droplets injected into a flame, cannot be separated experimentally from the total spray cooling effect. In theoretical works, such as Log's [35], Lage and Rangel's [34] or Stephenson and Coward's[33], the water droplet absorptivity was estimated. Log modelled the radiant heat attenuation in fine water sprays dependent on droplet size distribution and spray load. The effect of scattering of radiation on droplet surfaces was found to play a dominant role compared to absorption. To achieve a significant radiant blocking effect, extremely small droplet sizes were required, with diameters less than 50 μm . The data of Ravigururajan and Beltran [54] in fire radiation, confirmed these results, since the maximum attenuation factor was found to correspond to those droplet radii of the order of the incident wavelength, i.e. from 0.6 to 25 μm for infrared radiation. In both of these works, the significant role of droplet loading in radiation attenuation is outlined.

The connection between radiation absorption and water droplet evaporation for small droplets in the range of 50-100 μm was studied by Lage and Rangel [34]. It was found that radiation absorption can play a potentially significant role in droplet vaporisation. In

addition, absorption fraction increases rapidly during droplet vaporisation as the droplet diameter decreases [34] indicating that under usual combustion conditions of 1500-2000K, there is an insufficient amount of radiative energy to induce explosive boiling of water droplets. Water droplet emissivity was neglected by Chen and Trezek [55] in their work on thermal performance of water sprinklers.

2.1.2.2 Fuel coverage

Fuel coverage due to direct impact of water to the fire base, in order to cool and wet the combustibles, is the most common fire suppression mechanism. However, the interaction between droplets and burning fuel have been studied by a limited number of workers [56], and governing parameters of extinguishment have not yet been established. Rasbash *et al.* [4] in small scale laboratory experiments described the interaction between droplets and different liquid fuels, but only qualitative explanations of the extinguishment phenomena were given. The mechanisms of extinguishment of solid combustibles were also investigated by Yang *et al.* [29] using small scale experiments where the droplet diameters and water flow rate were indicated as the main governing parameters affecting the extinguishment time. It was found that the larger the diameters, the longer was the extinguishment time. This conclusion does not apply to large scale fires controlled by standard sprinklers, where larger diameters have better penetrative abilities and suppression results [27, 28, 40]. The difference can be attributed to the effect of hot gas buoyancy on droplets of varying sizes. This problem falls within the area of scaling which in many cases of experimental fires does not exist [14].

2.2 CRITERIA FOR FIRE EXTINGUISHMENT

In this thesis, the phrase ‘criteria of extinguishment’, implies a gauge of sprinkler effectiveness in terms of fire extinguishment. As classified by Pepi [57], there are three possible sprinkler performance objectives:

- fire suppression, i.e. a sharp reduction in the rate of heat release with no re-growth;
- extinguishment, i.e. complete suppression of a fire with no burning combustibles

-
- control which is limiting the fire growth by controlling gas temperature.

Thus, sprinkler performance in fire can be estimated in terms of three modes: fire extinguishment, fire control and failure. Depending on safety objectives, an acceptable sprinkler design ensures prevention of the fire spread by controlling or extinguishing the fire. Hence, qualitatively, sprinkler performance can be described based on “pass/fail” consideration depending on fire development after sprinkler activation. However, there is a lack of quantitative criteria of sprinkler performance or fire suppression/extinguishment in the fire literature. Some of the attempts to quantify water spray performance in compartment fire fighting are listed below.

Extinguishment is due to the removal of heat by water droplets, which causes a reduction in the compartment gas temperature. Spray heat removal effectiveness was measured by Kung [25] and specified as the spray heat absorption ratio (SHAR). SHAR is expressed as the heat actually extracted by the water spray divided by the total heat release rate. Following Wighus [42], SHAR can be calculated or measured based on the conservation of energy equation:

$$Q = Q_{\text{water}} + Q_{\text{wall}} + Q_{\text{ceil}} + Q_{\text{floor}} + Q_{\text{vent}} \quad (2.1)$$

where Q is the total heat release rate (HRR) of a fire; Q_{water} , Q_{wall} , Q_{ceil} , Q_{floor} and Q_{vent} are the heat absorbed by the water, walls, ceiling and floor, and convected by ventilation, respectively. Then, SHAR can be derived as follows:

$$\text{SHAR} = 1 - \{ Q_{\text{wall}} + Q_{\text{ceil}} + Q_{\text{floor}} + Q_{\text{vent}} \} / Q \quad (2.2a)$$

or

$$\text{SHAR} = Q_{\text{water}} / Q \quad (2.2b)$$

Therefore, SHAR can be found in two ways: indirectly, by measurement of the total losses to the environment as in Equation (2.1), or directly, by estimating the heat absorbed by the water, including convective heating and evaporation.

$$Q_{\text{water}} = m_{\text{ev}} L + m_w C_{\text{pw}} (T_{\text{ev}} - T_w) \quad (2.3)$$

where L is the latent heat of evaporation of water; C_{pw} is specific heat of water; T_{ev} and T_w are the water evaporation (boiling) and initial temperatures, respectively; m_w is the water discharge rate, and m_{ev} is the water evaporation rate. In Wighus's work, SHAR was estimated experimentally. It was reported that a spray that does not instantly absorb more than 60% to 70% of the HRR of the fire would fail in extinguishment.

Evidence of successful sprinkler operation or theoretical extinguishment in several works implies partial heat extraction, for example, up to 90% in Yao's work [27]. Some of the computational works use SHAR only to characterise the sprinkler effectiveness without modelling suppression, as in [32, 38]. In the case of water mist systems, another mechanism of fire extinguishment is oxygen depletion due to evaporation. Hence, extinguishment may be achieved with a mist system even when the quantity of heat removal is less than required for $\text{SHAR} \geq 90\%$.

One of the possible approaches to the problem, especially in fire zone or field modelling, is to determine whether the sprinklers provide the pre-established safety level in terms of temperature distribution [16]. For example, Pietrzak *et al.* [48] used an average room temperature drop below 150°C and wall/ceiling temperature reduction below 200°C as the fire control criteria in their fire-sprinkler interaction model. This approach to assessment of sprinkler performance seems to be most reasonable from a practical point of view.

The adiabatic flame temperature is used to determine the threshold of extinguishment in [43]. Novozhilov *et al.* [43] used a constant adiabatic flame temperature of 1600 K in the simulation of fire suppression due to sprinkler operation. This approach would have been correct if it had taken into account the dependence of the flammability level on the fuel-air-water vapour mixture fraction [26, 58]. In fact, 1600 K would have been appropriate only for premixed hydrocarbon fires.

2.3 MODELLING OF THE INTERACTION BETWEEN FIRE AND SPRINKLERS

This section reviews the ways of modelling two of the main parameters of Table 2.1 water spray properties and fire scenario. To illustrate the modeling of water spray properties, droplet models are considered, while to describe the fire scenario, zone and field models are reviewed. The numerical approaches to fire-sprinkler interaction are also summarised. The description is restricted to enclosure fires which evolve in confined spaces inside buildings, with little dependence usually on the outdoor environment. No discussion is included on fires in an open atmosphere or accidental industrial fires which are usually associated with explosion development and external fire spread.

2.3.1 Droplet models

There are two distinct approaches to model the effects of a spray as a collection of moving droplets on a fire environment: Eulerian-Eulerian and Eulerian-Lagrangian approaches. The first approach treats the fire and droplets as two continua occupying the same space. The second method treats the droplets as individual particles, i.e. as a discrete phase in the continuum fluid phase. Computational works studying multi-phase processes, such as spray drying and cooling, and usually use the second approach. In this approach, three equations governing heat, mass and momentum exchange for a discrete phase are solved separately, and then, droplet momentum, heat and mass flow rates are introduced as source/sink terms in the gas flow equations. This coupling technique was first applied by Crowe et al. [59] to describe the dynamics and heat-mass transfer of two-dimensional gas-particle systems. The resulting model is known in the literature as the Particle-Source-in-Cell (PSI-Cell) method. The method is popular in modelling fire-sprinkler interactions [4, 3, 43, 38, 60, 61], and it is employed in this thesis. The restrictions of this technique arise from the assumptions of low droplet concentration and low gas turbulence [22].

More specifically, in the Eulerian-Lagrangian treatment of a discrete liquid phase, a number of individual particles can be characterised by a droplet distribution function. For this purpose, either a monodisperse case of initial single droplet diameter, or a polydisperse case of initial droplet diameter variation, for example, as defined by the Rosin-Rammler function, can be considered. The droplet trajectories and mass and temperature histories

are obtained by integrating the equations of motion for each of the droplets in the gas flow and solving the mass and heat balance equations at the interfaces. In the basic equation of motion, the drag force on each particle is taken into account and relative velocities are calculated. The rates of droplet temperature change and mass flow are determined through considerations of convection heat transfer and evaporation mass transfer, as in Equation (2.3). The model governs the multi-phase processes, such as spray drying and cooling, and the resulting heat-mass transfer model is known in the literature as the 'drier model' [53, 59, 62]. The drier model is the best known application of the PSI-Cell technique. A literature review on the existing approaches to the problem of particle transport in a turbulent gas flow can be found in [63]. The stochastic droplet dispersion due to turbulence can be included within Lagrangian formulation using the technique proposed by Gosman and Ioannides [64] in connection with spray combustion.

There is agreement in the literature regarding the heat and mass transfer coefficients, since the basic Ranz-Marshall [65] correlations for Nusselt (Nu) and Sherwood (Sh) numbers have been found to be satisfactory by most researchers [4, 22, 53]. Much less agreement exists with respect to the droplet drag coefficient. In Paji and Galustov's work [50, p.40], 17 different approximations for the drag coefficient are compared for different conditions. The assumptions that the droplets are spherical, isothermal, and sufficiently distant from each other, i.e. non-interacting, are justified in spray cooling processes [22, 38, 55].

No distinct radiation model exists for water droplets within fire-sprinkler interaction models. The discrete transfer method of Lockwood and Shan [66], is used widely to approximate radiation exchange between solid boundaries with known geometry [3, 43, 62,]. In this method, the radiant heat transport equations are solved along a specified representative ray between the two boundaries. The gas and soot particles between the two boundaries are considered as an absorbing, emitting and scattering medium with known isotropic coefficients. The discrete transfer method is usually available in CFD packages, such as Furnace or FLOW-3D. This method is not applicable to a medium with anisotropic scattering properties where the rays' path length can not be specified *a priori*, as the theory demands. In addition, for a system with many particles, such as a mist spray system, the

incoming radiation is scattered many times, and the scattering function is anisotropic [33]. In this case, the radiation exchange can be modeled randomly using the Monte Carlo technique [67], but there has been no attempt to apply this technique to investigate spray performance in fire.

2.3.2 Numerical models of fire environment

Numerical models that simulate heat and mass transfer processes associated with a known enclosure fire source, fall into one of two categories: zone models and field models. The essential difference is in the way they treat the fire induced hot gas movement or buoyancy and their utilisation of experimental information.

2.3.2.1 Zone models

In zone modelling, the hypothetical fire compartment is divided *a priori* into several distinct zones, or layers of consistent fire behaviour. The assumption is based on experimental observation of gas layering. One or more zones may be specified. Typically, up to three zones are considered:

1. A lower layer of cool air, assumed to be effectively stagnant and isothermal;
2. A higher layer of hot gases beneath the ceiling, again assumed to be effectively stagnant and isothermal; and
3. A rising plume of hot gases above the burning object, which entrain the surrounding air. This is the only boundary that is penetrated. The mixing of horizontal layers is otherwise neglected [20].

The buoyancy generated by any burning object, causes the formation of a plume which acts as an upward force to move heat and mass from the lower layer into the upper layer [68, p.5]). As the fire progresses, the thickness of the lower cool layer decreases, causing the interface to move downward. If the growing upper layer radiates a sufficient amount of heat to unburnt combustibles, they will ignite, causing sudden fire growth known as flashover.

The mathematical approach in zone modelling is based on solving a set of fundamental equations for conservation of mass and energy, which describe the interaction between assumed zones. Within these zones, empirical expressions are used to describe the physical properties of the fire, such as the maximum gas velocity in the plume [58], ceiling jet velocity and temperatures [69], temperature distribution as a function of the vertical distance from the fire source, flame height and width [58] and hot layer thickness.

Calculations can be performed relatively quickly with zone models, even on moderate size computers, and they result in acceptable predictions of the centerline temperature and hot layer thickness. As a result, zone models are attractive in engineering practice, and their development continues [14]. Some of the commonly used zone models are listed in Appendix A together with their applicability criteria, input and output parameters. The main weaknesses of the zone approach are the difficulties in determining the number and location of representative zones, the uncertainty of the existing empirical expressions in some applications and the absence of experimental data to determine related empirical constants [14].

Zone modelling has been used in engineering applications to predict the characteristics of fire-sprinkler interaction. A one-zone model with uniform compartment gas temperature was employed by Pietrzak *et al.* [44, 47, 48], Morgan [36], Wighus [42] and Unoki [70] to estimate their experimental results. Gardiner [41] developed a quasi-zone-field model, describing the interaction between a sprinkler and buoyant layers of hot gases due to fire, as mentioned by Hoffman and Galea [22]. Pietrzak *et al* [48] studied the optimum droplet diameter in fire suppression with both gas and fuel cooling mechanisms. However, no mathematical description of their model exists. Chow [32] employed the Harvard V fire compartment zone model, to estimate sprinkler effectiveness. Hinkley [20] used zone modelling to describe sprinkler-fire interaction. In these works, only the sprinkler 'macro-characteristics', as referred to by Chow and Fong [38], have been obtained. These are, the total heat extracted by the spray [32,42], and the overall drag-to-buoyancy ratio (D/B), i.e. the ratio of the overall drag force on the spray, D, to hot gas buoyancy, B. This ratio can be used to estimate the stability of the smoke layer [36]. In terms of these macro-parameters,

zone modelling gives acceptable agreement with experiments. However, sprinkler-fire interaction with a comprehensive account of droplet dynamics and heat transfer has not been simulated within a zone model, and this gap is filled by the present work.

2.3.2.2 Field Models

Another deterministic way to model the fire environment is through field modelling which gives a much more detailed prediction of the fire environment behaviour than a zone model. Field models divide the room into a large number of elemental cells in which mass, momentum and energy transport equations are solved numerically point by point by applying appropriate boundary conditions. Field modelling in fire simulation falls within the area of Computational Fluid Dynamics (CFD). It involves the numerical solution of a set of three-dimensional, time dependent, non-linear coupled partial differential equations of linear momentum, i.e. the Navier-Stokes equations, to describe the gas flow. Based on the method of turbulence treatment, two main approaches are used in fire simulations: a $k-\epsilon$ type of turbulence model [22,38, 71, 72] and Large Eddy Simulations (LES) [73,74]. A review of traditional field models with $k-\epsilon$ type turbulence models and a brief description of LES can be found in [75]. Direct numerical simulation (DNS) is an upcoming CFD approach in fire modelling. [76]. This technique avoids the inaccuracy due to averaging and empiricism involved in $k-\epsilon$ type simulations, but even with modern computational hardware, it is still unacceptably expensive. The question of applying one or another CFD technique to fire modelling relates to the question of creating or improving the relevant sub-models for the combustion zone, water droplet performance, radiation transfer, etc [77]. To receive a realistic picture of the overall fire phenomena, all aspects of the problem must be studied. The objective of the present research has been to prepare a complete sub-model related specifically to water droplet behaviour with relevant study of all aspects of fire-sprinkler interactions. Although the sub-model has been used only with a zone model so far, it can be used in conjunction with a field model as well. A summary of selected CFD works in fire modeling follows.

Using the PSI-cell coupling technique, Hadjisophocleous *et al.* [4] obtained from 10 to 20 times lower suppression times than indicated experimentally with a three-dimensional CFD-code, TASC-flow. Using the same approach for the simulation of sprinkler-fire interaction, Chow *et al.* [38,39] developed a three-dimensional field model and indicated both fair and poor agreement for the same compartment. Large deviations from experimental results were observed at the positions within the compartment close to the combustion zone (100% and more) and the ceiling's vents. The authors explained these discrepancies by the absence of a combustion model, and by the lack of data for free boundary conditions. On the other hand, Hoffman and Galea [22] obtained their best results for a location directly above the fire source rather than for a location away from the fire. They used the Eulerian-Eulerian approach and a commercial computer program, PHOENICS, for the three-dimensional analysis of the fire environment with sprinkler implementation. For their work, the suppression phenomenon and combustion were not modelled, but a comprehensive investigation of gas re-circulation caused by spray intervention was performed. However, the effects of different sprinkler properties, such as droplet diameter or water flow rate have not been investigated in any of the above mentioned works.

One of the CFD packages, used to model fire is FURNACE, developed by Boyd and Kent [78] and modified by CESARE (Centre for Environmental Safety and Risk Engineering, VU). FURNACE is written in FORTRAN. It uses the basic $k-\epsilon$ model for turbulence, and a discrete transfer model for radiation [66]. An attempt to add a droplet sub-model to FURNACE has already been made by Novozhilov *et al.* [43], together with one of the co-authors of FURNACE. However, this combination contains only one macro characteristic of spray thermal performance, namely, a critical water flow rate as a function of droplet diameter. In addition, droplet trajectories are calculated for small droplets; whereas water demand for suppression are calculated for large droplets.

Another commercially available package, CFX, has been employed by different authors to model water droplet and fire interaction. The program provides two selective approaches to modelling the continuum-discrete phase interactions, Eulerian-Eulerian and Eulerian-

Lagrangian. The Eulerian-Lagrangian approach has been used in a study of 2D fire-sprinkler interaction [37]. The authors demonstrated the results of momentum exchange between the two phases. However, they do not provide either a comparison with other results or the droplet input characteristics. Hoffman and Galea [22], using the Eulerian-Eulerian approach, ran test problems using CFX4 (Harwell, UK) flow modelling software, and qualitatively correct results were presented for fire-sprinkler interactions. These authors also outlined that the utilisation of CFD packages is first of all a computer time issue. A Lagrangian particle transport model available in the library of CFX applications, allows to study droplet movement and convective heat transfer with surrounding gas flow. The drag coefficient and heat-mass transfer coefficients of this model can be modified by the user. However, no other flexibility exists. This particle transport model cannot be separated from the rest of the software, and hence, it can not be used in connection with a zone model. In addition, convection is the only mode of heat transfer, considered.

3 DROPLET DYNAMICS

3.1 INTRODUCTION

Although many publications on fire-sprinkler interaction contain models of spray droplet dynamics, only a few provide sprinkler trajectories in fire induced gas flow and related spray characteristics. On the other hand, most experimental and numerical results in fire suppression by water sprays can be explained with a clear understanding of droplet dynamics. One of the problems in comparing model spray dynamics with experimental evidence is the lack of input data, such as initial velocities and angle distribution within the spray. A droplet sub-model has been developed in this study for zone modelling of fire environments. In this chapter, trajectories are described based on the numerical solution of the equations of droplet motion in gas flow under gravity and drag forces. Heat transfer is excluded, and consequent changes in gas and droplet temperatures or droplet mass, are not accounted for. Droplet residence time is identified as a key factor of droplet dynamics affecting spray thermal performance. With droplet residence time, the dynamics model is linked to heat and mass transfer between water spray and hot gas as described in Chapter 4.

In this chapter, a sensitivity analysis has been carried out to determine the effect on droplet residence time on droplet diameter and distribution, initial droplet angle and velocity, and gas velocity profile. The results are analysed with respect to three different relative fire-sprinkler locations. These numerical results indicate the existence of an optimal droplet diameter in gas cooling.

3.2 BACKGROUND

A droplet sub-model has been developed for the purpose of predicting fire-sprinkler interaction. This sub-model serves to predict the different effects imposed by injected water spray into a fire environment. The fire environment can be presented as a gas flow characterised by temperature and velocity distributions. The basic continuity, energy and momentum conservation equations are then applied to this flow. Representing the spray as a discrete particle flow, the presence of droplets in a gas flow can be accounted for by

introducing source/sink terms into gas equations. In order to evaluate these terms, droplet trajectories, mass and temperature histories should be predicted first based on solving momentum, mass and energy balance for the droplets. In this chapter the droplet trajectories are obtained explicitly from the equation of motion. Analysis is simplified to the case of one-way coupling, e.g. it is assumed that the droplets do not affect the gas velocity distribution, while gas velocity affect the droplets. The droplets in a spray are considered to behave as isolated spherical particles and their motion is governed by friction drag and gravity [32, 36, 41, 59, 79] forces only.

Complicated particle interaction is difficult to account for and errors may arise from the consideration of droplet motion as single particle flow rather than within a spray. Particle interactions in a dense flow can cause reductions in heat transfer up-to 38% as stated in [63]. The drag coefficient and droplet motion can also be affected. For dense spray flows, the drag coefficient of a single droplet within the spray, C_d , can be corrected by the following empirical expression [50]:

$$C_d/C_{ds} = (1-\gamma)^{-4.65} \quad (3.1)$$

where γ is the droplet volume concentration in the continuous phase equal to V_n/V . V_n is the total volume of all droplets, and V is the total volume of the spray space. C_{ds} , the drag coefficient of a single isolated droplet, can be calculated using any standard single droplet equation. It is also stated in [50] that for $\gamma < 0.015$, the droplets can be considered as independent from the presence of other droplets in the spray.

The problem with real sprays arises from the fact that the droplet density is not uniform along the spray path. Near the nozzle the droplets may occupy a significant volume of the gas phase in comparison with distances further down. Another limiting value of γ is given in [80]. For $\gamma > 0.05$, the droplet trajectories are close to each other and the following expression is suggested to correct the droplet drag coefficient, C_{ds} [80]:

$$C_d/C_{ds} = 1 + 3.5\gamma \quad (3.2)$$

For common fire spray discharge rates (1-2 kg/s) and ratios of total droplet to spray cone volumes, the values of γ were found to be below the threshold for interacting droplets. Estimated values of γ are about 3×10^{-4} to 6×10^{-4} for the whole spray, and 0.01 to 0.03 at a distance of 0.1m from the nozzle for 1-2 kg/s water sprays.

In the remainder of the spray ($\gamma < 0.05$), even though the droplet trajectories are separated, the effect of droplets following each other in a line may cause the reduction in the drag coefficient. As explained in [80], gas motion induced by droplets can reduce the overall resistance to the movement of the following drops. This reduction depends on droplet size and, as indicated in [80], it can reach as much as 30% for 300 μm droplets. No data are provided regarding water flow rates or larger diameters.

In [80], it was shown by CFD simulations with particle tracking that a water spray of 1.57 kg/s and droplet diameters from 0.5 to 1.2mm had a negligible effect on the gas flow field. Therefore, no correction has been used for C_d in the present study considering that sprays below this rate are not dense enough to have droplets affect each other's movement.

In relation to droplets' effect on their surrounding as suggested in [81], the Stokes number can be used for spray spreading in "an organised turbulent structure":

$$St = 2\rho_l R^2 \Delta_u / (9\mu_g L) \quad (3.3)$$

where ρ_l is the liquid density, R is droplet radius, Δ_u is a characteristic slip velocity between droplets and gas, μ_g is the gas viscosity, and L is a characteristic length associated with the gas flow. According to [81], if $St \leq 1$ the droplets can follow the gas flow. If $St \geq 1$, then droplets do not have time to interact with flow vortices, and their behaviour is independent of the flow if $St = O(1)$, then droplets interact with the flow, and there is a non-zero slip velocity between the droplets and the flow.

In [81], how to estimate L in Equation (3.3) is not explained. It has been assumed here for preliminary estimations, that L is the same order as the fire plume radius in fire environment. For Class 2 and Class 3 mist and sprinkler sprays, the conditions for fire sprays are more likely to fall into the third category of $St = O(1)$. This condition is actually applied in the present study.

Special consideration should also be given to the reduction in the friction drag coefficient due to droplet evaporation causing the so called “blowing effect” around droplets [63]. High droplet evaporation rates may cause a substantial reduction in C_d . This may become especially important for mist spray applications when small droplets are immersed into high gas temperatures. Possible corrections for C_d and heat and mass transfer coefficients connected to the effect can be found in [59, 63], and these will be discussed in the heat-transfer section (Chapter 4) of the present thesis.

3.2.1 Basic Equations

Assuming that only gravity and drag forces act upon droplets, Newton's second law of motion for a particle of constant mass can be expressed as follows [59]:

$$m_d \frac{dv}{dt} = -0.5 C_d A_d \rho_g |v-u| (v-u) + m_d g; \quad (3.4)$$

$$\frac{dX}{dt} = v \quad (3.5)$$

where m_d , v , X and A_d are the mass, velocity, position vector and cross-sectional area of the droplet, respectively and u is the gas velocity vector. The first term on the right hand side in Equation (3.4) is the friction drag force, D , opposing the motion. The drag coefficient in these equations corresponds to that of a single solid sphere, and it is expressed by the following relationships:

$$C_d = (24/Re_d) (1 + 0.11 Re_d^{0.81}) \quad \text{for} \quad Re_d < 21 \quad (3.6a) \quad [80]$$

$$C_d = (24/Re_d) (1 + 0.15 Re_d^{0.667}) \quad \text{for} \quad 21 < Re_d < 1000 \quad (3.6b)^1 \quad [41, 59, 64]$$

The Reynolds number, Re_d , depends on droplet relative velocity and droplet diameter: $Re_d = d |v-u| \rho_g / \mu_g$; where d is the droplet diameter, μ_g is the gas film average viscosity, and ρ is the free stream density [63]. The second term in Equation (3.4) corresponds to gravitational force.

Air entrainment into the spray due to spray movement is not considered in the zone-type environment discussed here. As indicated by Sirignano [63], air entrainment caused by the momentum coupling between liquid droplets and gas, is governed by friction drag, pressure drag and thrust forces. Pressure drag associated with air entrainment due to voids, and thrust associated with droplet evaporation are not accounted here for the droplet trajectories [50, 82]. However, it can be assumed that the effect of all these forces are indirectly accounted for by the empirical friction drag coefficient in droplet momentum balance equation. This coefficient has been evaluated for moving and evaporating water droplets, and it includes the effect of all forces contributing to the resulting droplet motion.

In this study, gas flow is taken to be steady and two dimensional, and it is represented by a given gas velocity distribution. The new particle velocity and coordinate as the droplet traverses the hot layer is obtained from the integration of the system of ordinary differential Equations (3.4) and (3.5) with defined initial conditions, for a given gas velocity. Both numerical [38] and analytical solutions [12,36,59,62] of Equations (3.4) and (3.5) exist in the literature for different $C_d(Re)$. However, experimental data are not available for droplet trajectories and instant velocities.

The effects of internal fluid circulation and oscillation of the droplet shape on droplet behaviour are considered to be negligible, when the Reynolds number range is between 80

¹ In [80], the range of Re_d for Eq. (3.6b) is limited by 400. The experimental corrections for C_D for the range of $Re_d > 400$ for the case of polydisperse sprays can be found in [80]. However, the range of Re_d in present study usually does not exceed this limit.

and 300, for droplet diameters less than 1 mm and gas to fluid viscosity ratio, μ_g/μ_d of much less than unity [83,84]. Levich [85] states that even for larger Reynolds numbers and higher relative velocities, the effect of internal circulation is negligible due to usually existing water contamination on the droplet surface.

3.3 DYNAMICS: RESULTS AND DISCUSSION

3.3.1 Droplet trajectories in terms of relative fire-sprinkler location

In the present study, sprinkler discharge is represented by a mean droplet diameter, initial droplet velocity and set of initial starting angles which vary from -90 to 90 degrees from the vertical axis. Two types of sprays, mist and coarse, are represented by two droplet diameters, 0.3 mm and 0.7 mm, respectively. Droplet trajectories are calculated based on the fourth order Runge-Kutta numerical integration of Equations (3.4) and (3.5). Initial conditions include droplet size, location and velocity vector (i.e. water bulk velocity with specified discharge angle). The initial time step of integration can be automatically changed by the program based on the solution convergence. Droplet trajectories are shown in different gas flow directions for fine and coarse droplets. The origin of the Cartesian coordinate system in the room is at the sprinkler head. The vertical axis, Y, is negative in the downward direction. The three types of relative sprinkler-fire locations are represented by the three gas flow directions. In this work, they are identified as Locations 1, 2 and 3 in Figure 3.1.

Location 1: a horizontal (X-direction) gas flow (no vertical component), as usually exists in the hot layer. This scenario corresponds to spray operation far away from the fire source (corridor or remote site in the apartment of fire origin).

Location 2: spray nozzle activated in gas flow with both vertical and horizontal components. This scenario can represent the plume turning point.

Location 3: a vertical gas flow (positive Y-direction), as usually exists in the fire plume. This scenario corresponds to nozzle activation directly above the fire source.

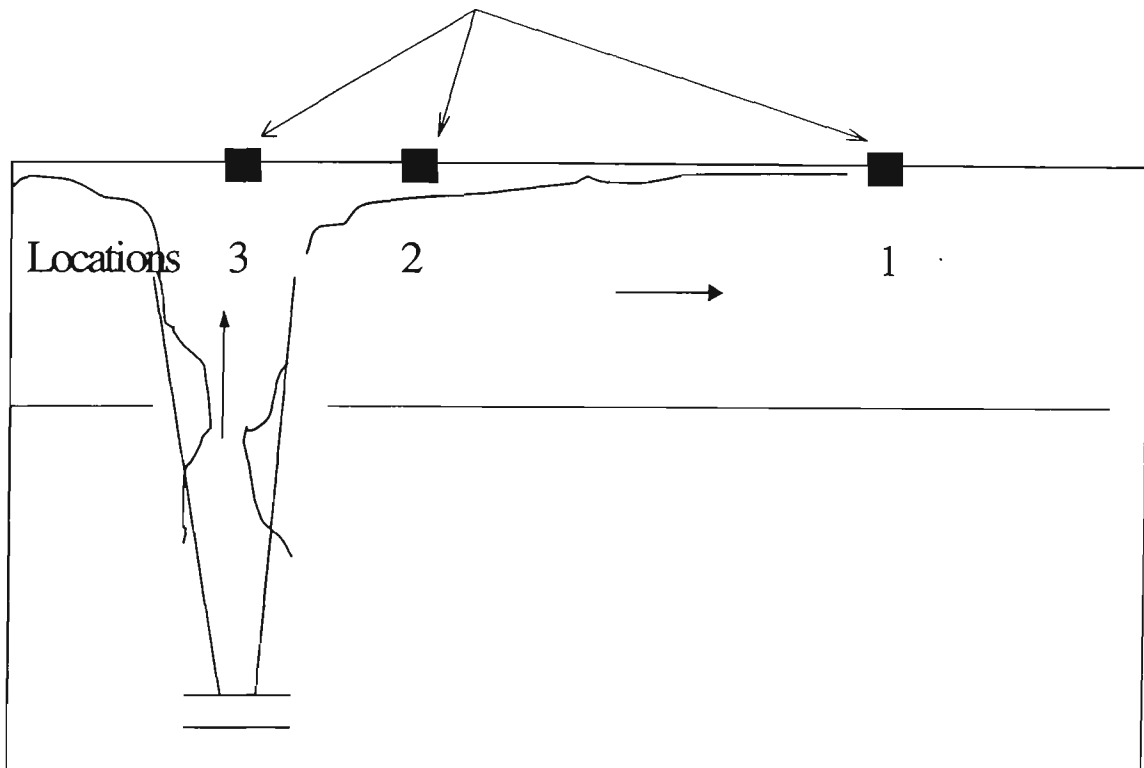


Figure 3-1. Three cases of gas flow relative to fire sprinkler location. Gas velocity distribution is assumed to be uniform in all cases. Gas velocity magnitude is taken as 2m/s with an initial droplet velocity, V_0 , of -5m/s.

Among the three representations in Figure 3.1, Location 3 is the most critical when analyzing droplet movement. At this location, the high sensitivity of droplet dynamics to droplet diameter and gas-droplet relative velocity is indicated in Figure 3.2 (c and f). At Location 3, the mist spray represented by 0.3mm droplets is blown away to the ceiling, whereas the coarse spray of 0.7mm droplets penetrates downwards successfully for the same initial velocities. At Location 1, although both sprays get deflected due to the horizontal gas flow (and finer droplets get deflected more than coarser ones, as expected), the effect is less than at Location 3. Location 2 represents the intermediate case (Figure 3.2b and e).

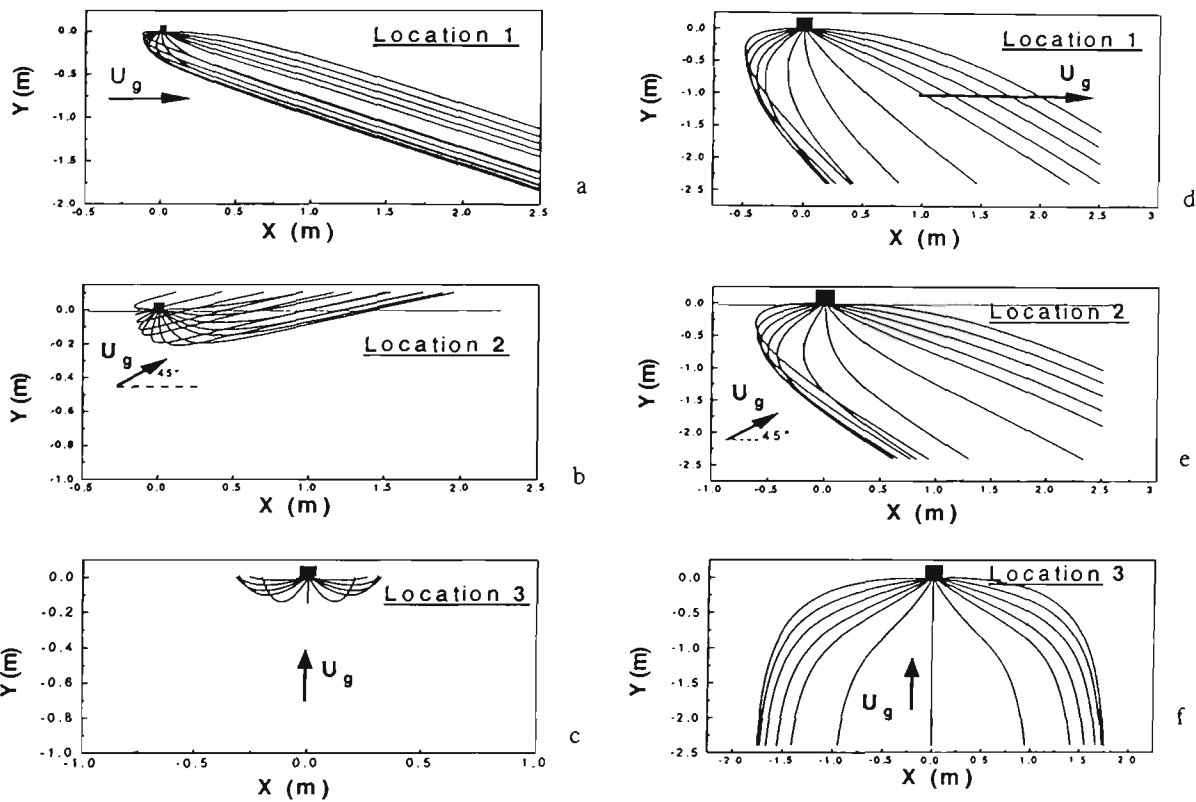


Figure 3.2. Droplet trajectories in uniform gas flow of 2m/s at the three relative fire-nozzle locations. The thirteen different trajectories correspond to the different droplet initial angles, α , at the sprinkler head. Droplet initial horizontal and vertical velocity components are calculated using: $V_{ox} = V_0 \sin(\alpha)$ and $V_{oy} = V_0 \cos(\alpha)$, respectively. Locations are represented by the different gas flow directions. (a) and (d) correspond to uniform horizontal gas velocity; (b) and (e) correspond to gas velocity at 45° to horizontal; (c) and (f) correspond to updraft vertical gas velocity. (a) to (c) correspond to the 0.3 mm droplet spray, and (d) to (f) to the 0.7mm droplet spray.

From a comparison between the shapes of the sprays given in Figure 3.2 (a and d) for 0.3 and 0.7mm droplets, respectively, the trend of small droplets to move closer to the centerline in comparison with heavier droplets can be observed, regardless of the initial angles. This observation is consistent with the limited experimental data of Chan [86] as described by Nam [46]. The fact that the uprising fire plume does not allow the water droplets to reach the fire base can be found in the experimental observation [87] for mist droplet (0.3-0.5mm) sprays. High sensitivity of spray effectiveness to the relative fire-nozzle location has also been indicated by Wighus [42] in his full-scale experimental study of propane fire extinguishment by ceiling mounted sprays.

3.3.2 Droplet velocities and residence times

Droplet dynamic characteristics, such as droplet velocities and residence times, affect spray number density. The spray number density, i.e. the number of droplets per unit volume, in turn determines sprinkler heat transfer effectiveness. As seen from Figure 3.2, the relative fire-sprinkler locations have a profound effect on water spray behaviour, especially on small droplets.

In Figure 3.3, the effect of the same three locations on droplet residence times is shown. As indicated previously, a sprinkler is represented by either ‘mist’ (0.3mm) droplets or ‘coarse’ (0.7mm) droplets discharged at different angles. Figure 3.3a corresponds to the 0.3mm, and Figure 3.3b to the 0.7mm sprays. As in Figure 3.2, gas profiles are uniform, and gas velocity magnitude is 2m/s. The results are presented for 1m of vertical travel distance. The residence times of light mist droplets of 0.3mm diameter at Location 3 are small and much less than the residence times of coarse sprays with 0.7mm droplets. On the other hand, in horizontal gas flow corresponding to Location 1, finer droplets are suspended for longer periods of time and have almost double the residence times of coarser droplets.

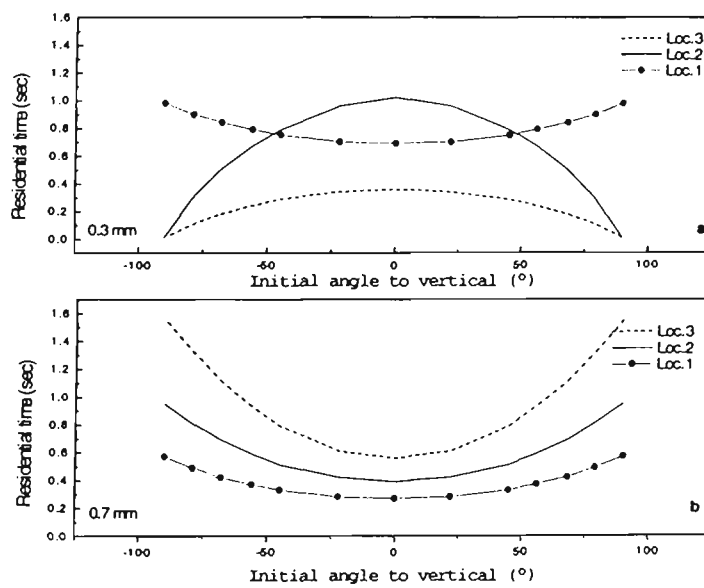


Figure 3.3. Droplet residence times as a function of initial discharge angles. The residence time corresponds to either a vertical distance of 1m or when the droplets (only the 0.3mm diameter ones) strike the ceiling. (a) 0.3mm droplet spray; (b) 0.7mm droplet spray.

In Figure 3.4, the relation between droplet diameters and their residence times is shown for the range of diameters from 0.3mm to 1.5mm. Location 1 is chosen to allow all droplets to cover a similar distance without being diverted. It can be seen that the droplets smaller than 0.5mm show significantly higher residence times.

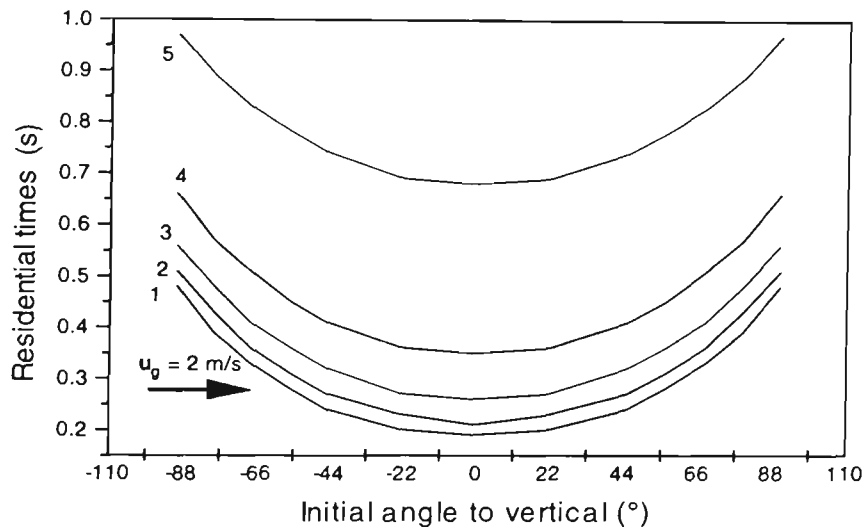


Figure 3.4.. Droplet residence times for different mean droplet diameters: 1 - 1.5mm; 2 - 1mm; 3 - 0.7mm; 4 - 0.5mm; 5 - 0.3mm. Location 1 is chosen due to its common use in the literature. Horizontal gas velocity is constant, 2 m/s; layer depth is 1m and droplet initial velocity is 5m/s.

In terms of initial angles, coarser sprays have higher residence times at the periphery ($\sim 90^\circ$), and mist type sprays have longer times at the centre, 0° , when they are both discharged at Location 3, as shown in Figure 3.3. Therefore, coarse sprays are more effective with broader discharge angles, whereas mist sprays are more effective with narrow, more centralized spray patterns when directed downwards. The experimental data of Salzberg *et al.*[49] on two spray patterns show the effect of the initial discharge angle on sprinkler effectiveness. Sprays of 60 and 90-degree initial angle were discharged by a high pressure hose equipped with a spray nozzle. The results indicate that the angle becomes important when an ‘upwind attack’ is present (co-current droplet motion and gas flow). In this particular case, the best performance in fire extinguishment was obtained with a 90-degree spray. An explanation for this result can be given in terms of the present model calculations. In Figure 3.5, the residence times of mist droplets (0.3mm) discharged

upwards (co-current flow) and downwards (counter-current flow) in an uprising gas flow of 2 m/s, are plotted. The advantage of 90-degree initial discharge compared to a 60-degree one in the ‘upwind’ (co-current) direction is clearly shown, since the residence time for the larger angle is much higher, and consequently, so too is sprinkler effectiveness. The residence times for the downward spray direction are given for comparison, and to outline the advantage of upwind direction for mist sprays. The advantage of a 60-degree discharge angle spray in downward direction [49] is confirmed by the lower curve in Figure 3.5.

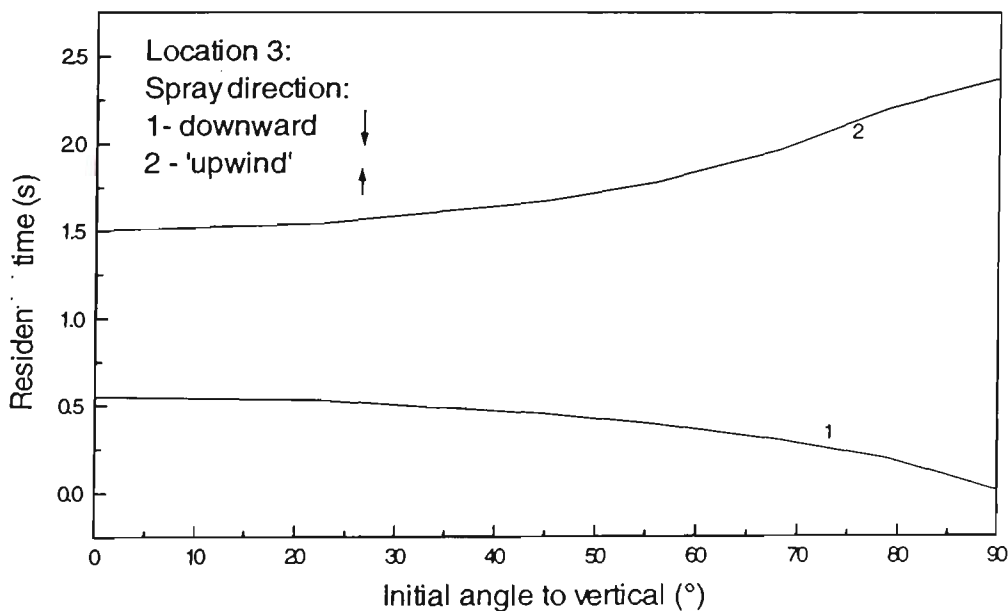


Figure 3.5. Comparison of mist spray droplet residence times in upward and downward discharge directions. The spray is represented by 0.3mm droplets discharged under 10 initial angles from 0 to 90°. The uniform updraft velocity is 2m/s.

To investigate the link between droplet momentum characteristics and droplet residence times in updraft gas flow, droplet vertical coordinates are plotted against instant velocities and time in Figure 3.6 and Figure 3.7 (a and b), respectively. In Figure 3.6, vertical velocities of 0.3mm to 3mm droplets are shown along the vertical distance from the sprinkler head in zero gas flow. Depending on the droplet diameter, droplets either accelerate (the heavier ones), or decelerate before reaching certain terminal velocities.

In Figure 3.7a, the vertical distances versus vertical velocities are plotted for the droplets of different sizes with equal initial velocities moving in the 2m/s updraft gas flow (Location 3). Some of the droplets that decelerate, finally stop (the velocity drops to zero). These droplets then change their direction of motion, and their velocities change sign. There is a critical droplet diameter below which droplets turn up, and above which they go down. As shown in Figure 3.7b, the critical diameter is about 0.5mm at Location 3 for 2m/s updraft gas velocity. The 0.5 mm droplet quickly decelerates and attains its terminal velocity, after which the droplet slowly moves up with the gas flow. The upward motion of the droplet is so slow that it gets suspended in vertical gas flow. The value of the ‘suspended diameter’ corresponds to when a balance of gravity and opposing drag forces exists, and it depends on the magnitude of the gas velocity. As seen in Figure 3.7, ‘the suspended’ diameter becomes the diameter at which terminal velocity is close to the magnitude of the opposing gas velocity. The higher the gas velocity, the higher the droplet terminal velocity needs to be to balance it, and only heavier droplets can achieve this balance. These results are in agreement with experimental observations that the heavier the droplets, or the larger the droplets momentum, better is their penetration into the uprising fire plume [40].

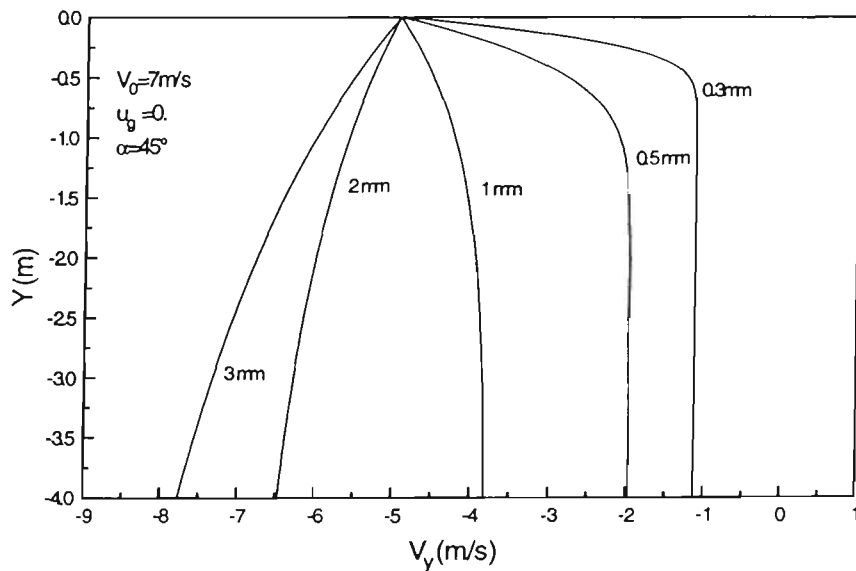


Figure 3.6 The vertical components of droplet trajectories for different diameters for zero gas velocity. Droplet diameters are listed next to corresponding curves. Initial conditions are the same for all droplets, consisting of 7m/s droplet initial velocity and 45° discharge angle.

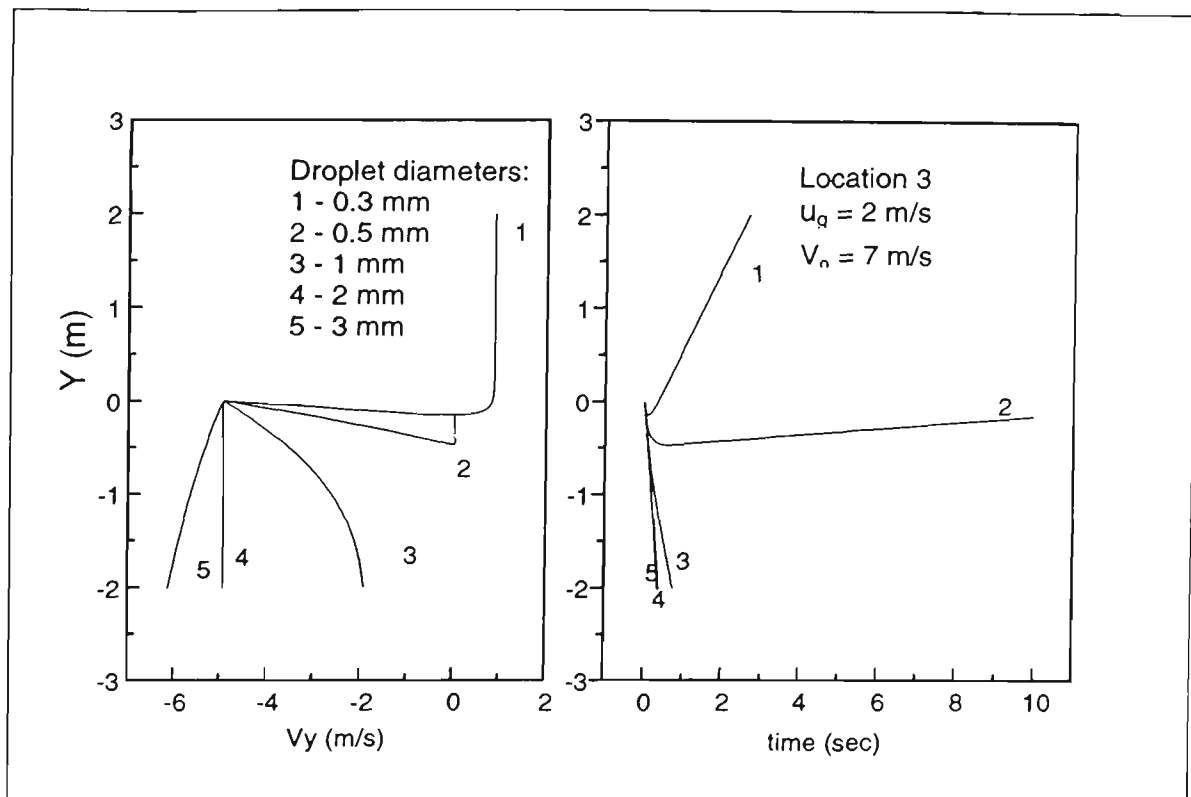


Figure 3.7. Droplet vertical trajectories as a function of vertical velocities (a) and time (b) in the uniform updraft gas velocity of 2m/s. The droplet diameters are as listed. Location 3 is chosen as the most critical case. Initial conditions for droplets are the same as in Figure 3.6.

3.3.3 Effect of gas velocity profiles: modelling fire induced gas flow

In terms of *gas velocity distribution*, a real fire environment can be represented either by CFD models (with turbulence and velocity field modelling, and with or without combustion), or by zone models. Zone modelling is based on fundamental equations (continuity and energy conservation), and it describes the main zones of the fire environment by semi-empirical formulas [58]. In order to investigate the sensitivity of droplet dynamics to gas velocity distribution, a zone modelling approach has been adopted here. The following relationships proposed by Heskestad [88], for a plume rising above a fire source are used in the present study to describe the mean excess temperature and corresponding mean velocity at the centerline of the plume:

$$b_{\Delta T} = 0.12(T_0/T_\infty)^{1/2}(z-z_0) \quad (3.7)$$

$$\Delta T_0 = 9.1[T_\infty/(gc_p^2\rho^2_\infty)]^{1/3}Q_c^{2/3}(z-z_0)^{-5/3} \approx 25 Q_c^{2/3}(z-z_0)^{-5/3} \quad (3.8)$$

$$u_0 = [3.4[g/(c_p^2\rho^2_\infty)]^{1/3}Q_c^{1/3}(z-z_0)^{-1/3}] \approx 1.03 Q_c^{1/3}(z-z_0)^{-1/3} \quad (3.9)$$

where ΔT_o and T_∞ are the mean temperature rise above the ambient at the centerline of the plume (K) and the ambient temperature (K); respectively; u_o is the mean gas velocity at the centerline of the plume (m/s); $b_{\Delta T}$ is the plume radius to the point where the temperature rise has fallen to half of the centerline temperature rise (m); Q_c is the convective heat release rate of the fire (kW); z is the elevation above the fire source (m); z_0 is the elevation of the virtual origin above the source (m); g is the gravitational acceleration (m/s²); c_p and ρ_∞ are the specific heat capacity (J/kgK) and density (kg/m³) of ambient air, respectively.

For pool fires, the virtual origin can be determined from the following expression ([58, Ch.4]):

$$z_o = -1.02D + 0.083Q^{2/3} \quad (3.10)$$

where Q is the total heat release rate (HRR) of the fire (kW), and D is the initial diameter of a circular fire source (m), equal to $\sqrt{(4A)/\pi}$. A is the burning area (m²), which can be calculated as the ratio of a given total heat release rate to a nominal fire load density (kW/m²), such as 250kW/m² for office fires [89]. In the present calculations, the convective heat release rate is taken as 70% of total heat release [58, 90].

In the flame zone, not considered in the present dynamic calculations, the temperature is usually considered to be uniform (1100-1700°C), and velocity increases as the square of height, z , above (or below) the fire source [90]. The flame length, L , can be estimated by the following simplified equation of Heskestad [88]:

$$L = -1.02D + 0.23Q_c^{2/5} \quad (3.11)$$

A summary of the different expressions is available to estimate the virtual origin, flame length and plume centerline temperatures and velocities [90]. As stated in [90], the temperature and velocity radial profiles were originally considered as "top hat" profiles (uniform profiles in the present study). This was modified into a Gaussian distribution by

Zukoski *et al* [90] without any theoretical background, using only experimental observation, resulting in the following expressions:

$$\Delta T = \Delta T_0 e^{-(r/\sigma_{\Delta T})^2} \quad (3.12a)$$

$$u = u_0 e^{-(r/\sigma_u)^2} \quad (3.12b)$$

where ΔT_0 and u_0 are given by Equations (3.8) and (3.9), respectively, $\sigma_{\Delta T}$ and σ_u correspond to the radii where local values of temperature rise and velocity are $e^{-1} = 0.368$ times the centerline values. For Gaussian profiles, these values are as follows [88]:

$$\sigma_{\Delta T} = 1.201 b_{\Delta T} \quad \text{and} \quad \sigma_u / \sigma_{\Delta T} = 1.1.$$

The effect of gas velocity profiles on droplet trajectories and residence times are shown in Figure 3.8 and Figure 3.9. In Figure 3.8, six trajectories of 0.7mm diameter droplets are compared in 0.2 and 0.5 MW Gaussian fire plumes and in a uniform gas velocity of 3.5m/s at Location 3. As shown in Figure 3.8, in the case of Gaussian gas velocity distribution, only the central part of the sprinkler discharge (from 0° to 68°) will reach the floor, while the periphery is diverted. The uniform upward velocity of 3.5 m/s ‘blows away’ the whole discharge. In comparison with the 0.7mm droplet trajectories in a 2m/s upward gas flow, given in Figure 3.2 (f), the behaviour in 3.5m/s gas velocity is quite different. These results relate to the problem of spray penetration described previously. Spray penetration depends on both droplet diameter and gas velocity vector (magnitude and direction). The residence times for the cases shown in Figure 3.8, are plotted in Figure 3.9. Times were recorded at 2m of vertical distance, or, if droplets are diverted, when they strike the ceiling (at the level of sprinkler head). As seen from Figure 3.8, the spray has zero penetration to the fire base in 3.5 m/s updraft gas flow velocity. On the other hand, as indicated in Figure 3.9, the sprays above 0.2 and 0.5 MW fires of Gaussian velocity distribution and 3.5m/s uniform gas velocity distribution have similar trend and values of residence times for large discharge angles. Thus, if the fire plume is represented by a uniform upward velocity, attention should be paid to the magnitude of this velocity. If the same gas cooling effect

needs to be achieved, then the droplets have to have approximately the same residence times. If penetration is important in modelling, then gas velocity should not exceed the ‘fluidization’ level for the given mean droplet diameter.

For horizontal gas flow, for a given distance from the fire, gas velocity and temperature distributions across the layer in a burn room are close to uniform, according to experimental data available in the literature [91, 92a]. However, to allow a sensitivity study of droplet dynamics to gas velocity distribution, two types of horizontal gas velocity profiles were adopted here. The first is a uniform profile, characterized by one velocity value, as used in the previous calculations to characterize Location 1 (e.g. Figure 3.2a, and Figure 3.2d). The other is a ‘triangular’ or linear gas velocity distribution across the layer with a neutral plane (zero velocity) located at the bottom of the layer.

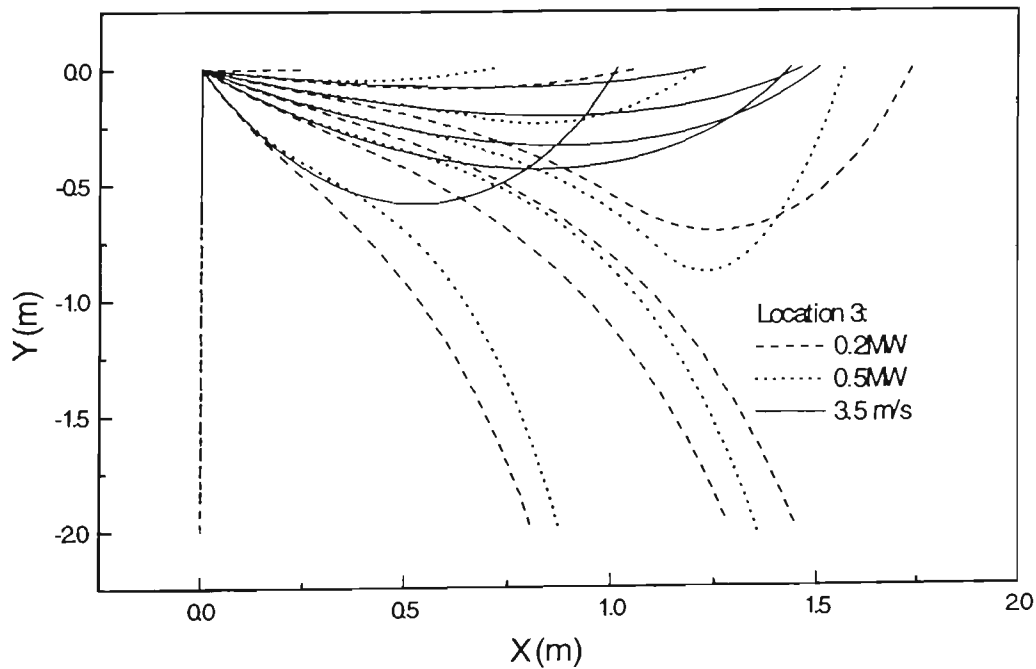


Figure 3.8. Trajectories of 0.7mm droplets in fire plumes modelled by Gaussian and uniform gas velocity distributions. The Gaussian distribution is for 0.2 and 0.5MW fires. The uniform distribution is modelled by 3.5m/s gas velocity.

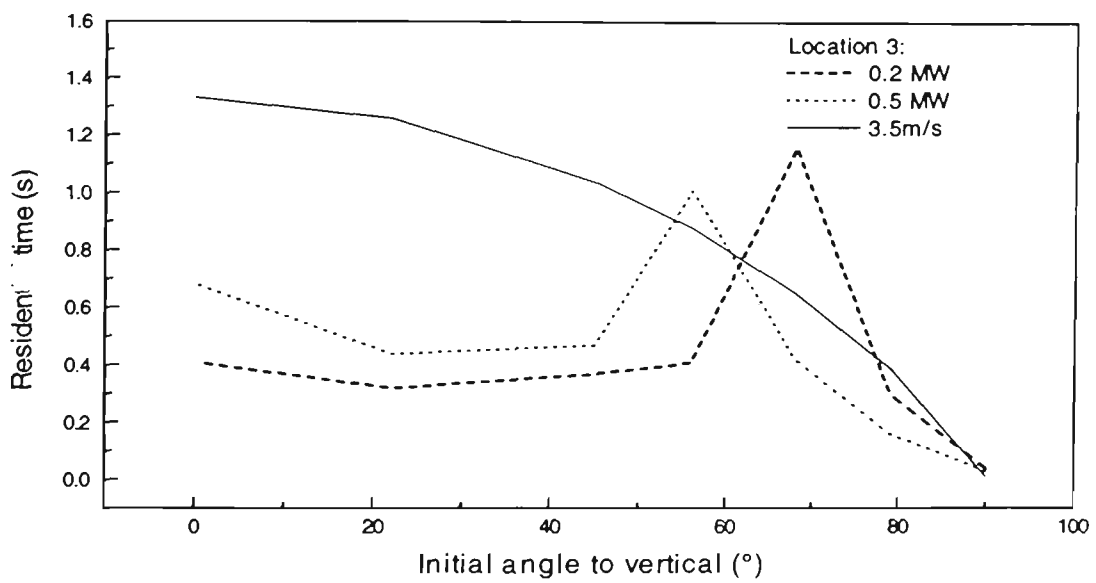


Figure 3.9. Residence times as a function of initial discharge angle for the same conditions as those given in Figure 3.8.

This type of distribution is available, for example, in the room of fire origin with an ‘open door’ scenario. There are two flows in such a compartment: the inflow of fresh air that entrains into the fire plume through the bottom part of the door and outflow of hot gas at the upper part of the door [92b]. Such triangular velocity profile can also exist in the corridor [92a]. The following equation is used to describe the ‘triangular’ profile in this study:

$$u = u_m(D-y)/D \quad (3.13)$$

where u is the horizontal gas velocity at a specified vertical distance from the ceiling, y ; D is the hot layer depth; u_m is the maximum velocity value. Ceiling jet is not considered in this study, and the maximum value is taken just below the ceiling.

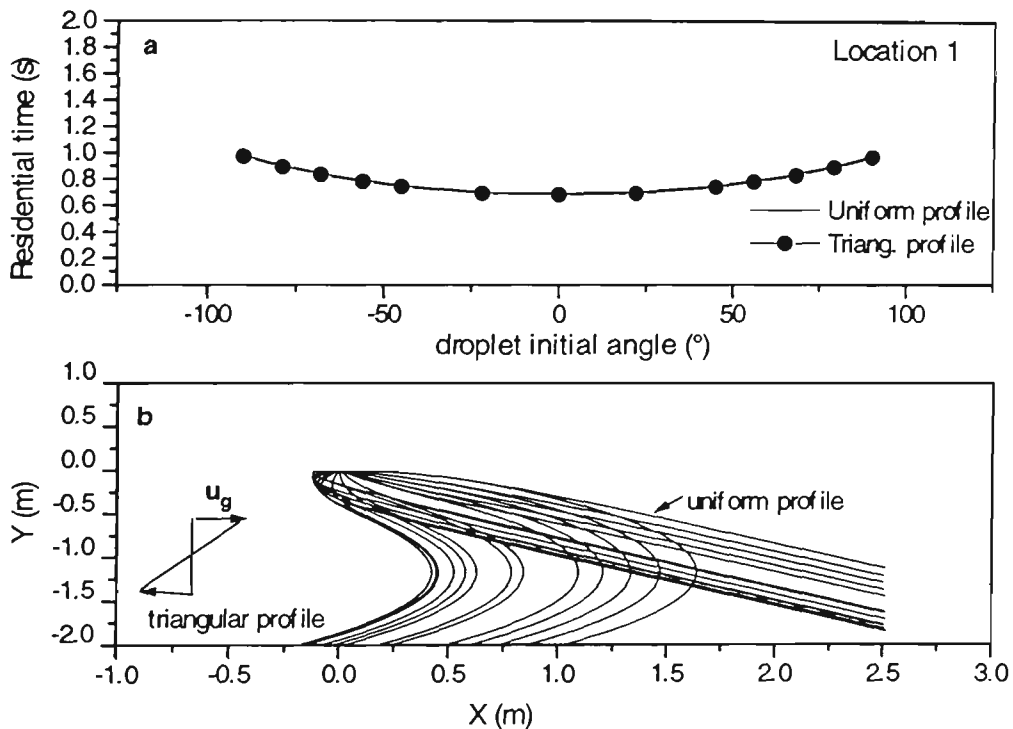


Figure 3.10. Residence times of 0.3mm droplets in uniform and triangular gas velocity profiles (a), and trajectories of 0.3mm droplets in uniform and triangular gas velocity profiles (b). The triangular profile has its minimum, i.e. the zero gas velocity, at $Y=-1.0\text{m}$ from the ceiling, that is the bottom of the hot layer. The maxima are at the ceiling, $Y=0\text{m}$, and at $Y=-2\text{m}$ (entraining flow).

A comparative analysis of trajectories under different gas velocity profiles at Location 1 is given in Figure 3.10 for the 0.3mm droplets. In Figure 3.10a, a comparison of residence times is given of 0.3mm droplets as calculated with the uniform and triangular gas velocity distributions. In Figure 3.10b, 13 trajectories of 0.3 mm droplets discharged under different initial angles are shown in the same uniform and triangular gas velocity profiles as in Figure 3.10a. The results indicate that even though the trajectories depend on velocity distributions, the residence times are unaffected by them for the selected magnitude of maximum gas velocity of 2m/s. This magnitude is considered reasonable for most pre-flashover compartment fires [41]. Accordingly, if droplets of 0.3 mm or larger diameter are discharged far away from the fire, the horizontal gas velocity can be represented by a uniform gas velocity profile for the purpose of heat transfer calculations. From Figure

3.10b, it can also be concluded that in a fire environment, circulation of the small droplets of 0.3 mm or less, is also possible. The droplets can turn with entraining air, and they can be sucked in by the plume.

3.3.4 Comparison with data available in the literature

One of the problems in comparing model spray dynamics with experimental evidence is the lack of input data, such as initial velocities and angle distribution within the spray. There is a limited number of papers with experimental information on dynamic spray characteristics, such as droplet trajectories, velocity distributions or residence times. Most of the available information relates to the terminal values of either velocities or trajectories, usually without initial conditions. In the absence of such experimental data, a comparison has been made between the present predictions and the values given by Nam [46] of average actual delivered densities (ADD) and water flux distributions for sprinklers with and without fire. Both the experimental and CFD (computational fluid dynamics) results of [46] have been used to validate the droplet dynamics treatment by the present droplet sub-model.

The experimental and computational ADD results taken from [46] correspond to two areas located at 2.69 m below the sprinkler head. The two areas, Area 1 and Area 2, are 1.486 m^2 and 5.226 m^2 , respectively, around the spray centerline. The results are for two ESFR (early suppression fast response) sprinklers produced by different manufacturers, referred as ESFR-A and EFSR-B. The volumetric mean droplet diameter is given as $2.65 \times 10^{-3} G_w^{-2/3}$ and $2.268 \times 10^{-3} G_w^{-2/3}$, respectively for ESFR-A and ESFR-B sprinklers. In these two expressions, the water flow rate, G_w , is in litres per second, and the resulting mean droplet diameter is in meters. In Nam's CFD predictions, discharge angles are determined as follows:

$$\theta_j = \theta_i + (\theta_o - \theta_i)[(j-1)/(n-1)]^p \quad (3.14)$$

where θ_j , θ_i and θ_o correspond to the j^{th} , innermost (3°) and outermost (90°) discharge angles, respectively. The total number of discharge angles, n , is kept as 25, and p is an exponent which determines the degree of non-uniformity of the distribution. Ten droplet diameters, from $0.5d_{\text{pmean}}$ to $2d_{\text{pmean}}$, where d_{pmean} is the volumetric mean diameter, are assigned to each discharge angle, resulting in 250 trajectories. For 1.88, 3.15, 4.42 and 6.23

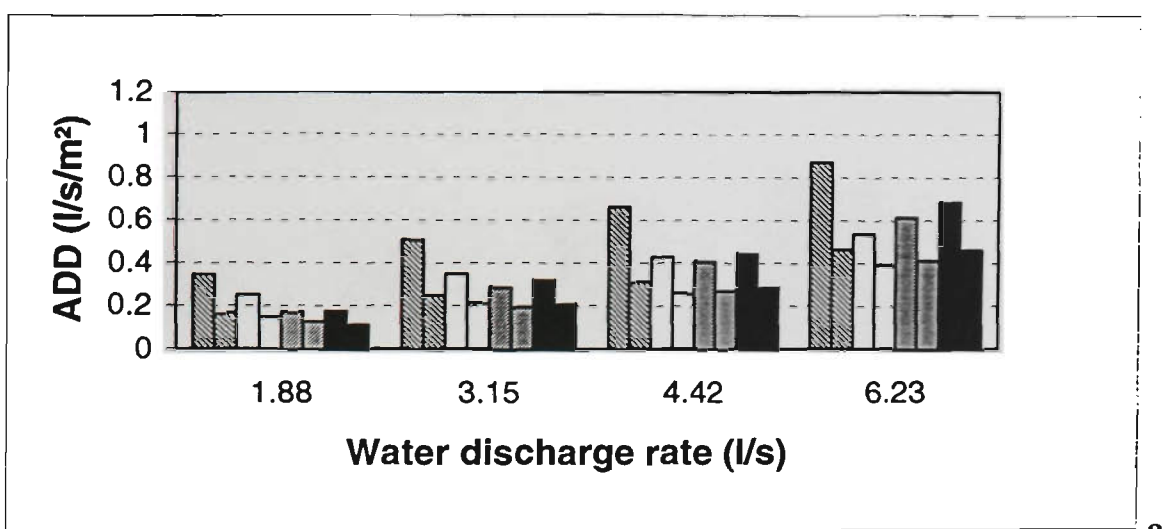
l/s, respectively, the values of d_{pmean} were, 1.74 mm, 1.237 mm, 0.987 mm and 0.785 mm for the ESFR-A sprinkler, and 1.49 mm, 1.05 mm, 0.842 mm and 0.669 mm for the ESFR-B sprinkler. In addition, to account for the effect of a central jet, 25 large droplets were discharged at the spray centerline. In the present calculations, Nam's droplet diameter and discharge angle distributions were used. For the cases with a central jet, each droplet diameter and the central jet constituted $1/11^{\text{th}}$ of the total water mass. The central jet was kept within 3° . For the cases without a central jet, each droplet diameter corresponded to $1/10^{\text{th}}$ of the total mass.

In Figure 3.11, the present predictions with $p = 1.25$ in Equation (3.14) are compared with Nam's numerical and experimental ADD results for water discharge rates of 1.88, 3.15, 4.42 and 6.23 l/s to determine the effect of the central jet in the calculations. For each volume flow rate, four pairs of columns are given corresponding to the present predictions with and without a central jet and Nam's experimental and computational results. The first column of each pair corresponds to Area 1, and the second column is for Area 2. Figures 3.11a and 3.11b are for EFSR-A and ESFR-B sprinklers, respectively. This figure indicates that the central jet becomes effective at higher volume flow rates for Area 1. For Area 2, the difference in ADD calculations with and without jet is almost negligible. At lower volume flow rates, the present results without a jet are similar to Nam's experimental and numerical results. At the highest two volume flow rates, the present prediction of ADD compares well with the experimental values of ESFR-A without a central jet and of ESFR-B if a central jet is modelled. This difference is attributed to the different droplet diameter distributions of the two sprinklers. ESFR-A has in general larger droplets than ESFR-B. Hence, ESFR-B is more conducive to modelling with a jet due to the possible coalescence of droplets close to the spray centerline. These results point out to the importance of the correct modelling of the central jet in predicting ADD with ESFR sprinklers.

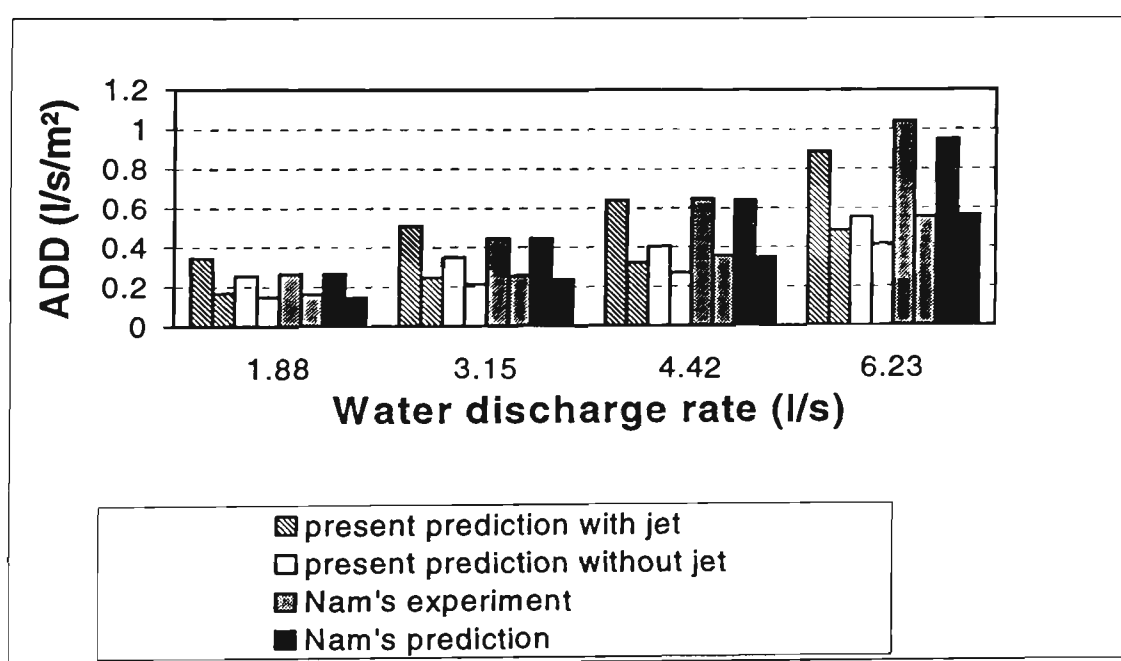
In Figure 3.12, the effect on the predicted ADD of different discharge angle distributions is examined. In Equation (3.14) above, $p = 1.25$ and $p = 0.75$ are used to represent uneven distributions, and $p = 1$ corresponds to a uniform distribution. In addition, a comparison is made between the use of a droplet diameter distribution and a constant volumetric mean

droplet diameter to represent the whole spray for $p = 1$. A central jet has not been included in these calculations due to the modelling uncertainty, as demonstrated in Figure 3.11. Figure 3.12 indicates that for all four volume flow rates used in the calculations, the type of discharge angle distribution has negligible effect on ADD. The droplet distribution can be replaced by one mean droplet diameter for ADD calculations for volume flow rates of 4.42 l/s or less. As the volume flow rate approaches the highest value used here, 6.23 l/s, the calculations with a mean droplet diameter underestimate ADD.

In Figure 3.13, the present predictions of water flux as a function of radial distance from the spray centerline are compared with the experimental data of Chan [86] as reported in [46]. Water flux is calculated for the ESFR-A sprinkler for 4.42 l/s and 6.23 l/s. A central jet is not modelled. The present numerical results are given by the solid and dashed lines in Figure 3.13, corresponding to Nam's droplet diameter distribution and one mean droplet diameter, respectively. The symbols correspond to Chan's experimental data [86]. As seen in this figure, the present numerical results are in agreement with Chan's experimental results.

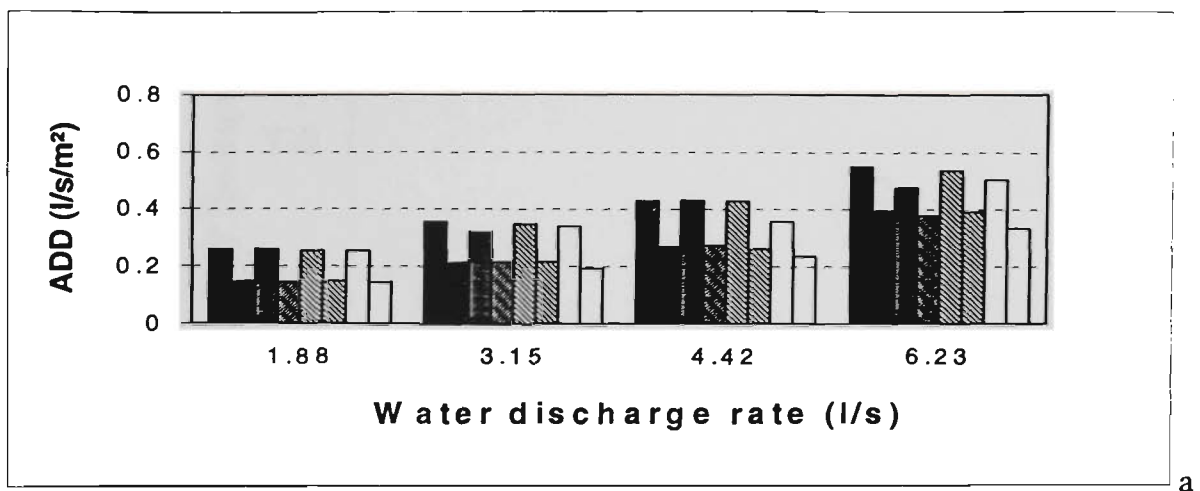


a

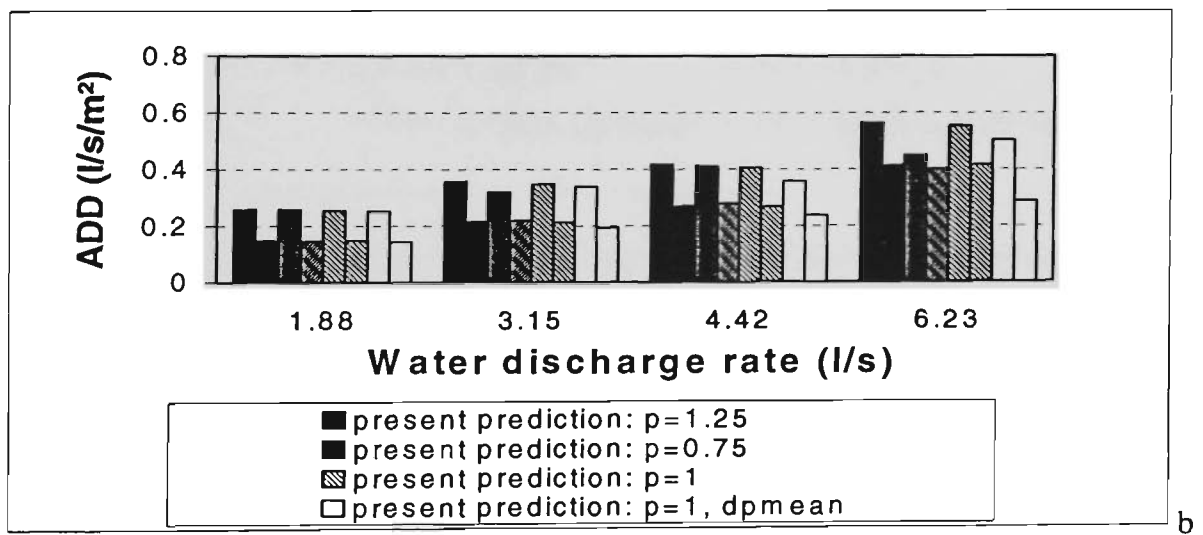


b

Figure 3.11. Actual Delivered Density in the 1st area (ADD1) and 2nd area (ADD2). Comparison between prediction and experiments: a (ESFR-A sprinkler) and b (ESFR-B sprinkler). 1st column – ADD1; 2nd column – ADD2.



a



b

Figure 3.12. Actual Delivered Density in the 1st area (ADD1) and 2nd area (ADD2). Comparison between ADD in terms of spray representation by different angle and diameter distributions. Angle distribution modelled by power law (p is a power value). Diameter distribution either corresponds to Nam's distribution or given by one mean droplet diameter. a (ESFR-A sprinkler) and b (ESFR-B sprinkler). 1st column – ADD1; 2nd column – ADD2

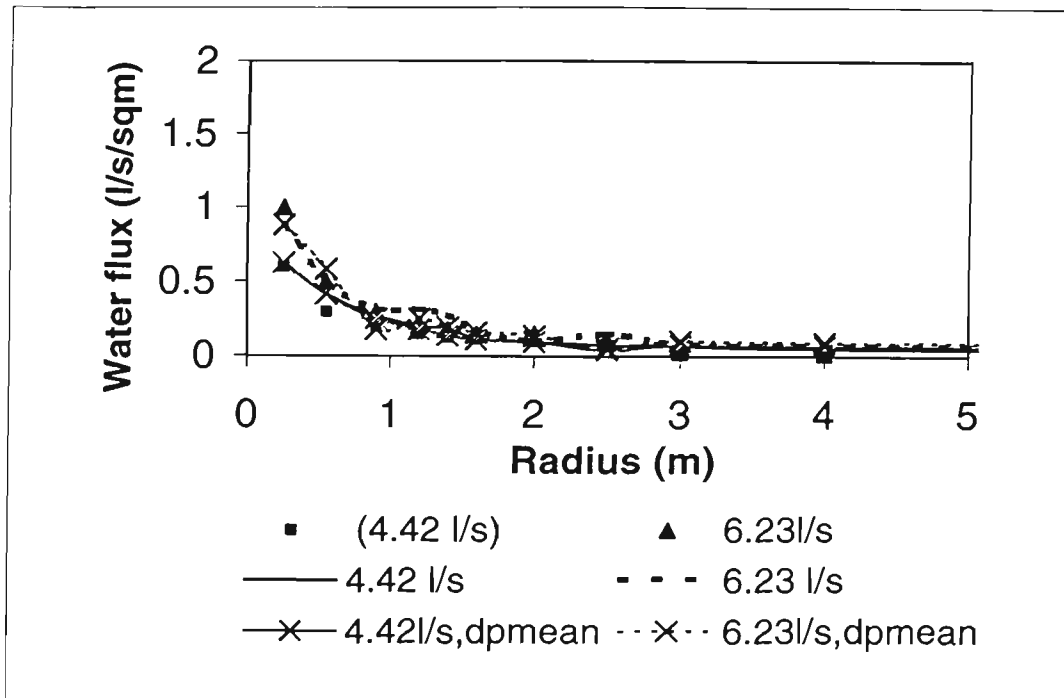


Figure 3.13. Comparison of the water flux distribution obtained from the present model with the experimental data of Chan [86] given in [46]. Two different water flow rates are used in the calculations, as indicated. Chan's experimental data for two ESFR-A sprinklers are given by symbols. Calculations correspond to droplet distribution (lines with symbols) and mean droplet diameter (single lines), both discharged at 25 initial angles. Sprinkler height = 2.69m from the floor.

3.4 NUMERICAL EVALUATION OF THE EFFECT OF MOMENTUM COUPLING BETWEEN WATER SPRAY AND GAS FLOW

Based on the Stokes number ranges as listed following Equation (3.3), there may be interaction between droplets and turbulent gas flow in the discussed range of droplet diameters. However, in zone modelling, turbulence and gas flow field are not modeled explicitly. Hence, the momentum coupling between spray and gas flow is only “one way”: droplet trajectories are affected by gas velocity vectors, while possible changes in gas velocity due to droplet injection are not taken into account. In order to understand the effect of two-way couplings between gas flow and droplets, CFD simulations have been utilised here. Two-dimensional steady planar gas flow has been studied with and without liquid spray injection in terms of a Lagrangian-Eulerian formulation. All simulations have been done using a commercial CFD package, CFX-F3D, Version 4.1 [93].

3.4.1 Channel flow

A long (8mx0.5m) plane symmetrical horizontal channel has been used to simulate a gas flow. This case has been chosen as a well-studied with results widely available in the literature for comparison and similar worked examples available in CFDX-F3D Examples Manual [93]. To solve the problem in CFX-F3D, user needs to read a *command file* from the suitable reference example (say, “Introductory Example 4: Turbulent flow”) to user’s own directory and then modify the geometry, boundary conditions and model variables appropriately. The certain changes can be easily made under certain commands, subcommands and key words given in a *command file* and explained in details in User Manual [93]. After the CFX has been run with new command file and geometry, the output can be examined using CFX-F3D post-processing facilities, such as CFX-Visualise window (to view so-called dump files), or can be accessed through the output files containing a log of simulations, i.e. all the information stored in text or numerical form.

The fluid flow is treated as steady isothermal with default reference temperature (293.15K) air flow with mass flow boundary conditions applied at the inlet and exit to ensure a constant mass flow rate. Because it is a low speed flow, the default status of weakly compressible (practically incompressible [93]) flow was used. The flow profile at the inlet is assumed to be flat with bulk velocity of 2m/s. As recommended in [93], the two dimensional problem is treated as three dimensional with single internal plane in the Z direction.

The flow is turbulent and the default turbulence model, which is the standard k- ϵ model, is used. The wall boundary conditions are set as the default non-slip with zero turbulent kinetic energy k. Since variables change rapidly near the wall, a non-uniform grid is used with a finer mesh in this region. The results of grid refinement, plotted in terms of U (horizontal, X direction) and V (vertical, Y direction) velocity profiles calculated across the channel at different distances from the inlet, are presented in Appendix B. For flow calculations without a sprinkler, a 78x42x1 grid was chosen, after calculations showed that a finer grid,

$78 \times 84 \times 1$ led to negligible variations. Based on the results, it was concluded that the CFD code successfully predicts the developed turbulent gas flow in a channel.

3.4.2 Two-phase flow: gas and water droplets interaction.

A water spray is injected by one nozzle located in the middle of the channel upper wall at 4 m from the inlet perpendicularly to the gas flow. The spray is represented by spherical droplets of a uniform diameter distribution and by 13 injection angles similar to the calculations presented earlier in this chapter. The simulation involves calculation of trajectories and velocities of dispersed droplets and two-way coupling through the source terms between the dispersed and continuous phases [93, Ch. 12]. With 13 trajectories, the whole 2π -discharge angle is divided into twelve sectors of 15° each. The droplet diameter was either 0.3 or 0.7 mm. Spray total mass flow rate was 1.84 kg/s.

The momentum transfer between the phases is equal to the change in the momentum of droplets passing through each control volume:

$$F = N(3/4\pi p_p d_p^2) C_d \rho |V_R| (V_R) m_p \Delta t \quad (3.16)$$

where N is the total number of particles of given diameter; V_R is a vector of droplet relative velocity equal to $V_p - V$; d is the particle diameter, ρ is the density, C_d is the droplet drag coefficient which is a function of Reynolds number [93] similar to the function used in present calculations; m_p is the mass flow rate of the dispersed phase; Δt is the integration time step. The variables with index “ p ” relate to particles, with no index to the continuous phase. The particle Reynolds number is defined as $Re = \rho |V_R| d / \mu$. The momentum transfer from the particles leads to a source (sink) of momentum for the continuous phase. Convergence is considered to be achieved when the values for residuals of the conservation equation for the gas phase becomes smaller than 10^{-6} , while the residuals for the other variables (enthalpy and velocities) are calculated accordingly. An average of 300 iterations was needed to achieve convergence.

The results of simulations of this spray-air flow system are shown in Figure 3.14. In this figure, the V-velocity distributions along the channel at 0.25m from the inlet port are given for 0.3 and 0.7 mm droplets. For grid-independence simulations for 78x42 and 78x84 grids, are also presented in the Figure 3.14 a and b. Gas flow velocity is found to be slightly affected by the droplets in the centre, in vicinity of sprinkler cone. The gas is “pushed-down” by spray. The smaller the droplets, the larger the effect. This effect is similar to hot layer lowering during sprinkler activation since it has a similar trend towards droplet diameters (as discussed in Chapter 4).

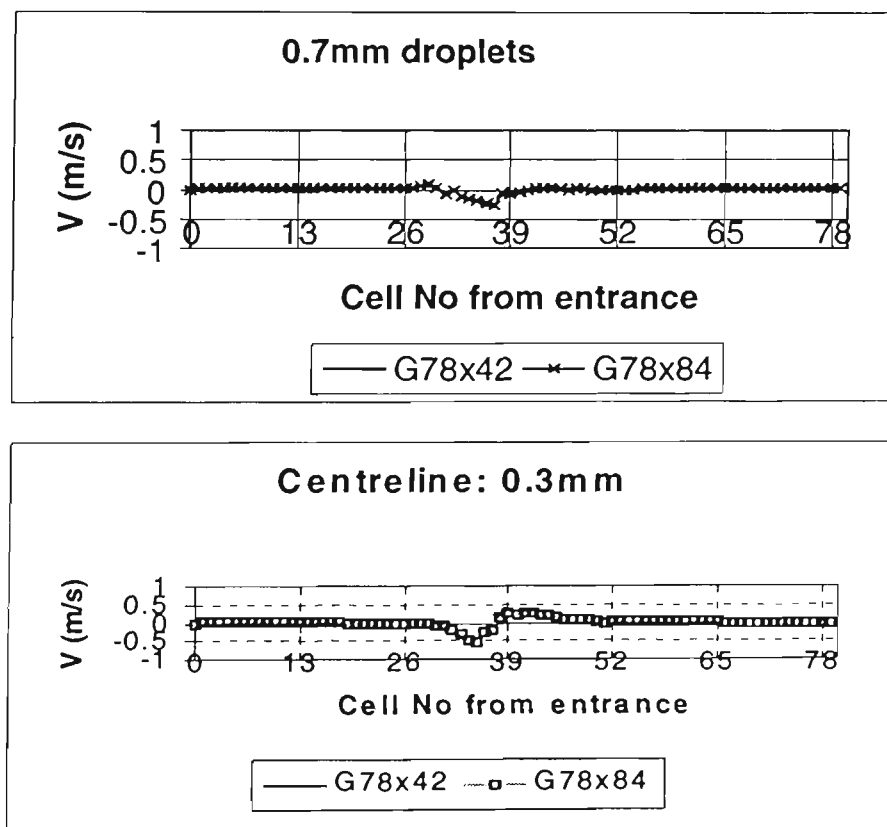


Figure 3.14. The effect of the sprinkler spray on V-velocity distribution at the channel centreline, $y = 0.25\text{ m}$, along the channel length. The spray nozzle is located in the middle of the channel ceiling ($x = 4\text{ m}$ and $y = 0.5\text{ m}$). The grid independence is also demonstrated. (a) droplet diameter 0.7 mm; (b) droplet diameter 0.3mm.

The vector plot of gas velocity field with spray injection is shown in Figure 3.15 and Figure 3.16, reflecting the trajectories and gas velocity vector field in the presence of 0.3 and 0.7 mm sprays.

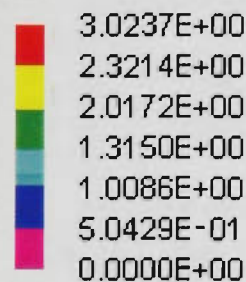
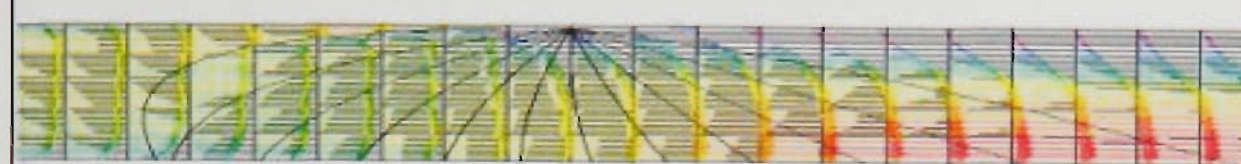


Figure 3.15. Droplet trajectories for a mono-disperse spray of droplet diameter 0.7 mm injected downward from the centre of the upper wall. The gas velocity vectors as indicated.

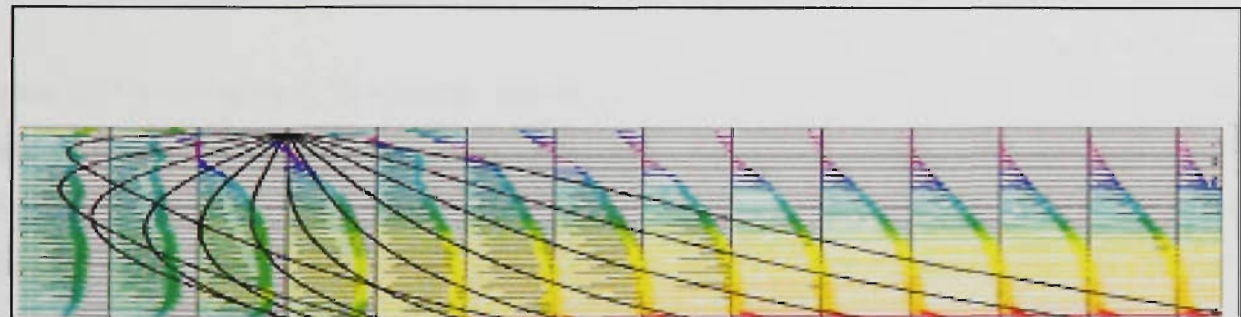


Figure 3.16. Droplet trajectories for a mono-disperse spray of droplet diameter 0.3 mm injected downward from the centre of the upper wall. The gas velocity vectors as indicated.

The comparison between the droplet trajectories obtained through the simple zone modelling approach, presented earlier in this Chapter and those from the CFD results has been done in terms of droplet residence times. The results of this comparison are shown in Figure 3.17 for 0.3 and 0.7 mm sprays for all discharge angles.

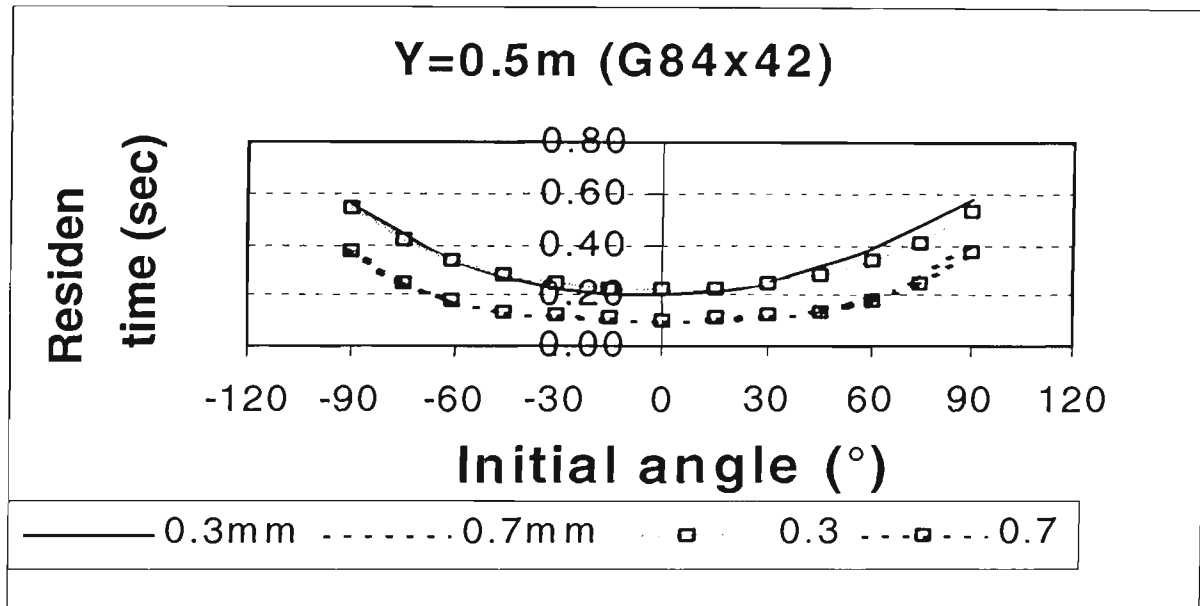


Figure 3.17. Residence time comparison between CFX predictions and those of the present sub-model. Solid and dashed lines, CFX predictions for 0.3 and 0.7 mm droplets, respectively. \square , 0.3-mm and \diamond , 0.7mm droplet residence times, respectively, as predicted with the present sub-model.

Figure 3.15 and Figure 3.16, indicate that the presence of droplets does affect the initial gas velocity field. The trajectories are also affected by gas velocity, but only at the first coupling. There is no “four-way” coupling (a term used in [63] for dense sprays), and the changed under droplet influence gas flow field does not change back the droplet trajectories. Thus, in terms of droplet residence times which, as shown in Chapter 4, is a key factor in heat transfer and spray effectiveness, “one- way” coupling is acceptable instead of “two-way” coupling in zone modelling.

In the obtained results, there is no evidence of the gas turbulence affecting the liquid flow. This result is well aligned with the explanation given in [63]. In a forced gas flow, its mass flux and mean kinetic energy, usually substantially exceed the kinetic energy

of the dilute liquid sprays, as well as of those of the turbulent field. Therefore, the spray flow is much more likely to receive its kinetic energy from the mean gas flow, than from the turbulent field. Also, the turbulent field is also much more likely to be affected by the mean gas flow, than by the droplet flow².

3.5 CONCLUSIONS

Two-dimensional droplet movement in gas flow under different initial conditions has been simulated. The fourth order numerical Runge-Kutta integration scheme was used to solve the system of ordinary differential equations of droplet motion under gravity and drag forces to obtain droplet velocities and trajectories in gas flow. The effects of input parameters, such as droplet diameters, initial angles, gas velocity distribution, direction and magnitude, are investigated. The features of real fire-sprinklers and fire environment are assigned to droplet and gas initial parameters, respectively. Consequently, the sprinkler spray droplet dynamics is studied using a zone-type fire environment description. The conclusions of this study can be summarised as follows:

- 1 Droplet residence times are found to be highly sensitive to droplet diameter and initial angles, especially in vertical (counter) gas flow, at Location 3. At this location, the residence times of 0.3 mm diameter fine droplets can be an order of magnitude different than the residence times of 0.7 mm diameter coarse droplets. At a given location, for one droplet diameter, the residence time can vary by approximately a factor of three depending on the initial discharge angle.
- 2 It is possible to represent fire induced gas flows by uniform gas velocity profiles, provided that an equivalent to non-uniform case droplet residence time is used
- 3 A limiting droplet diameter exists at Location 3, i.e. valid if the counter-flow is established. The spray penetration ability through a fire plume depends on whether the spray mean droplet diameter exceeds this limiting value. The magnitude of limiting diameter depends on the relative gas-droplet velocity: the limiting diameter

² During fire in domestic size room (20m^3), the usual mass flow rate of gases is about 30 kg/s , while nominal sprinkler flow rate is 1kg/s .

-
- corresponds to the case when droplet terminal velocity close to gas velocity, i.e. relative velocity close to zero
- 4 The present results and their comparison with experimental and numerical works have revealed the importance of realistic spray representation in terms of droplet diameter distribution, range of initial angles and central jet. However, one mean droplet diameter, derived from a realistic droplet distribution, can be used in place of the distribution to represent the whole spray in terms of the total created by droplets interface. This conclusions is valid for volume flow rates of 4 l/s or less for residential or ESFR type sprinklers.
 - 5 The CFD calculations are compared with the present zone model approach in terms of droplet trajectories in a gas flow. This comparison revealed that “two-way” momentum coupling exists between spray and gas flow. However, for the range of gas velocities, spray flow rates, and diameters used here, one way coupling is sufficient in determining the droplet trajectories and residence times.

4 DROPLET HEAT TRANSFER: GAS COOLING

4.1 INTRODUCTION

It is believed that the most important mechanism by which water sprays act to suppress a fire is heat extraction from the fire compartment [94]. Other mechanisms in fire-sprinkler interaction are oxygen displacement by steam, direct impingement, wetting and cooling of the combustibles. In a number of cases reported in the literature, fire suppression or extinguishment has been under-predicted, i.e. the computed time of suppression is much shorter than that achieved experimentally, (Hadjisophocleous *et al.*, [87]). There are also cases where sprinklers have been unable to suppress fires, even though they complied with the sprinkler performance requirements³. The unsuccessful use of steam for fire protection on marine vessels at the beginning of the century was also reported [57]. All these cases indicate that there is no uniform answer yet on how sprinklers act in different situations, and how the different mechanisms of suppression contribute to the overall result. However, the main factors that affect fire-sprinkler interaction are known [19, 48] as the following: the discharge rate of water, mean droplet diameter, fire size (or room temperature) at the moment of sprinkler activation, relative location of the sprinkler and fuel and ventilation conditions. The present study is an attempt to explain how and why these factors act, and how sensitive the total cooling is to each of these factors.

4.2 BASIC EQUATIONS

In most cases of compartment fires, the water is sprayed and delivered to the fire zone either by sprinklers, or by mist nozzles. This division is usually due to different type of fuel available in a room and, consequently, environmental conditions set up by the possible fires. While basic equations of heat and mass transfer for either type of spray are similar, the results are different due to different external conditions and spray properties. Thus, there are two main sections in this chapter, following section 4.2, Basic Equations: In Section 4.3, heat transfer from a moving hot gas layer to a sprinkler spray is examined, for

droplet diameters of 0.3 to 2mm and gas temperatures less than 200°C. In Section 4.4, heat absorption capacity of mist sprays is examined, covering droplet diameters of 0.2 to 0.5mm within gas temperatures 600°-1200°C. Hence, Section 4.3 deals mostly with standard sprinklers, or Class 3 mist sprays, and Section 4.4 covers Class 2 mist sprays, as defined in Chapter 1. These two classes of sprays were chosen due to their common usage.

4.2.1 The model of droplet-gas flow

In the present study, a preliminary mathematical model of droplet dynamics and heat transfer has been developed to investigate the transport processes in gas flows typical for fire environment. The thermal performance of spray in cooling hot gas flow has been calculated as a function of operating conditions and dimensions.

The general concept of calculation of gas-droplet coupling can be described by the Crowe *et al's* [59] model of gas-droplet flow. In this model droplets are treated as sources of mass, momentum and energy to the gaseous phase. This model is known as the particle-source in-cell (PSI-Cell) model and can be illustrated by Crowe *et al's* [59] computational scheme given in Figure 4-1..

The concept of solution of droplet-gas flow equations illustrated by Figure 4.1 can be described as follows:

1. The calculation starts by solving gas flow equations assuming no droplets are present
2. Using the obtained gas flow characteristics (temperatures and velocities), the droplet trajectories, size and temperature histories are calculated
3. The mass, momentum and energy sources for each cell are determined
4. The flow equations are solved again using source terms and accounting for the effect of the droplets on the gas
5. The new gas flow field is used to re-calculate droplet trajectories and temperatures, producing new source terms and accounting for the effect of the gas on the droplets

³ One of such cases was an experimental fire in a toy warehouse. The warehouse was equipped with sprinklers according to the standards. The video with this fire is available in Standard Services Laboratory (SSL), Melbourne.

6. Repeat steps 2, 3, 4 and 5 until gas characteristics converge.

The computational process usually takes several iterations to converge. The cycle in which the mutual interaction between droplets and gas is accounted for, is called “two-way” coupling in [59]. In the present work, the momentum coupling is accounted for only in one-way fashion, e.g. dynamics and thermodynamics (heat and mass transfer) are uncoupled. Droplet trajectories are calculated, once under initial gas flow conditions and the calculated time of the droplet to traverse through the computational cell (residence time) is then used to account for total number of droplets permanently available in the control volume.

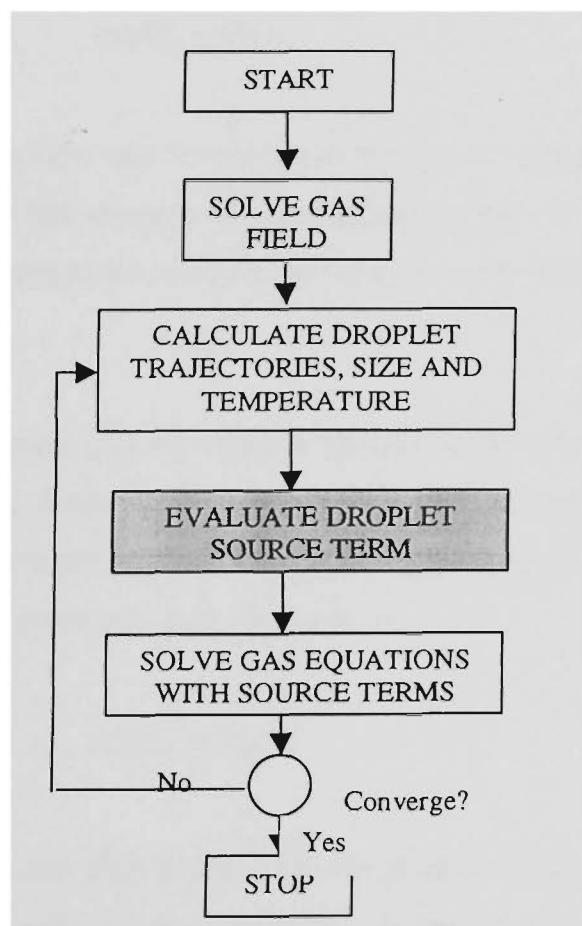


Figure 4-1. Flow chart of gas-droplet flow computational scheme (reproduced from [59]).

In PSI-Cell model, the number and consequently, the size of the computational cells may vary significantly depending on a gas model in use: from thousands of small cells (CFD) to one or two zones (zone models). Each zone (layer) can be subdivided into several sub-

layers. The sources from numerous droplets can also be considered as one source term from one large droplet (“superdrop” or “meandrop” in Kumar *et al*’s terminology [95]) of the same surface area as the group of droplets, having an evaporation and heat absorption rates as the sum of the rates of all droplets in a group. The number of these “superdrops” can vary from one to few in different approaches and will be discussed further in this chapter.

In the light of the “superdrop” approach, the total mass flow rate of all individual droplets, M_d , is discretised into weighted finite number of flow rates determined by the number of droplet size groups:

$$m_d(d_i) = M_d f_i \quad (4.1a)$$

where $m_d(d_i)$ is the mass flow and f_i is the mass fraction of droplets with *initial diameter* d_i in the total discharge. While droplets are moving across the control volume, their size and mass flow rate are assumed to be constant, equal to the inlet values. Droplets do not collide or shatter.

In the general case, droplets can be injected (or ejected) in (or from) more than one port. Thus, another weighting factor f_j , is suggested [59] to account for the mass fraction of droplets originating from a port j . In this case, the mass flow of droplets, $m_{dj}(d_i)$ of size d_i which enters the control volume at port j is given by:

$$m_{dj}(d_i) = M_d f_i f_j \quad (4.1b)$$

The weighting factor, f_j , can also account for the number of spray emission sectors if the spray cone is sub-divided into sectors [95]. The weighting has to be adjusted to give the pre-specified total sprinkler flow rate, M_d [95].

The number flow rate ($N_j(d_i)$, s^{-1}) of discrete class of droplets of size d_i at port j is then determined as weighted spray mass flow rate divided by the mass of an individual (representative) droplet:

$$N_j(d_i) = \frac{6M_d f_i f_j}{\pi d_i^3 \rho_d}$$

For this approach, droplets are spherical and ρ_d is the density of droplet substance.

Now, the most important spray characteristics, total number of droplets (N_{ij}) with diameter, d_i , accumulated by each cell, can be calculated as follows:

$$N_{ij} = N_j(d_i) \tau_d \quad (4.3)$$

where τ_d is the residence time of a representative droplet in the computational cell. This time is a result of the calculation of droplet trajectory traversing the cell (as described in Chapter 3). The total number of droplets with diameter d_i , is then used to calculate the total surface area of the “superdrop” and, consequently, momentum, energy and mass sources from the whole group of droplets. A coupling between droplet dynamics and *thermodynamics* is, therefore, based on estimated time of the droplet as it traverses through the computational cell (*residence time*).

4.2.2 Droplet-Gas flow equations

A complete description of the gas flow, with distributions of temperature and vapour concentration requires derivation of differential equations in three-dimensional space with specified boundary conditions. These equations in their differential form can be found elsewhere and represent conservation of mass, energy and momentum laws written for each control volume with source terms [22].

In general form, the conservation equations for the closed transient gas-water system can be given as follows [96]:

$$\Sigma_{in} \begin{pmatrix} \text{mass} \\ \text{energy} \\ \text{momentum} \end{pmatrix} - \Sigma_{out} \begin{pmatrix} \text{mass} \\ \text{energy} \\ \text{momentum} \end{pmatrix} + \begin{cases} +\text{source} \\ -\text{sink} \\ \text{terms} \end{cases} = \text{rate of accumulation} \quad (4.4)$$

where the symbol Σ relates to gas flow changes and reflects summation of all input/output streams. Different streams for the same quality may relate to different mechanisms of changes, such as, for example, mass/heat transfer by molecular diffusion and convection. The *rate of accumulation* term shows the change in mass (energy, momentum) with respect to time in the volume of interest. For the cases of steady state, such as discussed in [59], this rate equals zero.

From the engineering thermodynamics point of view, a steady flow with imbalance between inflow/outflow due to source/sink terms can be considered as a steady open system [97] where energy carried by gas is removed by a suitable mean (see Figure 4.2).

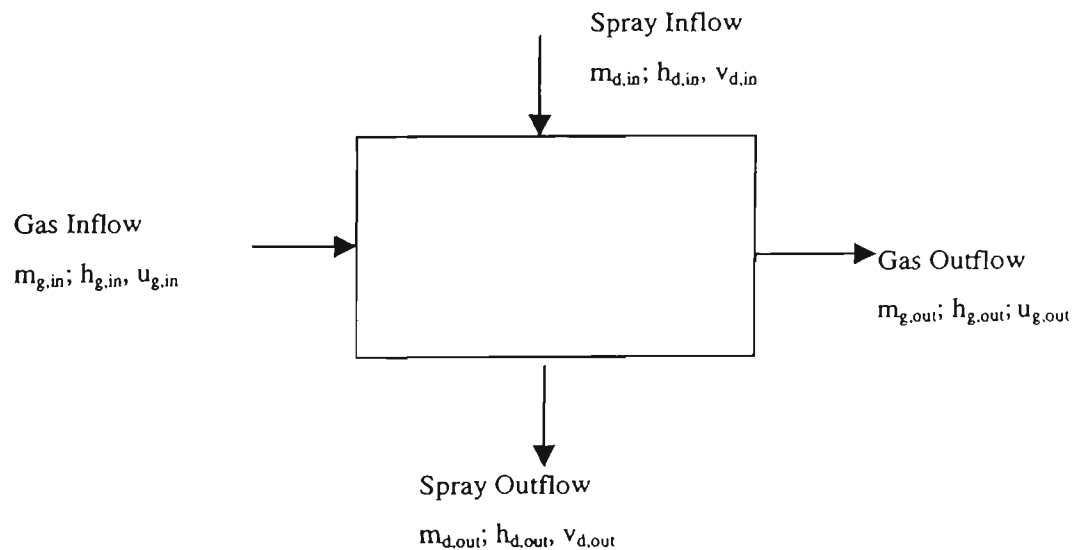


Figure 4.2. Steady droplet-gas system: fire induced hot gas flow cooled by spray

Dealing with moist air (air-vapour mixture), it is common to operate with the term “enthalpy” instead of “energy”. For the system shown in Figure 4.2, conservation equation (4.4) can be re-written as follows:

$$(\text{enthalpy flow out}) - (\text{enthalpy flow in}) = \Delta Q$$

i.e.

$$(m_g h_{\text{mix}})_{\text{out}} - (m_g h_{\text{mix}})_{\text{in}} = \Delta Q \quad (4.5)$$

where indices “in” and “out” correspond to gas flow before and after interaction with the droplets; “mix” relates to gas and denotes mixture of air and vapour; h_{mix} is the gas enthalpy and m is the gas mass flow rate in kg/s. ΔQ is heat transferred from the gas to the droplets. In terms of thermodynamic coupling, ΔQ causes water enthalpy change and includes droplet heat-up and evaporation.

Gas, or air-vapour mixture, enthalpy, h_{mix} , consists of enthalpies of dry air, h_g and water vapour's, h_v . It can be calculated as follows:

$$h_{\text{mix}} = h_g + h_v = C_{pg} T_g + (C_{pv} T_g + L)x_v \quad (4.6)$$

where T_g is the gas temperature (K), L is the latent heat of vaporization of water, C_{pg} and C_{pv} are the specific heats for gas and vapour, respectively; x_v is the specific humidity (kg of water vapour/kg of dry air) of gas at temperature T_g (air-vapour mixture). Since $C_{pv}T_g \ll L$ in most engineering calculations, equation (4.6) is simplified to the following expression:

$$h_{\text{mix}} \approx C_{pg} T_g + Lx_v \quad (4.7)$$

where properties, C_{pg} and L^4 , are generally the functions of temperature, T_g .

Assuming constant average values of gas properties and unchanged total mass flow rate, m_g , equation (4.4) can now be re-written as follows:

$$m_g(C_{pg} T_{g,\text{out}} + L x_{v,\text{out}}) - m_g(C_{pg} T_{g,\text{in}} - L x_{v,\text{in}}) = \Delta Q \quad (4.8)$$

where $T_{g,\text{out}}$ and $x_{v,\text{out}}$ are unknown and can be defined through the ΔQ and a series of iterations as shown in the next section.

⁴ In present work, C_{pg} and L are taken as constants, corresponding to a gas temperature of 25°C [97].

4.2.3 Droplet heat absorption term, ΔQ

In this work it is assumed, that the temperature change of traversing the control volume droplet, results from the following: a) convective heat transfer from hot gas-vapour mixture to the droplet surface, governed by the gas-droplet surface temperature difference; b) phase change due to evaporation (latent heat) governed by the difference of vapour concentration on the evaporating droplet surface and in the bulk gas flow. There is no radiative coupling between droplets and gas, or droplets and walls, at least for the range of droplet sizes studied (Class 2 and 3 sprays), flow rates (1-2 kg/s) and gas temperatures (100-600°C). However, the radiative cooling of droplets can be accounted for by introducing the correction term [55] to the convective heat transfer coefficient.

Droplets are assumed to be totally mixed and characterised by the uniform temperature. Therefore, heating due conduction is neglected. The assumption of completely mixing isothermal droplets is reasonable for low thermal resistance or low values of the Biot number, Bi , which is the ratio [98] of droplet conduction thermal resistance to convective thermal resistance. Low Biot numbers refer to $Bi < 1$. For the range of the investigated sprinkler-gas parameters, $Bi = hd/k_d$ (d is the droplet diameter, h is the convective heat transfer coefficient and k_d is conductivity of the droplet substance) was estimated to be less than 10^{-2} .

The total heat transferred from the gas to the droplets, ΔQ is equal:

$$\Delta Q = \sum_i N_d a_d h (\langle T_g \rangle - \langle T_d \rangle) \quad (4.9)$$

where summation corresponds to the number of droplet size (d_i) groups. h is a heat transfer coefficient. $\langle T_g \rangle$ and $\langle T_d \rangle$ are the average (over the droplet path) gas and droplet surface temperatures (K), respectively; N_d is the number of droplets with diameter d in a control volume; a_d is a surface area of a single droplet (πd^2) with diameter d .

The heat rate used to evaporate the droplets is:

$$Q_L = \sum_i N_d m_{dev} L \quad (4.10)$$

where m_{dev} is evaporation rate of the droplet with diameter d , or diffusion rate (kg/s).

The rate of droplet surface evaporation is governed by the difference of vapour concentration on the evaporating droplet surface (or saturation partial pressure) and in the bulk gas flow and can be found as follows:

$$m_{dev} = a_d h_D (\langle p_{sat} \rangle - \langle p_\infty \rangle) \quad (4.11)$$

where p_{sat} is the saturation vapour partial pressure at the droplet surface which is a function of droplet surface temperature, $p_{sat}(T_d)$; p_∞ is the vapour partial pressure, or specific humidity, in a bulk gas flow, far away from the interface ($p_\infty(T_g)$); h_D is the mass transfer coefficient.

Looking at Equations (4.9) and (4.11), where the product, $N_d a_d$, denotes the total surface area, the importance of product $\tau_d d^l$ can be seen as follows. Based on Equations (4.2) and (4.3), N_d is proportional to τ_d / d^3 , while a_d is proportional to d^2 , therefore $N_d a_d$ is proportional to τ_d / d or $\tau_d d^l$. Therefore, later on in this chapter, this parameter will be studied instead of total spray surface area, in connection with spray effectiveness in gas cooling.

Then the heat available for heating-up droplets from $T_{d,in}$ to $T_{d,out}$ can be obtained as the difference between ΔQ and Q_L :

$$M_d C_{pd} (T_{d,out} - T_{d,in}) = \Delta Q - Q_L \quad (4.12)$$

where M_d is the total spray mass flow rate, T_d relates to droplet temperature. "in" and "out" correspond to the droplet temperatures at the inlet and the outlet to the gas-droplet system, or control volume, respectively.

Thus, combining Equations (4.9), (4.10) and (4.12), temperature change of spray, ΔT_d can be calculated as follows:

$$\Delta T_d = T_{d,out} - T_{d,in} = [\sum_i N_d a_d h (\langle T_g \rangle - \langle T_d \rangle) - \sum_i N_d a_d h_D L (\langle p_{sat} \rangle - \langle p_\infty \rangle)] / (M_d C_{pd}) \quad (4.13)$$

where $\langle p_{sat} \rangle$ and $\langle p_\infty \rangle$ are functions of $\langle T_d \rangle$ and $\langle T_g \rangle$, respectively.

The following expression has been used in the present study for the vapour pressure of steam over water surface, p_{sat} , up to 100°C:

$$\log p_{sat} = 28.59051 - 8.2 \log T_d + 0.0024804 T_d - 3142.31/T_d \quad (4.14)$$

where T_d is average droplet temperature in K and p_{sat} is pressure in bars. Equation (4.15) developed from National Engineering Laboratory Steam Tables [99], applies to water only. Vapour pressure in a bulk gas mixture, p_∞ can be calculated based on the ideal gas law at ambient temperature:

$$p_\infty = x_v R_v T_g \rho_g \quad (4.15)$$

where x_v is the specific humidity of gas flow; R_v is a gas constant for water vapour; T_g and ρ_g are the ambient gas temperature and density, respectively.

Gardiner [41] used the assumption that due to the large entrainment rate of ambient air into the seat of the fire, the specific humidity of the fire gases is the same as that of the ambient (outdoor) air. This assumption has not been confirmed, but it is adopted in the present work in terms of an idealised adiabatic drier model [59].

Equations (4.8 to 4.15) are solved in order to predict gas and water temperature change using a simple iterative scheme, as follows:

- Find the outlet droplet temperature, $T_{d,out}$, from Equation (4.13), assuming that $\langle T_g \rangle$ and $\langle T_d \rangle$ at the right hand side of equation have their initial values instead of average.

-
- determine each droplet evaporation rate, m_{dev} , using Equation (4.11)
 - determine gas specific humidity, $x_{v,out}$ using $x_{v,out} = x_{v,in} + \sum_i N_d m_{dev} / m_g$
 - calculate $T_{g,out}$ from Equation (4.8)
 - recalculate ΔQ^{new} and $T^{new}_{d,out}$ based on the difference between average gas and droplet temperatures, i.e. $\langle T_g \rangle - \langle T_d \rangle = (1/2)\{(T_{g,out} + T_{g,in}) - (T_{d,out} + T_{d,in})\}$. The p_{sat} is also based on average T_d .
 - calculate new value $T_{g,out}^{new}$ based on new ΔQ^{new}
 - repeat the process until T_g^{new} converge, i.e. it will differ from T_g^{old} by no more than 1°C .

4.2.4 Heat transfer coefficient

The Ranz and Marshall correlation [22, 55, 83, 100]

$$Nu_d = 2 + 0.6 Re_d^{0.5} Pr(Sc)^{0.33} \quad (4.16)$$

has been used to predict convective heat transfer between sprays and open atmosphere. The heat transfer coefficient is therefore given as follows:

$$h^5 = Nu_d k_d / d \quad (4.17)$$

where d and k_d are the diameter and thermal conductivity of droplets, respectively. The Reynolds number, $Re_d = V_R d / v$, in Equation (4.16) is based on droplet diameter, relative gas-droplet velocity, V_R , gas phase viscosity, v . The mass transfer coefficient, h_D , is determined using the Lewis law [55,15]:

$$Le = h_D C_{pg} / h \approx 1, \quad (4.18)$$

⁵ As it is suggested by Chen and Trezek [55,] h can be corrected ($h \Rightarrow h + h_r$) by radiative term $h_r = \epsilon \sigma (T^4 - T_e^4) / (T - T_e)$, where T_e is droplet equilibrium temperature, i.e the maximum temperature that a droplet can attain at a given gas temperature.

The reduction of heat transfer rate at high gas temperatures due to droplet evaporation, mentioned in [15] as ‘transpiration blocking effect’ can be corrected by the Spalding (or mass-transfer) number, B_M , following Crowe *et al.* [59]:

$$Nu_d = Nu_{d0}/(1+B) \quad (4.19)$$

where Nu_{d0} is determined from Equation (4.17), and experimental values for B at the range of ambient gas temperature from 100°C to 1000°C for water droplets can be found in [101]. B varies from 0.024 at 100°C to 0.43 at 1000°C. The detailed study and validations of mass and heat transfer numbers is presented in Section 4.4 in connection with rapidly evaporating mist spray droplets exposed to high gas temperatures.

Another well-known correlation of McAdams [101] for Nu_d in the range of Reynolds numbers from 20 to 150000, was successfully used by Morgan [36] in his fire-sprinkler interaction study:

$$Nu_d = 0.37(Re_d)^{0.6}(Pr)^{0.33} \quad (4.20)$$

Equation (4.20) is used in the present study for small droplets with a diameter of 0.5 mm or less, when the Ranz-Marshall correlation, originally obtained [65] for droplets of 0.6 – 1.1 mm, may produce an error.

4.2.5 Local humidity assumption

Droplet evaporation rate depends on the difference between the humidity or partial pressure in the vicinity of a droplet (at droplet surface) and the ambient air humidity. In this context, there are two wind conditions affecting on a choice of the values for “ambient” air humidity discussed in the literature [55]. The assumption of “critical wind condition” states that if the air flow rate is equal to, or greater than the evaporation rate, all the vapour produced will be removed so that the local air humidity (or partial pressure) can be taken as the ambient humidity. The confusion should be avoided in terminology. Under “*local*” conditions, the ambient gas conditions in immediate neighborhood of the droplets are understood in the

literature [41,55]. Under “*ambient*” conditions in [41,55], the ambient conditions of fresh, entraining air are supposed.

The critical wind speed was experimentally determined in [55]. This validated the estimate values of 4.5-5.5 m/s for *ambient* humidity, while 2.5m/s and less indicates the need to take the *local* average humidity. At the “low or zero wind conditions”, the *local* humidity as then stated in [41] and [55], is not readily defined, and a suitable average value can be used. No explanation was given to what is “suitable”.

In the present study, “local” humidity (not to be confused with “local” in [55]) was determined based on droplet surface conditions using Equation (4.15) or (4.16), while ambient (those in spray in [55]) corresponded initially to those of free stream gas with further changing due to droplet evaporation.

The present heat transfer model describes only one part of the complex mechanism of fire extinguishment, namely, gas cooling. Prior to introducing this sub-model into ‘overall’ fire model, a sub-model calculates total heat losses in zone modelling or source terms in CFD simulations, and the sensitivity of the model to gas and spray characteristics in terms of heat absorption and evaporation rates, has been analysed.

4.3 WATER SPRAYS

4.3.1 Model validation

Prior to predicting fire suppression by integrating the droplet sub-model into any fire model, some validation of the sub-model itself has to be done. The set of equations proposed both for droplet dynamics (Chapter 3) and heat and mass transfer (Section 4.2 of present chapter), which actually constitutes Crowe *et al*'s PSI-Cell model [59] (see section 4.2.1), has been used: first to confirm the results presented in [59]. Assuming a gas flow with uniform initial temperature and velocity, the same as in Crowe *et al*'s work, but not modeling momentum exchange and gas internal turbulence, the problem was solved for Crowe *et al*'s spray cooling towers. Hot water at 60°C is sprayed into a vertical two-

dimensional duct of radius, $R = (1.5 \pm 2)$ m. The comparison is shown in Figure 4.3 [109]. In this figure there are two sets of three curves, the curves with symbols and plain lines, reflecting three droplets. The upper curve corresponds to the smallest droplet of 0.7 mm, and the lower to the largest droplet of 1.38 mm. The present results are shown by plain lines, and the results taken from [59] have symbols (small spheres). The temperatures along the droplet trajectories obtained in [59] are given in brackets next to the temperatures calculated in the present work. The relative discrepancy in terms of temperatures is about 3%. The trajectories are qualitatively similar (larger droplets penetrate deeper in both cases), while quantitatively differ by about 10% along the vertical distance.

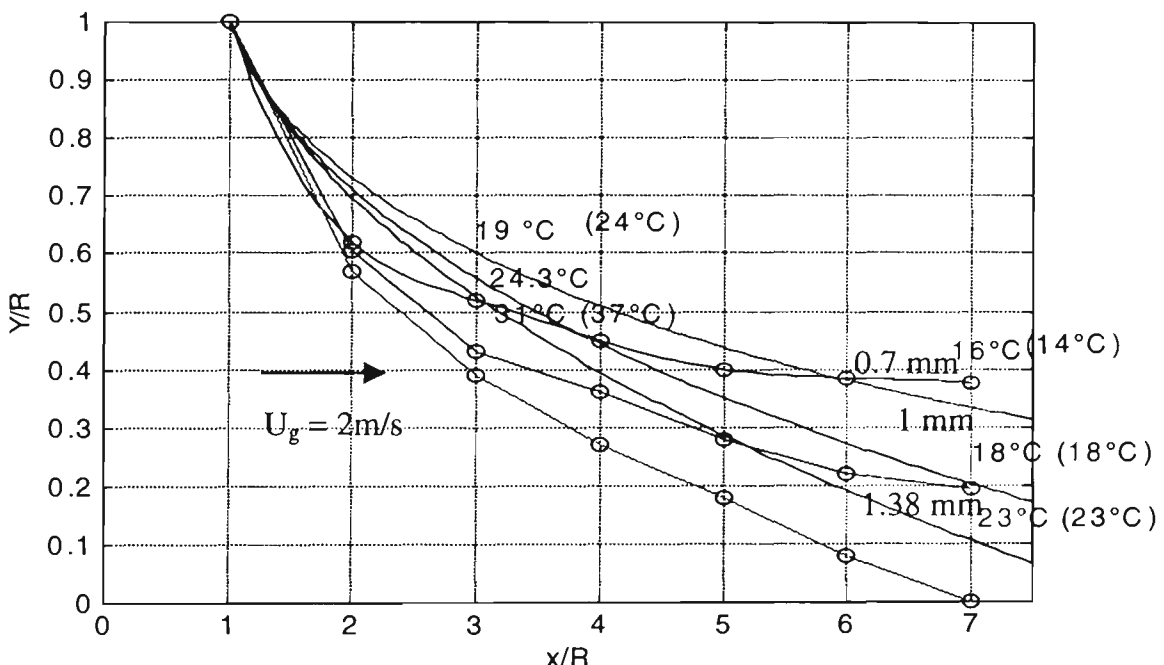


Figure 4.3. Trajectories (lines) and temperatures (shown near the lines in °C) of droplets with initial diameters of 0.74 mm, 1 mm and 1.38 mm. Comparison between Crowe et al's [59] (lines with sphere-symbols and temperatures in brackets) and present (solid lines) calculations. Initial droplet temperature is 60°C, and velocity is 2 m/s. Gas initial velocity is 2 m/s, initial relative humidity is 30% and temperature is 20°C.

Such a discrepancy in trajectories can be assigned to the different methods of solution of droplet motion equation used in [59] and in the present work. Thus, while Crowe et al [59] solved equations analytically, the present approach is based on numerical solution. Another source of discrepancy may also be due to uncertainty of the initial angle of the droplets. In

[59] it is said that angle ranged between 25 and 35°, but it is not actually clear which angle has been used for trajectories shown in Figure 4.3.

4.3.2 Sensitivity Analysis

The governing equations for heat and mass transfer between moving droplets and gas flow are given in the previous sections. The objectives of this section are to analyse the results of modeling under different initial conditions and to understand the sensitivity of the model to the input parameters, before conclusions are drawn on sprinkler thermal performance.

As summarized in [102] where the spray behaviour in gas flow is studied, the main properties of the dispersed liquid phase that affect droplet behavior and spray thermal performance are

- 1) droplet size,
- 2) droplet relative velocity,
- 3) droplet location,
- 4) number of droplets in a given control volume (or droplet number density).

The 2D sketch of the physical situation in zone compartment with the spray activated beneath the ceiling and droplets traversing the hot layer, is given in Figure 4.4.

Figure 4.4 reflects the computational approach in the following way: the whole compartment is divided into zones: hot layer and cold layer. The zone of interest is the hot layer which is sub-divided into finite number of horizontal sub-layers. The number of sub-layers is based on error analysis. If the results (gas temperature drop) do not change with an increase in the number of sub-layers, then this minimum number is sufficient. The sub-layers are not mixing and no heat or mass exchange between them is allowed [41].

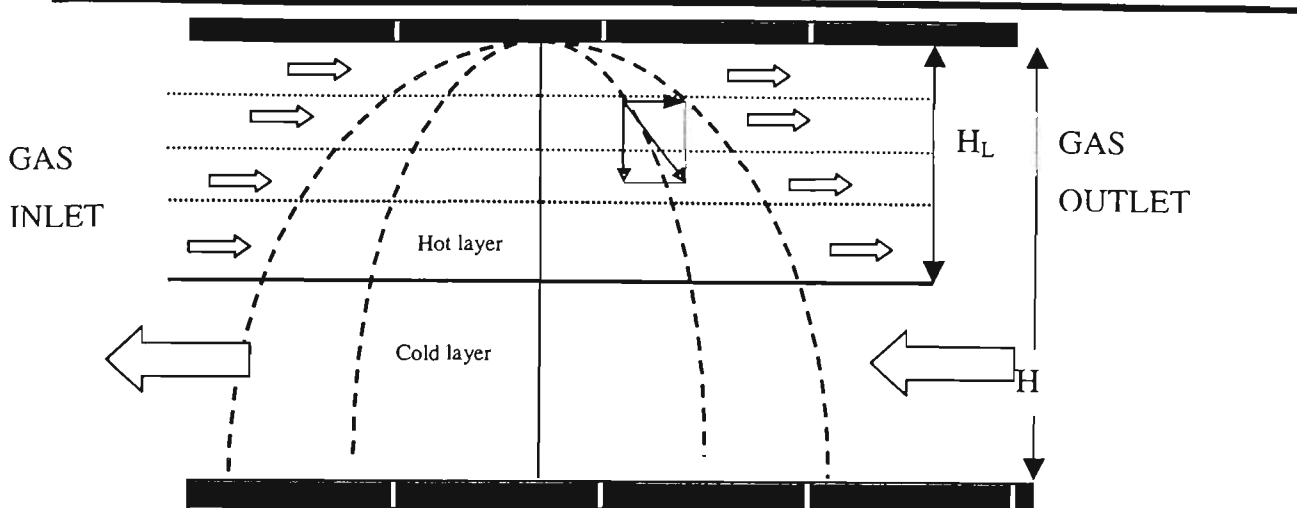


Figure 4.4. Schematic shows the water spray (thick dotted lines) activated in a moving hot layer. The hot layer divided into sub-layers shown by the faint dotted lines.

The mass gas flow rate in each sub-layer is defined as the gas velocity multiplied by the cross-sectional area of the sub-layer. Inlet (initial) gas conditions are defined as conditions prior to spray activation, and outlet - just after gas passed a spray cone. The change in gas conditions is determined by the values of source/sink terms produced by the droplets in each sub-layer. The spray represented by a set number of droplets is characterised by the total number of droplets of each class, permanently available in each sub-layer. These numbers are used to calculate total heat absorption in each sub-layer and depend on droplet moving time across the sub-layer. For steady state, the main outcome of this two-phase modelling is heat and mass transfer rates and their spatial distributions, produced by spray constantly operating within the hot gas layer.

In this study, gas flow is represented by three parameters: the gas temperature, specific humidity, and velocity. Three cases of gas movement are discussed: Horizontally moving hot layer, Location 1; plume turning point where gas velocity vector has equal horizontal and upward vertical components, Location 2; and upward moving fire plume, Location 3.

For the sensitivity analysis, the heat-and-mass transfer model was simplified to a one-dimensional one-step model. The time step is the time interval over which a droplet interacts with gas flow. Depending on the control volume size, the time step can be either the total droplet residence time, or a reasonable fraction of it for convergence. The total droplet residence time is obtained from the solution of the two-dimensional motion

equations within a given control volume for each representative droplet in the spray. The droplet residence time is limited geometrically either by the hot layer depth, or by the natural boundaries, such as ceiling or wall. Based on the droplet residence times, the number of droplets (Equations 4.2 and 4.3) and total spray interface can be calculated, and subsequently, the heat transfer equations can be solved. In the present calculations the gas mass flow rate through the sprinkler spray is taken as the product of gas velocity and spray radial cross-section, similar to the approach of Cooper [103].

4.3.2.1 Droplet residence times and spray surface area

As discussed previously, the droplet residence time is the coupling parameter between droplet dynamics and heat transfer. A summary is given in Table 4.1 of the residence times of different droplets discharged at the three locations, as described in Chapter 3. Initial droplet velocity is 5m/s and initial angle 68° as in [41]. At Location 3, e.g. in an uprising gas flow, droplets of 0.5 mm diameter are nearly suspended in a 2m/s updraft gas flow (see Figure 3.2c) when the drag and gravity forces on each droplet balance each other. In this case, droplets move very slowly, and the residence time goes to infinity when there is no connection between droplet evaporation and droplet motion. This phenomenon was mentioned by Gardiner [41] when the author referred to the ballistic calculations of Lapple and Shepherd [104]. For small droplets of 0.2 to 0.3mm diameter, the residence times and the product $\tau_d d^l$ (see discussion in section (4.2.3)) are much smaller when they are discharged in updraft gas flow, Location 3, in comparison with a horizontal gas flow, Location 1. If droplets move in a horizontal gas flow, the product $\tau_d d^l$ decreases as the diameter increases. If the droplets are discharged against gas flow, Location 3, then the value of $\tau_d d^l$ increases sharply as the droplet diameter decreases down to a critical value which depends on upward gas velocity. For uprising plume velocity of 2m/s, the critical diameter is about 0.5 mm, whereas for 1 m/s, it is about 0.3 mm. For diameters smaller than the critical value, the values of τ_d are low and decrease faster than the diameter. Thus, under certain conditions, fine sprays can be less effective in comparison with large droplet sprays due to lower values of $\tau_d d^l$.

Table 4.1. Residence times (s) for 0.8m distance (or until droplets hit the ceiling) for different droplet diameters, initial droplet velocity of 5m/s, droplet initial angle of 68°. Gas velocity is 2m/s.

d (mm)	LOC 1		LOC 2		LOC 3	
	τ_d (sec)	$\tau_d d^{-1}$ ($s m^{-1}$)	τ_d (sec)	$\tau_d d^{-1}$ ($s m^{-1}$)	τ_d (sec)	$\tau_d d^{-1}$ ($s m^{-1}$)
0.2	0.77	3.85e3	0.27	1.35e3	0.12	0.6e3
0.3	0.66	2.2e3	0.78	2.6e3	0.31	1.03e3
0.5	0.41	0.82e3	1.21	2.42e3	6.7	13.8e3
0.7	0.34	0.48e3	0.54	0.77e3	0.82	1.17e3
1	0.3	0.3e3	0.37	0.37e3	0.43	0.43e3
1.5	0.27	0.18e3	0.31	0.2e3	0.33	0.22e3

In Table 4.2, a comparison between different sprays is given in terms of the number of droplets and total spray surface area. Each spray is represented by a different mean droplet diameter with the same total discharge rate. The residence times were obtained based on the droplet dynamics at Location 1 as an example. The values of initial gas temperature, 99.5°C, and water mass flow rate, 1.84kg/s, correspond to the experimental values published by Gardiner [41, p.165]. A hot layer depth of 0.8m was used in the calculations. The results given in the first 5 rows in Table 4.2 are based on the assumption that the spray is represented by one droplet diameter corresponding to the mean droplet diameter of the spray [53]. The effect of droplet diameter distribution, $f(d)$, on the total surface area is shown in the last row. The distribution was taken to consist of 0.5 mm, 0.7 mm and 1 mm droplets of 25%, 50% and 25% mass fraction, respectively. This example droplet diameter distribution, at Location 1, does not change the total interface area substantially in comparison with the area of a mono-disperse spray represented by a single size 0.7mm droplets at the same location. A similar conclusion was reached in [105] regarding the reasonable insensitivity of CFD predictions to the type of droplet diameter distribution, especially for coarse sprays. Thus, in the following calculations, a spray is represented by one mean droplet diameter. Such an approach is viable for Locations 1 and 2. At Location 3, it may not be possible to determine one mean droplet diameter to represent the whole spray, if there is a substantial number of suspended droplets in the spray, since the residence times of such droplets tend to infinity.

Table 4.2. The total surface areas calculated as for water sprays represented by single-size droplets (first five rows) and by droplet distribution (the last row). The droplets' residence times are shown in the second column for each diameter. Water mass flow rate is 1.84kg/s, gas and droplet velocities are the same as in Table 4.1.

Droplet diameter (mm)	Residence times for 0.8m (sec)	Total number of droplets, N	Total surface area, m ² (N x F _d)
0.3	0.66	85x10 ⁶	24
0.5	0.41	1.1x10 ⁶	9
0.7	0.33	3.4x10 ⁶	5.36
1	0.3	1.x10 ⁶	3
2	0.27	0.1x10 ⁶	1.49
25% (0.5) +50% (0.7) +25% (1.0)	As above for corresponding diameters	As above for corresponding diameters	$\Sigma f(d)(N \times F_d) = 5.68$

4.3.2.2 Droplet initial angles

The sensitivity of the droplet residence times to the initial angles has been investigated in Chapter 3. and, the influence of the droplet initial angles on sprinkler thermal performance through the residence times is evaluated next. In Table 4.3, the rate of convective heat transferred to a water spray is given in terms of the different initial droplet angles. The results are listed for two different locations. In each case, the spray is represented by single size droplets of one initial angle (one trajectory spray) at the same total discharge rate. Within the same location, the spray heat absorption rate is sensitive to the discharge angle, since the residence times are sensitive to it. The sensitivity to discharge angle, in practice, means that the different shapes of spray cone (whether it is hollow or filled, narrow or broad, etc.) affect sprinkler thermal effectiveness, and therefore, it needs consideration in sprinkler design.

The representation of a sprinkler by one trajectory should be based on a reasonable value of the initial angle. Looking at the results in Table 4.3, it is worth to note that a realistic spray with droplet angles from 0 to 90°, can be substituted by “one-angle” spray as far as this spray produces an average between 0 and 90° heat absorption rate (Gardiner's [41] angle 68° is close to such average value).

Yet, there is no uniform answer in the literature, on how real sprinklers have to be represented, as well as how the number of trajectories affect the results. Some of the authors represent sprinklers by one initial angle (usually, either 45° , or 90°) and one diameter [32,49,106], others use from few [41] to few hundreds discrete trajectories [46,105] with discrete initial angles with either one droplet diameter or a diameter distribution. In all calculations, the total flow rate is uniformly distributed among the discrete initial angles. A literature review on this issue was prepared by Kumar *et al* [95].

Table 4.3. Convective heat absorption rate, kW, of the sprays, represented by one diameter (0.7mm) and one initial angle taken to the vertical. The residence times are calculated for Locations 1 and 3. Water mass flow rate, gas velocity and initial temperature are the same as in Tables 4.1 and 4.2.

		Initial droplet angle to vertical ($^\circ$)			
		0 $^\circ$	45 $^\circ$	68 $^\circ$	90 $^\circ$
Convective heat absorbed (kW)	Loc.3	78	122	158	223
	Loc.1	60	77	94	125

Another validation of the one-size, one-angle spray representation in comparison with real droplet distribution is given in Table 4.4, where total spray surface areas are calculated both for Nam's [46] and a simplified sprays. The choice of representative initial angle plays an important role in obtaining the realistic values of the area. This angle determines the length of droplet trajectory and, consequently, droplet residence time and total number in given spray. The relationships between total spray area and droplet mean diameter given both in Tables 4.2 and 4.4 are in agreement with results presented in [107].

The results of heat and mass transfer calculations based on spray representation by different number of discrete trajectories are given in Table 4.5. The total mass flow rate and discharge angles from -90° to 90° were evenly distributed among these trajectories. The gas temperature and sprinkler discharge rate are the same as in Table 4.1. The results are considered for two locations. It follows from Table 4.5 that the sensitivity to the number of

trajectories is higher at Location 3, since at this location the residence times and trajectories are affected more by the initial droplet angles.

Table 4.4. Calculated total spray interface area (m^2) for many-droplet (250 trajectories) and one-droplet (one trajectory) sprays.

Sprinkler discharge rate l/s	ESFR-A sprinkler			ESFR-B sprinkler		
	Droplet distribution 250 trajectories (Nam's distribution)	One volume median droplet diameter and one angle 45°	85°	Droplet distribution 250 trajectories	One volume median droplet diameter and one angle 45°	80°
	1.88	4.8	3.3	4.85	5.32	4.02
3.15		11.7	7.34	11.7	12.95	8.97
4.42		20.4	11.3	19.11	23.78	14.5
6.23		41.31	18.12	30.05	46.	24.
						44.7

It can also be concluded that in both cases of locations, the division of 7-19 trajectories is sufficient. In fact, even one trajectory with an initial angle of 45° can be used to represent a spray at Location 1, if the total spray angle is 180° , as indicated in Table 4.5. Similarly, for Location 3, if the spray is represented by a single angle, 30° is appropriate. Using hundreds of trajectories is not necessary, especially in zone modelling where only thermal coupling can be accounted for and the adequate spray interface area plays the main role.

Table 4.5. Comparison of the convective heat absorption rate (kW) between sprinklers represented by one diameter (0.7mm) and by different numbers of trajectories in the range -90-0-90°. Water mass flow rate, gas velocity and initial temperature are the same as in Tables 4.1 and 4.2.

Convective heat absorption rate (kW)	Location 1 ($U_g=2\text{m/s}$)	Number of trajectories						
		1 at 30°	1 at 45°	7	12	19	25	30
heat absorption rate (kW)	Location 3 ($U_g=2\text{m/s}$)	68	76	80	77.6	76.6	76	76
		102	122	111	98	94	93.6	93.6

4.3.2.3 Mean droplet diameter

In this study, a spray is represented by one volumetric mean droplet diameter and one trajectory to assess sprinkler thermal performance. In Table 4.6, the convective cooling rates for sprays represented by different droplet diameters are given in terms of three relative fire-sprinkler locations. At Locations 2 and 3, the finer sprays produce higher heat absorption rates only with a critical droplet size, as discussed previously in connection with Table 4.1. In addition, if droplets are heavy enough to move down in updraft gas velocity, Location 3, then sprinklers have higher effectiveness in comparison with droplets in horizontal gas flow, Location 1. Due to lack of experimental data on heat absorbed by water droplets, direct comparison is not available with experiments. An experimental value [41] is given in the last column of Table 4.6. Although the exact relative sprinkler location is not known for this entry, the quoted convective heat transfer rate has the same order of magnitude as some of the calculated values, keeping the same initial gas temperature of 99.5°C.

Table 4.6. Convective heat absorption rate, kW , of the sprays, characterized by one diameter and one angle of 68°. Water mass flow rate, gas velocity and initial temperature are the same as in Tables 4.1 and 4.2.

LOC\dia	0.3mm	0.5mm	0.7mm	1mm	1.5mm	2mm	Exper. [41]
LOC 1	241	162	92	54	31	22.7	157
LOC 2	176	290	122	67	35	24	
LOC 3	86	500	155	71	36	25	

4.3.2.4 Initial gas temperature

The effect of initial gas temperature on the droplet evaporation and heat absorption rates are shown in Figure 4.5a and b. In these figures, the droplet diameters vary from 0.3 mm to 1.5 mm, while the initial gas temperature varies from 70°C to 150°C. In Figure 4.5(a), the fraction of evaporation rate varies from 0.2% to 5% of the total water mass flow rate, and it is sensitive to the droplet size for the relatively small droplets of 0.5 mm or less. For larger droplets, the results become insensitive to droplet size. In Figure 4.5(b), the convective heat absorption rate is plotted for the same parameters. The

weak dependence of the heat absorbed on the spray mean droplet diameter is observed for droplets larger than 0.5 mm. Figure 4.5(b) can be taken as an illustration of the results presented in Table 4.1 and Table 4.2 for Location 1.

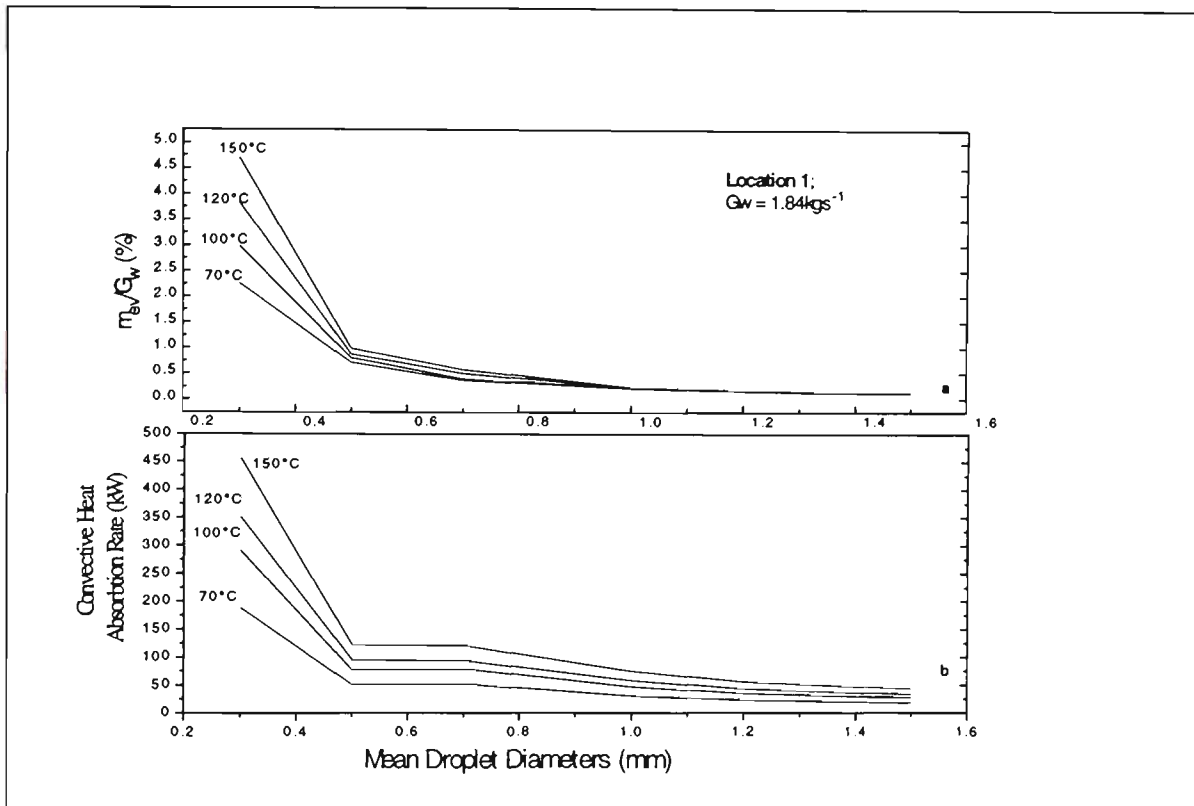


Figure 4.5. Ratio of the evaporation rate of the spray to total mass flow rate of the spray (a) and spray heat absorption rates (b) for different mean droplet diameters for five initial gas temperatures. Initial gas temperatures are given on the curves. Location 1 is chosen due to its common use. The initial droplet discharge angle is 45°.

4.3.3 Results and Discussions

4.3.3.1 Prediction of optimal droplet parameters

The spray characteristic that is usually varied in practice to achieve sprinkler performance objectives, is the water discharge rate. To illustrate the effect of this parameter, the results of heat transfer calculations for different discharge rates at the Location 3 are shown in Figure 4.6 and Figure 4.7. The discharge rate values are the same as Gardiner's [41]. Location 3 (updraft gas velocity) is chosen as the most critical, where small droplets can be blown away and contribute little to heat transfer. In Figure 4.6, the discrete calculated points are joined by straight lines, showing a peak value of cooling rate for droplets of

0.5-mm to 0.6-mm diameter. As indicated in [41], sprinkler effectiveness can be substantially increased by decreasing the droplet diameter to some optimal value. A similar conclusion can be found in [42] based on experiments of fire extinguishment with fine droplet sprays. In Figure 4.6, peak values of heat absorption rate correspond to an updraft gas velocity of 2 m/s where 0.5mm droplets are ‘suspended’. If the gas velocity increases or decreases, the peak will shift to the right or to the left, towards larger or smaller droplet diameters, respectively. The gas-cooling rate by large droplets is relatively low and insensitive to the droplet diameter and discharge rate. Therefore, large-droplet sprinklers are not effective in gas cooling, but they can be used for fuel wetting and cooling. In the range of 0.5 to 0.7mm droplet diameters, the gas cooling rate is much more sensitive to droplet diameter than to sprinkler discharge rate. In this range, effective cooling can be achieved by choosing the appropriate droplet diameter with a minimal flow rate of water. This result clearly shows the existence of an optimal combination of mean droplet diameter and water flow rate.

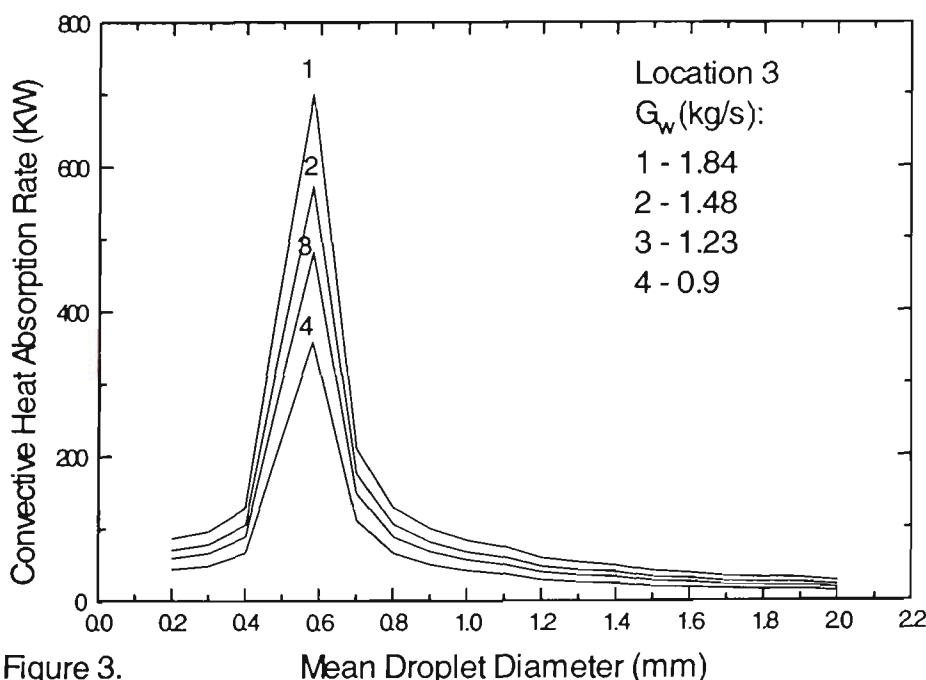


Figure 3.

Figure 4.6. Effect of spray diameter and discharge flow rate on convective heat absorption rate. The uniform vertical gas velocity is 2m/s. The sprinkler discharge rates are listed as numbered. Location 3 is chosen as the most critical.

The results given in Figure 4.6 of effective heat absorption rate as a function of droplet diameter for fixed discharge rates are plotted in Figure 4.7 to show discharge rate as a function of droplet diameter for fixed effective heat absorption rates. Two rates of 100kW and 300kW are considered. The minimum discharge rates of the curves in Figure 4.7, correspond to the same optimum droplet sizes as those given for the maximum cooling rates in Figure 4.6. The smaller the diameter, the lower is the required flow rate to provide the same heat transfer. However, in updraft gas flow, if the diameters are too small and residence times too short, more water is needed to absorb the same amount of heat.

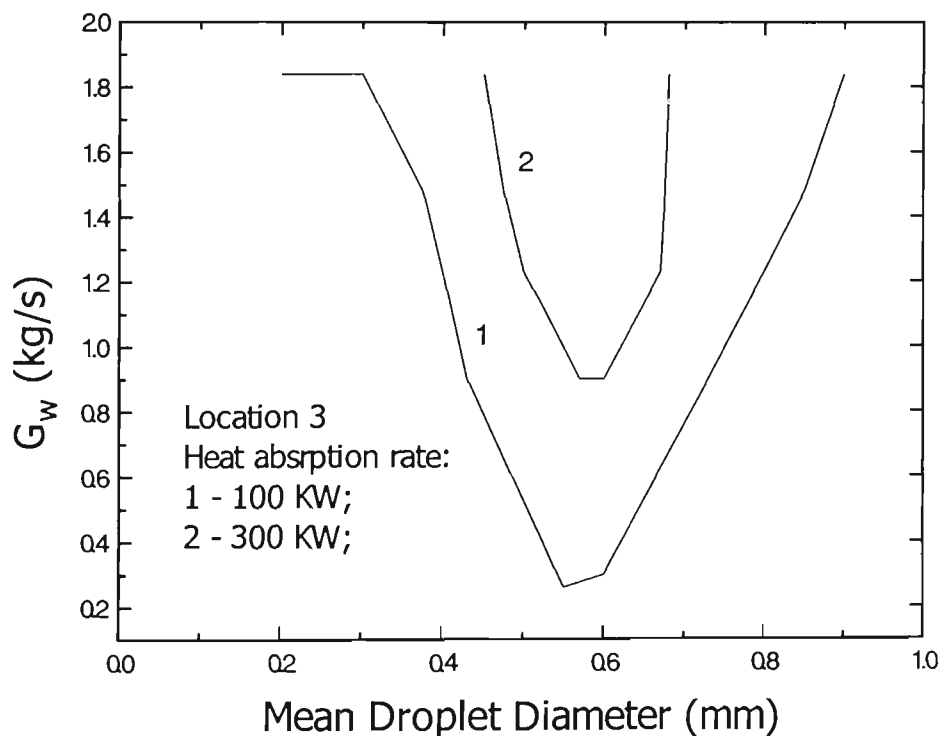


Figure 4.7. Variation of the sprinkler discharge rate with the spray mean droplet diameter for two convective heat transfer rates: 100kW (curve 1) and 300kW (curve 2). The environmental conditions and spray characteristics are the same as in Figure 4.6.

The type of relationship plotted in Figure 4.7 is a conventional way of describing sprinkler performance for thermal effectiveness. Most of the works in fire-sprinkler interaction try to predict or measure the minimal discharge rate needed for extinguishment [25, 44, 105] and qualitatively look like the right half of the two curves given in Figure 4.7 (see, for example,

experimental data given in Figure 3 of [44], or data given in [42]). It is difficult to provide the quantitative comparison with this type of data, since the clear criteria of extinguishment are not usually given. The figures based on calculations with a clear minimum and two branches similar to those plotted in Figure 4.7 were first published by Pietrzak *et al.* [44]. One of the figures taken from their later publication [55] is reproduced in Figure 4.8 for comparison. In this figure, the successful combinations are given of water delivered density and mean droplet diameter in controlling fire. Three cases of fuel exposure to water spray are discussed there: 0% - means no fuel is exposed to water; 50% - means that half of the fuel surface is covered by water and 100% - corresponds to full fuel coverage. The curve for 0% fuel exposure involves gas cooling, only, and it has a clear minimum in water flow rate corresponding to an optimal droplet diameter. Of the three curves given in Figure 4.8, only this one can be compared with the present gas cooling results. Although the 0% curve in Figure 4.8 is similar to the present results qualitatively, a quantitative comparison cannot be made due to lack of gas and sprinkler input parameters of [55] leading to this curve. The curve for 50% exposure in Figure 4.8, also has a minimum, but the optimal diameter is not as obvious. The 100% fuel exposure curve has no minimum, and it is insensitive to droplet diameters of 0.4mm and larger. Hence, the larger the diameter, the more likely it is for the spray or fraction of the spray to reach and cover the fuel, providing suppression regardless of the droplet diameter. These conclusions do not contradict the present results, but only highlight that fuel removal and surface cooling mechanisms should also be studied. The unique results given by Pietrzak *et al.* [44, 48] do not contain the details of calculations or quantitative comparison with other experimental results, but only a general discussion is provided. Since fire was represented in their work [48] by uniform updraft gas velocity, the nozzle pressure and droplet velocity must be important.

Based on the present results, it can be further considered that if sprinkler activation is delayed, extinguishment may not be possible due to increased gas velocity [25]. Gas velocity is expected to increase with the heat release rate, HRR, of the fire before sprinkler activation, proportional to $HRR^{1/3}$. Late activation has the effect of shifting the rate of heat absorption curves to the right in Figure 4.6 due to the higher gas velocity, hence increasing the necessary optimal droplet diameter for extinguishment. If the spray does not include

this particular size, droplets might be blown away by gas flow, unable to reach the fire base to provide effective cooling.

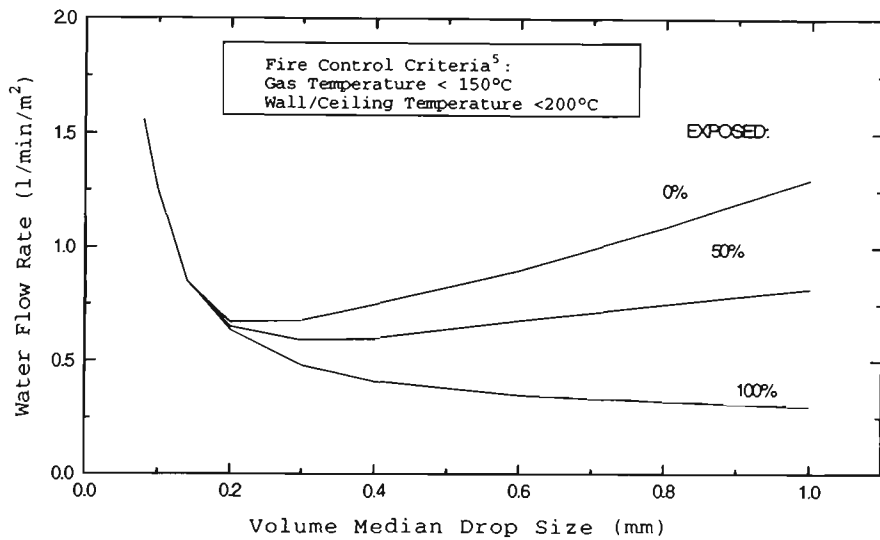


Figure 4.8. Successful combinations in controlling fire of mean droplet diameter and water delivered density (Replication of Figure 3 of Pietrzak et al.[48]). 0% exposure curve corresponds to the present results given in Figure 4.7.

4.3.3.2 Stability of Hot Layer after Sprinkler Activation

From a momentum conservation point of view, a group of decelerating droplets can have a significant effect on gas flow causing it to accelerate if their momentum reduction is significant [59]. Even if the droplets' momentum does not change, they still affect gas flow due to the steady non-zero drag force [82, 108] caused by the non-zero relative velocity. The criterion of layer stability suggested by Bullen [106] and used elsewhere is based on the overall Drag-to-Buoyancy Ratio, D/B. D corresponds to the vertical component of the total drag force (see Equation 3.4) experienced by moving droplets. The buoyant force B can be calculated as follows [41]:

$$B = (\rho_\infty - \rho)gVol \quad (4.21)$$

where ρ_∞ and ρ are the densities of ambient air (at T_∞) and room gas (at T_g), respectively; g is the gravitational constant; Vol is the gas volume embraced by the spray envelope.

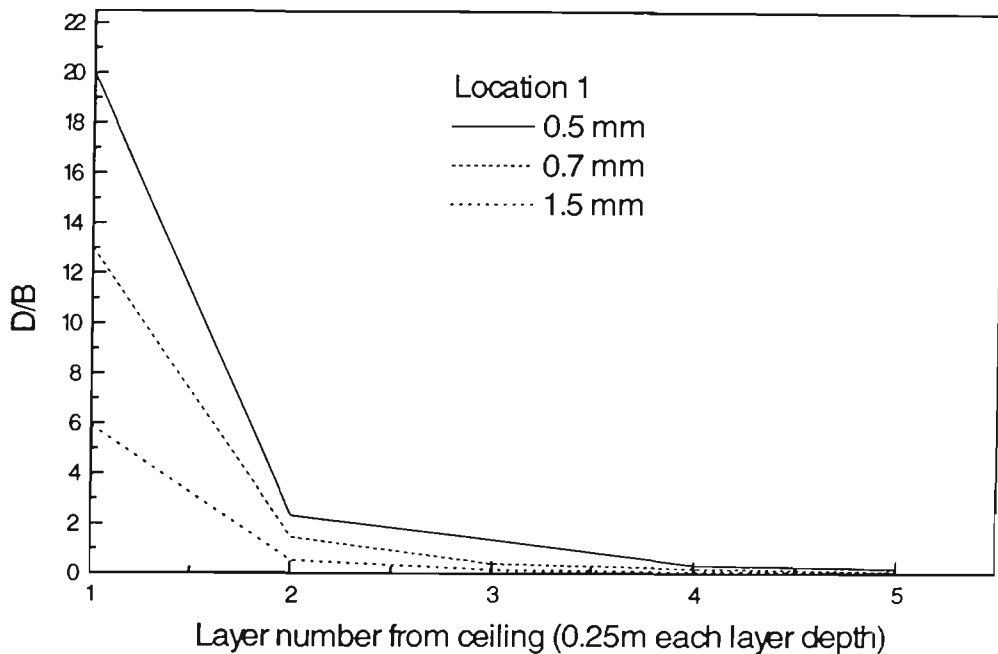


Figure 4.9. The Drag-to-Buoyancy ratio distribution across the hot gas layer. Initial gas temperature is 99.5°C . Water mass flow rate is 1.84kgs^{-1} . Three droplet diameters are considered, as indicated. Location I is where hot layer lowering can be observed.

In the present study, by dividing the horizontally moving hot layer into five sub-layers (see explanations to Figure 4.4), the Drag-to-Buoyancy Ratio distribution across the layer was calculated for each sub-layer. The control volume was taken as the volume of a cylinder with height equal to the sub-layer depth, and diameter of the spray cone at the given height. The time interval corresponded to the droplet residence time in each sub-layer. The heat transfer model was applied consequently to calculate heat absorption and gas temperature reduction in each sub-layer. The D/B ratio distributions across the hot gas layer for three one-size droplet sprays are plotted in Figure 4.9. The droplet diameters of 0.5, 0.7 and 1.5mm were investigated. The trend of the curves is similar for different diameters: the closer the distance to the sprinkler head, the higher is the D/B ratio. A similar pattern was mentioned by Cheung [100] in his CFD study of fire-sprinkler interaction. For the same water flow rate, the D/B ratio is much higher for the small droplets, especially at the beginning, in comparison with large droplets. The reason is that the smaller the diameter, the greater the droplet number accumulated within a given gas volume, and consequently,

the drag force is larger. The D/B ratio for all sprays is much higher than unity at the two sub-layers closer to the sprinkler head. Further away, D/B falls below unity. These results confirm the suggestion of Cheung [100] that the usual calculation of the D/B ratio for the entire hot layer is not appropriate to characterize the layer stability. The stability of the hot layer can be disturbed down to a certain distance below the sprinkler head [103], initiating the downward movement. This distance depends on droplet diameter and gas temperature, and it is a result of the balance between two forces – droplet drag force and gas buoyancy confined in the spray cone.

As it was shown earlier [109], the stability of hot layer may be also disturbed by the “negative” buoyancy phenomenon, which is caused by non-uniform gas cooling within a hot layer by sprinkler spray. Interacting with cold water at the sprinkler head, the hot gas is cooled more at the top than at the bottom of the hot layer, providing buoyant gas flow in the downward direction due to the temperature difference. This additional downward flow contributes to gas lowering if the initial gas temperature distribution is almost uniform. To illustrate “negative” buoyancy, the uniform initial hot-layer temperature distribution was used for the present 2D calculations. The resulting gas temperature profile after sprinkler activation indicates the presence of “negative” buoyancy, i.e. the temperature gradient across the hot layer. In Figure 4.10, the present results are also compared with the numerical results from [41] to validate the present droplet sub-model. Labeled lines in Figure 4.10 correspond to the Gardiner’s [41] input (gas temperature distribution across the layer *before* spray activation) and output (temperature across the layer - *after* spray activation) results. Given that gas input (initial) temperature in present calculations was taken similar to the Gardiner’s input (i.e. labeled “before” in Figure 4.10), the output results correspond to unlabeled curve in the series “after”.

The following estimation can be made in terms of contribution of the “negative” buoyancy in total gas buoyant term, B. The temperature difference across the hot layer is, $\Delta T_{lr} = (T_{up} - T_{low})$, where T_{up} and T_{low} are the temperatures of the upper and lower sublayers respectively. Buoyancy can be defined as being proportional to the temperature difference between the maximum hot layer temperature and ambient temperature; $B \sim \Delta T_{max} = (T_{max} - T_{amb})$.

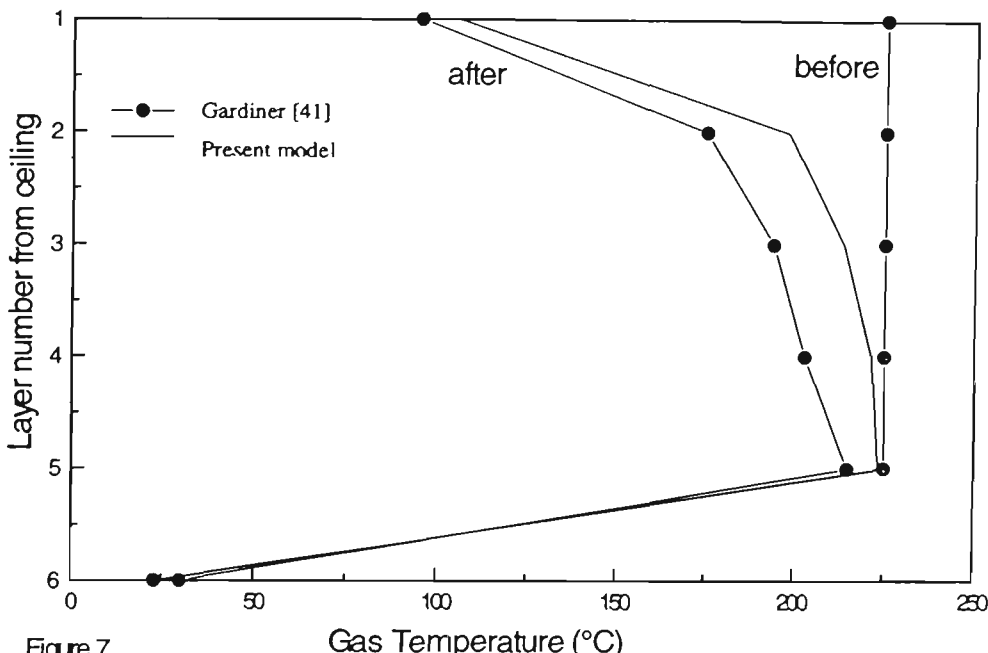


Figure 7.

Figure 4.10. Temperature distribution across hot gas layer of 1.5m depth before and after sprinkler activation. The comparison is given with computational results of Gardiner [41]. Sprinkler is represented by 1.48 kg/s discharge rate, 0.7mm droplets with 45° initial angle, initial gas temperature of 225°C.

A new buoyancy term, B' , caused by non-uniform layer cooling, can be defined as $B' \sim -\Delta T_{lr}$. This new buoyancy appears as an addition to the average buoyancy term. The sign of the ΔT_{lr} is negative in Figure 4.10, indicating negative buoyancy. The term B' , taken with its sign can be used to express the overall drag to buoyancy ratio, as $D/(B+B')$ or $D/((\Delta T_{maxr} + \Delta T_{lr}) / T_{max}) \rho g Vol$, where $\rho g Vol$ is weight of air contained within the sprinkler spray. The additional term, B' , if negative, increases the D/B ratio only in the upper sub-layer, closer to sprinkler head

As a more realistic case, the effect of a non-uniform hot layer temperature profile before the sprinkler interaction was investigated based on the results of a full-scale real furniture sprinkler test. The full-scale tests were carried out by the Centre for Environmental Safety and Risk Engineering (CESARE) of Victoria University of Technology [110]. The burn room was 3.6m x 5.4m x 2.4 m, and the fuel load was 30 kg/m² of wood crib equivalent.

Two sprinkler heads were placed 0.5m on either side of a thermocouple rack at 85 mm below the ceiling. Both sprinklers were discharged: the first at 270 seconds, and the second sprinkler at 381 seconds after ignition.

In Figure 4.11, the temperature histories are given along the thermocouple tree placed at the north edge (remote from fire) of the centerline north-south thermocouple rack. One sprinkler head was placed at the south edge of the centerline of burn room (0.5 m from the edge of thermocouple rack) just above the burning object, another sprinkler was placed at the north edge of the centerline; both sprinkler heads were located at 85 mm below the ceiling. Both sprinklers were charged: the first at 270 seconds; the second sprinkler at the 381 seconds. The temperature profile across the hot layer, for peak temperatures along thermocouple tree just before and after first sprinkler activation are chosen for comparison with the prediction.

In Figure 4.12, the dashed line is the experimentally measured temperature across the hot layer before sprinkler activation, the experimental hot layer temperature profile after the first sprinkler activation is distinguished by the square symbols. In this figure, three sets of calculated hot layer temperature profiles are also given, each corresponding to a different water to gas mass flow rate ratio. The spray is represented by one mean droplet diameter of 0.7mm. In the experiment, the first sprinkler discharge was about 0.8 kg/s (3/8" BSP at 70 kPa) and air ventilation rate was of about 1300 l/s. From a comparison of the experimental and calculated temperatures after activation, a mass flow rate ratio of 0.5 appears to be reasonable.

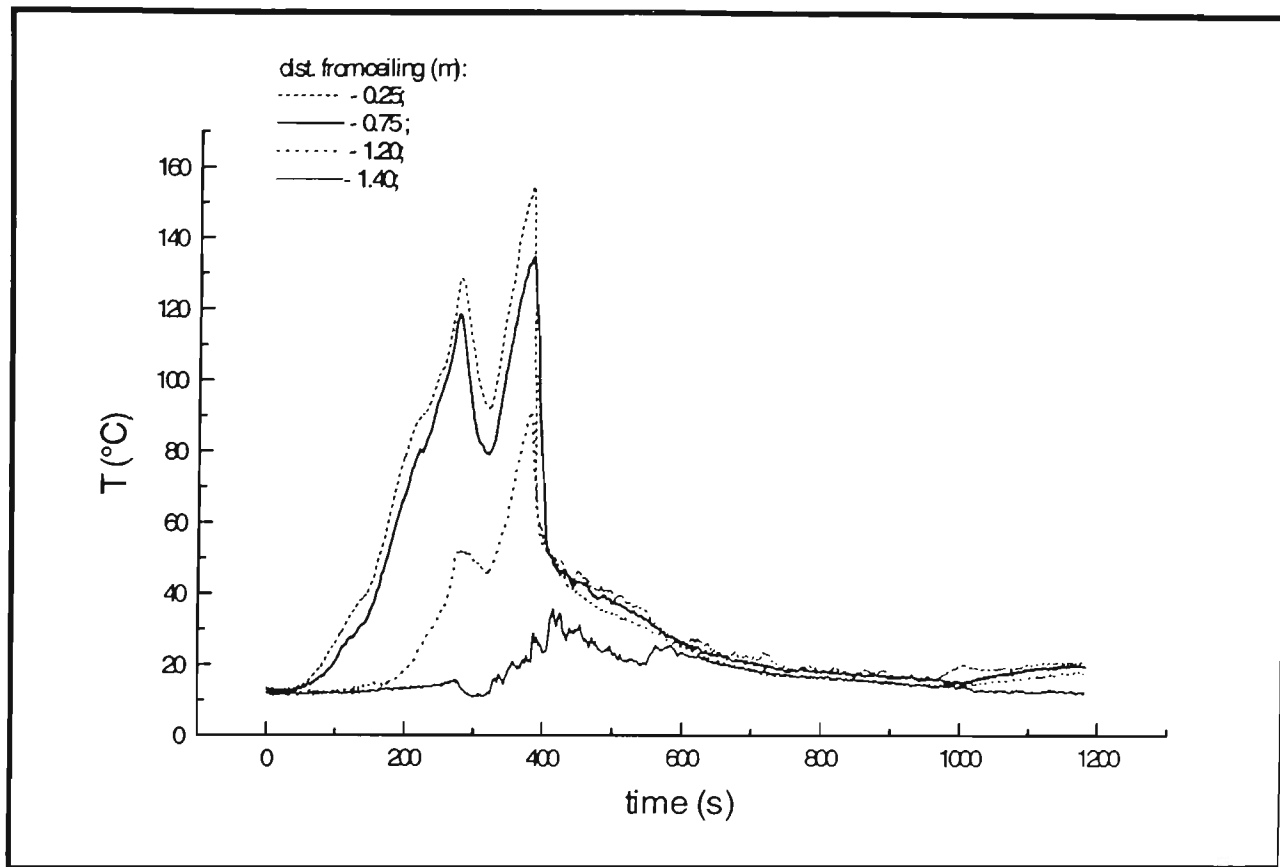


Figure 4.11. Temperature histories within the hot layer of a burn room taken at the distances 0.25, 0.75, 1.25 and 1.4 m below the ceiling. First sprinkler activation time is 270 sec; the second sprinkler was activated at 381 sec.

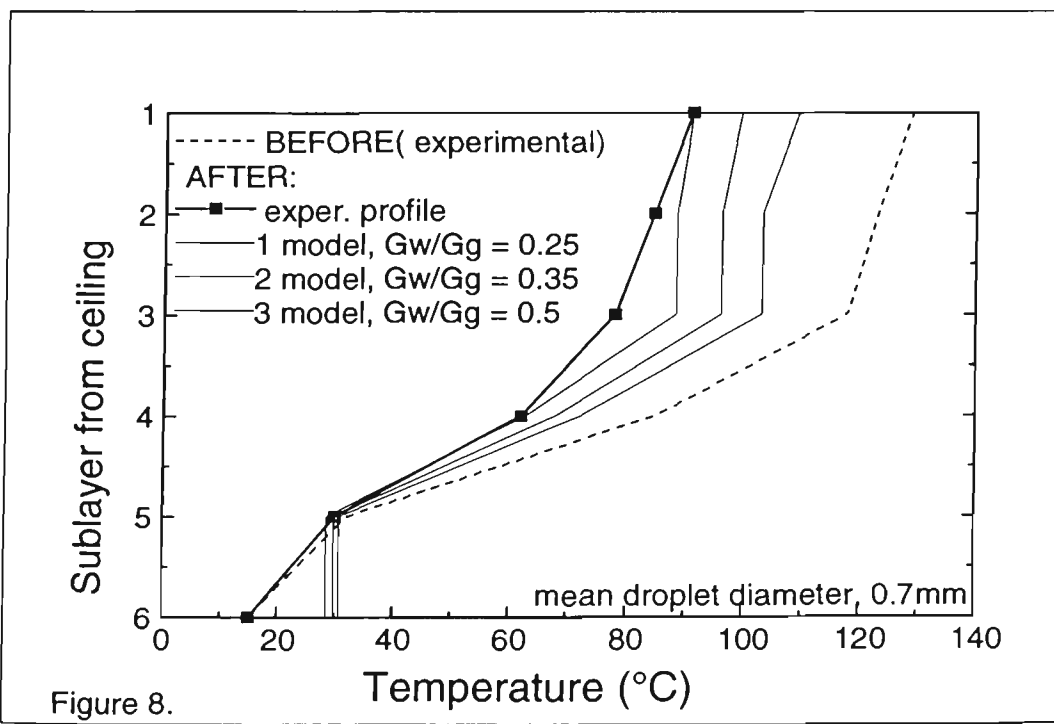


Figure 8.

Figure 4.12. Experimental and predicted temperature profiles before and after sprinkler interaction for different water to gas mass flow rate ratios: $G_w/G_g = 0.25, 0.35$ and 0.5 .

4.3.4 CONCLUSIONS – SPRINKLER SPRAYS AND SENSITIVITY ANALYSIS

The quantitative sensitivity analysis has shown the importance and effect of different input parameters on the resulting sprinkler thermal performance. The conclusions of this part of the study can be summarized as follows:

1. The ratio of droplet residence time to droplet diameter, τ_d/d , defines spray cooling effectiveness for a given volume flow rate. This governing parameter also links droplet dynamics and heat transfer.
2. The classification given in Chapter 3 for the relative nozzle and fire source locations is appropriate for prediction of gas cooling. Hence, thermal performance of sprinkler in fire suppression will also depend on relative fire-sprinkler location.
3. An optimal droplet diameter, which provides the maximum heat absorption for the same water mass flow rate, exists in gas cooling. This optimal diameter is based on the longest residence time that can be attained by the droplet in a given gas flow. The optimal droplet diameter is location dependent. The state of fire development at the moment of sprinkler activation, particularly in terms of the magnitude of maximum plume velocity, dictates the necessary optimal droplet diameter. This diameter has to be large enough not to be immediately dismissed by gas flow and small enough to produce the most effective cooling.
4. For the wide range of water sprays (from coarse to fine) activated at gas temperatures below 200°C, the evaporation rate does not exceed more than few percent of the total spray mass flow rate. The heat absorption and evaporation rates are rather insensitive to droplet diameters in the range of 0.6 to 1.2 mm, while for smaller droplets the sensitivity increases sharply (see Figure 4.4).
5. The effect of initial discharge angle on gas cooling effectiveness has been found to be significant. In fact, depending on the choice of the initial discharge angle, a spray can be represented by an equivalent mean droplet diameter having the same interface area as the real spray.
6. The stability of the hot layer after sprinkler activation calculated in terms of drag-to-buoyancy ratio distribution was found to be mostly affected ($D/B \gg 1$) in the vicinity

-
- of spray head. It was also more destabilised under the effect of smaller droplets in comparison with larger ones.
7. The presence of negative buoyancy within the hot layer due to essential gas cooling at the top, near the spray nozzle, depends on the initial temperature distribution across hot layer. In some cases it can be balanced by the non-uniform gas temperature profile with higher temperatures in upper area.

4.4 MIST SPRAYS

4.4.1 Background

Upon activation, cold droplets are released within a high temperature (above 400°C) gas environment. This sudden immersion changes the relative contribution of droplet different mechanisms of heat absorption into the total heat absorption rate as droplets progress in the gas layer, and their temperature rises. According to the droplet evaporation theory presented in [111], at normal droplet injection temperatures, the concentration of steam around droplets is low providing relatively low mass transfer (evaporation) rate. At this stage, almost all of the heat supplied to the droplets is used to rise the droplet temperature. This period is called the “heat-up” period [111] and its duration depends on surrounding gas temperature, droplet diameter, relative velocity and thermal properties [111]. After the “heat-up” period has finished, each droplet reaches its steady “wet-bulb” temperature corresponding to the ambient conditions. Starting from this moment, the heat absorption continues only due to droplet evaporation (if radiation exchange is neglected). Depending on the comparative length of the heating-up period and droplet residence time (or distance traversed), this steady temperature may or may not be attained. As droplets attain their equilibrium temperatures, all heat that is supplied to droplets is utilized to provide droplet evaporation [111]. This second period in droplet life time is characterised by intensive mass loss and reduction in droplet diameter.

Mathematically, the achievement of steady “wet-bulb” temperature by droplets can be expressed in terms of values of mass transfer (or Spalding) and heat transfer numbers. According to [111], mass transfer number, B_M , can be defined as follows:

$$B_M = \frac{X_s}{1 - X_s} \quad (4.22)$$

where X_s is the water vapour mass fraction at the droplet surface corresponding to the saturation state at the surface temperature and ambient pressure, P_a . X_s can be expressed as follows:

$$X_s = \frac{P_s M_w}{P_s M_w + (P - P_s) M_a} \quad (4.23)$$

where P_s is the vapor pressure at droplet-air surface (see Equation (4.12)), M_w and M_a are the molecular weights of droplet (water) and air respectively.

The heat transfer number, B_T , denotes the ratio of available enthalpy in the surrounding gas to the heat required for droplet evaporation. The following expression is recommended [111] for B_T :

$$B_T = \frac{C_p (T_g - T_s)}{L} \quad (4.24)$$

where L is the latent heat of vaporization corresponding to the droplet surface temperature, T_s . T_g is the temperature of surrounding gas far away from the droplet surface. As soon as these two numbers become equal, the droplet reaches the steady-state condition and wet-bulb temperature.

4.4.2 Results and discussion

4.4.2.1 Single droplets

The development of heat and mass transfer numbers, B_T and B_M , respectively, during droplet movement through the 1m hot gas layer at different gas surrounding temperatures are plotted in Figure 4.13. The relative values of these two numbers reflect the relative contribution into gas cooling of two mechanisms: droplet heating (B_T) and evaporation (B_M).

The sprays are represented by 0.3mm, 0.5 mm and 1 mm droplets that correspond to a, b and c, respectively. The different series of curves in these figures correspond to different surrounding gas temperatures (T_g), namely, 100, 200 and 400°C. The intersection of the B_T and B_M lines indicates steady temperature, given as T_s in Equation (4.15). Thus, in Figure

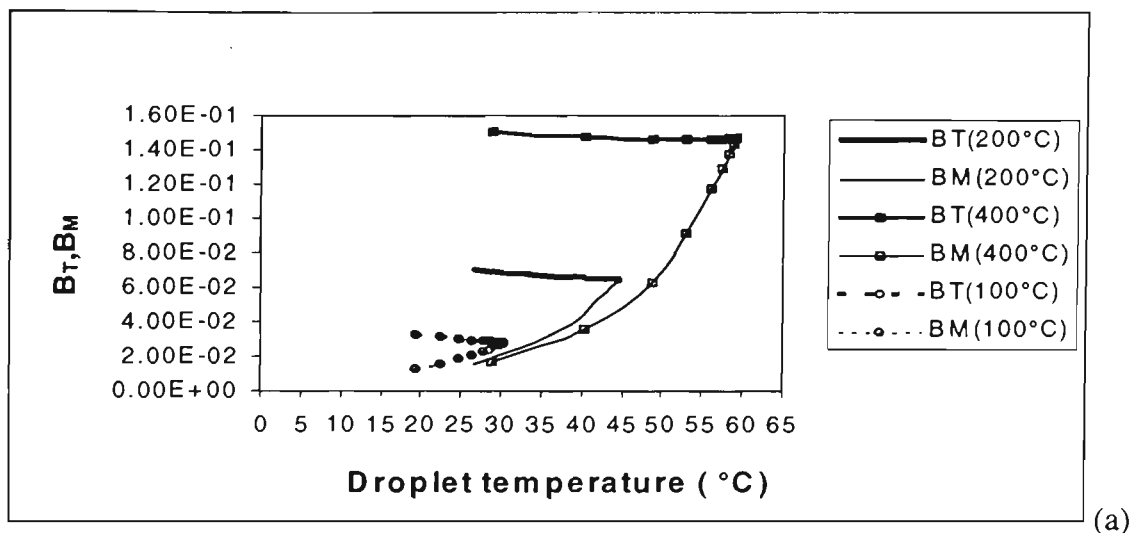
13a, at $T_g = 400^\circ\text{C}$, $B_T = B_M \approx 0.17$ and $T_S \approx 60^\circ\text{C}$, while at 100°C , $B_T = B_M \approx 0.04$ and $T_S \approx 30^\circ\text{C}$. This graphical method of determining equilibrium droplet temperature can not be considered accurate, especially if the B_T and B_M lines intersect each other at a narrow angle [111].

Omitting the basic heat and mass balance equations and intermediate expressions for an ideal gas, Lewis law given in the previous section and applied to any size of droplets and ambient conditions, only the expression for mass evaporation rate at steady state (equilibrium) conditions can be given below [111]:

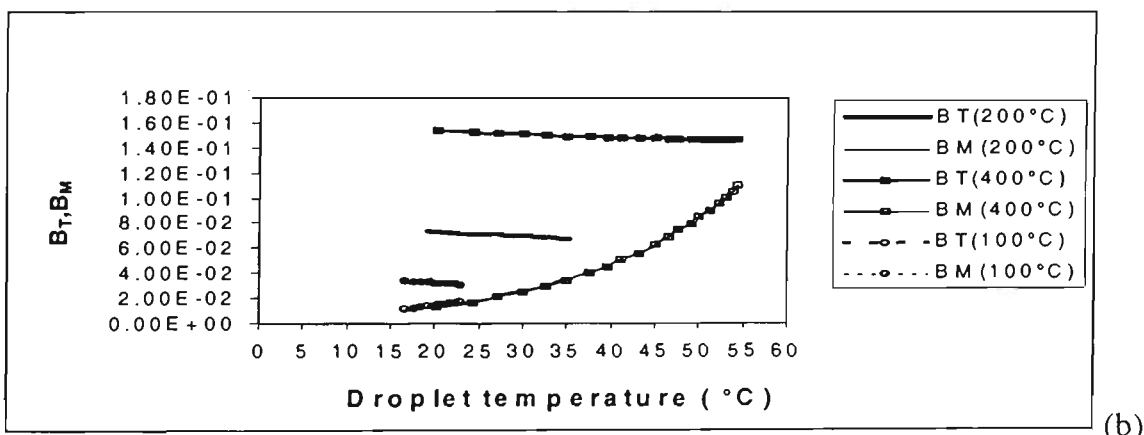
$$m_{ev} = 2\pi D(k/C_p)_{mix} \ln(1+B) \quad (4.25)$$

where k and C_p are the thermal conductivity and specific heat of vapour-gas mixture, respectively, and B can be either B_T or B_M at equilibrium.

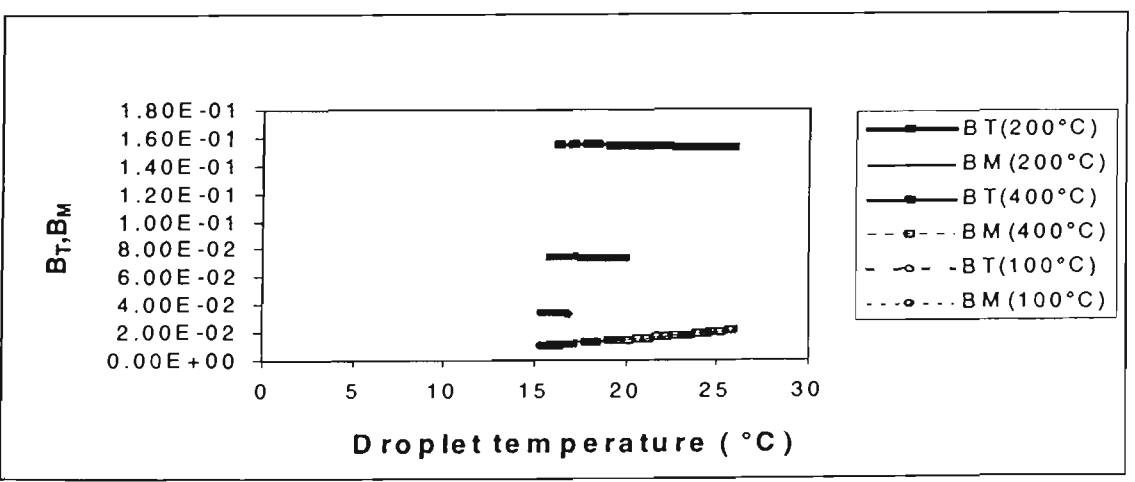
An illustration of the sensitivity of “heat-up” period to the initial droplet diameter is given in Figure 4.14. In this figure, the temperature histories of two droplets (of 0.3 and 0.5mm initial diameters), along their vertical coordinate are shown. The droplets are injected with the same initial velocity ($V_x = 0.7\text{m/s}$ and $V_y = 0.7\text{m/s}$) and temperature (15°C) into steady 1m deep hot gas layer of 600°C . The droplet temperatures, until they reach their steady values, are calculated based on the approach presented in Sections 4.1 to 4.3. A steady state is reached by 0.3 mm droplets at the short distance from the injection point (about 0.3m, or in 0.2s in terms of time), while 0.5mm droplets are only close to equilibrium at the very end of their traveling distance (about 0.6s in terms of time). The equilibrium or “wet-bulb” temperature for both droplets is the same (about 67°C) and depends only on ambient conditions. In all calculations, the ambient pressure is taken as atmospheric (101 kPa).



(a)

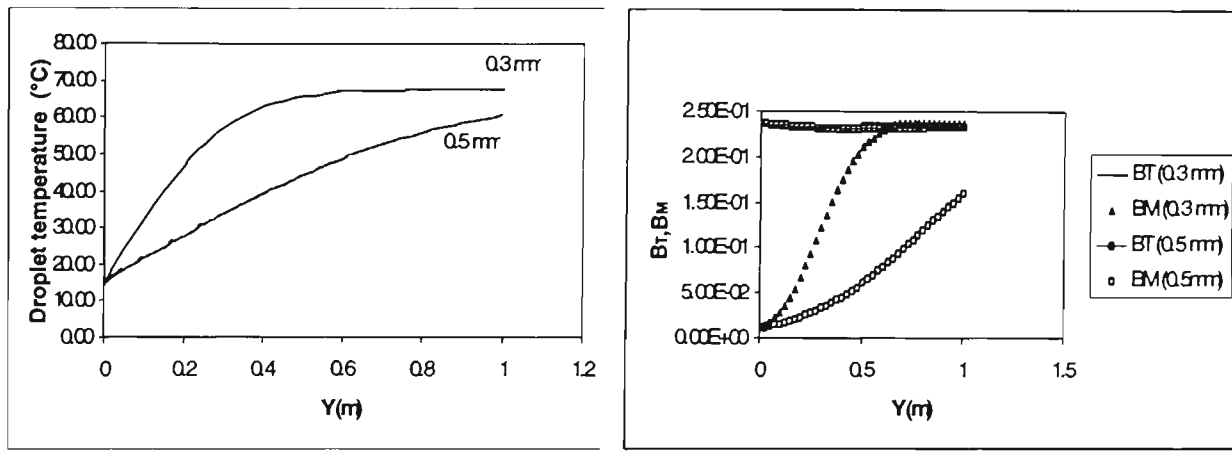


(b)



(c)

Figure 4.13. Variation of transfer numbers, B_T (upper curves) and B_M (lower curves) with droplet temperature rise at different surrounding gas temperatures. Droplet diameters correspond: a) 0.3mm; b) 0.5 mm; c) 1mm. Corresponding gas initial temperatures are shown at the legend.



(a)

(b)

Figure 4.14. a) 0.3 and 0.5mm droplets temperature change along vertical axis. Gas temperature is 600°C and initial diameters are indicated near the corresponding curves. Initial droplet temperature is 15°C. Initial droplet velocity is 1m/s and discharge angle 45°. b) Development of B numbers at $T_g = 600^\circ\text{C}$ for 0.3 and 0.5 mm droplets along the droplet trajectory.

To better illustrate the connection between droplet trajectories, residence times and gas temperatures, vertical droplet coordinate histories, $Y(t)$, obtained numerically (Chapter 3) for evaporating droplets are plotted in Figure 4.15a and b. Initial droplet diameters are taken as 0.3 and 0.5mm, velocities are the same as at Figure 4.12 and droplets are injected under different gas surrounding temperatures. The change in the behavior of function $Y(t)$ with gas temperature is due to different rates of droplet evaporation and, consequently, reduction in droplet diameter. It is assumed in this study that the droplets reduced to 10 μm size are evaporated completely. It can be seen that smaller droplets (0.3mm) evaporate totally at high (800°C) temperature before they traverse the whole distance of 1m. The higher the gas temperature, the shorter is this “evaporation” distance (Y). The trajectories of larger droplets (0.5 mm) are not affected by the change in gas temperature since these droplets do not reach the intensive evaporation regime along their travelling distance.

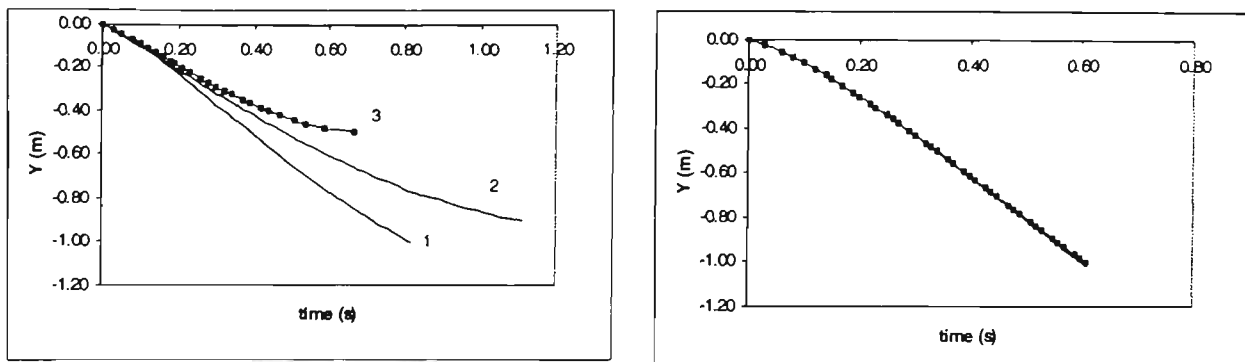


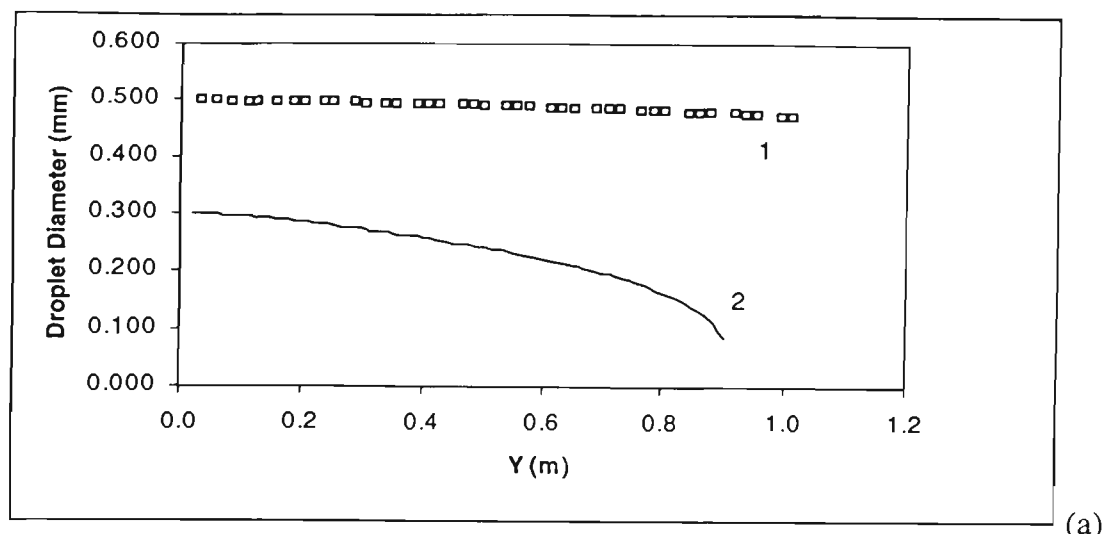
Figure 4.15. Vertical droplet coordinates versus time in steady gas environment. Droplet initial diameters are: a) 0.3mm and b) 0.5mm. Surrounding gas temperatures are: 1-200°C; 2-600°C; 3- 800°C. Droplet initial angles and velocities are similar to those in Figure 4.14.

An illustration of the effect of droplet initial diameter on its behavior in hot gas environment is shown in Figure 4.16. Two droplets of 0.3 and 0.5 mm are exposed to the same gas temperature of 600°C. The difference in the rate of diameter change is as expected. While smaller droplets (0.3mm) lost about 75% of their initial diameter (the size has been reduced to about 70μ) larger ones (0.5mm) are nearly unchanged. For the cases shown in Figure 4.16, the 0.3mm droplet trajectories (or residence time) across 1m hot gas layer have not been long enough to allow droplets to fully evaporate. The diameter change is plotted in two ways: along the droplet traveling distance (a) and along with the residence time (b). The Figures 4.15 and Figure 4.16 help to complete the physical picture of droplet behavior at high temperature.

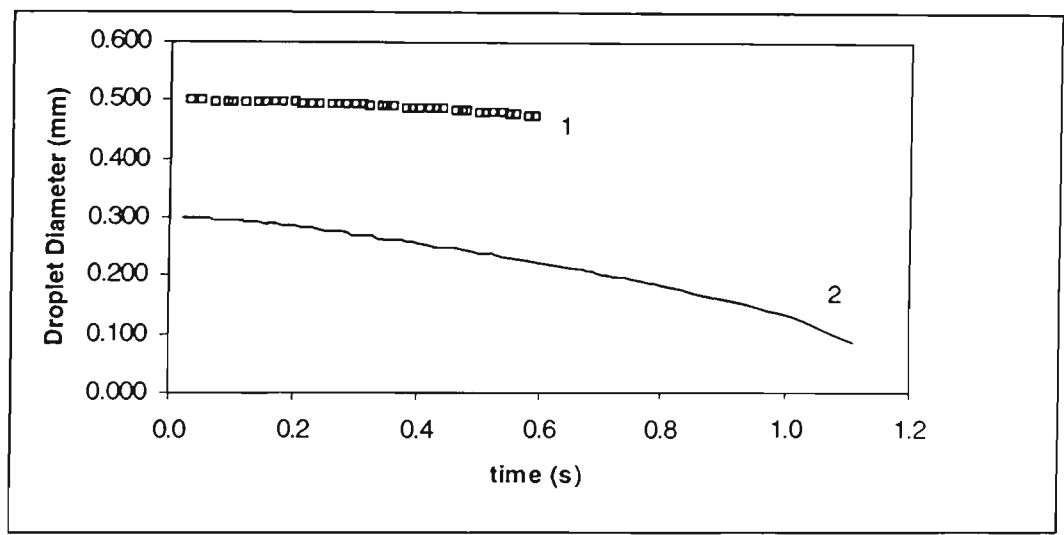
In Figure 4.17, the effect of gas temperature on duration of “heat-up” period and achievement of equilibrium for 0.5mm droplet moving along vertical distance is shown.

The “heat-up” period is significantly shortened and the droplet achieves equilibrium or “wet-bulb” temperature as gas temperature rises faster.

It can be noticed that at very high temperature, the “wet-bulb” droplet temperature is close to its boiling temperature [111] at the corresponding ambient pressure.



(a)



(b)

Figure 4.16. Droplets' diameter reduction as they move at surrounding gas temperature of 600°C: a) along their trajectories; b) over residence time. Curve 1 corresponds to 0.5 mm of droplet initial diameter and Curve 2 to 0.3 mm.

In addition to understanding the difference in droplet relative contribution of heating and evaporation to heat absorption, the following simple calculations can be shown.

Assuming that 1 kg of water is heated by 50° it will consume 210 J (Q_{heat}) amount of heat, while to evaporate the same amount will need 2500 J (Q_{ev}) of heat consumption:

m_{water} (kg)	ΔT	$Q_{heat} = mC_p\Delta T$ (kJ)	$Q_{ev} = mL$ (kJ)
1	50	210	2500

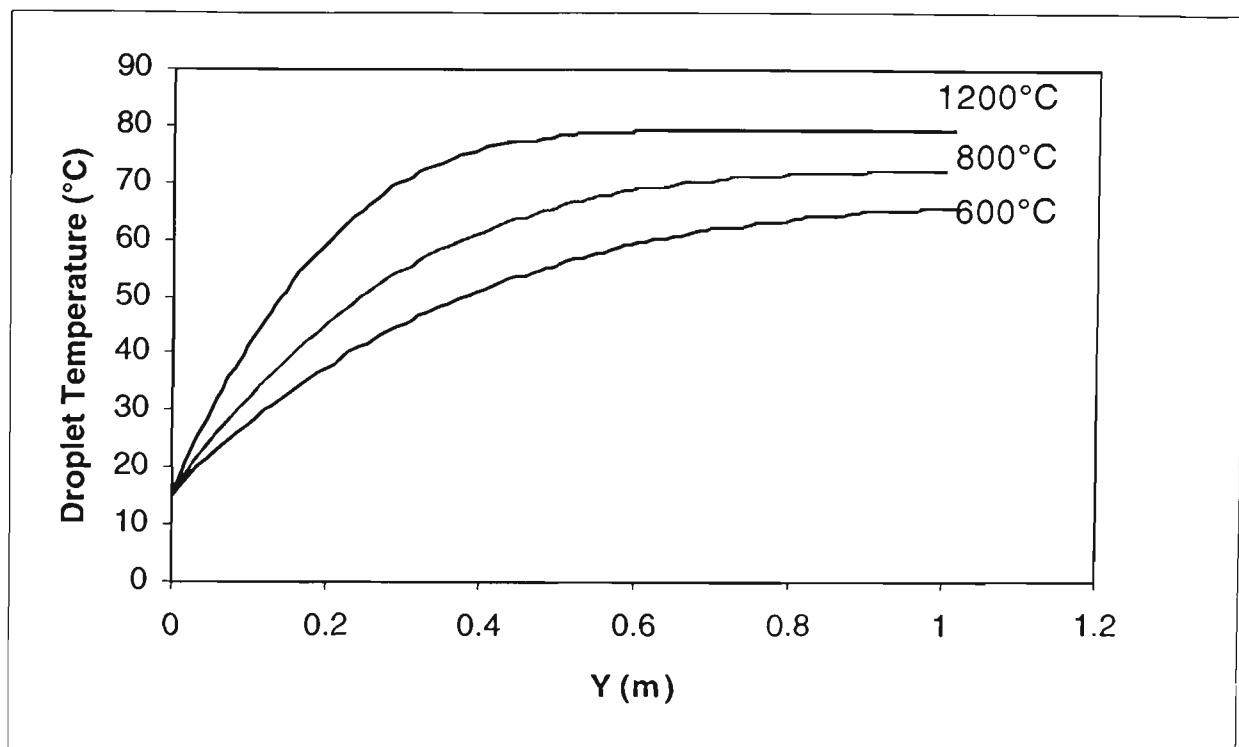


Figure 4.17. Unsteady 0.5mm droplet heating at different gas temperatures ($600^{\circ}\text{C} - 1200^{\circ}\text{C}$), as the droplet moved downwards across the hot layer of 1m depth. Initial conditions are the same as in Figure 4.14.

However, it should be understood that depending on droplet dynamics and heat transfer rate, only part of this whole amount of water may be evaporated during droplet residence time in the hot layer. For this reason, even though the evaporation is a much more powerful mechanism of heat absorption, it still can produce a small contribution as illustrated in Section 4.1.

4.4.2.2 Sprays

As the mass of droplets reduce as a result of water evaporating from their surface, their diameters diminish. If the droplet diameter reduction is plotted in the traditional way [4], namely, the square of droplet diameter (d^2) against time (t), then one of the most important quantitative characteristics of droplet evaporation, namely, the evaporation constant, can be determined.

As an example, in Figure 4.18, the $d^2(t)$ behavior is given for 0.3 mm droplets together with their temperature change at 600°C gas temperature. The curves consist of two parts. The slope at the first part is quite small (low evaporation rate). This initial stage corresponds to “heat-up” period. The slope at the second part is much steeper, and reflects the steady evaporation state. According to the “ d^2 law”, the square of droplet diameter, d^2 , diminishes linearly with time following the expression:

$$d_0^2 - d^2 = \lambda t \quad (4.26)$$

where d_0 is the droplet initial diameter, t is the time interval, λ is generally known as evaporation constant [111], and it represents the slope of the straight line in the $d^2(t)$ curves.

The location of transition point between the two parts in Figure 4.18 denotes the establishment of steady or equilibrium state. The higher the surrounding temperature, the earlier is the transition, and the steeper is the slope, in addition, more intensive is evaporation. Actually, the value of λ consists of two components, λ_{hu} and λ_{st} , corresponding to the “heat-up” period slope (usually negligibly small) and steady evaporation part, respectively. The corresponding time interval (Δt) also consists of two distinct parts: the “heat-up” period (Δt_{hu}) and the time of droplet steady evaporation (Δt_{st}) to its completely disappearing. The expressions for the two parts of λ are the following:

$$\lambda_{hu} = (d_0^2 - d_1^2)/\Delta t_{hu} \quad (a) \quad \text{and} \quad \lambda_{st} = (d_1^2)/\Delta t_{st} \quad (b) \quad (4.27)$$

where d_1 is the new value of the diameter after the heat-up period.

Based on Equation (4.27), droplet lifetime (t_{life}), an important characteristic, can be derived as follows [111]:

$$\begin{aligned} t_{life} &= (\Delta t_{hu}) + (\Delta t_{st}) = \Delta t_{hu}(1 - \lambda_{hu}/\lambda_{st}) + (d_0^2)/\lambda_{st} \\ &\approx \Delta t_{hu} + (d_0^2)/\lambda_{st} \end{aligned} \quad (4.28)$$

Since evaporation during the “heat-up” period is usually low, the ratio $\lambda_{hu}/\lambda_{st}$ is close to zero, and it can be neglected.

For the steady evaporation period, and transforming Equation (4.27b) into a single spherical droplet mass loss rate, the following is obtained:

$$m_{ev} = (\pi/4)\rho_d \lambda d \quad (4.29)$$

where ρ_d is the droplet density corresponding to its temperature. The total heat used by droplets (or spray) to vaporise the water is:

$$Q_{ev} = N_d m_{ev} L \quad (4.30)$$

where N_d is a number of droplets of diameter d in a given volume as defined by Equation (4.3)).

Combining Equations (4.25) and (4.28), the following expression can be drawn for λ :

$$\lambda = 8k_{mix}\ln(1+B)/C_{Pmix}\rho_d \quad (4.31)$$

Using Figure 4.18 as an example to estimate the life-time of 0.3mm droplet injected in air of 600°C and atmospheric pressure, the following results are obtained.

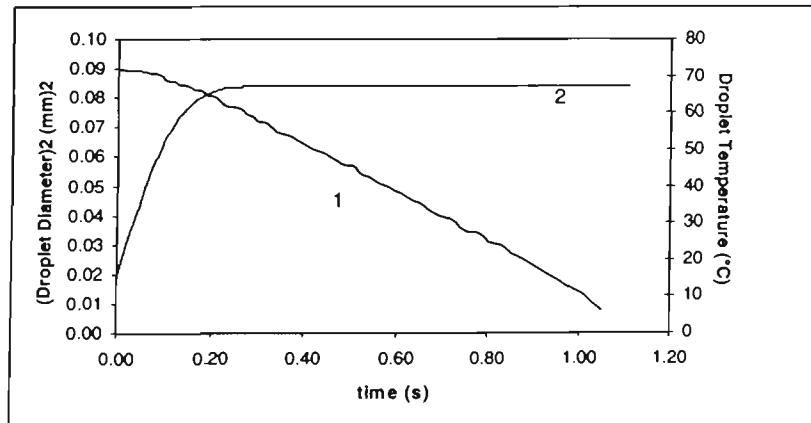


Figure 4.18. Change in temperature (2) and in square of diameter (1) of 0.3mm droplet during heating and evaporation at 600°C. Droplet initial angle is 15°, velocity 1m/s.

Although the transition point between droplet heat-up and evaporation periods is not clearly defined with this type of graphs, it is estimated that $\Delta t_{hu} = 0.1\text{s}$. Consequently, the average value of λ is about $0.08 \times 10^{-6} \text{ m}^2/\text{s}$ for the 0.3mm droplets immersed into 600°C hot gas environment. Using Equation (4.28), the droplet lifetime is estimated as 1.23s.

The heat absorption curves for the sprays represented by droplets of different diameters are plotted in Figure 4.19. For this graph, the sum heat absorption rate (kW) of the spray are varied against surrounding gas temperature. Different sprays are represented by uniform droplet diameter distributions and similar water flow rates (80 l/min). The 1m hot layer is divided into 50 sub-layers (this number has been pre-determined as suitable grid refinement for any gas temperature). It should be noted that the higher is the gas temperature and the smaller the diameter, the finer division should be done, especially near the nozzle, since the temperature of the droplets changes dramatically at the beginning. The initial angle is varied from 0 to 90° with 3.6° increment (25 sub-angles). Droplet velocity is 1m/s.

The heat absorption curves plotted in Figure 4.19 show the existence of linear proportionality between heat absorption and surrounding gas temperature (or temperature difference between droplet and gas). However, this proportionality is valid only up-to certain level of heat absorption or evaporation. As far as droplets attain the level of heat absorption of about 2000 kW for given water flow rate, they perform this rate steady, independently on gas temperature (plateau at the curve 3). Thus, there is a certain maximum level of total spray heat absorption rate corresponding to the particular total water flow rate. This level is defined by the maximum possible evaporation rate, i.e. depends on the total amount of droplets in the hot layer, their diameters and residence times (see Equation 4.20). Since droplets evaporate constantly in hot gas, their amount in spray seize and can be totally consumed while they traversing the hot layer. This fact leads to the limitations in total heat absorption and evaporation rates.

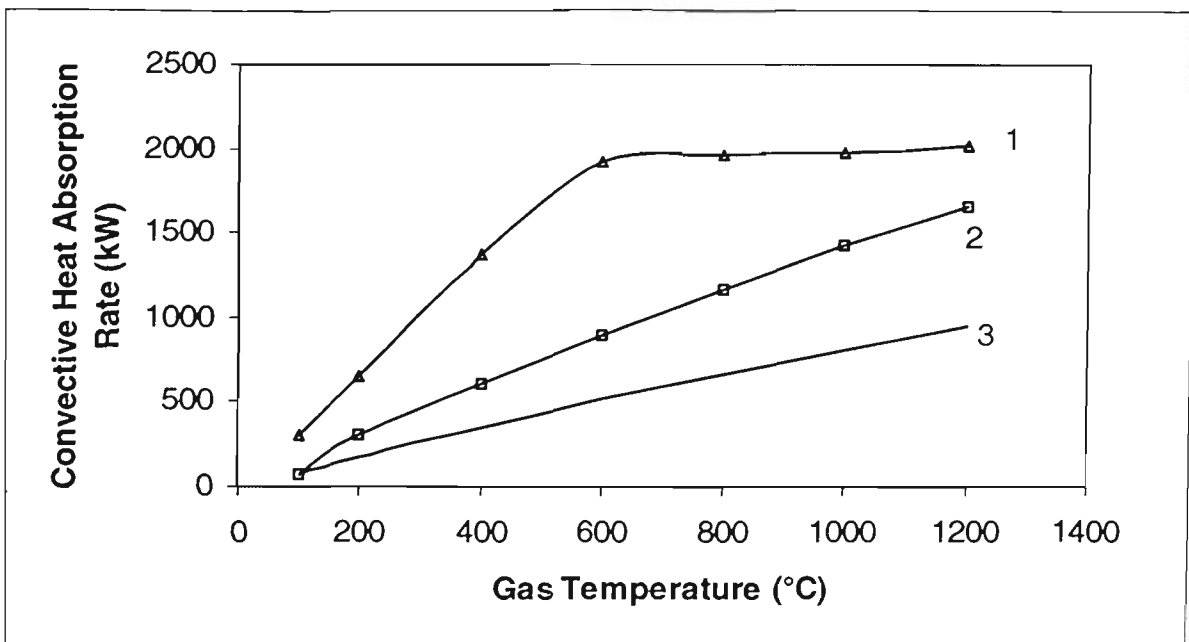


Figure 4.19. Spray heat absorption: 1- 0.3 mm; 2- 0.4 mm; 3 – 0.5mm. Total water flow rate is 80 l/min. The discharge angle range –90 to 90°. Hot layer depth is 1m.

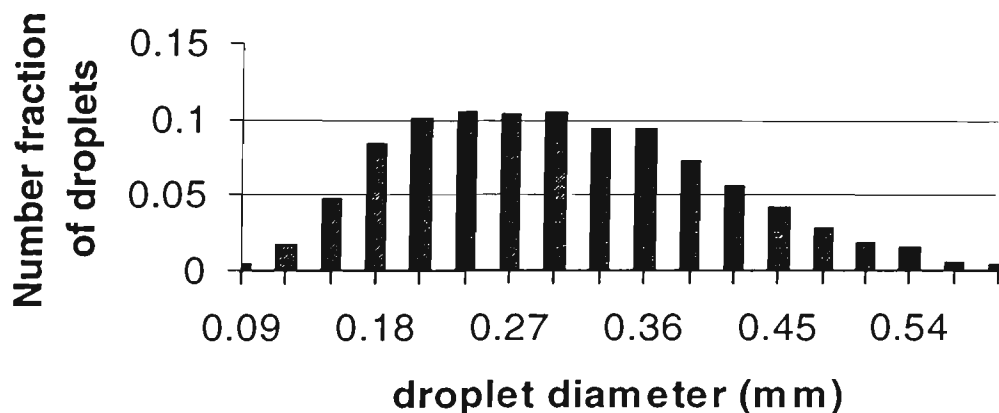
It has to be noted here that the theoretical limits of heat absorption will be slightly higher since in present numerical study, the droplet lifetime is limited by the diameter reduction only to 10 μ m, while theoretically the full evaporation is allowed.

In Figure 4.20a, droplet size distribution for AM24 mist nozzle [112] is presented to highlight the effect of mist droplet diameter distribution on total spray heat absorption rate, as presented in Figure 4.20b. In Figure 4.20b, the effect of water discharge rate on spray heat absorption level is shown for two cases: 80 l/min (curve 1 and 3) and 40 l/min (curve 2 and 4). The reduction in heat absorption is approximately the same as in water flow rate (i.e. twice as less). Thus, the heat absorption rate is proportional to water flow rate and the coefficient of proportionality will be different for different mean droplet diameters representing the spray.

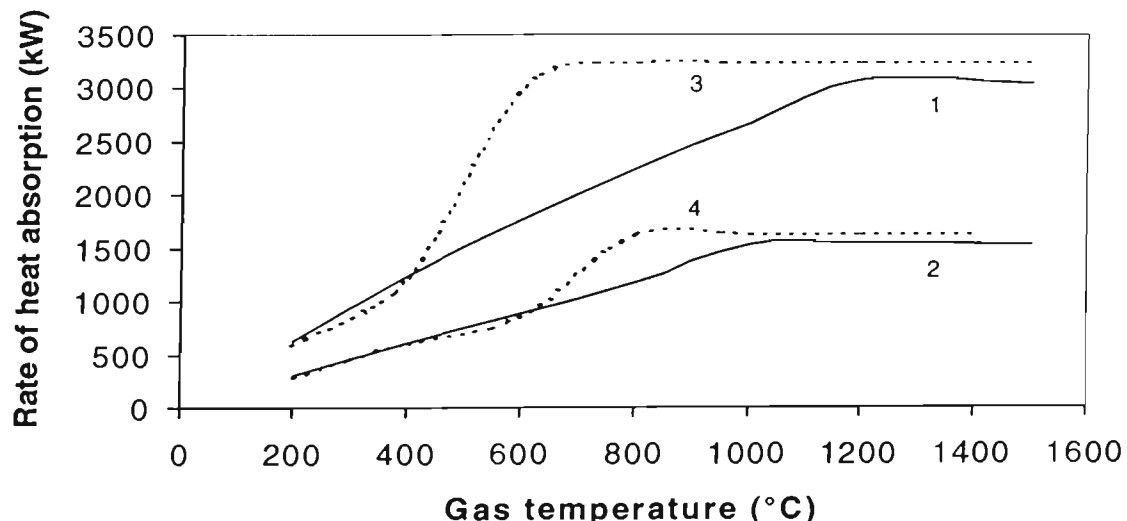
It is worth to notice that even though the water flow rate is twice reduced, it still absorbs more heat at the same temperature as sprays with approximately twice larger droplets (0.5 mm). Comparison of heat absorption rate for 0.3mm spray with 40 l/min water discharge in

Figure 4.20b and for 0.5 mm (80 l/min) in Figure 4.19, for example, for 600°C, show that 0.3 mm spray at 80 l/min absorbs approximately twice more heat than 0.5 mm spray at 80 l/min. This makes the variance of droplet diameter much more effective mean in fire cooling and suppression than change in water flow rates. Present conclusion is in a good qualitative agreement with experimental data of Japanese researchers [113], where they indicated a failure of oil room fire extinguishment by 140 µm spray discharged at 1.5 l/min, while it was extinguished by 85 µm droplets injected at the double reduced rate of 0.75 l/min.

AM24 mist nozzle



a)



b)

Figure 4.20 a) Droplet size distribution for the AM24 mist nozzle; b) Heat absorption for 0.3mm uniform droplet spray (lines 3 and 4) and AM24 nozzle (lines 1 and 2) as a function of water flow rate. Curves 1 and 3: 80 l/min; Curves 2 and 4: 40 l/min.

To connect the results of this section with the “droplet diameter optimality” study in Section 4.3 built on the understanding of droplet residence times, Figure 4.21 has been drawn. At this figure, the droplet trajectories at 1200°C for 0.3 and 0.4mm sprays are plotted. Examining Figure 4.13a, it can be seen that both 0.3 and 0.4mm sprays are close to the same limiting heat absorption rate. However, in terms of droplet dynamics, the spray with heavier droplets exists longer in a given hot layer and penetrate further, traversing the whole hot layer depth of 1m, as shown in Figure 4.15. The increase in droplet diameter above 0.4 mm will lead to essential reduction in heat absorption (see curve 3, Figure 4.13a), with no benefit to droplet penetration capabilities for the same surrounding conditions. Thus, for high surrounding gas temperature with intensive droplet evaporation provided, the spray optimal (minimal) droplet diameter can be identified depending on this temperature and the hot layer depth involved into cooling process.

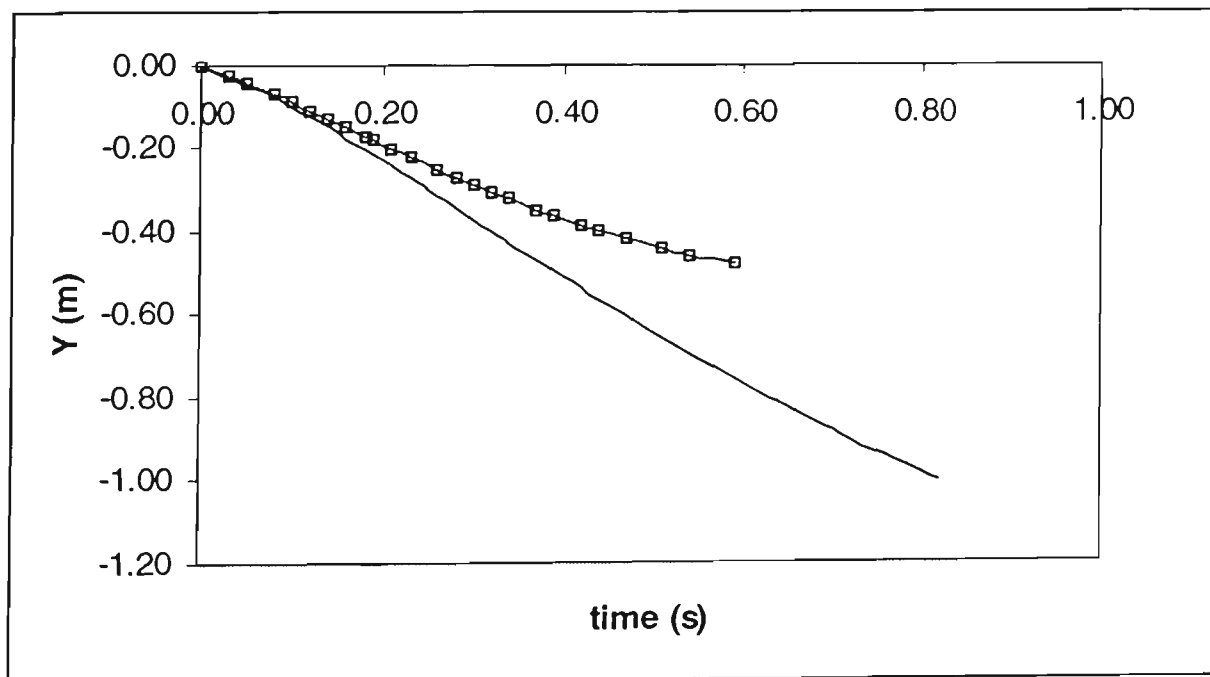


Figure 4.21. Vertical trajectories over time for 0.3mm (symbols) and 0.4mm (solid line) droplets injected into 1 m hot layer of 1200°C. Initial velocity is -1 m/s with a 45° angle.

4.4.2.3 Heat absorption distribution within the spray occupied space

In order to substitute heat absorption rate as a sink term in a one-dimensional one-zone model of a fire environment, the uniformity of real heat absorption rate distribution within the occupied by the spray has to be analyzed. Figure 4.22 shows the trajectories distribution of 0.3 mm mist spray with evaporating droplets discharged within 400°C gas environment. Spray is represented by 20 angles and the hot gas layer of 1 m depth is divided into 20 sub-layers. The heat absorption rate distribution (Q-distribution) shown in Figure 4.23 for the spray occupied 2D-space of 1mx1m. The Q-distribution is not as smooth since the spray division into 20 sectors is not sufficiently fine. However, it is important to note the trend: the peak of heat absorption happens at the very tiny space (nearly point) close to the nozzle, while for the rest of the space the Q-distribution can be considered as uniform. This fact can be of importance if the effect ceiling of jet cooling is of interest in modelling spray-fire interaction, otherwise spray can be modelled as a point sink term in a one zone fire enclosure.

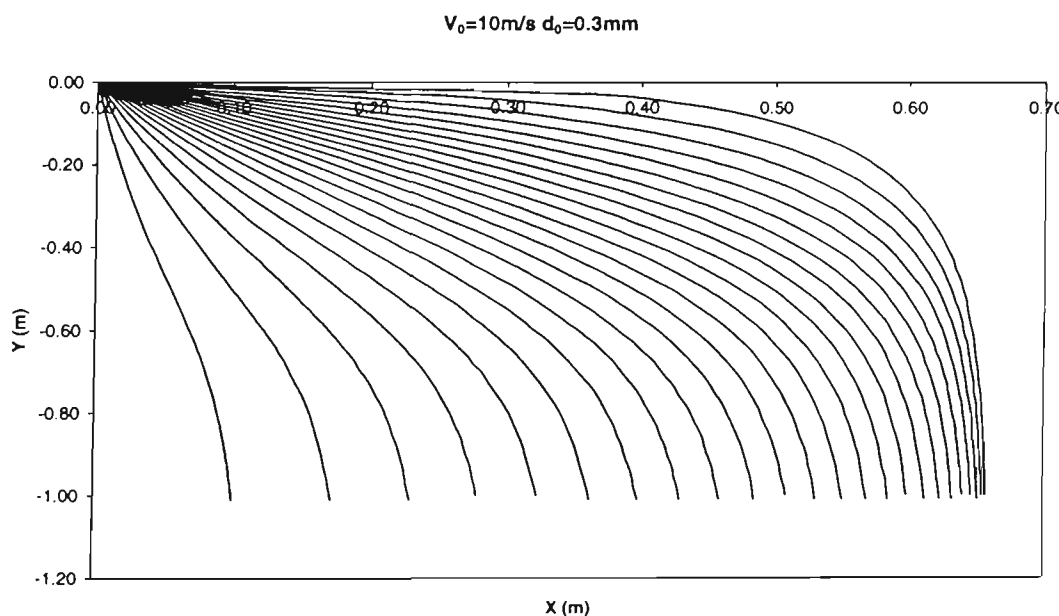


Figure 4.22. Droplet trajectories of 0.3 mm unconfined spray discharged with 10 m/s initial velocity in steady 400°C gas environment.

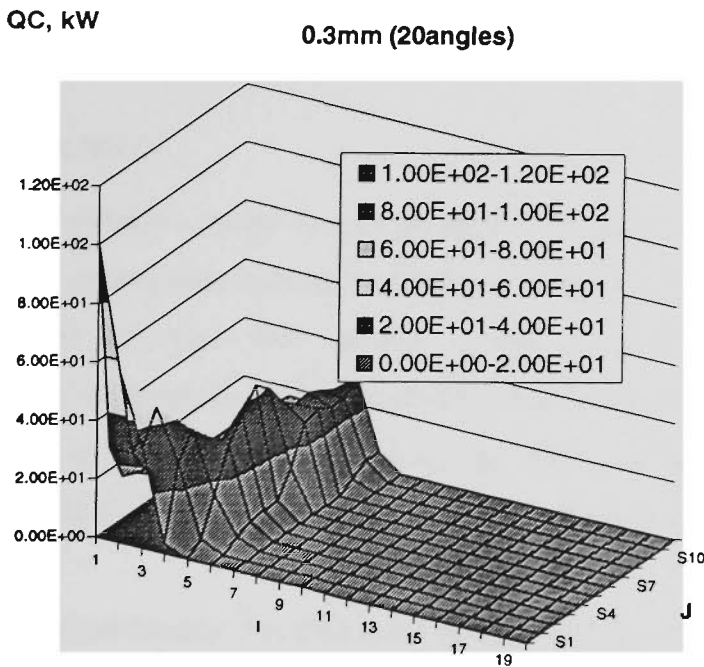


Figure 4.23. Heat absorption rate (kW) distribution along the ceiling (I) and across the hot layer (J) inside 400°C gas environment.

4.4.3 Conclusions - Mist Sprays

1. The sprays released under high surrounding temperatures can produce only a limited heat absorption rate. This limitation or “plateau” depends on total water flow rate. The lowest gas temperature at which this “plateau” occurs depends on droplet diameter or the level of evaporation rate.
2. The effect of droplet size on heat absorption during gas cooling is twice as important than the role of total spray flow rate at similar ambient conditions.
3. Droplet dynamics plays an important role in spray effectiveness. Thus, even though fine water mists are very effective in heat absorption, they still are not as effective in penetration and filling the space as coarser ones.
4. Heat absorption rate distribution is not totally uniform within the space occupied by the spray. However, it still can be modelled as a point sink term if the spray cone occupies most of the space of the fire enclosure.

5 SURFACE COOLING

5.1 INTRODUCTION

In the design of sprinkler systems, it is generally assumed that water spray can reach the fuel surface. The consequent interaction between water droplets and fuel surface, from fuel coverage to fuel cooling, then becomes one of the major mechanisms of fire extinguishment. Of the phenomena associated with such interaction, fuel cooling due to water impact has not been studied systematically in the literature. In the present Chapter, a model of fuel thermal behavior during fire before and after water application is presented.

5.1.1 Fire Extinguishment due to Fuel Cooling with Water

Although a number of works exists on fuel cooling during extinguishment, their scope is limited. There are experimental works in fire extinguishments using solid combustibles, that examine the effect of water delivered density [27, 114, 115] together with the effects of fuel type, orientation, configuration and distance from sprinkler [29]. In these works, the interaction between water droplets and hot fuel surface has not been studied. In the suppression of gas fires, on the other hand, the role of spray droplet diameter and velocity has been studied [30, 116, 42, 46]. In spite of these mostly experimental studies on fire suppression, little has been done to provide a theoretical background and a model for fuel cooling processes due to water application in a fire environment. One such attempt can be found in [117], where a simple model is developed for the spray cooling of a hot body with uniform temperature distribution in order to predict a water heat absorption rate. The model is based on experimental results for the spray cooling of a carbon steel plate. The surface temperature is taken to be at the Leidenfrost⁶ point [118], and the effects of spray properties are not studied. No account is given to real fuel properties, and the assumption of

⁶ As described in [118], “in 1756, Leidenfrost noted that small spherical droplets formed on a hot smooth iron spoon took a relatively long time to evaporate. He was the first scientist who started to investigate the film boiling of discrete masses. In his honor the stable film boiling of discrete masses is termed as the Leidenfrost phenomenon.”

Leidenfrost boiling which is associated with a critical heat flux level depending on the surface properties [119], is not justified.

In [56, 120], a comprehensive analysis is given of wood combustion in terms of temperature distribution inside fuel and external fire dynamics using CFD. The surface temperature history of wood is predicted during fire with no water application, and the numerical results are compared with the experimental results in [56]. These experimental and numerical results are compared with the present results with no sprinkler interaction in Section 5.3.

The model of [120] has been extended to include a sprinkler sub-model in [56]. In this combined model, a standard sprinkler sub-model is used for gas cooling. The surface cooling model is based on the assumption of complete water evaporation on top of a hot surface. The effect of incomplete evaporation is not accounted for, although the simplified model of [117] could have been used for this purpose. In [56], extinguishment is defined based on the decay of mass burning rate for different water application rates. Fuel temperature history are not shown, although cooling rate across a sample thickness is considered to be of the main importance in the extinguishment of charring combustibles, such as wood.

In [14], the extinguishment of plastic combustibles is discussed using the same simplification for sprinkler heat absorption rate as in [56], where complete water evaporation is assumed. In [121], similar to [56], thermal behaviour of fuel before and after sprinkler activation is not explicitly shown, although it is stated that for plastics, extinguishment is governed by fuel surface temperature. However, qualitative agreement is presented with experimental results in terms of critical water flow rate needed for suppression for different external heat fluxes applied to fuel.

5.1.2 Basic Surface Cooling

Several studies on surface cooling can be found in the literature. The fundamentals of heat transfer during evaporation and boiling of liquid on a heated surface were studied by

Kutateladze [122] in 1962. Another detailed description of surface cooling regimes, especially due to a spray which forms a shallow layer on top of the hot surface, can be found in [123]. The description and quantification of Leidenfrost phenomenon for dilute sprays with low Weber number (We) droplets resulting in droplets bouncing on the hot surface, is given in [124, 125]. The behaviour of thin liquid film caused by spray application with high We , is experimentally studied in [126]. The experimental and theoretical study of the behaviour of a single droplet on a heated surface can be found in [119, 127, 128].

The common feature of the works listed above is that the measurements related to boiling phenomena are usually taken on hot polished metal surfaces. Correlations for rough surfaces of low conductivity, such as plastics, wood, char or polyurethane (PU) foam, are uncommon. The influence of surface roughness on the occurrence of a particular boiling regime is studied in [139, 127], and the effect of surface thermal diffusivity is given in [128]. Although these correlations have been obtained in connection with different metal surfaces, they are utilised in the present thesis.

In the present study, water heat absorption in fuel cooling is studied in detail. Emphasis is given to fuel thermal behaviour before and after water application. Fire effect is simplistically accounted for by an external heat flux applied to the fuel surface. This part, along with Chapters 3 and 4, serves the development of an overall sprinkler performance model in terms of fire-sprinkler interaction. The present Chapter completes the sprinkler-fuel interaction part. However, the resulting model can be used as an independent sub-model either in a zone or CFD model of the fire environment.

In the following section, the possible mechanisms of surface cooling are covered first in a detailed description of the physical model. After this qualitative description, a quantitative analysis of spray cooling is presented in the following two subsections. The first subsection describes the droplet wetted area, and the second provides information on surface heat flux during water impact. The behaviour of hot solid fuel before and after water impact is then described by unsteady conduction. The final section before the conclusions presents the

Results and Discussion of this Chapter, incorporating the ideas of fire extinguishment due to fuel cooling with water as well as the basics of surface cooling. Comparisons with available experimental and numerical results are also given in this section.

5.2 MECHANISMS OF SURFACE COOLING

In the present study, fuel cooling is modelled as a one-dimensional unsteady heat conduction problem with boundary conditions specified by either incident radiative heat flux or convection. As a first step in understanding the local heat transfer mechanisms associated with fuel coverage by a water spray, the general classification of evaporation regimes is discussed next.

5.2.1 Physical model

Several studies exist on the evaporation of a single droplet or of liquid jets and films impacting on flat hot surfaces [122,119,127,128, 129]. The present investigation is limited to a shallow liquid layer of depth less than 10 mm [123], caused by a spray on top of a flat hot surface. Hence, the case of freely flowing liquid over a heated surface is being considered. Typical applications of such cases can be found in technological processes, such as quenching and cooling of cutting tools, where the surface may be wetted by a spray.

Generally, all cases of liquid impingement on a heated surface are covered by ordinary evaporation, nucleate (or bubblewise) boiling, transition and/or film boiling regimes [122, 123]. A sketch of these three possible spray cooling regimes is given in Figure 5.1. According to Kutateladze [122, p.375], the behavior of water droplets falling on a hot surface can be described as follows. When the temperature of the heated surface is below the liquid saturation temperature (liquid boiling point), droplets of liquid spread into a thin layer and evaporate slowly (Case 1). When the temperature of the heated surface is higher than the saturation or liquid boiling temperature, this temperature difference is referred as the surface superheat. In this case, until the surface heat flux exceeds some critical value, q_{\max} , nucleate boiling can be observed in the spreading liquid (Case 2). At heat flux values close to q_{\max} , transition to film boiling occurs. During film boiling, surface heat transfer is

sharply reduced due to the insulating effect of vapour interlayer produced by droplet evaporation from the lower droplet surface. The value of surface heat flux then decreases down to the value of q_{\min} , and the surface temperature reaches its maximum value or Leidenfrost point [118]. Between q_{\max} and q_{\min} , the falling liquid can either collect into spherical droplets which intermittently make contact with the surface during the entire period of evaporation (rebounding process – Case 3a), or the liquid forms a stable vapour interlayer causing total interruption of contact between droplets and surface (Case 3b). If heat flux drops below the value of q_{\min} , the transition from film boiling back to nucleate boiling can occur [130]. The summary of empirical equations for q_{\min} can be found in [130].

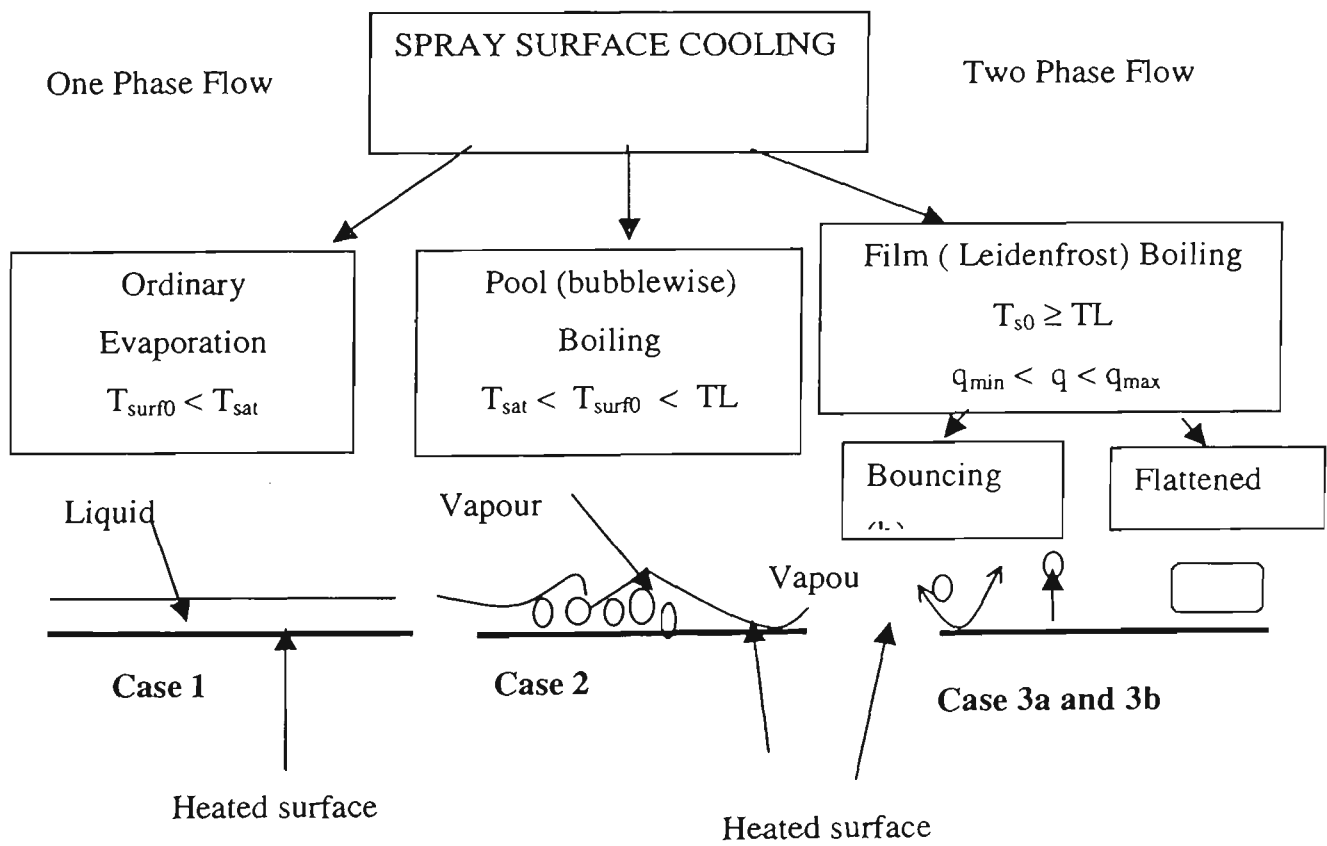


Figure 5-1. Regimes of heat transfer in a thin liquid layer due to droplets deposited on a hot surface of temperature $T_{\text{surf}0}$. T_{sat} is the saturation temperature under atmospheric conditions ($T_{\text{sat}} = 100^\circ\text{C}$ for water). q_0 is the heat flux corresponding to the beginning of boiling, TL is Leidenfrost point (around 200°C for water on metal plates [122, 127]). q_{\max} is the maximum heat flux corresponding to the occurrence of film or Leidenfrost boiling, and q_{\min} is the minimum heat flux corresponding to transition from film boiling back to nucleate boiling.

The magnitude of the Leidenfrost temperature, LT, or equivalently, the amount of heat flux corresponding to the maximum life time of droplets, depends on wettability and thermal diffusivity of a hot surface [128]. It also depends on whether the surface temperature changes in cooling or heating. In [128], experimental data on Leidenfrost temperature as a function of surface thermal diffusivity, α , are given. For surfaces with smaller diffusivities, the Leidenfrost temperature is higher. Thus, for carbon steel ($\alpha \sim 10^{-5} \text{ m}^2/\text{s}$, where α is thermal diffusivity, $\alpha = k/\rho C_p$), LT is about 200°C, while for stainless steel ($\alpha \sim 1.5 \times 10^{-6} \text{ m}^2/\text{s}$), it is 300°C in cooling and 280° for heating. Given that for most solid fuels (wood, plastics, foams), thermal diffusivity is about $10^{-7} \text{ m}^2/\text{s}$ [117, 135], even higher LT values are expected.

The typical behaviour of water droplets on a hot metal surface is illustrated in Figure 5.2 taken from Figure 122 of [122]. This figure represents the lifetime, or the evaporation time, of a water droplet of 0.0465 cm^3 in volume (or 2.23 mm in radius), as a function of the surface temperature of a polished metal plate. The minimum corresponds to intensive nucleate boiling occurring at a certain surface superheat above the saturation temperature ($\Delta T_s \sim 50\text{-}60^\circ\text{C}$). With further temperature rise, the evaporation rate slows down, and at a surface temperature of about 225°C, the deposited droplet shows a maximum life time, corresponding to Leidenfrost boiling. The presence of such a maximum is independent of the surface properties [118, 122, 123, 127] as well as of the initial droplet diameter [119, 122]. During the period of Leidenfrost boiling, the thickness of liquid layer remains practically constant [122].

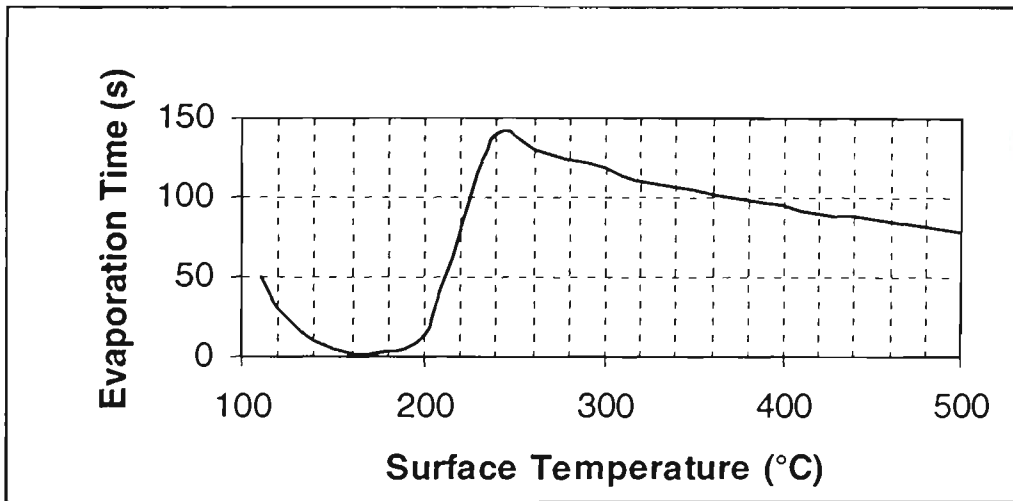


Figure 5.2 Time of evaporation of a droplet of 0.0465 cm^3 volume as a function of surface temperature [122, p.375].

In Table 5.1, the values given in Figure 5.2 are converted into data commonly used to quantify spray cooling regimes. In this table, droplet evaporation rate, m_{ev} , has been calculated as the ratio of the droplet mass to total evaporation time. Heat flux absorbed by the droplet, q_w , is calculated as m_{ev} multiplied by the latent heat of vaporization and divided by the droplet base area taken as πr^2 . In the table, m_{ev} in kg/s is converted to an evaporative density, D_{ev} , in mm/min by using the droplet base area. D_{ev} allows comparison with a standard delivered density of about 2.5 mm/min. As seen in Table 5.1, if the surface temperature is between 110 and 220° C, nucleate boiling, more than 2.5 mm/min of delivered density is required to allow enough water deposit on the surface for evaporation. At a surface temperature of 160° C, the surface heat flux reaches its maximum value of about 3.7 MW/m². This point is also the peak of intensive nucleate boiling with minimum droplet life time of around 2 seconds. When the surface temperature is high enough to cause stable film boiling, at about 240° C, the surface heat flux reduces to its minimum value of 0.053 MW/m². At this point, the droplet life-time rises to its maximum value of 140 seconds.

Table 5.1 The single droplet evaporation characteristics obtained from Figure 5.2.

Surface Temperature (°C)	Evaporation Time (s)	$m_{ev}/\pi r^2$ kg/(sm ²)	D _{ev} (mm/min)	q _w (kW/m ²)
110	50	0.0595	3.572	148.82
120	30	0.0992	5.953	248.03
140	10	0.2976	17.858	744.10
160	2	1.4882	89.292	3720.52
180	3	0.9921	59.528	2480.35
200	13	0.2290	13.737	572.39
220	80	0.0372	2.232	93.01
240	140	0.0213	1.276	53.15
260	130	0.0229	1.374	57.24
280	123	0.0242	1.452	60.50
300	118	0.0252	1.513	63.06
320	110	0.0271	1.623	67.65
340	107	0.0278	1.669	69.54
360	102	0.0292	1.751	72.95
380	98	0.0304	1.822	75.93
400	95	0.0313	1.880	78.33
420	90	0.0331	1.984	82.68
440	88	0.0338	2.029	84.56
460	85	0.0350	2.101	87.54
480	81	0.0367	2.205	91.86
500	79	0.0377	2.261	94.19

5.3 QUANTITATIVE DESCRIPTION OF SPRAY COOLING

5.3.1 Wetted area

The radius of wetted area, or as it is often called, projected base area, is an important parameter in heat transfer considerations [128, 129]. Specifically, in the case of low density sprays when a limited number of droplets reach the surface, to cover it gradually before flooding, the radius of wetted area needs to be considered. The limited amount of data

found in the literature relate usually to particular types of surfaces or temperature ranges, and this information is summarized below.

The radius of wetted area, R , non-dimensionalised with the undeformed sphere radius, R_0 , of equivalent initial liquid volume, will give the wetting parameter, $\beta = R/R_0$. R depends on surface temperature, roughness, contact angle (shown by θ in Figure 5.3) and the speed of droplet deposition. Thus, for sprayed water, β can be of order up to 4.5 [129] at the near-saturation surface temperature prior to nucleate boiling of about 100° C. For droplets “softly” [129] deposited on a surface, i.e. from a height less than 1 cm, the value of β is in the range of 1.2 to 1.5. It is also reported in [129] that the radius of the wetted area is constant through most (90 to 95%) of the total evaporation time. Figure 5.3 shows the relationship between the radius of a spherical droplet, R_0 , before it impacts a solid surface and the droplet base area radius, R , after deposition. Figure 5.3 has been generated from Figure 1 of Reference [129].

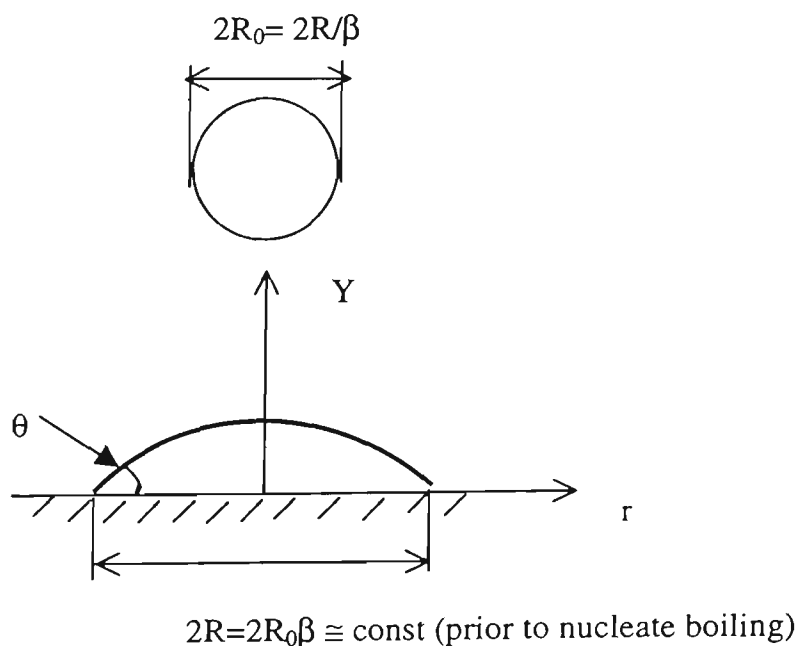


Figure 5.3. Lens-shaped [131] deposited droplet on top of a flat surface. θ is the droplet contact angle. R is the initial radius of the base area. Reproduced from Figure 1 of [129].

In [131], water droplet evaporation is studied at a low surface overheat, ΔT_s , of about 30° C to 100° C above saturation temperature, leading to nucleate boiling. It is shown that the time averaged wetted area, $(\pi R^2)_{av}$, is approximately half of the initial droplet base area (πR^2). The droplets discussed in [131] are of sufficiently low Weber number, and hence, they do not break when they hit the solid surface. Given that for most practical cases, β is not exactly defined, and taking into account the reduction of R during evaporation, the base projected area is taken as $\pi R_0^2 (\beta = 1)$ in the present study.

The volume, V , of lens-shaped droplets deposited on the surface with a constant contact angle, θ , can be determined as follows:

$$V = \frac{\pi}{3} R^3 F(\theta), \text{ where} \\ F(\theta) = \frac{(1 - \cos \theta)^2 (2 + \cos \theta)}{\sin^2 \theta} \quad (5.1)$$

Equation (5.1) is utilised in the present heat transfer calculations, as explained in Section 5.3.2.

5.3.2 Surface Heat Flux

In order to understand, and consequently, quantify the local heat transfer mechanisms that follow fuel coverage by water spray in fire, the three cases given in Figure 5.1 are re-visited below.

Case 1: One-Phase Heat Transfer

When water temperature does not exceed T_{sat} , the resulting one-phase heat transfer is governed by conduction through the water layer, although negligible convection can also exist. The water film is considered completely transparent to radiation energy in the present model. The surface heat flux is calculated using the following equation:

$$q_w = k_w(T_s - T_w)/D \quad (5.2)$$

where k_w is the water conductivity, T_s and T_w are the surface and bulk water temperature, respectively. In other words, $(T_s - T_w)$ is a surface superheat, ΔT_s . D is the water characteristic length. In the case of drop-wise wetting, $D = 2R$, and the value of R can be calculated by equating the volume of a deposited droplet given by Equation (5.1) to the volume of a non-deformed spherical droplet ($4\pi R_0^3/3$). In the case of flooding of flat surfaces, D is taken as water film thickness which depends on the water flow Reynolds number, and consequently, on temperature through water viscosity [132].

Case 2 and Case 3a: Wetting Regime

If the water temperature exceeds T_{sat} , one of the three boiling regimes can occur, corresponding to Cases 2, 3a and 3b. Comparison between actual surface heat flux and the critical heat flux, q_{max} , identifies the regime, as indicated in Figure 5.1. The following formula suggested in [98] for fully wetted regime in surface cooling can be used for this purpose:

$$q_{max} = \frac{\pi}{24} \rho_v^{1/2} L [\sigma g (\rho_l - \rho_v)]^{1/4} \quad (5.3)$$

where ρ_l and ρ_v are the liquid and vapour densities, respectively; σ the surface tension between water and vapour, and L is the latent heat of vaporization. For water, q_{max} is typically $1.1 \times 10^6 \text{ W/m}^2$.

On the other hand, the value of time-averaged heat flux absorbed by a single water droplet in the transition region can be estimated by using the empirical expression given in [127]:

$$q_w = 770 \times \Delta T_s^{2.78} \quad (5.4)$$

where ΔT_s is the surface superheated above liquid boiling temperature. Equation (5.4) is obtained for smooth metal plates, and it can overestimate the values of heat flux for rough surfaces with low values of $k_p C_p$ [127]. Equation (5.4) has been found to compare favorably with the experimental data of Kutateladze [122] given in Table 5.1.

If the calculated value of heat flux from Equation (5.4) exceeds q_{\max} from Equation (5.3), then the system must be operating in the film boiling regime. In the present calculations, Equation (5.4) is applied to determine the onset of a specific regime in fuel cooling because of lack of specific experimental data for the surfaces of low thermal diffusivities and high roughness. Thus, for example, for water coming on top of solid combustible surfaces of about 400°C [58], corresponding to pyrolysis for most such surfaces, q_w is about 5×10^9 W/m², and Leidenfrost or film boiling (Case 3) can be expected more than nucleate boiling (Case 2).

When $q_w > q_{\max}$, in film boiling, Cases 3a and 3b, Equation 5.4 is not valid. Instead, the time averaged heat flux can be calculated using a semi-empirical equation [128] obtained for a wide range of temperatures (80-450°C) and materials:

$$q_w = \frac{1.5}{\tau} \times \frac{\rho_l L}{1.813} \times 3V_0^{1.3} \quad (5.5)$$

where the total evaporation time, τ , is defined as follows:

$$\tau = \frac{\rho_l L}{1.1 \times 1.813} \times \left(\frac{\mu_v}{k_v \rho_l \rho_v L^* g} \right)^{1/4} \times \Delta T_{sat}^{-3/4} \times \frac{12}{5} V_0^{5/12}$$

and the reduced latent heat of evaporation, L^* , is:

$$L^* = L \left[1 + (7/20) C_{pv} (\Delta T_{sat} / L) \right]^3$$

where L is the latent heat of evaporation; ρ_v , μ_v , k_v and C_{pv} are the density, viscosity, thermal conductivity and constant pressure specific heat of steam, respectively. ρ_l is the density of water. ΔT_{sat} is the surface superheat above water saturation temperature. V_0 is the initial droplet volume.

In [128], experimental results are shown to be in a good agreement with Equation (5.5). With this equation, a heat flux of about 10×10^6 kW/m² can be calculated for a ΔT_{sat} of

300°. The distinction between Cases 3a and 3b depends on the surface superheat, the normal velocity component of droplets approaching the surface and surface roughness.

Case 3b: Bouncing Droplets

The dynamic Leidenfrost phenomenon, or film boiling with bouncing droplets, described earlier in Section 5.1, is often referred in the literature in connection with spray cooling of hot metal (smooth) surfaces [118, 117]. The recent investigation of Buyevich [124], showed that the position of the maximum in Figure 5.1 depends on surface roughness and the normal component of droplet approach velocity. This maximum evaporation tir (5.6) corresponds to the surface superheat that leads to the establishment of stable film boiling. It was also shown [124] that the magnitude of the repulsive force generated by an excessive vapour pressure is a function either of the surface superheat if the droplet size and normal velocity are maintained constant, or of the droplet fall velocity for the same surface overheat, for a given surface. The theoretical study in [124] of bouncing droplets led to the following expression for the critical impact velocity of a droplet as a function of the surface superheat and wall roughness for a given droplet size:

$$u_{cr0} = \left[\frac{3\nu_v k_v R_0 \Delta T}{2\rho_l L \delta^3} \right]^{1/2} \quad (5.6)$$

where ν_v and k_v are vapour kinematic viscosity and conductivity, respectively; ρ_l is liquid density; δ is wall surface roughness, L is the latent heat of evaporation, ΔT is surface overheat above saturation temperature, and R_0 is the droplet initial radius. If droplet impact velocity, u_0 , does not exceed this critical value, u_{cr0} , then droplets will bounce on the vapour cushion. The droplets with impact velocities more than the critical value will be collected at the surface.

Alternatively, Buyevich [124], provided an expression for the dynamic Leidenfrost temperature of droplets with a constant diameter and velocity. If the surface temperature exceeds this critical amount, then droplets bounce off of the surface:

$$T_L \approx T_s + 0.65 \frac{\rho_l L u_0^2 \delta^3}{\nu_v k_v R_0} \quad (5.7)$$

Equations (5.6) and (5.7) were obtained with the assumption of dilute spray or low droplet concentration in the vicinity of the surface. Another limitation of the model proposed in [124] is that the droplet temperature as it approaches the surface coincides with liquid boiling temperature. Therefore, in reality, the value of T_L for subcooled water (water temperature lower than liquid boiling temperature) can be higher and critical velocity smaller than predicted by Equations (5.7) and (5.6), respectively.

In this study, it is assumed that most burnt surfaces would be rough, with a δ of about 50-100 μm . It is further assumed that most of the sprayed droplets are likely to be captured by such a surface, provided that the wetted mode falls into either Case 2 or 3b of Figure 5.1**Error! Reference source not found.**, depending on heat flux. In addition to expecting high roughnesses for most solid fuel materials, low droplet We numbers, or terminal velocities, are also expected, contributing further to the wetting mode rather than the bouncing regime. In addition, if the surface is large enough, even the bouncing droplets are expected to be captured.

5.4 FUEL BEHAVIOUR: UNSTEADY CONDUCTION

The conservation of energy within a solid substance can be expressed by the heat conduction equation [98]. For a semi-infinite body (one with much larger longitudinal dimensions than the transverse ones), the one-dimensional transient thermal conduction equation is written in the following form:

$$\rho \ C_p \ \frac{\partial T}{\partial t} = k \ \frac{\partial^2 T}{\partial x^2} + q_G \quad 0 \leq x \leq \delta \quad (5.8)$$

where ρ , C_p and k are the fuel density, specific heat and thermal conductivity, respectively. q_G is the internal energy generation per unit volume inside the control volume. T and δ are the material temperature and thickness, respectively. The combination $\alpha = k/\rho C_p$ is earlier referred to as thermal diffusivity. Since heat generation or sink terms are not considered, $q_G = 0$. The boundary conditions are written as follows:

$$-k \frac{dT}{dx} \Big|_{x=0} = q_{in} \quad \text{and} \quad -k \frac{dT}{dx} \Big|_{x=R} = 0 \quad (5.8a)$$

where q_{in} is the resulting incident heat flux at the top material surface ($x = 0$), and the bottom surface ($x = R$) is considered to be adiabatic. Similar one dimensional treatment was found satisfactory by Novozhilov *et al.* [105, 120] in modelling of wood combustion.

Considering the fuel as a semi-infinite plate, Equation (5.8) can be solved numerically with appropriate initial and boundary conditions. With a control volume approach, dividing the domain $0 \leq x \leq \delta$ into $N-1$ equal segments of width $\Delta x = \delta/(N-1)$, and with a time step of $\Delta t = t_{m+1} - t_m$, Equation (5.8) can be written in an explicit final difference form as follows [98]:

$$T_{i,m+1} = T_{i,m} + Fo(T_{i+1,m} - 2T_{i,m} + T_{i-1,m}) \quad 2 \leq i \leq N \quad (5.9)$$

where Fo is the Fourier number, $Fo = \Delta t \alpha / \Delta x^2$, and $T_{i,m} \equiv T_{i,\text{old}}$ and $T_{i,m+1} \equiv T_{i,\text{new}}$, where old and new refer to the previous and present time steps, respectively. The initial condition corresponds to a uniform temperature T_0 at all nodes, usually taken as 20°C :

$$T_{i,1} = T_0 \quad 1 \leq i \leq N, m = 1. \quad (5.10a)$$

For fuel exposed to external heat flux, the explicit boundary conditions are as follows:

$$T_{1,m+1} = T_{1,m} + [2\Delta t / (\rho C_p \Delta x)](q_{in} + k(T_{2,m} - T_{1,m})\Delta x) \quad \text{and} \quad T_{N,m+1} = T_0 \quad (5.10b)$$

The solution of the system of explicit equations (5.9) and (5.10) is straightforward. However, there is a limitation on the time step [98]:

$$\Delta t < \Delta x^2 / 2\alpha \quad \text{or} \quad Fo < 0.5 \quad (5.11)$$

As indicated by Equation (5.8a), or equivalently by Equation (5.10b), the fuel surface temperature is governed by the external heat flux, q_{in} . In this study, the external heat flux is

taken to be heat release rate per unit area, $q_{in} = q_{fire}$. Expressing q_{fire} as a function of time for a medium-size fire [133], the external heat flux becomes,

$$q_{in} = q_{fire} = 0.0117t^2 \quad (5.12)$$

where q_{fire} is in kW/m^2 , t is in seconds.

5.5 RESULTS AND DISCUSSION

5.5.1 Before Water Application

The heat flux history corresponding to Equation (5.12) is plotted in Figure 5.4. With this external heat flux, Equations (5.9) and (5.10) were solved for a PU (polyurethane) slab of 0.1 m thickness, divided into 20 equally spaced nodes. The properties used in the calculations for PU foam were taken as follows: $\rho = 29 \text{ kg/m}^3$, $C_p = 1.3 \text{ kJ/(kgK)}$ [32], and $\alpha = 1.2 \times 10^{-6} \text{ m}^2/\text{s}$. Sample temperature histories across the slab are plotted in Figure 5.5. The heat loss from fuel surface due to radiation and convection is not accounted for in this calculation. The constant surface temperature of 400°C corresponds to the known phase transition (pyrolysis) of PU at this level. Lack of detailed experimental data in fuel heating during fire does not allow validation of the results presented in Figure 5.5. Limited comparison is given next with two different sets of available data.

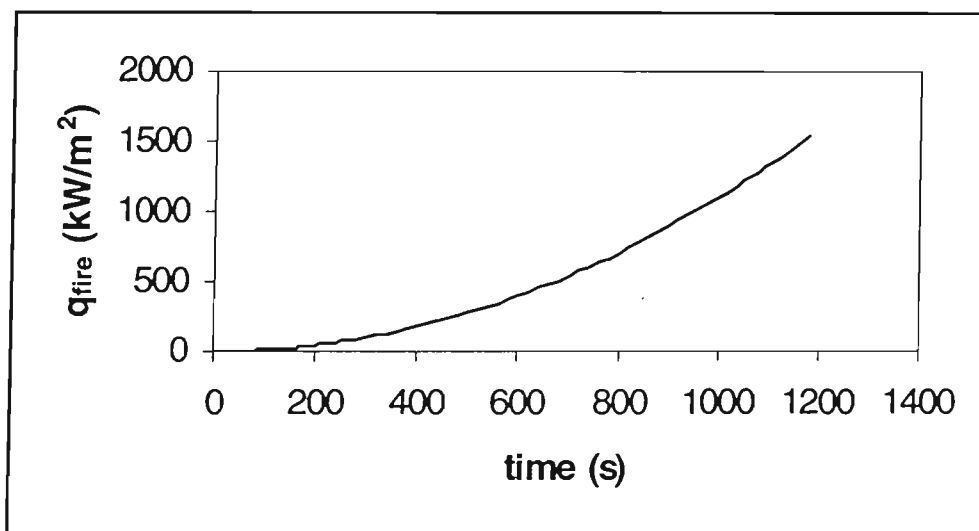


Figure 5.4. Medium fire heat flux history

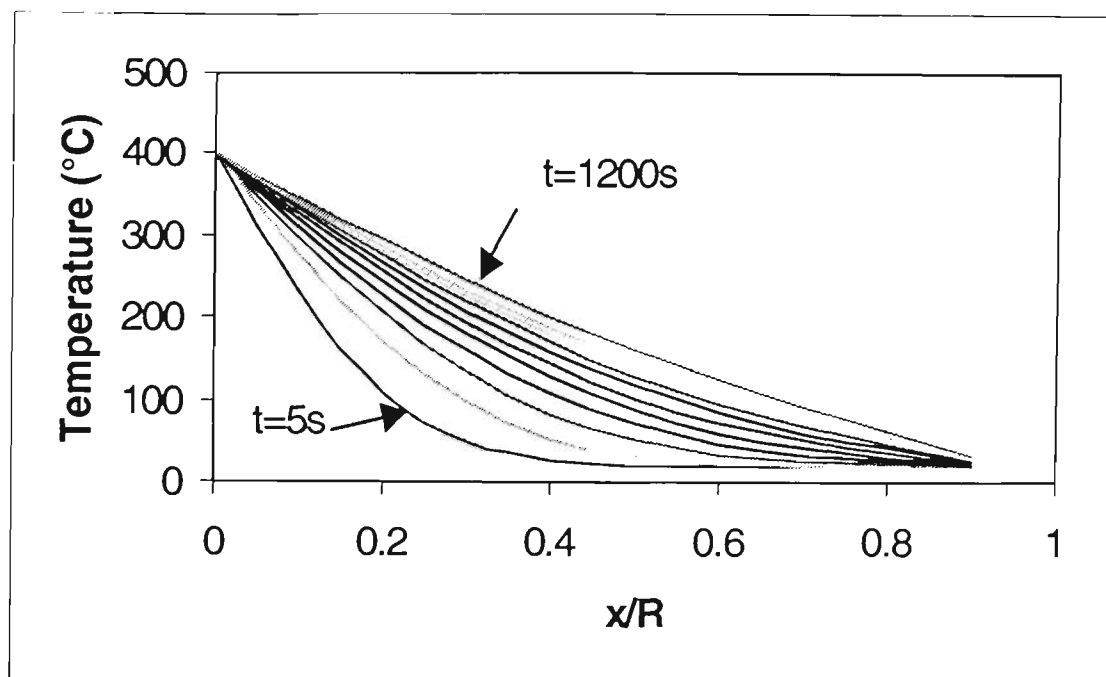


Figure 5.5. Temperature profile history in a PU slab across the non-dimensional depth x/R ($R=0.1m$). Each curve corresponds to a different time starting at 5 s with a time step 100 s.

In Figures 5.6 and 5.7, comparisons are shown of the present numerical results with the experimental results from [120] and with the present experimental results, respectively. For the experimental results given in Figure 5.6, a rectangular vertically oriented piece of wood (particle board) was exposed to a constant surface radiant heat flux [120] of 31 kW/m^2 during a small scale experiment. The following properties needed for the calculations are taken from [120]: $\rho = 663 \text{ kg/m}^3$; $C_p = 2.52 \text{ kJ/(kgK)}$, and $\alpha = 7.5 \times 10^{-8} \text{ m}^2/\text{s}$. The symbols in Figure 5.6 represent the surface temperature history. The solid line in Figure 5.6 represents the present calculations. The incident surface heat flux q_{in} in Equation (5.8a) has been taken as follows:

$$q_{in} = q_{fire} - q_{irad} - q_c \quad (5.13)$$

where q_{fire} is the constant radiative heat flux applied to the wood surface, taken as 31 kW/m^2 . q_{irad} is the gray body Boltzman irradiation from hot fuel surface to the surroundings, and q_c is the convective heat loss from the heated surface to ambient gas. q_{irad} is calculated with fuel emissivity taken as 0.9 [120].

For q_c , the convective heat transfer coefficient, h , has been calculated based on an empirical correlation for the Nusselt number as a function of the Grashoff and Prandtl (Gr,Pr) numbers: $Nu = C_1(GrPr)^n$ [58, p.56], where the coefficients C_1 and n depend on the value of product ($Gr \times Pr$). Thus, for $(Gr \times Pr) < 10^9$ $C_1=0.59$ and $n= 0.25$, for $(Gr \times Pr) > 10^9$ $C_1=0.13$ and $n= 0.33$. Then, $h = Nu k_{air} /D$, where k_{air} is the air conductivity, D is the sample characteristic length generally equal to the ratio of the surface area to surface perimeter. The calculated values of the average heat transfer coefficient, h , did not exceed 10 $W/(m^2 \cdot ^\circ C)$ for the range of plate temperatures up to $600^\circ C$. Hence, the effect of convection (both heating and cooling) was considered to be negligible. The calculated surface temperature history is plotted in Figure 5.6 shown by a solid line.

In Figure 5.6, the present numerical results are in closer agreement with the experimental results than those obtained in [120] using CFD modelling. The predicted temperature history approaches steady state due to the balance between the absorbed heat and heat loss, although in the modelling of wood combustion, unlike PU, there is no limitation of a constant surface temperature corresponding to pyrolysis. Wood external surface chars, and it remains exposed to fire. The difference between the present prediction and experimental results can be explained by the possible change in wood properties during charring which are not taken into account in the present model.

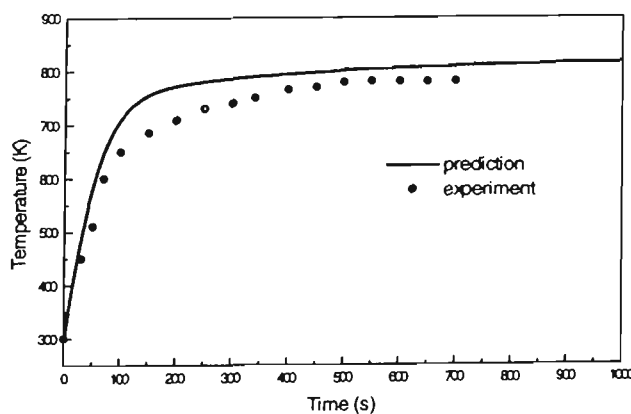


Figure 5.6. Comparison between predicted and experimental wood surface temperature histories. Wood is exposed to a constant external heat flux of $31 kW/m^2$ [120].

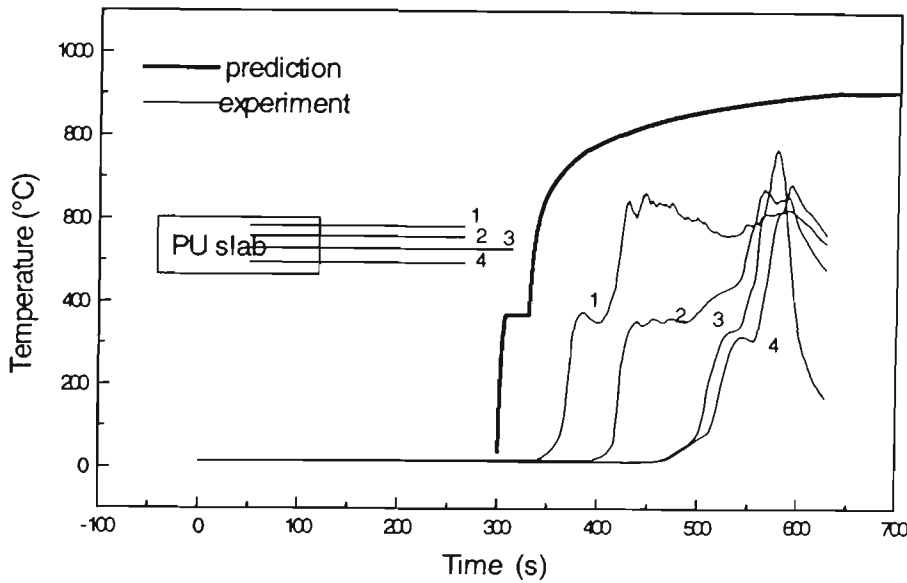


Figure 5.7. Time-temperature curves recorded during a flashover fire by 4 k-type thermocouples imbedded in a PU-slab [110]. Each curve corresponds to a different depth inside the PU-slab. The predicted surface temperature is given as a solid thick line.

In Figure 5.7, experimental datum are presented for a PU slab of $1 \times 1 \times 0.1 \text{ m}^3$ during a full scale fire test run at CESARE (Centre for Environmental Safety and Risk Engineering) of VU (Victoria University). Four k-type 0.5 mm thermocouples were inserted into the PU slab at equal distances along the depth as shown schematically in Figure 5.7. The first thermocouple was placed about 2 cm below the top surface. The thermocouples were not shielded. Further description of the experimental setup can be found in [110].

In the model, a constant heat flux was applied to the burning surface. The reason for this assumption is that by the time the first 2-cm depth of the PU slab burnt out to expose the first thermocouple, in about 300 s from the ignition, the fire had already reached a quasi-steady state. Consequently, the fuel was exposed to a constant heat flux. This value was taken to be 9 kW/m^2 in the present calculations, corresponding to the critical flux needed for the ignition of PU [134]. Unlike wood, all plastics and PU [58,121] are known to burn at a constant surface temperature in the region of 270 to 370°C during pyrolysis. Thus, in the model, as indicated in relation to Figure 5.5, when the PU surface reaches a pyrolysis

temperature of about 400°C , it is kept constant until the upper layer burns out. Further thermal degradation of material has not been modeled. The calculated surface temperature history is qualitatively similar to the experimental behavior.

A further comparative analysis is given in Figure 5.8 of wooden and PU slabs' surface temperature behavior in a t^2 -fire. The curves reflect the well known fact that to ignite wood by the same amount of heat flux as PU would take longer.

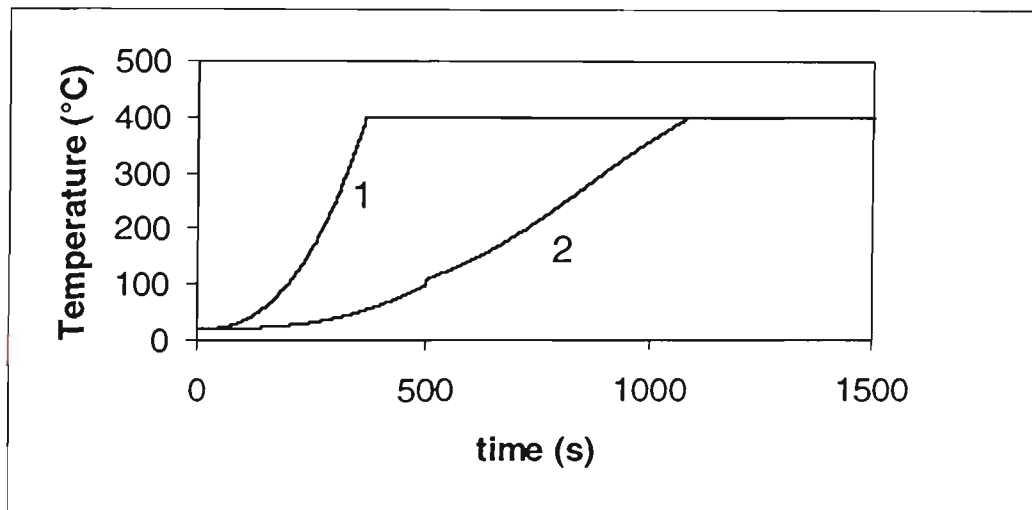


Figure 5.8. Surface temperature histories for PU (curve 1) and wooden (curve 2) 0.1m thickness slabs during t^2 fire without sprinkler activation.

It should be added here that Equation (5.8) is valid until the fuel temperature reaches the pyrolysis point, T_{pyr} . Then, an additional heat sink term will appear in Equation (5.8) due to the latent heat of pyrolysis ($q_{\text{in}} = q_{\text{fire}} - q_{\text{pyr}}$), and the fuel depth, R , will no longer be constant. From this point, the surface temperature remains constant in the present calculations, but no consideration to fuel surface degradation is given.

5.5.2 After Water Application

With water applied on top of the fuel during the fire, the term q_{in} in Equation (5.8a) will change to include water heat absorption rate per unit area, q_w .

$$q_{\text{in}} = q'_{\text{fire}} - q_w \quad (5.14)$$

where q_w takes one of the values described by Equations (5.2), (5.4) or (5.5) depending on the cooling regime established, as described in relation to Figure 4.1. The heat flux from fire, q'_{fire} is also weakened by the water film due to radiant energy absorption. q'_{fire} may be expressed by:

$$q'_{fire} = q_{fire}(1-e^{-kx}) \quad (5.15)$$

where k is the absorption coefficient, x is the distance of penetration into medium, and q_{fire} is the radiant heat flux at $x = 0$. Equation (5.15) is similar to the radiation term in Equation (4.3) with the subsequent discussion concerning k . Due to the uncertainties in evaluating k and penetration length, the water film is considered here to be completely transparent to radiation energy and heated only by conduction, as governed by Equation (5.2).

In the present model, the choice of cooling regime is determined based on the water temperature which changes according to the following heat balance:

$$T_w^{(new)} = T_w^{(old)} + q_w/C_{pw}/DD \quad (5.16)$$

where T_w is the bulk water temperature and the DD is delivered density of water spray in $\text{kg}/(\text{sm}^2)$. Depending on the bulk water temperature, the cooling regime and consequently, q_w , are determined as described next.

If $T_w > T_{sat}$, then, one of the two boiling regimes is present. Hence, q_w is calculated using either Equation (5.4) or Equation (5.5) depending on q_{max} produced by the surface. When T_w reaches T_{sat} , it is kept constant till all water evaporates [127]. If $T_w < T_{sat}$, then, one-phase heat transfer is present. Hence, q_w is calculated using Equation (5.2).

The results of surface temperature behaviour for different types of fuel after sprinkler activation are shown in Figure 5.9. In this figure, water is applied when the fuel surface reaches 400°C for both wood and PU. The surface temperature drops immediately at the time of contact, and then, it starts to rise slowly since external heat flux is still acting on the

fuel through the transparent water film. The incident heat flux for both wood and PU is the t^2 -fire given in Equation (5.12).

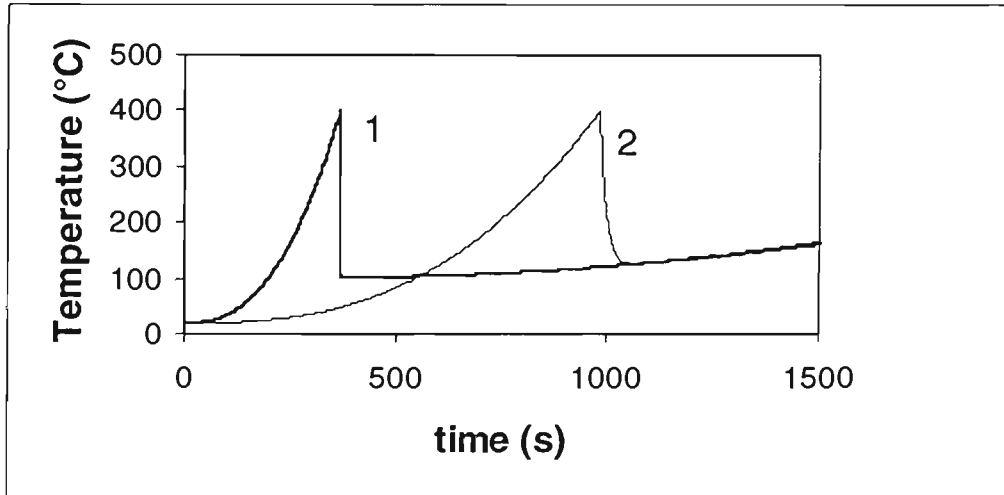


Figure 5.9. Surface temperature histories during continuous water application on top of burning fuel for PU (curve 1) and wood (curve 2). A sprinkler of delivered density 3 mm/min is activated when surface temperature reaches 400°C.

In Figure 5.10, the case of one-shot water application is shown when the fuel temperature reaches 400°C. This case can correspond to an on/off sprinkler application. The results in Figure 5.10 correspond to a t^2 -fire. In this figure, the PU curve exhibits a plateau at 100°C for a while, approximately 400 s, until the water layer totally evaporates. In the case of wood, this plateau is almost non-existent. Of the two, wood has a thermal diffusivity about an order of magnitude lower than that of PU. Consequently, it takes longer for wood to reach 400°C compared to PU. As such, at the moment of water application to the wood, the incident heat flux is greater in comparison to the PU. This can be seen in the figure by different evaporation times: for wood (right after sprinkler activation) all water evaporates within a few time steps, in about 0.5 s.

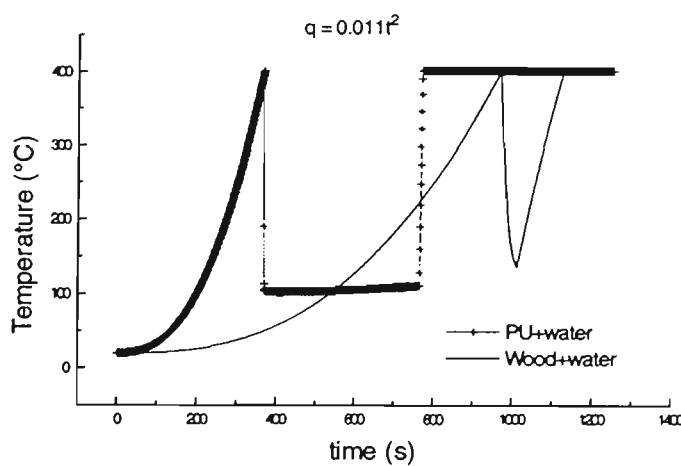


Figure 5.10. Surface temperature history with fully interrupted water application on top of burning fuel for PU and wood of 0.1-m thickness slabs. Applied heat flux is the t^2 -fire.

5.5.2.1 Critical water flux

In connection with extinguishment, the critical water flux or DD (delivered density) refers to the volume flow rate when either visible flames disappears in experiments or mass burning rate totally decays in simulations [121]. In the present model, the critical water flux is calculated as the minimum flux below which all droplets on top of fuel within a time step will evaporate faster than the rate of surface coverage. For this purpose, the following procedure is applied starting from the moment of water application. The time to evaporate all droplets, TT1, is calculated as follows:

$$TT1 = WW/(m_{ev}A_f), \quad (5.16)$$

where A_f is the exposed fuel area, and WW is the total droplet mass on top of fuel. $WW = N\text{Vol}_1\rho_1$, where Vol_1 is the volume of a single deposited droplet, N is the maximum droplet number on top of fuel surface with the assumption that droplets cover the surface by one layer equal to A_f/A_1 , where A_1 is the single droplet area. m_{ev} is the mass flow rate of evaporation of droplets calculated based on q_w at a given time and equal to q_w/L , and L is the latent heat of evaporation.

The time to cover the whole surface, TT2, is equal to the $A_f/(A_1N)$ where N is the droplet number flow rate (1/s). The critical water flux corresponds to the case when TT1 becomes

less than TT2. In this case, the water layer evaporates before it is renewed, and the fuel surface temperature quickly rises as there is no water on top. Hence, the value of critical water flux varies linearly with applied heat flux, as described next. A similar variation has been shown in [121]. The critical water flux depends on fuel type, in addition to heat flux.

The critical water flux calculated with the present model for a wooden slab is presented in Figure 5.11. This result can not be compared quantitatively with the experimental values summarised in [121], since no values for external radiation are given. However, most of the experimental values for wood are listed in the range of 1.2 to 3.8 g/(sm²) in Table 2 of [121], of about the same order as the predicted values in Figure 5.11.

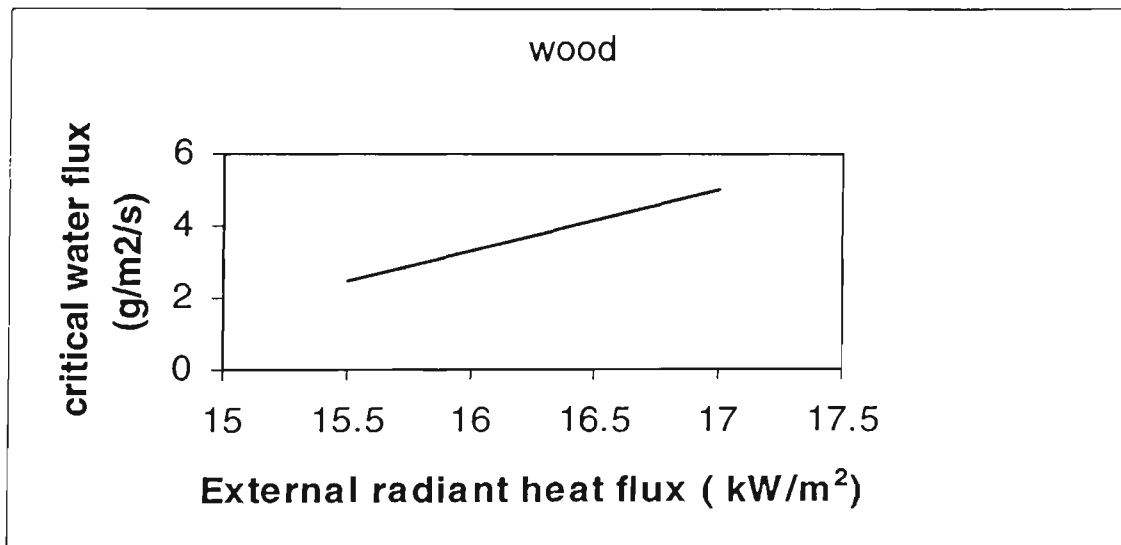


Figure 5.11. Calculated critical water fluxes for a wooden slab exposed to different levels of radiant flux.

Similarly, the experimental results of Unoki [70] indicate values in the range of 3.17 – 7.02 g/(sm²) for wooden pallets. As indicated in Figure 5.11, if the external heat flux increases as a function of time, then, the critical water application rate depends on the time of sprinkler activation. When water flux is above the critical value, the surface temperature remains below the boiling point regardless of water flux magnitude, in agreement with [121].

5.6 CONCLUSIONS

Fuel thermal behaviour prior to pyrolysis has been investigated as a transient heat conduction problem with boundary conditions specified by the radiant heat flux due to fire with and without water on the surface. The water film on the fuel surface is considered transparent for external radiation. The following conclusions can be drawn:

1. The heat absorbed by water impinging on hot ($T > T_{sat}$) fuel surface depends on the boiling regime which occurs after contact with the surface. This regime is defined by the surface temperature overheat above T_{sat} . The resulting evaporation rate defines the critical water flux.
2. The critical water flux corresponding to the amount of water needed for complete fuel coverage, depends on the value of external heat flux and fuel properties.
3. Further experiments in fuel cooling during fire, providing surface temperature histories, are needed.

6 INTEGRATION OF SPRAY COOLING MODEL WITH NRCC-VUT ZONE MODEL

A quasi-steady two-dimensional spray-cooling model has been developed based on the fundamental heat and mass balance equations written for water droplets and hot gas flow induced by a compartment fire. This model is described in Chapters 3 to 5. After verifying the capabilities of the model as outlined in these chapters, it has been used to simulate fire suppression within a compartment. For this purpose, the model has been integrated with the NRCC-VUT (National Research Council, Canada – Victoria University of Technology) one-layer zone model, FGM (Fire Growth Model), and transient fire-sprinkler interaction has been simulated with the combined code. The zone model was needed for the simulation of a realistic fire environment. The combined code allows to evaluate the contribution of two of the suppression mechanisms, namely, gas cooling and fuel coverage in terms of different spray characteristics.

6.1 INTRODUCTION

Many studies have been conducted to investigate large droplet and mist sprinkler performance during fire extinguishment. Experimental studies include full-scale [25, 31, 70, 135] and small-scale [29] fire suppression experiments where single or multiple fire parameters, such as temperature, heat release rate, oxygen concentration and visible flame extinguishment, have been registered versus varied sprinkler characteristics, such as water flow rate, droplet diameter and discharge angle, to evaluate sprinkler effectiveness. The conclusions generally relate to rooms of a certain size, ventilation conditions, fuel type and configuration and a fixed way of water application.

In practice, depending on specified class of occupancy hazard and floor area, standard sprinklers are designed to provide a certain prescribed minimum water application rate over a specified area. This approach is called the Area/Density Method [136], and it can be safely applied only to sprinklers and fire scenarios which are similar to the testing procedure. In this method, all calculations and measurements are based on the assumption

that the whole water discharge is delivered on top of fuel. The available results are for standard residence sprinklers. For sprinklers other than standard ones, for example for Fast Response (FR) sprinklers, separate experiments are needed. As for mist systems, there are no uniform design criteria, nor enough experimental data available to understand the mechanisms of suppression and to prescribe the operational parameters. There is a definite need for a computational tool that can relatively quickly and cheaply predict sprinkler performance in non-standard fire/enclosure situations.

Existing computational studies in this area include CFD modelling of the fire environments usually coupled with a particle tracking approach to assess sprinkler effectiveness [37, 39, 43, 73]. Most CFD models do not practically allow the implementation of multiple extinguishing mechanisms in the suppression process. The effects of different spray parameters in combination with various burning conditions have not yet been considered using CFD [77].

An alternative computational approach to predict single and multi room fires is zone modelling. Although zone models require extensive empirical input, they are practical engineering tools to calculate fire development and suppression. In spite of the relative simplicity of zone modelling, little has been done to account for the effects of sprinkler parameters in combination with external fire conditions on sprinkler performance. Few models published in the literature contain a heat transfer model of sprinkler interaction with hot gases [32, 36, 41]. However, a transient fire environment has not been modelled satisfactorily in these works, and consequently, suppression has not been calculated adequately.

Some of the existing fire codes based on zone models contain sprinkler response and suppression calculations. In these models, such as FAST (Fire Growth and Smoke Transport) and its versions [68, 137], suppression calculations are based on experimental correlations between water application rate and fire heat release rate as discussed by Evans [138]. Generally, the correlations proposed for suppression calculations are one-parameter expressions [89], depending only on water application rate, and limited by fuel type,

configuration and conditions of water application. Spray dynamics and its direct effect on gas temperature and velocities have not been modeled yet [68].

One of the fire models that includes water suppression, where droplet trajectories and heat transfer effects are considered, is the Fire Demand (FD) model [48]. It was developed in the United States in the 1980s. Only post-flashover compartment fire suppression was modelled by FD, and later, the results were shown of agree reasonably with the experiments of Tuomissaari [13] in terms of heat release rate and temperature histories [13].

For the work summarized in this chapter, the sprinkler submodel [139, 140, 141] has been incorporated into an existing zone model [142]. As described in Chapters 3 to 5, the submodel includes droplet dynamics and associated heat and mass transfer between gas flow and water droplets as well as between fuel and water. The objective is to simulate suppression phenomena due to gas cooling and water-fuel interaction. The capabilities of both the sprinkler submodel and the zone model, NRCC-VUT FGM, allow investigation of fire development and suppression with respect to various sprinkler parameters, such as mean droplet diameter, discharge rate, RTI (Response Time Index), fuel exposure to water, room geometry and ventilation conditions. The model predictions are compared with fire suppression experiments in a burn room using residence fast-response sprinklers of different discharge rates. In these experiments, only total fuel surface coverage with water spray has been studied [143]. Hence, the predicted contribution of suppression from gas cooling has not been verified for residence sprinklers. For mist sprinklers, experimental data of Tuomissaari [13] has been used for comparison with the present gas cooling prediction.

6.2 MODELLING OF SPRINKLER IMPACT ON FIRE: ZONE MODEL AND SPRINKLER SUBMODEL

In this work, a one-zone model is used to predict fire growth in terms of fuel mass loss, average room temperature and exhaust condition histories in a burn room. The model was

originally developed by Takeda and Yung in 1992 [144] as the NRC (National Research Council of Canada, later NRCC) Fire Growth Model (FGM). After being validated against full-scale experimental data, it was further modified by Cooper and Yung [134]. In collaboration with CESARE (Centre for Environmental Safety and Risk Engineering, Victoria University (Australia), it was developed into the NRCC-VUT Fire Growth Model. Most of the corrections to the original NRC model have been implemented to achieve more accurate prediction of fuel mass loss rates for different types of fuels [134] and species production rates [134, 145], while the basic equations and one-zone approach remain unchanged.

In the present study, fire suppression due to gas cooling and fuel coverage by water sprinkler has been predicted using the NRCC-VUT FGM [145]. The idea of such calculations within a zone model appeared in [134] as a suggestion for further work. However, neither appropriate algorithms, nor extinguishment results have been produced since then.

In Figure 6.1, the algorithm for the NRCC-VUT FGM is given. This flowchart is taken in part from the original work of Cooper and Yung [134]. In Figure 6.1, there are two major additions to their flowchart, namely, the occurrence of sprinkler activation time, t_{ACT} , and the calculation of sprinkler heat absorption rate after sprinkler activation. The sprinkler submodel is referred as SHAR (Spray Heat Absorption Rate) here. The use of this abbreviation, SHAR, is similar to the terminology of Kung [25]. The two present additions are highlighted in gray in Figure 6.1. The subprogram SHAR takes gas temperature as an input and returns the additional heat loss and steam production rate to the main program. Therefore, after the sprinkler is activated, the part of the algorithm labeled “SPECIES BALANCE” receives the spray steam production rate over the current time step. In addition, the part with “COMPARTMENT ENERGY BALANCE” obtains the additional heat loss due to heat absorbed by droplets. Further details of the zone model and its combination with the sprinkler submodel are discussed in the next two sections.

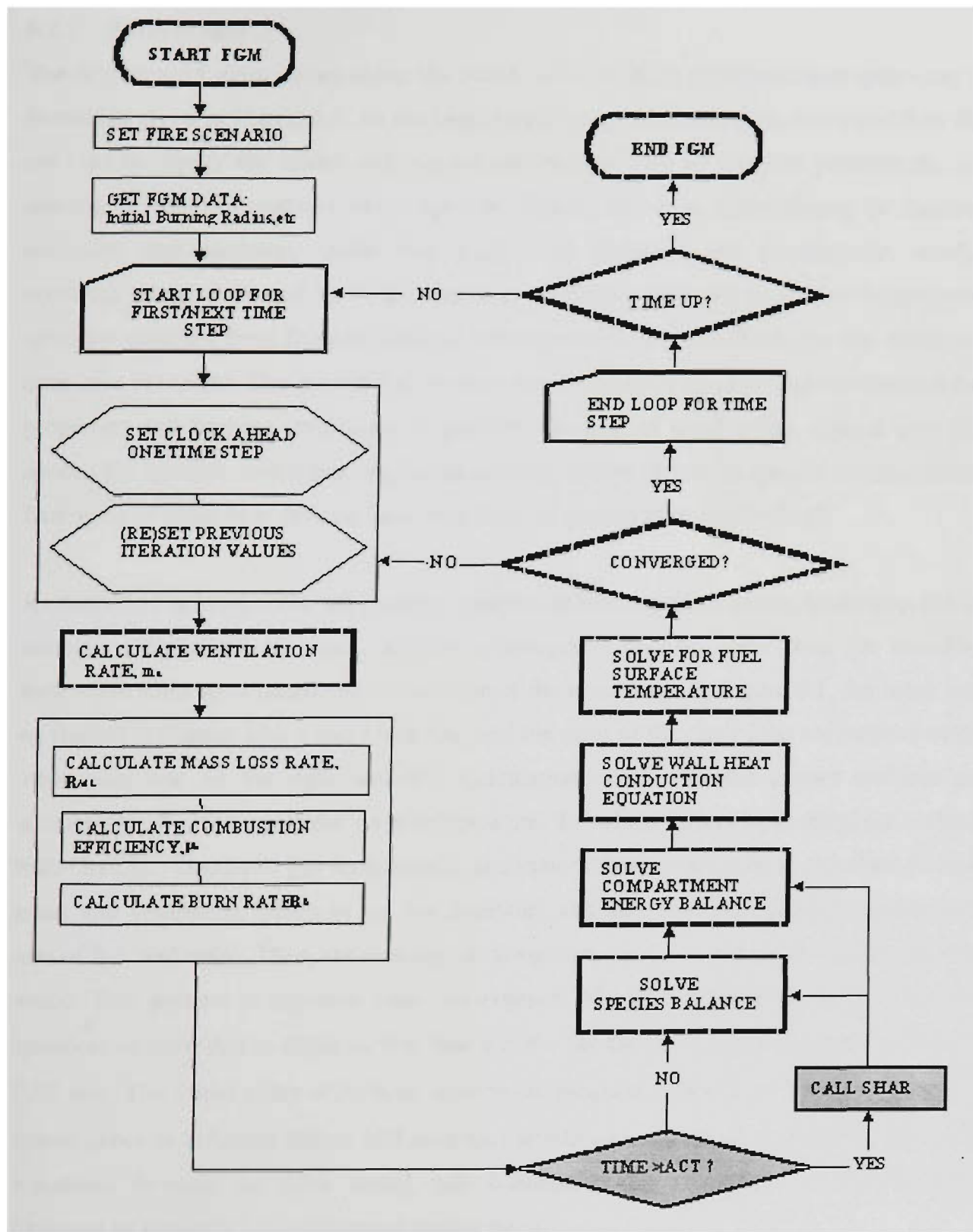


Figure 6.1. Flowchart of the NRCC-VUT FGM taken from Fig.4 of [134]. The two shaded boxes are the new additions to the NRCC-VUT FGM, and these correspond to the sprinkler activation time, t_{ACT} , and the spray sub-model SHAR.

6.2.1 Zone Model

The sequence of calculations using the NRCC-VUT FGM is explained next following the flowchart given in Figure 6.1. At the beginning of the calculations, the two input data files are read to supply the model with needed information. One of the files provides the data relating to the fire scenario (door open or closed), fire type (smouldering or flaming), enclosure and openings, initial fuel mass, wall thickness and conductivity, window breakage temperature and sprinkler parameters: sprinkler RTI and glass bulb temperature, sprinkler distance from fire and nominal water pressure. It also defines the fire simulation time (fire duration). The second file contains the information on chemical and thermal fuel properties and burning conditions. It provides the heat of combustion, critical heat flux needed for ignition, initial burning radius and magnitudes of critical species concentrations. Examples of these user-defined input data files are presented in Appendix C.

As described in [134, 144], the program consists of two nested loops: an inner loop for the iterative calculations to check solution convergence, and an outer loop for marching forward in time upon successful completion of the inner loop. In Figure 6.1, the inner loop on the left is framed with a thin black line, and the steps of the outer loop are marked with a wide gray line on the right and left. Calculations start with the known ambient gas temperature, T_0 , and a guessed room temperature, T_G , which differs from the given ambient value by 2%. These two gas temperatures and their difference are used to calculate all heat, mass and ventilation fluxes in the fire enclosure and also the corresponding temperature rise of fuel and walls. Then, the guessed gas temperature is corrected by the newly obtained value. This process is repeated until convergence. The convergence criterion is for two consecutive iterations to differ by less than 0.01%. The time step, Δt , is recommended to be 0.02 min. The initial value of Δt is an input to the program, and it is defined by the user. If convergence is achieved before 100 iterations within a time step, Δt is doubled. The basic equations forming the zone model, and consequently, the contents of the flowchart elements in Figure 6.1, are discussed further below.

- Compartment ventilation

The calculation for fire growth begins with the ventilation rate, m_a , which represents the fire induced gas inflow to the room from the opening [134]:

$$m_a = \frac{2}{3} \sqrt{2g} C_D \rho_{G0} A_0 \sqrt{H_0} \left[\left[1 - \frac{T_0}{T_G} \right] \left[\frac{T_0}{T_G} \right] \right]^{0.5} \left[1 - \frac{n}{H_0} \right]^{1.5} F \quad (6.1)$$

where g is the gravitational constant, C_D is the discharge coefficient for the compartment opening, ρ_{G0} is the gas density at ambient conditions, A_0 and H_0 are the area and total height of the opening, respectively. n is the height of the neutral plane [144], or interface between hot and cold gas layers. In this one zone model, it is assumed to be $0.5H_0$ (halfway up the compartment opening) [134]. F is an empirical flow correction factor [134, 144].

- Mass loss and burning rate

The NRCC-VUT FGM is one of few models that correlates the burning rate of fuel, R_B , with burn room conditions [134]. Expressing the mass loss flux of fuel, m'' [$\text{kg}/(\text{sm}^2)$] for flaming fires as a function of radiation feedback to the fuel, the following general heat balance equation can be written [58]:

$$m'' = (q_F + q_E - q_L) / \Delta H_v \quad (6.2)$$

where q_F is the heat flux from flame to fuel surface, which is strongly dependent on the oxygen concentration in the surrounding air. q_E is the total external radiant heat from external sources, such as hot gas layer and walls. q_L is the total heat loss. The difference ($q_E - q_L$) is the net heat flux delivered to the fuel surface by the compartment enclosure. ΔH_v is the latent heat of fuel vapourisation (for liquids) or gasification (for solids). It is also referred as the heat required to produce volatiles for polymeric materials in [58]. In the NRCC and NRCC-VUT models, the net flux or the heat feedback to the fuel, q_r , is expressed as follows [144]:

$$q_r = q_E - q_L = \sigma [\varepsilon T_G^4 + (1 - \varepsilon) T_{W1}^4 - T_S^4] \quad (6.3)$$

where ε is the gas emissivity, T_G , T_{w1} and T_s , are the gas, inner wall and fuel surface temperatures in a room, respectively. The rise of q_r is limited by the minimum heat flux needed for ignition, q_{0ig} (13 kW/m² in the NRCC-VUT FGM). To avoid negative heat fluxes at the beginning of the fire, the surface temperature of fuel is assumed to be tied to T_G in the model.

The maximum (ideal) burning rate, $m_{id} = q_F/\Delta H_v$, is the rate of burning of material if all heat losses are exactly compensated by an imposed heat flux, $q_E = q_L$ [58]. Hence, Equation (6.2) can be re-written as follows:

$$m'' = m_{id} + (q_E - q_L)/\Delta H_v \quad (6.4)$$

m_{id} [kg/(sm²)], ΔH_v and other thermal properties for some typical furniture materials can be found in the Table 1 of [134]. For PU, wood and PMMA (polymethylmethacrylate), the values of m_{id} [kg/(sm²)] and ΔH_v (MJ/kg), are, PU: 0.045 and 2.08; wood: 0.013 and 1.82; and PMMA: 0.024 and 1.63.

- Mass conservation for oxygen

q_F in Equation (6.2) is a linear function of oxygen mass concentration, Y_{O2} , for flaming fires [58]. The complete relationship for fuel mass loss rate in kg/s, R_{ML} , can be written as follows [134]:

$$R_{ML} = m'' A_v = (m_{id} Y_{O2i}/0.23 + \Delta r) A_v \quad (6.5)$$

where Y_{O2i} is the mass fraction of O₂ in the burn room before combustion; A_v is the burning area. $\Delta r = q_r/\Delta H_v$, and it is called the enhancement of mass loss due to heat re-radiation to the fuel. q_r is the net heat flux to the fuel surface ($q_r = q_E - q_L$) as given in Equation (6.3). The ignited area of the fuel is a variable. It is calculated as a function of time and flame spread velocity, V_f , until it reaches the specified maximum burning radius:

$$A_v = \pi [(A_{v0}/\pi)^{0.5} + \int V_f dt]^2, \quad A_{v0} \leq A_v \leq A_{vmax} \quad (6.6)$$

where A_{v0} is the initial burning area, i.e. the ignited area, specified as the initial burning radius by the user (Input 20 in the Sample Input Data File #1, Appendix C). A non-zero value of A_{v0} initiates fire growth in the NRCC-VUT FGM. A_{vmax} is the maximum possible burning area defined by the user as the equivalent fuel radius (Input 13 in Appendix C). This radius depends on fuel geometry and size, and it can be corrected within certain limits to fit the experimental data on burning rate [146].

Flame spread velocity, V_f , is, in turn, a function of radiated heat flux, q_r , and oxygen mass concentration, Y_{O2} [144,146].

$$V_f = \frac{a}{(b - q_r)^2} \left(\frac{Y_{O2} - Y_{O2crit}}{d} \right)^{0.5} \quad \text{for } Y_{O2} > Y_{O2crit}$$

$$V_f = 0.0 \quad \text{for } Y_{O2} < Y_{O2crit} \quad (6.7)$$

where a , b and d are empirical constants defined by the user. Y_{O2crit} relates to the critical value of oxygen mass concentration below which the fire will be extinguished under any level of the external heat flux. Y_{O2crit} is taken conservatively as 10% in the NRCC-VUT FGM. The constant b corresponds to the minimum ignition heat flux, q_{0ig} . To avoid infinite values of V_f for heat flux equal q_{0ig} , the maximum flame speed is limited to 0.01m/s [134].

Combustion efficiency, μ , is used to account for the ability of fresh oxygen to reach fuel vapours. Then, the real burning rate of fuel, R_B , is related to the mass loss rate, R_{ML} , through this coefficient as follows:

$$R_B = \mu R_{ML} \quad (6.8)$$

where R_{ML} is calculated from Equation (6.5) and μ is determined as follows [134]:

$$\begin{aligned} \mu &= \mu_0 & \phi &< 1 \\ \mu &= \mu_0/\phi & \phi &> 1 \end{aligned} \quad (6.9)$$

Here, μ_0 is the experimentally determined maximum efficiency for the fuel (about 0.9 for PU); ϕ is the compartment equivalence ratio, i.e. the mass ratio of the fuel vapour to oxygen present in the compartment, normalized by the stoichiometric oxygen to fuel ratio, γ :

$$\phi = \frac{0.23 \gamma [Y_{OFUE} \rho_c V + R_{ML} \Delta t]}{Y_{O2} \rho_c V + 0.23 m_a \Delta t} \quad (6.10)$$

where V is the compartment volume and Y_{OFUE} and Y_{O2F} are the mass fractions of vaporized fuel and oxygen, respectively. m_a is defined in Equation (6.1).

The variable ϕ considers all the fuel vapour and oxygen that will enter the compartment during a given time period, Δt . Values of $\phi < 1$ apply to the cases when oxygen is in excess, and burning is fuel-controlled. Values of $\phi > 1$ are for ventilation controlled cases, where the oxygen supply is a limiting factor [134].

- Species concentrations

According to the NRCC-VUT FGM, the species under consideration are oxygen, the product gases CO and CO₂, and unburned fuel vapour. The concentrations of species are calculated based on the assumption of the quasi-steady state at each time step, when suitable average values are used. The compartment is treated as a well-stirred reactor that is filled at the beginning of each time step and emptied to its initial volume at the end of each time step [134]. The concentrations of species, therefore, are calculated in relation to the total mass of gas in the compartment over the given time step.

The simplified expressions for species concentrations at the current time step can be written as follows:

$$Y_{O2} = M_{O2}/M_{tot}; \quad Y_{PRO} = M_{PRO}/M_{tot}; \quad Y_{FUE} = M_{FUE}/M_{tot} \quad (6.11)$$

where Y_{O2} , Y_{PRO} , and Y_{FUE} represent the concentrations of oxygen, product gases and fuel vapour over the current time step, respectively. M_{O2} , M_{PRO} , M_{FUE} are the total masses of oxygen, product gases and unburnt fuel vapour, respectively, contained in the whole

compartment during the current time step. The following mass conservation condition must be fulfilled:

$$M_{tot} = M_{O2} + M_{PRO} + M_{FUE} \text{ and hence, } Y_{O2} + Y_{PRO} + Y_{FUE} = 1.0. \quad (6.12)$$

Each mass is calculated as the sum of the mass of a particular gas which is already in the compartment, i.e. coming from the previous time step, and the mass injected over the current time step into the compartment.

$$M_{O2} = \rho_G V Y^f_{O2} + 0.23(M_a - R_{ML}\mu\gamma) \Delta t \quad (6.13)$$

Here, Y^f_{O2} represents the oxygen mass fraction at the end of the previous time step. The second term on the right represents the “true” oxygen concentration calculated as the difference between the oxygen injection ($0.23m_a$) and oxygen consumption ($R_{ML}\mu\gamma$) rates over the current time step. Before combustion, this second term consists only of one component, namely, $0.23m_a\Delta t$, while R_{ML} is equal to zero.

According to [134], when the oxygen concentration drops below 16%, an asymptotic scheme to calculate oxygen depletion is applied instead of Equations (6.10) and (6.13):

$$Y_{O2} = 0.10 + 0.06 \exp[k_{16}(t-t_{16})/0.06] \quad (6.14)$$

where t_{16} is the time when oxygen concentration reaches 16%, and $k_{16} = dY_{O2i}/dt$ at t_{16} . The maximum drop allowed in oxygen concentration is 6%. This value represents the difference between two thresholds, 16% and 10%. The former corresponds to the transition point from normal burning to burning under reduced oxygen (suffocation), and the latter corresponds to extinguishment.

The presence of a forced ventilation system is accounted for in the total gas flow rate, M_a . M_a represents the sum of fire induced gas inflow, m_a , and any other air supply or return rates, m_{vent} . The condition defined in the NRCC-VUT FGM is as follows:

$$M_a = m_a + m_{vent}. \quad (6.15)$$

Similarly, the mass of product gases is calculated as follows:

$$M_{PRO} = \rho_G V Y'_{PRO} + (1+0.23\gamma)R_{ML}\mu \Delta t \quad (6.16)$$

where the first term on the right side is the product gas mass from the previous time step, and the second term contains both oxygen and fuel mass forming the product gases.

The unburned fuel mass is calculated in the same manner as the available oxygen in Equation (6.13):

$$M_{FUE} = \rho_G V Y'_{FUE} + R_{ML} (1 - \mu) \Delta t \quad (6.17)$$

where Y'_{FUE} represents the concentration of fuel vapor contained previously in the compartment and $(1-\mu)$ denotes the unburned fraction of fuel vapor produced over the time period Δt .

M_{tot} is the total mass of all gases filling the compartment over the given time step, as defined in Equation (6.12). M_{tot} is calculated as the sum of Equations (6.13), (6.16) and (6.17), resulting in Equation (6.18):

$$M_{tot} = \rho_G V + (0.23M_a + R_{ML}) \Delta t \quad (6.18)$$

where the first term, $\rho_G V$, is the mass of gas already in the compartment, and the second term, $(0.23M_a + R_{ML}) \Delta t$, corresponds to the mass of gas entering the compartment over the current time step, Δt .

The mass flow rates in and out of the room satisfy the following mass conservation condition over a time step:

$$m_a + m_{asupply} + R_{ML} = m_{areturn} + m_{out} + m_{vent} \quad (6.19)$$

where m_{out} is fire induced gas outflow from the opening defined as follows:

$$m_{out} = m_a + R_{ML} \quad (6.20)$$

and m_{vent} is the difference between supply and return air mass flow rates:

$$m_{vent} = m_{asupply} - m_{areturn}.$$

- Energy balance

From an energy conservation point of view, if the material is burning in an enclosed fire, then, heat flux to the fuel is generated from its burning. Burning, on the other hand, is governed by irradiation from the hot layer to the fuel, determined by the gas temperature, T_G . T_G is calculated based on the heat balance between the fuel and the hot layer, as presented below.

The rate at which the fuel produces heat to the compartment (or heat release rate, HRR) is calculated from the following equations [58, 134, 144]:

$$Q_c = \Delta H_C \mu R_{ML} \quad (\text{fuel controlled fire}) \quad (6.21a)$$

$$Q_c = \Delta H_C \mu m_a \quad (\text{ventilation controlled fire}) \quad (6.21b)$$

where ΔH_C is the heat of combustion per unit mass of fuel burned, and R_{ML} and μ are defined in Equations (6.5) and (6.9), respectively. m_a is the air ventilation rate in kg/s given in Equation (6.1). The switch between Equations (6.21a) and (6.21b) is specified in detail by Drysdale [58, p311].

If a compartment is treated as a well-mixed combustor or one zone, then an average room temperature T_G can be obtained from the single transient energy balance equation [134]:

$$C_p \rho_G V \Delta T_G / \Delta t = Q_C - Q_L \quad (6.22)$$

where C_p and ρ_G are the specific heat and density of room air, respectively, at 20°C. t is time, and V is the compartment volume. On the right hand side, Q_C is the rate of heat released in the fire, and it represents the energy gained by the compartment air. Q_L is the

rate of heat loss from the compartment to the boundaries by radiation and convection. Q_L includes heat losses through the compartment walls, Q_w , through the openings by convection, Q_v , and by radiation, Q_o , and to the fuel by radiation, Q_r , leading to fuel heat-up and pyrolysis:

$$Q_L = Q_w + Q_v + Q_o + Q_r \quad (6.23)$$

Gas temperature rise, ΔT_G , during time step, Δt , obtained from Equation (6.22) provides a new gas temperature to calculate the net heat flux in Equation (6.3) and the corresponding burning rate using Equations (6.5) to (6.8). This iterative process is repeated for each time step until convergence is reached. As stated before, the convergence criterion is 0.01% or less variation in the predicted gas temperature for the current time step, T_G . At the beginning of each time step, the value of T_G is that calculated at the end of the previous time interval. The default time step of 0.02 min [144] is used in the present calculations.

- Heat loss through the compartment walls and to fuel surface

The conduction heat transfer is calculated through the wall boundaries by using one-dimensional transient conduction model. All walls are considered to be of the same thickness and thermal properties. The wall temperature needed in Equation (6.3) is determined by solving the following equation:

$$\frac{\partial T_w}{\partial t} = \frac{k_w}{\rho_w C_w} \frac{\partial^2 T}{\partial x^2} \quad 0 \leq x \leq L_w, t \geq 0 \quad (6.24)$$

where T_w is the wall temperature; x is the axis perpendicular to the wall surface; L_w is the wall thickness; k_w , ρ_w and C_w are the wall conductivity, density and specific heat, respectively. At $t = 0$, $T_w(x, 0)$ has the ambient temperature value, T_0 . The boundary conditions on internal surfaces are specified through the radiative and convective heat fluxes coming from the room:

$$\begin{aligned} 0 \leq x \leq L_w, t = 0, \quad & T_w = T_0 \\ x = 0 \text{ (inside surface)}, \quad & -k_w \frac{\partial T_w}{\partial x} = h_i(T_G - T_w(0, t)) + q_r \\ x = L_w \text{ (outside surface)}, \quad & T_w(L, t) = T_0 \end{aligned} \quad (6.25)$$

q_r is the net radiation heat flux received by the inside walls. h_i is the convection heat transfer coefficient on inside walls. Equation (6.24) is solved numerically using an explicit finite difference scheme by dividing the wall into a number of elements specified by the user (Input 18 in Appendix C). The resulting temperature history at the inside wall, $T_w(0,t)$ is of interest.

The equations and boundary conditions for obtaining the fuel surface temperature, T_s , in Equation (6.3), before water application, are similar to the set of Equations (6.24) and (6.25), as indicated in Chapter 5. The only difference is that instead of wall properties, those of the fuel are used.

- Fire decay and extinguishment

Burning enters the decay phase in the program when either the oxygen concentration or fuel mass drops below its critical value. In terms of oxygen concentration, the limiting condition defined in Equation (6.7) is used. If the oxygen concentration falls below 10%, the flame speed becomes zero, and fire stops.

The fuel mass degradation, FM, is calculated in the program at each time step, Δt :

$$FM^{new} = FM^{old} - R_B \Delta t$$

where R_B is calculated using Equation (6.8). The decay process under sufficient oxygen concentration starts due to fuel degradation when the fuel mass drops below its critical value. The critical fuel mass is an empirical value which is considered to be 20% of the total initial fuel mass [146]. The decay burning rate is modelled then by an exponential function of time, only: $R_B = f(e^{-t})$.

6.2.2 Sprinkler submodel

The present spray cooling model has been incorporated as a new module or submodel into the source code of the NRCC-VUT FGM. Prior to combining with this zone model, the submodel was used to calculate spray performance in hot gas for validation purposes [109, 139]. The computational scheme and gas-droplet interaction equations, when used within

the zone model, are similar to those described in the ‘Particle-Source-in-Cell’ method [59]. Gas and droplet governing equations are solved separately and then combined by means of the source terms. As indicated earlier, the addition of spray cooling follows the sprinkler activation time. Below, a description is given of how the submodel, Subroutine SHAR, works in combination with the NRCC-VUT FGM.

- Sprinkler Activation Time

The new submodel starts after a heat detector is activated. A glass bulb detector is considered. It is specified by the “glass bulb temperature”, i.e. the boiling temperature of bulb liquid, at which the sprinkler is activated, T_{bulb} (Input 44 in Appendix C). In addition, the sprinkler Response Time Index, RTI ($m^{1/2}s^{1/2}$), is specified (Input 46 in Appendix C). The time of sprinkler automatic heat detector activation, t_{ACT} , is calculated based on ceiling jet equations. The ceiling jet is modelled using the following equations [114]:

$$U_G = 0.96(Q_c/H_{det})^{0.33} \quad R_{det}/H_{det} < 0.15 \quad (6.26)$$

$$U_G = 0.195(Q_c^{0.33} H_{det}^{0.5} R_{det}^{-0.83}) \quad R_{det}/H_{det} \geq 0.15$$

where U_G is the ceiling jet velocity in m/s; Q_c is the fire HRR in kW from Equation (6.21). The height H_{det} is taken to be the difference between the ceiling height and half of the door height in the model, and R_{det} is the detector radial position from the fire source in m. R_{det} is defined by the user through the input file (Input 45 in Appendix C).

The temperature rise under the ceiling, ΔT_{det} , and heat detector’s temperature, T_{det} , are calculated by the following scheme:

$$\Delta T_{det} = \Delta t (T_G - T_{detO}) (\sqrt{U_G}) / RTI \quad (6.27)$$

$$T_{det} = T_{detO} + \Delta T_{det}$$

$$T_{detO} = T_{det}$$

where T_G is the gas temperature⁷ at the current time step, T_{det0} is the initial detector temperature taken as the ambient gas temperature, T_0 , at the first time step. Equations (6.26) and (6.27) are solved at each time step to obtain T_{det} which is compared with the given T_{bulb} to detect the activation time, t_{ACT} . When $T_{det} \geq T_{bulb}$, t_{ACT} takes the value of the current time.

- Spinkler heat absorption calculation

There are two types of suppression calculations presented here. The first is the calculation of gas cooling only, assuming that there is no interaction between water spray and fuel surface. The second type is fire suppression calculation due to direct water impact on top of fuel surface with and without gas cooling. These calculations are explained next.

In the first type of calculations, the sprinkler submodel uses as input parameters room gas temperature and gas velocity at the moment of activation. It returns to the main program sprinkler heat absorption and evaporation rates together with droplet average residence time at each gas solver time step.

Following the approach used in [64], the gas solver time step after sprinkler activation changes to the droplet residence (or traverse) time which is usually shorter than the initial gas solver time step. In this study, a sprinkler with a given discharge rate is characterised by droplets of uniform diameter and initial velocity (magnitude and angle), as indicated in Chapter 3. Droplet trajectories in the hot layer are considered first to obtain the droplet residence times. In the NRCC-VUT FGM, the hot layer depth is assumed to be half of the doorway height [134], as described in the previous section. Gas velocity is calculated based on gas outflow using Equation (6.20) and hot layer cross-sectional area. According to the classification given in Chapter 3, the sprinkler location is taken as Location 1.

⁷ The use of the average gas temperature in heat detector submodel may overestimate the sprinkler activation time. More accurate prediction of activation time should be based on the ceiling jet temperature [69], or at least, on the hot layer temperature higher than room average temperature.

Based on the residence time and corresponding total interface area, the heat absorption rate, Q_{abs} , imposed by the spray is calculated. Then, substituting the heat absorption rate as an additional heat loss term into the compartment energy balance, Equation (6.23), a new gas average temperature is calculated by the zone model:

$$Q_L = Q_w + Q_v + Q_o + Q_r + Q_{abs} \quad (6.28)$$

The details of Q_{abs} calculations are presented in Chapters 3 and 4 of this thesis.

The droplet evaporation in hot gas and consequently, oxygen dilution by steam production is also accounted for. The droplet mass evaporation rate, produced by the droplet submodel, Subroutine SHAR, is substituted as an additional concentration term into Equation (6.12). The following additions and changes to the species concentration equations, Equations (6.16) to (6.20), occur due to the new mass source term, M_{steam} . Steam mass concentration is defined as:

$$Y_{steam} = M_{steam}/M_{tot} \quad (6.29)$$

where

$$M_{steam} = \rho_G V Y_{steam}^f + R_{steam} \Delta t \quad (6.30)$$

where Y_{steam}^f represents the steam mass fraction at the end of the previous time step, R_{steam} is droplet evaporation rate. It should be noted that since air is the dominant component in a room, Equation (6.30) is written with the assumption that gas mixture density is equal to air density, ρ_G .

The total mass of all gases in the room, M_{tot} is changed to Equation (6.31) below, instead of Equation (6.18).

$$M_{tot} = \rho_G V + (M_a + R_{ML} + R_{steam}) \Delta t \quad (6.31)$$

The contribution to M_{tot} due to steam production can lower the oxygen concentration, and hence, it may affect the burning rate. Mass balance is modified as follows, instead of Equation (6.12):

$$Y_{O2I} + Y_{PRO} + Y_{VAP} + Y_{steam} = 1 \quad (6.32)$$

Due to the comparatively low value of the total droplet evaporation rate in the range of gas temperatures and droplet diameters considered here, oxygen dilution due to steam production is estimated to be negligible in the present study. On the other hand, at high temperatures, during post-flashover fire suppression, this term can be important if extinguishment is attempted prior to decay. Even in the extinguishment of post-flashover fires, if the spray activation time is close to decay conditions, then steam production contribution can still be negligible. Once the fire mechanism switches to oxygen starvation, oxygen concentration depends on no other parameter but time, as in Equation (6.14). If the switch is to a fuel controlled regime, then the burning rate is governed by the fuel decay rate.

In the second type of calculations, fire suppression due to burning surface reduction by droplet coverage is considered. The key factor in these calculations is the coverage rate, which is the number of droplets per unit time per unit fuel surface area enveloped by the spray at floor level. This rate is similar to the sprinkler delivered density. The droplet total coverage area on top of the fuel surface is calculated and extracted from the total fuel surface area at each time step starting from sprinkler activation. Two assumptions are made in these calculations. First, each droplet covers a surface equal to the droplet cross-sectional area. Secondly, droplets do not overlap as they reach the fuel surface. The following equations are solved by the program to account for the development of coverage area:

$$\begin{aligned} A_{cov} &= A_{cov0} + (Na_1\Delta t) \\ A_v &= A_v - A_{cov}, \quad \text{if } A_v < 0, A_v = 0 \end{aligned} \quad (6.33)$$

where A_{cov} is the area covered by the spray over time interval Δt ; A_{cov0} is the coverage area at the end of the previous time step; A_v is the burning area used in Equation (6.5). N corresponds to the droplet number rate (s^{-1}) explained in Chapter 4. $a_1 = \pi d^2/4$, is the droplet cross sectional area corresponding to the mean droplet diameter, d . It is further assumed in this study that as soon as the fuel is covered by water, there is no fuel left to

burn, and according to the fire development model, the fire begins to decay. As stated by Yu *et al.* [135], water depositing onto a burning surface will absorb heat from fuel surface until it is totally evaporated. In reality, however, the cooling effect of water is governed by the difference between water discharge rate and surface evaporation rate. As shown in Chapter 5, under the conditions of constant water supply above the critical, the water discharge rate exceeds surface evaporation rate, and fuel is protected from ignition.

The comparison between the two suppression mechanisms, gas cooling and fuel coverage, has shown the dominant effect of the latter, even for the values of water delivered density much below the standard levels required. These results are discussed next along with the experimental validation of the combined model.

6.3 EXPERIMENTAL CONDITIONS FOR THE SPRINKLER TESTS

The sprinkler tests described in this chapter were conducted in the Experimental Building-Fire Facility (EBFF) of the Centre for Environmental Safety and Risk Engineering (CESARE). The facility is a four-storey full scale building. The burn room (5.4 m x 3.6 m x 2.4 m) was connected to a corridor with an open doorway (0.8 m x 2.03 m). Opposite to the doorway was a 2.4 m x 1.5 m standard three-pane window. Detailed description of the facilities can be found in [110, 143, 147]. Nine full-scale tests, eight sprinklered and one unsprinklered, were conducted as part of this program [143]. The fuel was polyurethane (PU) slabs and timber cribs. In order to imitate real furniture, the mass ratio of foam to timber was 1:5 providing a similar fuel composition to that of a chair without covering. In total, 64 pieces of 90 x 35 x 1000 mm pine and 8 slabs of 1000 x 1000 x 100 mm PU were used. The material was loaded into four equal one-meter square stacks in a wood/foam/wood/foam arrangement.

A mass loss platform of 2.32 m x 3.52 m located at the window end of the burn room was used throughout this series of experiments. The total load on the mass platform corresponded to a wood mass equivalent fuel load of approximately 30kg/m^2 [143]. The fuel was arranged in the south-west corner of the room adjacent to the window. A residence pendant sprinkler of glass-bulb temperature 68°C and K-factor, the coefficient

proportionality between water flow rate and pressure, $3.9 \text{ gpm}/\text{psi}^{1/2}$ was installed as shown in Figure 6.2. The sprinkler was installed in the centre of the burn room, 2.66 m from the wall, instead of a standard 1.5m. The sprinkler used for the experiments was a concealed fast response domestic glass bulb sprinkler that discharges water in a hemispherical pattern. This sprinkler has a nominal orifice size of 9.5 mm, and the water pressure varies from 48 to 70 kPa. Gas spatial temperature distribution was measured with two thermocouple racks comprising of a total 70 thermocouple beads. The voltage from these thermocouples was recorded with 2 s resolution. Measurements were also made of species concentrations in the middle of the burn room and the corridor, and air velocity at the doorway during all experiments.

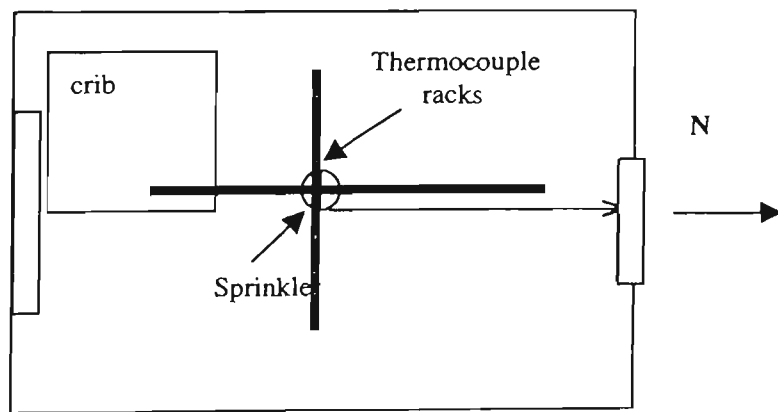


Figure 6.2. Layout of the burn room and locations of sprinkler, thermocouples and fuel in experiments. The opening on the right is the door, and the one on the left is the window.

6.4 RESULTS AND DISCUSSION

In this section, the results are presented which simulate the full scale fire experiments without and with sprinklers in the same 5.4 m x 3.6 m x 2.4 m burn room in EBFF in CESARE, as described briefly in Section 6.3. The present computational results are compared with the results of these experiments and with the results from [138].

6.4.1 Non-sprinklered fire

Prior to the sprinkler tests mentioned in Section 6.3, a series of experimental full scale furniture tests had been conducted in the EBFF within the same burn room for an FCRC (Fire Code Reform Centre) project [110]. Some of the results for these tests were used for the verification of the NRCC - VUT FGM. The details of this verification in terms of different fire parameters, such as fire growth, decay rates, and species concentration are given in [148]. In the present study, one of the verification cases was repeated to check that the model was used correctly, and that the input data was appropriate. For this purpose, the average room temperature history was predicted for the full scale flashover fire described in [110] as Experiment FO4 or Burn 5 in [147]. The initial fuel mass and fuel size, respectively, were taken as 232 kg and 100 cm x 30 cm (radius by thickness).

In Figure 6.3, the predicted average gas room temperature is compared with the experimental one. This comparison is similar to the comparison given in Figure 4.4 [146]. The input data file for the present prediction is given in Appendix C. The spatial average of measured gas temperatures is used for comparison with the calculated average room temperature. As shown in Figure 6.3, the predicted temperature history follows the experimental behavior closely.

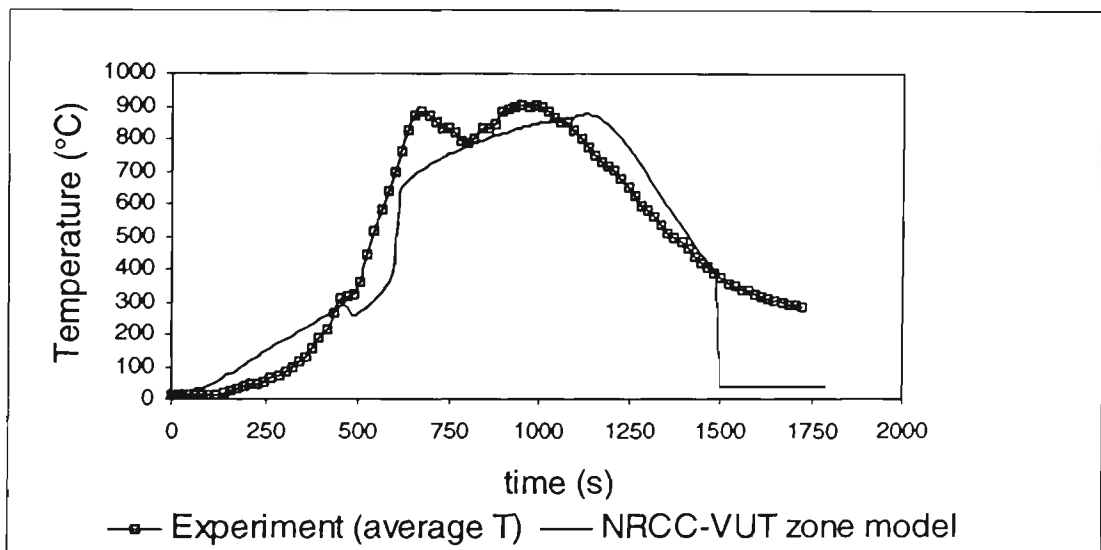
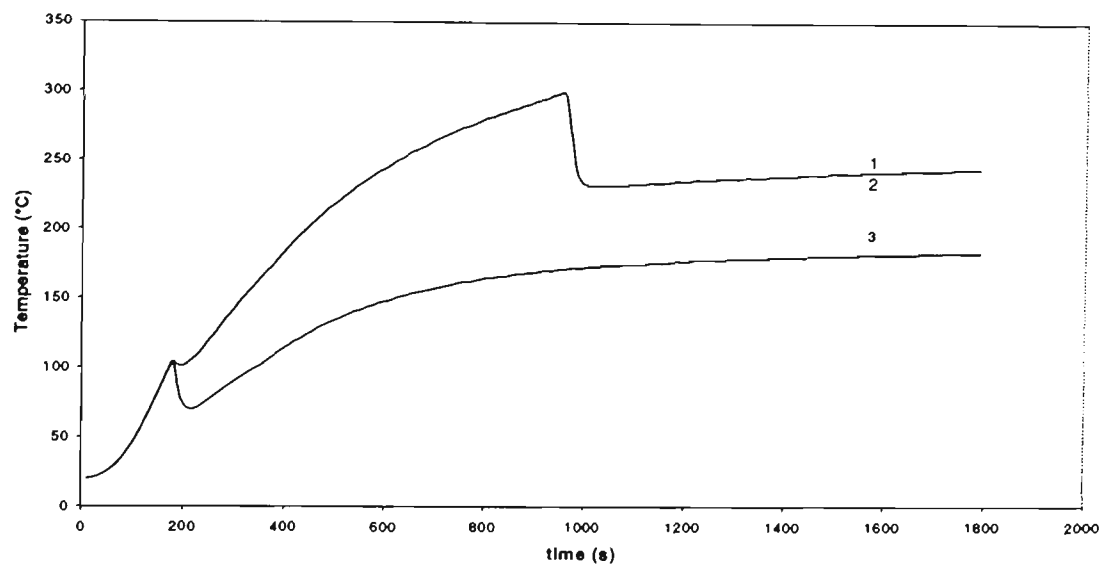


Figure 6.3. Comparison between the NRCC-VUT FGM prediction and spatially averaged experimental results for a full scale furniture burn.

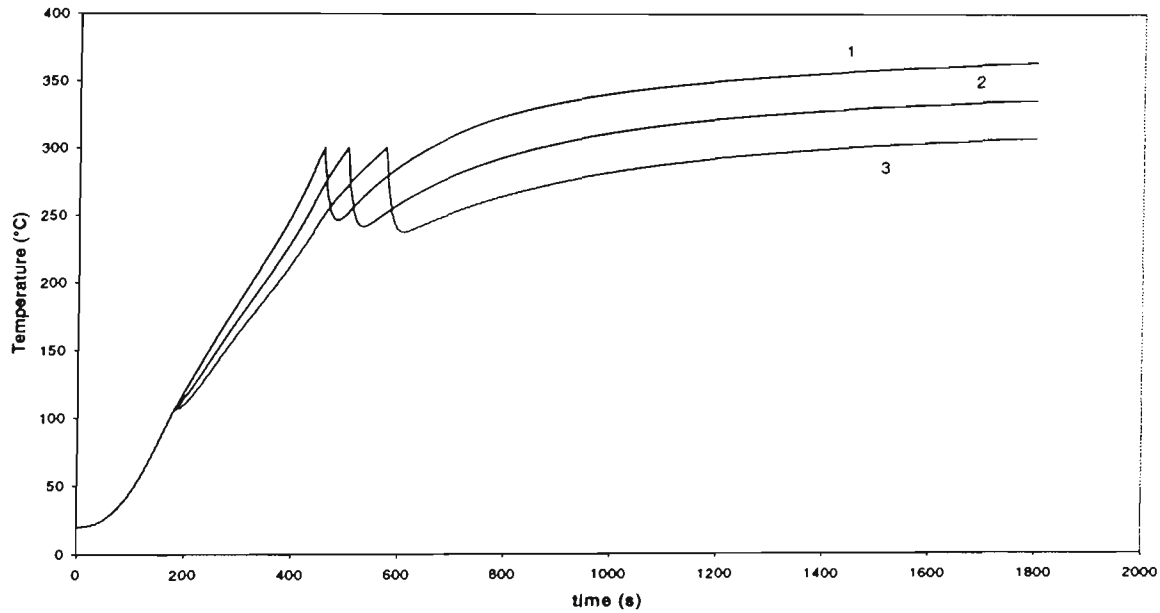
In [145], time-dependent heat release rate, HRR, and average room temperature were chosen to characterize the development of fire. The predicted effect of sprinkler interaction either with hot room gases alone or with fuel surface and hot gas, is discussed next in terms of these characteristics.

6.4.2 Sprinklered Fire: Gas Cooling

The effect of different spray parameters on overall gas cooling is shown next. Prior to variation of such determining spray parameters as droplet diameter and discharge rate, effect of relative fire-nozzle locations is discussed first. In Figure 6.4 the time-temperature histories are plotted for each of three possible locations described in Chapter 3. The results for 0.3 and 0.7mm sprays are given in Figure 6.4a and b, respectively. Gas velocity is taken 2m/s. This can be only applied for early activated sprinklers, when fire at the moment of activation does not exceed 4MW. For larger fires and later activation times another droplet and gas velocity ranges should be studied.



a



b

Figure 6.4. Comparison of temperature histories predicted presents for three possible fire-spray nozzle locations (Chapter 3). 1 – Location 1, 2 – Location 2, 3 – Location 3: a) 0.3mm spray; b) 0.7 mm spray. Water discharge rate 45 l/min.

According to Figure 3.2, the effect of relative location may be significant for stationary mounted mist nozzles (spray of 0.3mm). While locations 2 and 3 do not show any noticeable difference in terms of gas cooling (upper curve in Figure 6.4a), at location 1, this spray produces much better cooling effect (lower curve in Figure 6.4a). For 0.7mm spray,

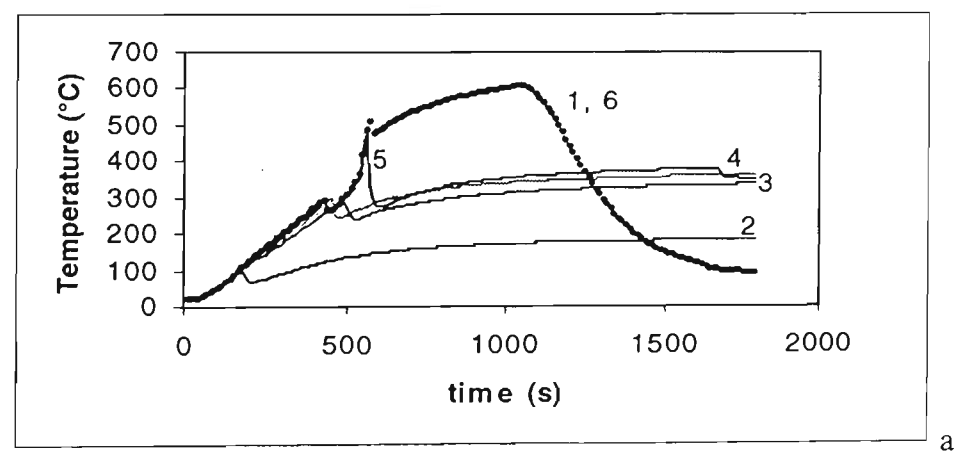
location effect is not as significant as for smaller droplets. For droplets larger than 0.7mm at specified 2 m/s gas velocity, choice of location does not affect on gas cooling. For further predictions, only Location 2 is discussed as the most similar to experimental arrangement.

Figure 6.5 shows the predicted transient temperature and heat release rate in the sprinklered compartment. The corresponding non-sprinklered results are also given for comparison. For the calculations, the initial fuel mass was taken as 117 kg with the same fuel size as in the non-sprinklered case. Fuel properties correspond to the properties of PU foam. To characterize the spray, a wider range of mean droplet diameters was considered computationally than used in the experiments. The computational range of droplet diameters was from 0.3 to 2 mm. The experimental diameter range, based on the pressure range of 0.5 to 1 MPa, was between 0.7 and 1.5 mm [143].

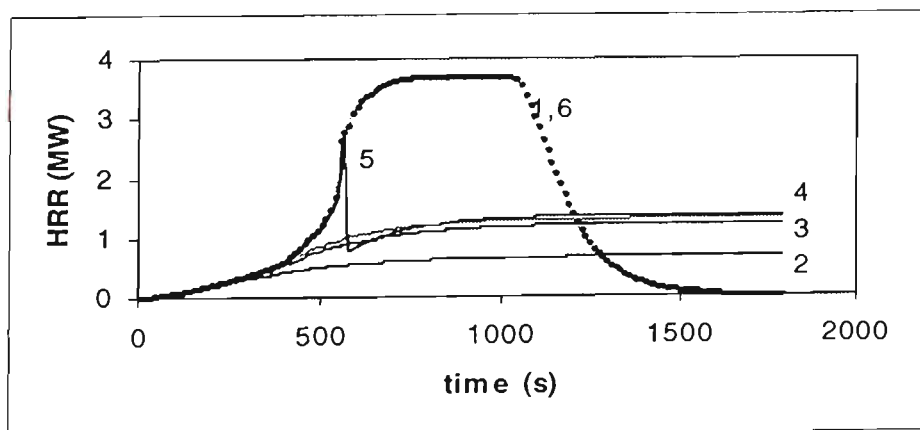
In Figure 6.5, the effects of window breakage, sprinkler intervention and droplet diameter on the average burn room temperature and HRR can be also seen. The upper curves, given by the dashed lines in Figure 6.5a and Figure 6.5b, show the effect of window breakage and additional cooling caused by this phenomenon due to fresh air entrainment. The initial temperature drop can be observed to occur at the window breakage point, 300°C in the present model. The cooling effect is counteracted by an increase in oxygen concentration in the enclosure, which causes a corresponding increase in fire growth rate. As explained in [149], the non-sprinklered fire reaches flashover around 500°C, and then the fully developed stage starts with further temperature rise up to about 650°C. The HRR reaches less than 4 MW as seen in Figure 6.5, and then the fire decays.

In Figure 6.5, the lowest curve, curve 2, corresponds to the fire cooled by a fine water spray of droplet diameter 0.3 mm and indicates no window breakage. Thus, the first temporary temperature drop in this curve is caused by additional gas cooling due to sprinkler activation. In this case, the spray cooling effect is sufficient enough to control fire, i.e. to prevent further fire growth to the window breakage point. In between the two extremes, the top and bottom most curves in Figure 6.5, there are three intermediate curves that indicate both sprinkler activation and window breakage occurrences. Initially, gas cooling due to

sprinkler activation, the first temporary temperature drop, is not significant enough to reduce fire growth and prevent window breakage. The fire control occurs later, due to the dual cooling effect of additional air entrainment and sprinkler spray on fire growth. In the model, the reduction in fire growth rate is followed by the reduction in radiative feedback to the fuel caused by the reduction in the average room temperature due to effective cooling. The reduction in burning rate leads to a moderate oxygen consumption, slower temperature rise and much later suppression caused by either oxygen starvation, or fuel burnout.



a



b

Figure 6.5. a) Temperature profiles and **b)** HRR rates predicted for gas cooling by the sprinklers represented by different mean droplet diameters. 2 – 0.3mm; 3- 0.5mm; 4 – 0.7mm; 5 – 1mm; 6 – 1.5 mm. ‘Unsprinklered’ case (curve 1) for the flashover fire experiment is given for comparison.

The curves corresponding to the fire cooled by a water spray of 1.5 mm droplets, curve 6, coincides with the non-sprinklered case, given by curve 1. As seen in Figure 6.5, with smaller droplet diameters, higher cooling effect is obtained, while spray represented by large droplet diameter, 1.5 mm, is not effective at all in fire suppression due to gas cooling. In all sprinklered cases, water flow rate was kept the same at 45 l/min, providing a standard delivered density, DD, of 2.5 mm/min. The sprinkler RTI was $30 \text{ (ms)}^{1/2}$, similar to that of experimental fast response residence sprinklers, which gave an activation time of about 180 s. The close agreement in terms of sprinkler activation times once more underlines the validity on NRCC-VUT FGM in predicting the domestic fires.

In Figure 6.6, the effect of water discharge rate on gas cooling is shown. The spray diameter kept at 0.7 mm, and water flow rate was varied from 29 to 45 l/min in accordance with the experiment. Other conditions, are the same as those in Figure 6.5. The effect of gas cooling coupled with water direct application on top of fuel is shown by the dotted line, curve 4, located below the solid curves in Figure 6.5. It should be mentioned here briefly that if the location of residence large droplet sprinklers is such that they provide total fuel coverage, then the effect of fuel blockage by water plays a major role in fire extinguishment. From Figure 6.6, it is seen that gas cooling can control fire in terms of preventing or delaying flashover, while water impact extinguishes fire.

The sensitivity of zone model predictions to compartment size is similar for unsprinklered and sprinklered fires with respect to the same parameter. In Figure 6.7, the effect of gas cooling is shown when identical sprinklers with the same discharge rate in compartments of different floor areas are simulated. For a small compartment, the temperature rise is much quicker, and water spray cooling is not sufficient to prevent flashover, as indicated by the dotted line in Figure 6.7. For a larger compartment, the spray cooling effect becomes the determining parameter, and the chosen sprinkler prevents flashover.

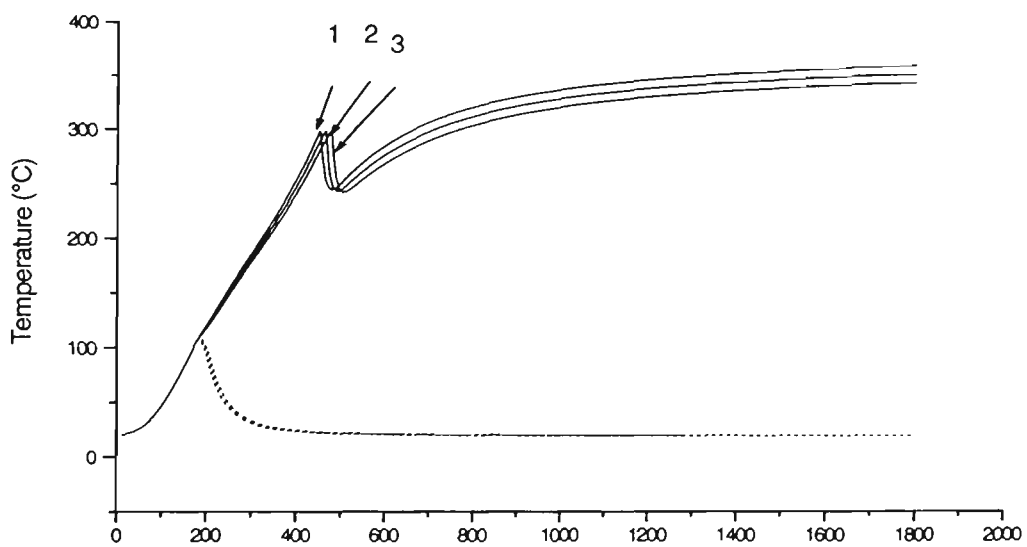


Figure 6.6. Effect of water discharge rate on gas cooling (curves 1,2 and 3) and suppression due to direct water application (dotted line). Water discharge rates: 1- 29; 2- 38 and 3- 45 l/min.

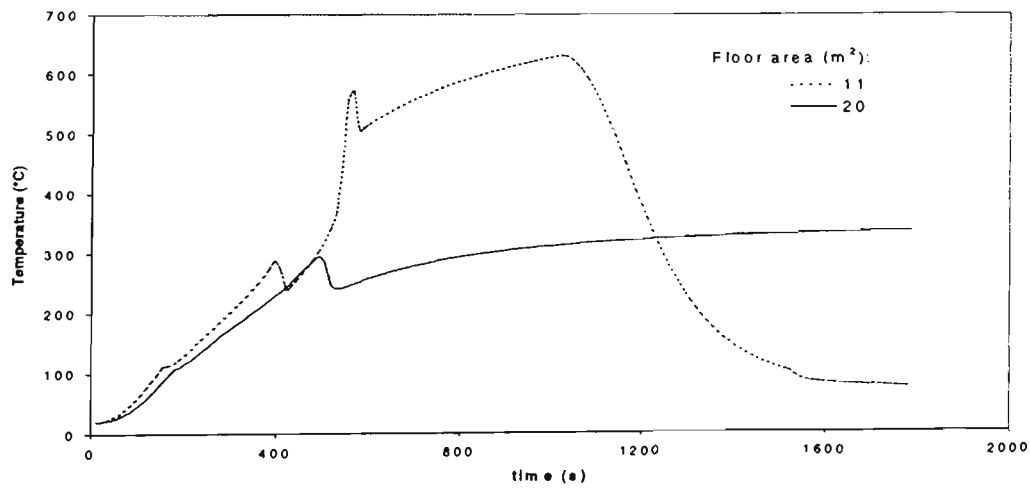


Figure 6.7. Predicted time-temperature curves for gas cooling by sprinkler with 1kg/s discharge rate, 0.7 mm mean droplet diameter, and RTI of $30 \text{ (ms)}^{1/2}$. Two curves correspond to the compartments of the same height (2.4m) and different floor areas. Window and door openings are the same in both cases.

6.4.3 Sprinklered fire: Fuel coverage. Prediction and comparison with experiments

In the present study, it has been assumed that heat release rate is proportional to burning surface area, and fire growth curves for different fractions of fuel exposure (or fuel mass left for burning) were investigated. In NRCC-VUT FGM, as the critical fuel level (less than 20% of initial mass) is achieved, the exponential decay process is initiated. In Figure 6.8, the time-temperature curves are plotted for the different fractions of fuel exposure (or fuel left uncovered) for identical sprinkler characteristics. The data are plotted together with one experimental curve, the dashed line is for comparison. It is expected that the fuel surface may not be totally covered by the water even when sprinklers provide total floor coverage. At this stage of the sensitivity analysis it has been assumed that 0.5% of fuel mass is still left for burning even though the outer fuel surface has been captured by spray envelope. It is obvious that fire extinguishment depends on the amount of fuel, or area left uncovered. According to the model (see Section 1.3.1), starting from 20% of unburnt fuel mass left with sufficient amount of oxygen present in the burn room, fire turns to decay stage.

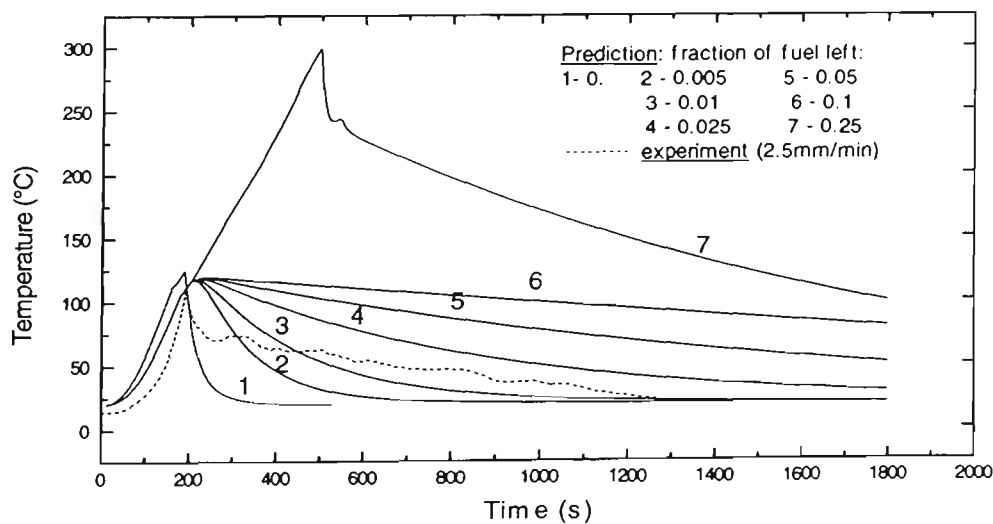


Figure 6.8. Time-temperature curves predicted for different fuel fractions exposed to water. In the model, the sprinkler is represented by 45 l/min flow rate (2.5 mm/min application rate), 1 mm mean droplet diameter and $RTI=30(ms)^{1/2}$. curves 1 to 7. The measured results are given by the dotted line corresponding to 2.5 mm/min sprinkler application rate.

In Figure 6., the computational and experimental results of fire extinguishment by different water application rates, from 2.5 to 0.6 mm/min, are given for comparison. In Figure 6.9, the fire decay time is under predicted due to the assumption of 99.5% fuel exposure. The numerical results follow the experimental trend qualitatively. The three calculated profiles given by the solid lines in Figure 6.9 have distinct maxima. In all of them, the higher the application rate, the less is the maximum temperature rise, and the faster the temperature decays. This trend is in agreement with experimental results given in the same figure by the dashed lines. From the predicted data given in Figure 6.9, it can also be seen that the decay time becomes less sensitive to water discharge rate as the later increases. Similar trends and values of temperature decay time in the extinguishment of a series of small scale PU fires can be found in the experimental data given by Yang *et al.*[29]. In their work, the time of extinguishment has been measured against water flow rate for direct impingement of the fine sprinkler spray on top of burning fuel. Quantitatively, the decay rate in HRR is overestimated by the present model.

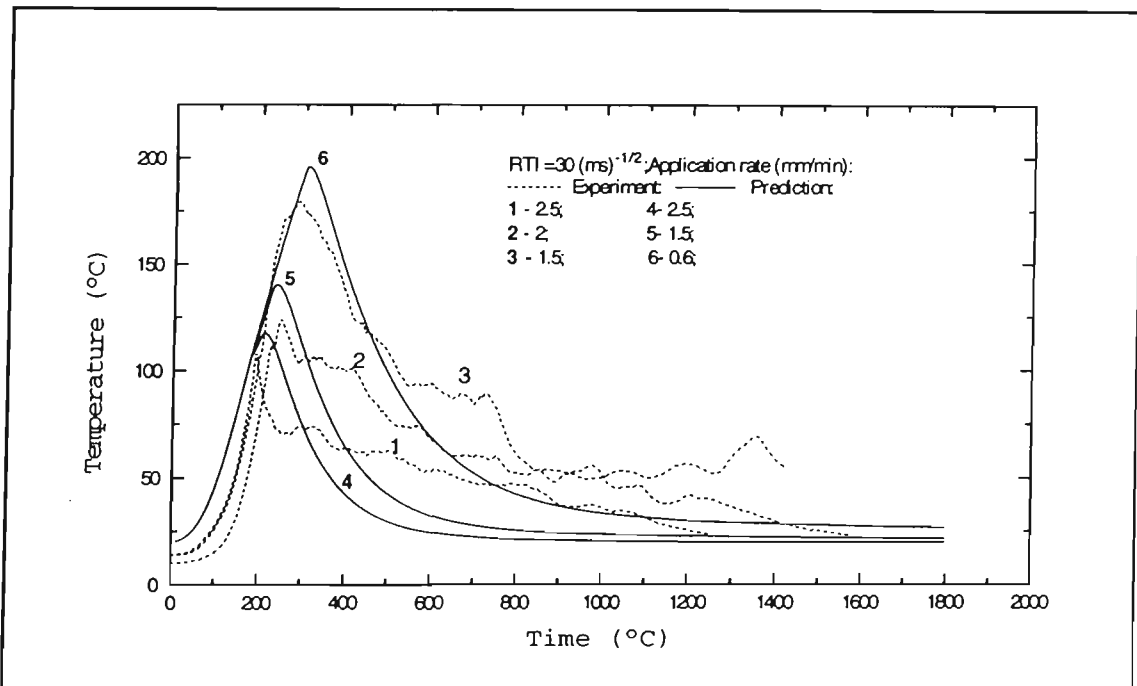


Figure 6.9. Time-temperature curves in fire extinguishment by the direct water application for the different sprinkler delivered densities. In the model initial fuel mass is 232 kg and sprinkler is represented by 1mm mean droplet diameter. Solid lines correspond to predictions; dotted lines – to experimental data.

In Figure 6.10, the predicted effect of mean droplet diameter on fire extinguishment due to water impact is shown. It is apparent that for a given water discharge rate, the decay time is shorter for a spray with smaller mean droplet diameters. This conclusion was also confirmed by the experimental data given in [29]. It can be shown that rate of area coverage by droplets is inversely proportional to droplet diameter: the smaller the diameter, the faster is coverage, and the more effective is suppression according to the present model.

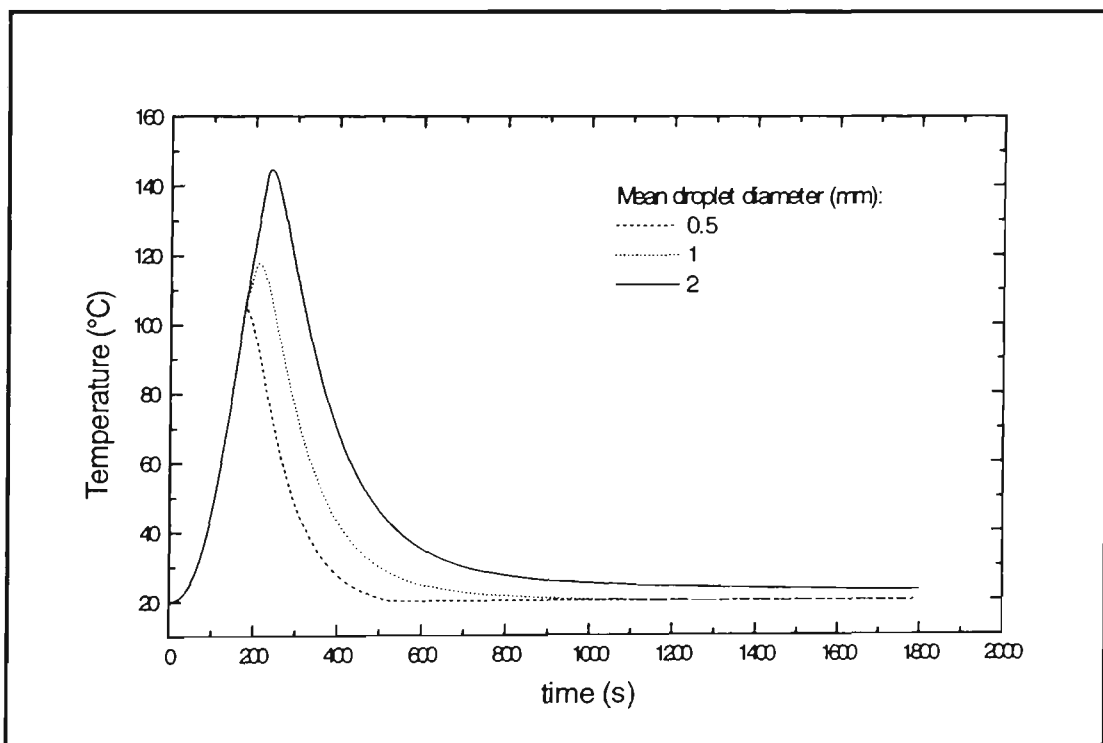


Figure 6.10. Prediction time-temperature curves for 99.5% of fuel exposure at the time of sprinkler activation. The sprinkler is represented by 1kg/s discharge rate and $RTI = 30 (ms)^{1/2}$.

The effect of sprinkler RTI on extinguishment can be seen in Figure 6.11. For higher RTI values, since the temperature and HRR rise are higher at the moment of sprinkler activation, the total extinguishment takes a longer time.

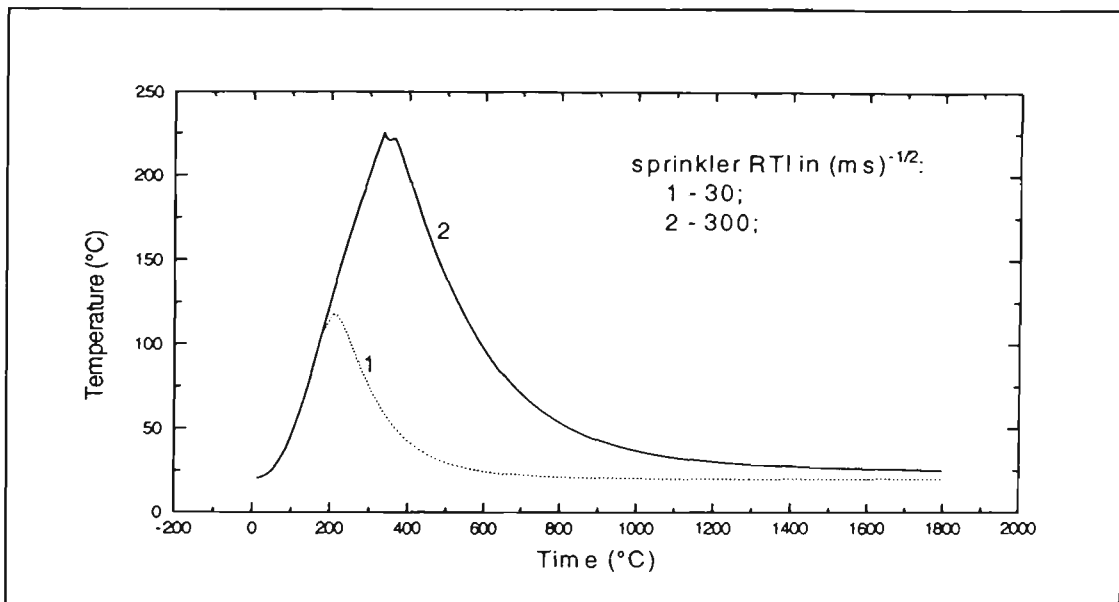


Figure 6.11. Prediction of fire extinguishment for 99.5% fuel exposure by the sprinklers with different RTI indexes. The sprinkler flow rate is 45L/min (2.5mm/min application rate) and mean droplet diameter is 1mm.

6.5 WATER MIST IN SUPPRESSION OF PRE-FLASHOVER AND POST-FLASHOVER FIRES

6.5.1 Pre-Flashover fire suppression

The nature of interaction of water spray with a fire is such that the cooling effect becomes essential for finely divided water droplets capable of creating a large interface between water and gas (Chapter 4). Prediction of suppression of pre-flashover and post-flashover fires by water mists using NRCC-VUT FGM combined with the present spray cooling model (SHAR) led to the results shown below. The pre-flashover fire has been modeled for the room size used in the CESARE experiments, even though the experimental data on the effect of pure gas cooling without water application are not available.

The effect of water flow rate on gas cooling effectiveness during pre-flashover fire suppression has been studied while mean droplet diameter was kept the same. The results are plotted in Figure 6.12. In all cases, the sprinkler was activated 5 minutes after ignition. The room has the same size, 20 m² area, and openings as it is shown in Figure 6.2. The spray was represented by one diameter shown at the top of each plot, and variation in water mass flow rates is indicated in the legends. To make a comparison, the same initial velocity

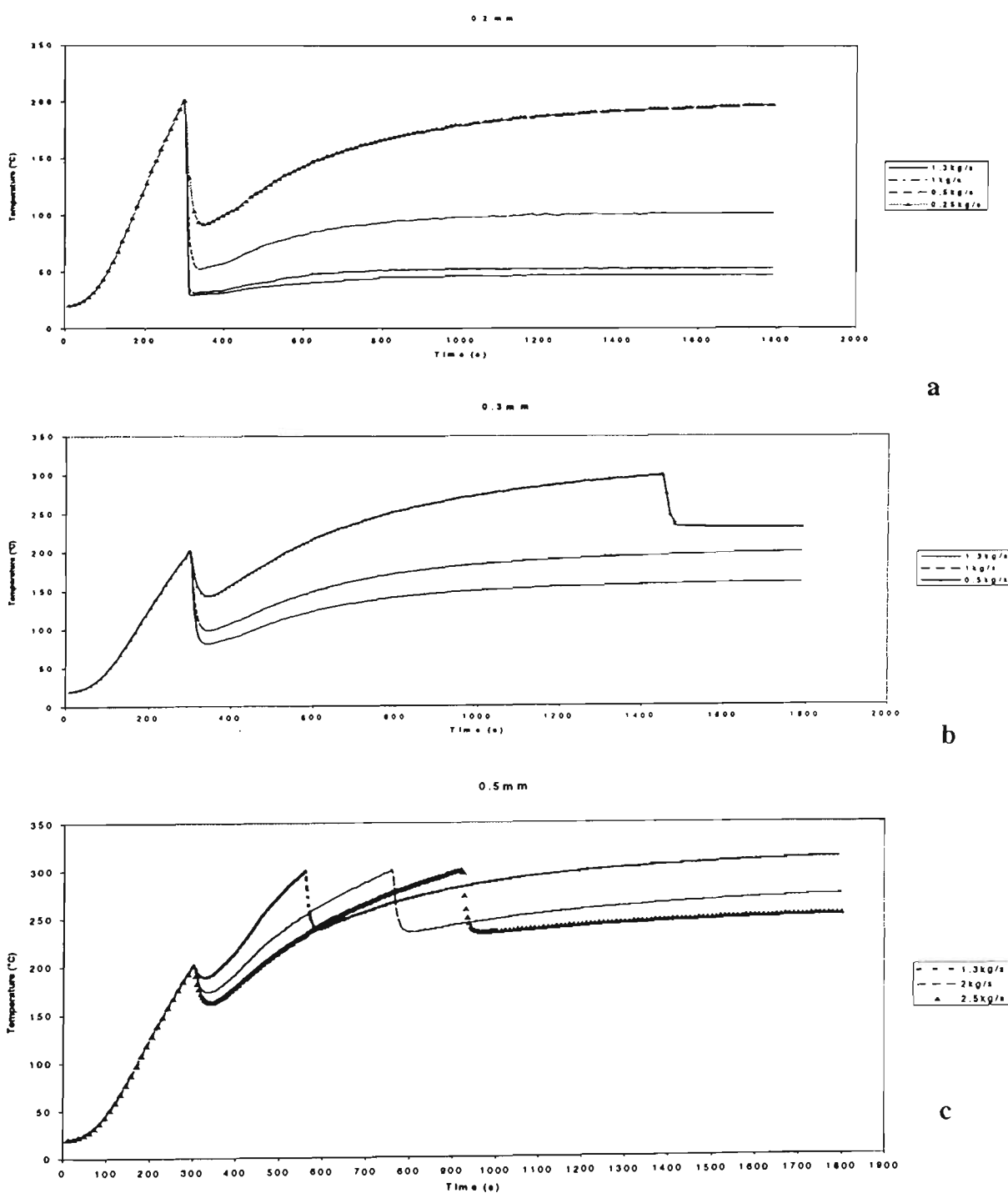


Figure 6.12. Sensitivity of gas room temperature to spray characteristics during gas cooling by water sprays. Droplet diameter used in calculations corresponds: a) 0.2 mm; b) 0.3 mm; c) 0.5 mm. Water flow rates are shown at the legends. Gas was assumed to be steady and droplet initial velocity was 1 m/s in all calculations.

(1m/s) of droplets was used in a steady gas flow. In Figure 6.12 (a), 0.2 mm water spray with water flow rates from 80 l/min (1.33 kg/s) to 0.25 kg/s demonstrates a high cooling capacity. During the 30 min fire, room temperature is kept below 300°C level that prevents window breakage and occurrence of flashover. This spray can also keep tenable conditions, gas temperature below 100°C, with flow rates down to 0.5 kg/s, and to control fire in all cases.

In Figure 6.12b, the gas cooling capacity of 0.3mm spray is shown. In this case the spray effectiveness is much less than for 0.2mm spray. Thus, window breakage is prevented only by 1kg/s and higher rates. None of the rates is capable of preserving tenable (100°C) conditions for the duration of at least 15 minutes. However, all sprays control the fire, i.e. keep the room temperature at constant level.

The 0.5mm spray, in Figure 6.12c, only delays the window breakage, but it can not stop it even though water flow rate is increased up to 2.5kg/s. However, the conditions during the first 30 minutes are still far below flashover, and the fire is controlled.

6.5.2 Post-flashover fire suppression

The nature of interaction of water spray with a fire is such that the cooling effect becomes essential for finely divided water droplets capable of creating a large interface between water and gas. According to NFPA classification, water sprays consisting of droplets with diameters less than 1mm can be considered as mists. Prediction of suppression of post-flashover fires by water mists using NRCC-VUT FGM combined with the present spray cooling model (SHAR) led to the results discussed below. Lack of measurements during Class A pre-flashover fire suppression by gas cooling mechanism only (shielded fire, for example) in CESARE tests, does not allow to provide quantitative comparison with NRCC-VUT FGM predictions. However, the data available in the literature for mist nozzles was for liquid pool heptane fires (4.5MW) in its post-flashover phase [13] were used for comparison.

The input file was changed to possibly meet the experimental conditions given in [13]. Thus, the room size was changed to $3.6 \times 2.4 \times 2.4 \text{ m}^3$ with one opening, a door of $2 \times 1 \text{ m}^2$ area and no window. Since NRCC-VUT FGM has not been designed for predictions of the liquid pool fire development, its fire growth curve can not exactly reflect the fire behavior described in [13]. Thus, the comparison between prediction and experiment can be considered only as qualitative. To make the prediction a little more appropriate to experimental conditions, the sprinkler initiation in NRCC-VUT FGM corresponding to the moment when the predicted time-temperature curve reached about 700°C , i.e. the temperature indicated in the experiments before the sprinkler activation.

In Figure 6.13 the upper curve corresponds to unsprinklered fire, while the three solid-line lower curves correspond to a fire cooled by 0.3, 0.35 and 0.5 mm water mists. Water flow rate of 80 l/min was used for both sprinklers, similar to the value used in the experiments [13]. The activation time was chosen as 10 min, when gas temperature was far above the flashover turning point of 600° [58]. The lowest labeled curve, which nearly coincides with the curve for 0.3 mm spray, corresponds to the 0.25 mm spray. This case is plotted to confirm the conclusion obtained earlier (Section 4.4), namely, that there is a limit in heat absorption which occurs at certain gas temperature for given droplet diameter. Thus, as discussed in Figure 6.13 gas temperatures for both 0.3 and 0.25 mm sprays achieve their limit and have the same effectiveness.

In Figure 6.14, the effect of water flow rate is shown. The rate of gas cooling is proportional to water flow rate. The four curves in Figure 6.14 display full fire control indicated by the plateaus prior to the natural decay due to the fuel “burn-out”. None of the sprays is capable of extinguishing the fire completely.

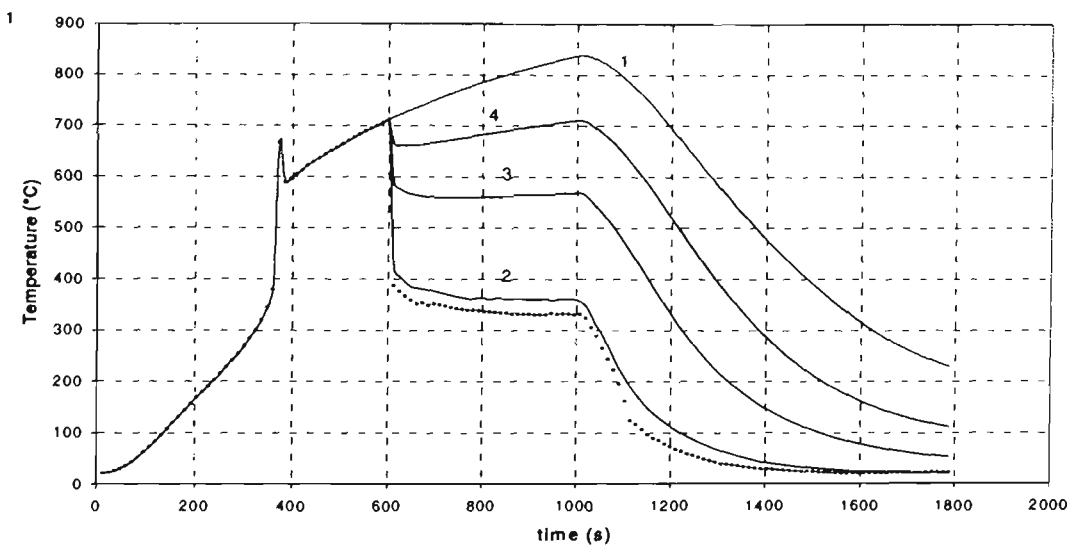


Figure 6.13. Prediction of post flashover fire suppression with spray of different droplet diameters. Gas temperature histories in RFO ($2.4 \times 3.5 \times 2.4 \text{ m}^3$) with (curves 2, 3, 4) and without (curve 1) sprinkler intervention. Droplet diameters correspond: 2 - 0.3 mm; 3 - 0.35 mm, 4 - 0.5 mm - 0.25 mm. Water flow rate in all cases - 80 L/min (1.3 kg/s).

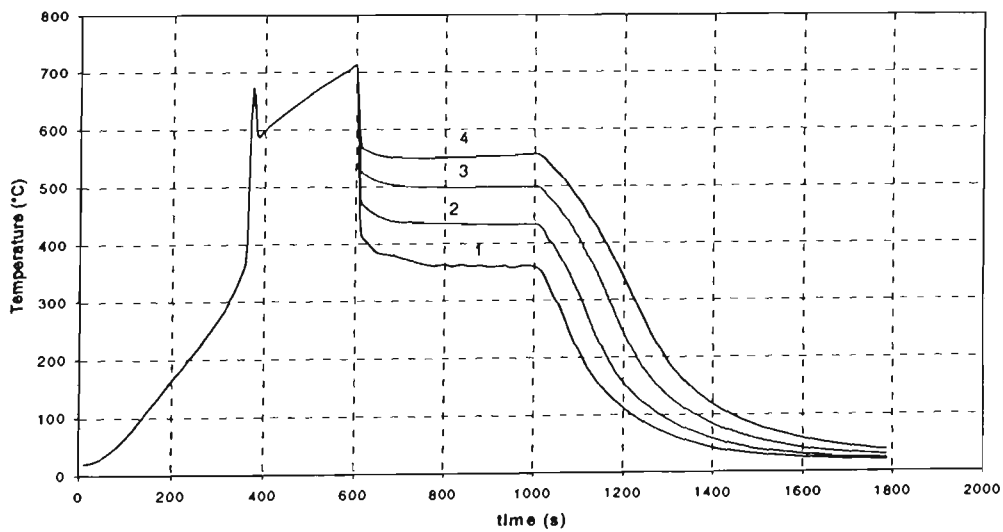
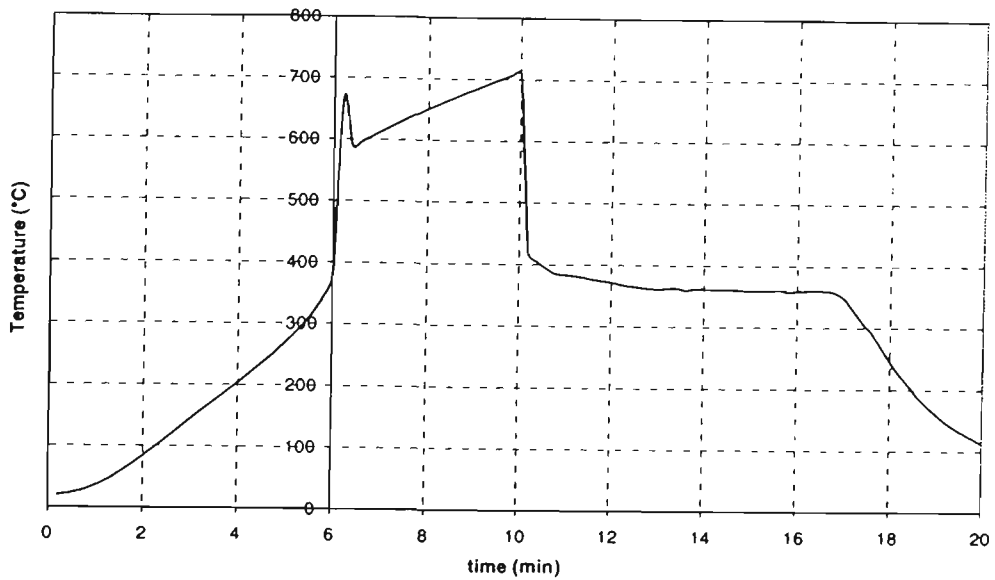
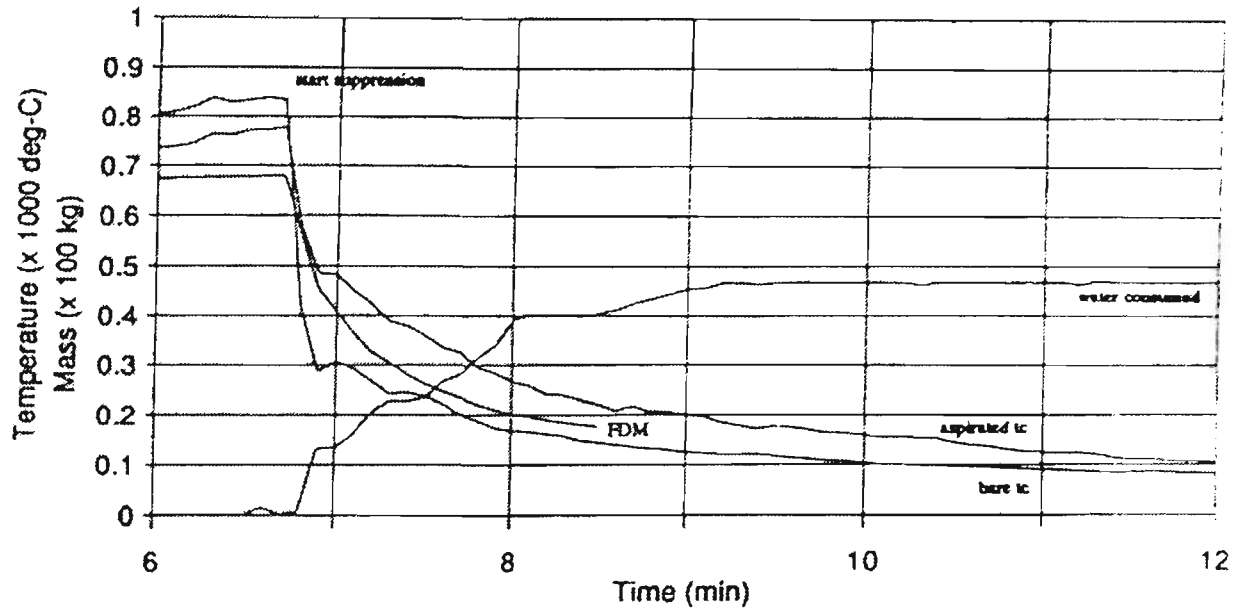


Figure 6.14. Prediction of post flashover fire suppression with sprays of different discharge rates and uniform 0.3 mm droplet diameter. The discharge rates are: 1 - 1.3, 2 - 1, 3 - 0.7 and 4 - 0.5 kg/s.



a)



b)

Figure 6.15. Comparison of the predicted in the present work post-flashover fire suppression (a) with suppression experiments of Tuomissaari [13] in full scale fire (b). The figure (b) is taken directly from the original paper [13] and reflects the temperature measurements taken by two types of thermocouples (upper and lower curves among the three decaying curves) as well as prediction (middle curve) using FD Model of Pieterzak et al. [48]. The water consumption rate is also plotted in the figure.

In Figure 6.15a and Figure 6.15b, the comparison between the present prediction and experiments described in [13] is shown. Figure 6.15a is a repetition of the curve for 0.3 mm spray given in Figure 6.13, while Figure 6.15b is taken from [13] and reflects the experimental data in fire suppression by a similar spray.

From a comparison of Figure 6.15a and Figure 6.15b, it is seen that the present results show longer extinguishment time, and therefore under-predict suppression. In [13], fire was completely extinguished in less than 1 minute, while in prediction for the similar 0.3mm spray, fire only starts to decay after about 3.5 minutes. The possible reason for this discrepancy can be assigned to the specific conditions for the decay mode prescribed by NRCC-VUT FGM. The decay in the model actually starts as either fuel mass or oxygen concentration reach their critical value.

6.6 CONCLUSIONS

This study has explored the possibility of predicting fire suppression by combining a sprinkler heat transfer model with a compartment fire zone model. Based on the results obtained, the following conclusions can be drawn:

1. The combined model allows the evaluation of the contribution of different mechanisms of extinguishment, such as gas cooling by water spray, oxygen displacement by steam due to spray evaporation and blockage of flame spread due to water direct impact on fuel.
2. The gas cooling mechanism was found to be sensitive to the droplet diameter of water spray. For a given water flow rate, the smaller the diameter, the higher is the heat absorption rate and the less is the risk of flashover occurrence.
3. Direct water impact over the fuel was found to be the main extinguishment mechanism for residence sprinklers with large droplet diameter and flow rate relatively lower than standard flow rate.
4. Extinguishment due to water impact is insensitive to water application rate and mean droplet diameter in a wide range of these parameters. However, it is sensitive to the percentage of fuel exposure to water.

-
5. Comparison with experiments has been done in terms of direct water impingement and gas cooling during fire. The comparison with water impingement experiments can be considered only as qualitatively reasonable. Further improvement of water-fuel interaction modelling with heat transfer effects are needed.
 6. The limited experimental data on gas cooling by mist sprays during liquid pool fire suppression were used for validation of model predictions. NRCC-VUT FGM has been successfully used to predict gas temperature and HRR histories before the nozzle activation, while temperature reduction histories after activation were different. The quantitative agreement has been achieved only for an immediate temperature drop after nozzle activation.
 7. All cases of fire development in this Chapter were studied in terms of fire sprinkler Location 1. The approaches used in this chapter can be further applied to the study of the effect of different locations on fire development.

7 CONCLUSIONS

Within the current state of knowledge, there has been a definite lack of reliable models of fire extinguishment due to water spray intervention. This gap is partially closed by the present work. As developed here, a relatively simple zone-type model of fire suppression by water sprays, can help to realistically identify water sprinkler or nozzle effectiveness under specified fire conditions, while avoiding excessive worse case scenario designs. Hence, the present model can be used in performance based fire safety assessments. The model can also serve for effective choice of sprinkler/nozzle parameters and suppression tactics. To summarize how this model has been developed in the present thesis, the general conclusions of each chapter are listed next.

The literature review in *Chapter 2* describes approaches and results available from studies of fire and sprinkler interaction. In this chapter, it was shown that to predict suppression accurately, fire development and spray parameters need to be interrelated. Through such models, sprinklers or mist nozzles thermal performance in fire can also be predicted. The more thorough works which describe fire suppression are mostly experimental, where fire characteristics, such as extinguishing time, fuel/gas temperature histories and wall temperature, are measured against spray parameters, namely, water discharge rate and droplet diameters. In some works, spray activation time and temperature are also reported. Experiments usually allow only one spray parameter, to be varied, such as spray discharge rate, while droplet diameters are presumed to be unchanged. There are few experimental works where the effects of change in more than one spray characteristic are measured and studied, yet these works do not provide generalisation and reliable formulas. The results and conclusions of experimental works can be applied only to similar types of fire, fuels, rooms, ventilation conditions and spray parameters.

In terms of the prediction and modeling of fire suppression, there are two main categories in the literature. In the first category are the in-depth studies of spray heat transfer and droplet dynamics in a gas flow. Most of these studies do not have fire development and suppression models. In the second category are studies with models of fire suppression.

These are usually CFD-based, and they mostly model fire as a heat source in a ventilated enclosure, although combustion models also exist. In these models, especially if they are not based on commercial software, but prepared as in-house program codes, sprays are represented poorly, usually as heat sinks without the necessary details of droplet dynamics. Fire extinguishment is not usually modeled by CFD, and spray effectiveness is judged by the pre-established gas temperature level drop.

In *Chapters 3 to 5*, the behavior of single droplets and water sprays is examined in two scenarios in order to determine the optimal thermal performance of sprays. Firstly, the interaction with fire induced gas flow is studied in Chapters 3 and 4. Secondly, the interaction with hot fuel surface is examined in Chapter 5. The complex transient process of fire suppression, with both gas cooling and fuel coverage, is presented in *Chapter 6*. For this purpose, the present model has been combined with a zone model. This combination is capable of simulating gas-droplet and fuel-droplet interactions to predict suppression. Hence, the combined code is an engineering tool that can be used to investigate fire behavior with possible modifications of spray characteristics and nozzle location, in addition to the relevant zone model parameters, such as the room size, heat release rate (or fuel size) and ventilation conditions. The conclusions of Chapters 3 to 6 are summarized next.

The numerical model of droplet motion under gravity and drag forces were discussed in detail in Chapter 3. The conclusions of this chapter can be summarized as follows:

- Three types of possible fire-sprinkler locations are specified, and spray dynamics is calculated in terms of these locations. The three locations cover the following cases: Case 1: Spray activation in a horizontal, slowly moving fire hot layer (Location 1); Case 2: Intermediate location in a plume turning point (Location 2); and Case 3: Activation just above fire, in uprising fire plume (Location 3).
- The effects of different gas velocity profiles generated by fire on spray behaviour are modelled. At Location 1, based on the available information in the literature, horizontal gas flow is characterised by two profiles: uniform and triangular. The comparison of the effects of these profiles has been done in terms of droplet

residence times. At this location, it has been shown that the gas velocity magnitude is more important in spray dynamics than the type of velocity distribution. At Location 3, an uprising fire plume is modeled by two types of gas velocity distributions: uniform and Gaussian, with characteristic centreline velocity related to heat release rate. At this location, similar to Location 1, the gas velocity magnitude has shown to play a major role in droplet penetration. In addition, the velocity distribution has been found to alter the effectiveness of the spray cone angle.

- The spray capability to penetrate through uprising gas flow, representing the fire plume, is calculated in terms of different droplet diameters. If the terminal droplet velocity exceeds the uprising gas velocity, then the droplets are capable of penetrating the plume. For example, to penetrate a 2m/s uprising uniform gas flow, the droplets of no less than 650 μm in diameter are needed. For larger diameters, terminal velocities are higher, and for the smaller ones, they are lower. Initial conditions affect only the distance at which this terminal velocity is established.
- Droplet residence time, e.g. the duration of droplets' flight through cooling area of study, is considered as the main output of droplet dynamics that affects whole spray heat absorption capacity. It is shown that this time defines a spray number density, i.e. the total number of droplets that is permanently available in a given control volume.
- Spray droplet residence times for different droplet diameters and locations are plotted in terms of initial angles, showing the effect of spray angle. At horizontal gas flow (Location 1), spray discharge angle does not have as significant an effect on spray dynamics as it has in a vertical gas flow (Location 3). In a horizontal gas flow, droplets at the spray periphery have slightly longer residence times in comparison with the central part. In an updraft flow, large droplets stay much longer at the spray periphery than at the centre, while small droplets are simply diverted to the ceiling with shortest times at the periphery, and longest at the centre.
- The effects of initial angles for 0.3mm sprays in co-current versus counter-current gas flows are also compared. A 90° spray is preferable in a co-current flow directed

upward, while a 60° spray is more appropriate in a counter-current flow (Location 3). These results are supported with experimental evidence.

- The main validation of the present numerical results in droplet dynamics is based on comparison with experimental values of spray Actual Delivered Density (ADD) distribution. ADD is seen as a cumulative result of droplet trajectories and gas and droplet velocity distributions. A close agreement between numerical results and experimental data has been obtained for this parameter. For this purpose, Early Suppression Fast Response (ESFR) sprinklers are studied.
- CFD modelling is used to evaluate the effect of two-way coupling and gas turbulence on droplet dynamics. For this purpose, a commercial code, namely CFX4, is used. The present model takes into full account of the effect of gas flow on droplet trajectories. Hence, one way coupling is used. To determine the effect of this simplification, the trajectories obtained with the present model in a horizontal smoke layer are compared with those obtained using CFX4. CFX4 has an imbedded droplet motion equation, similar to the present model, and takes into account two-way coupling and gas turbulence. The turbulence intensity was about 0.3 to 0.5% in the calculations. This comparison has pointed out that no appreciable effect could be determined coming either from two-way coupling or gas turbulence.

Analytical models have been developed to calculate heat transfer between water sprays and the hot gas fire environment at different regimes of gas and droplet movement as presented in *Chapter 4*. The study is conditionally divided into two cases: heat transfer at ordinary spray activation gas temperatures, of about 200°C or less, with practically non-evaporating droplets; and heat transfer under very high gas temperature conditions (600°C and more) that imply high droplet evaporation rates up to full droplet disappearance.

For ordinary sprays activated at nominal gas temperatures (below 200°C) the conclusions are summarised below:

- The original premise, developed in 60's, on the existence of spray optimal droplet diameter in heat absorption is numerically confirmed and explained based on droplet dynamics in fire-induced uprising gas flow. The predicted

values are in good qualitative and quantitative comparison with limited experimental data.

- The radiation absorption rate was shown to be too low in comparison with gas convective cooling.
- Convective heat transferred to droplets, is mostly used for rising droplet temperature, only a small part of it is utilised for evaporation (as shown in Figure 4.1). Droplet evaporation rate does not exceed 4-4.5% of the total discharge rate even for the spray smallest droplets.

For *mist sprays* activated at high gas temperatures (above 400°C) the conclusions are summarised below:

- Evaporation of water droplets becomes a decisive mechanism in gas cooling under high (about flashover) gas temperature conditions, when immersed droplets quickly attain an equilibrium steady temperature. This phenomenon is numerically predicted, and the dominating effect of droplet diameter in comparison with spray discharge rate on spray heat absorption capability is shown.
- The objective is to reduce average compartment temperature below the hazardous level due to heat absorption by spray during fire suppression. However, large rate of spray evaporation in the hot layer may hinder its penetration capability and sufficient amounts of water will not be delivered into the flame or other zones of fire. Therefore, mist thermal performance is calculated together with evaporating droplet dynamics in order to predict the penetration depth until droplet crosses through the hot layer. For example, to penetrate through 1m at 1200°C compartment temperature, droplets no less than 0.4mm are needed, while to penetrate 0.6m - 0.3mm droplets would be enough
- The heat absorption rate distribution within the spray cone is quite uniform below the distance from nozzle to about 5-7% of the hot layer depth. The droplet trajectories nearly fill uniformly the whole compartment space in this area. At the spray cone head within 5 cm downwards, heat absorption rate has

its peak and concentrated only in a small volume occupied by the spray in this close-to nozzle proximity.

Chapter 5 presents a one dimensional transient conduction model inside a hot solid fuel slab covered by water spray and subjected to fire environment to the incident radiative heat flux. The properties of fuel and spray characteristics are interrelated and results are plotted in terms of fuel surface temperature histories before and after water application. Two main ideas have to be accounted for when surface cooling is modelled:

- The heat absorption rate, or cooling regime provided by water sprayed on top of fuel surface, depends on surface “superheat”, e.g. fuel temperature rise above bulk water temperature. The form of heat transfer (regime) changes as fuel/water temperature difference changes below or above a certain value.
- A critical water flux, e.g. minimum water application rate needed for extinguishment, is shown to be a linear function of external radiant heat flux with a slope depending on fuel properties.

The prediction of fire suppression by combining a spray heat transfer model with a compartment fire one-zone model (namely, NRCC FGM) is presented in *Chapter 6*. One-zone model, originally developed in Canada and then extended in VU, Australia, consists of a number of independent modules (subroutines) which quantify phenomena in fire. Based on the solution of interrelated mass and energy conservation equations, a core model (main program) produces temperature, HRR, species and fuel mass histories by taking as input a specified initial ignition heat flux applied to given initial fuel mass.

The new module developed here is used as an additional sub-routine needed for evaluation of water spray impact, and consequently fire development during extinguishment or suppression. The combined model was then used to predict the additional gas cooling due to spray activation with accounting for different spray parameters. Mist and sprinklers were studied. The phenomenon of spray fuel coverage has been also included. The main outcomes are summarised below:

-
- The water delivered density needed for fire extinguishment in the case of complete fuel coverage by water is about 80% less than what is specified by fire safety standards values. The gas cooling mechanism is not as effective as fuel coverage and the standard delivered densities can not usually provide a sufficient safety level due to gas cooling.
 - Extinguishment due to water impact is insensitive to water application rate and mean droplet diameter in a wide range of these parameters. However, it is sensitive to the percentage of fuel exposure to water. It is shown that if percentage of uncovered area or subsequent fuel mass, exceeds the specified by the program critical level (20% of initial fuel mass in present study), a dangerous temperature rise can occur leading to flashover with sufficient amount of oxygen and fuel left
 - Comparison with large scale experiments in fire suppression due to direct water application on top of fuel showed a good qualitative agreement in terms of the effect of water delivered density. The quantitative agreement was not possible, since delivered densities in experiments could not be lowered to match those in the calculations.
 - The limited experimental data on gas cooling by mist sprays were used for validation of model predictions. Even though the experiments were based on liquid fuel fires, still NRCC-VUT FGM has been successfully used to predict gas temperature and HRR histories before the nozzle activation. The quantitative agreement has been achieved then for the immediate temperature drop after spray activation, while the further temperature histories did not show a reasonable agreement. The full extinguishment time was considerably longer in model prediction than in experiments.

8 SUGGESTIONS FOR FUTURE WORK

This thesis has considered the behaviour of single droplets of water in terms of heat, mass and momentum transfer of its droplets with gases and solids within a residential room-fire environment. e.g. an environment represented by certain temperatures, gas velocities and boundaries. The principles of integration of the droplet submodel into a fire zone model have been developed, and then the combined zone model has been used to predict room temperature history and fire suppression for different room, spray and initial conditions.

8.1 EXPANDING THE PRESENT SUB-MODEL

Further work towards prediction of fire suppression by water sprays, which is an extension of the presented approach, can be potentially expanded in **four** general directions:

- Extend (or improve) the existing droplet submodel;
- Expand the fire zone model;
- Use the existing combined model to study the effects of external factors
- Design and conduct the fire experiments using mists for extinguishment to verify the accuracy of prediction and validity of the combined zone model.

A number of concrete recommendations in terms of suggested directions for further research is given below.

8.1.1 Extend the existing droplet submodel

- Account for the collision of droplets (both coagulation and break-down) within the spray and examine the effect it has on heat transfer and motion. The first thing to do is to specify the conditions of whether or not the sprays can be treated in terms of single droplet relationships (some criteria can be found in [63, 80]); if they cannot then find out ways of accounting for interactions. Indirectly this effect could be accounted for through the adjusted transport coefficients [80]. In addition, understanding of the collision phenomenon would help to model the effect of overlapping sprinkler sprays.

-
- Examine the effect of water impurity and droplet coating (mentioned in Chapter 4 of the thesis) on heat transfer and motion and, as a result, on total room heat exchange and fire suppression. It may be interesting to estimate the fraction of coated droplets deposited on solid surfaces and, thus the risk of property damage in the compartment. Some works on coating are cited in [2]

8.1.2 Expand the fire zone model

- To include the fire plume and possibility of droplet discharge in this area. Separately, this phenomenon has been studied in Section 3.3.3 of this thesis, however, it has not been included into general fire zone model.
- Include the ceiling jet (which already exists to produce a sprinkler activation time) to account for possible heat transfer between droplets and the jet. It would be interesting to check the suggestion of [20] about possible delay of activation of remote sprinkler heads due to cooling of the ceiling jet by the spray activated earlier on.
- The effect of cooling of the ceiling jet can be also used to estimate the change in ventilation conditions.
- It would be useful to study the effect of the ceiling/wall wetting on fire suppression, or at least to quantify it. It is usually considered that ceiling wetting is a positive for fire suppression phenomenon since it cools the ceiling and reduces radiation feedback to the fuel.
- Develop or use some existing zone model, which has been verified for large compartment fires, combined with developed droplet submodel to investigate the effect of spatial distribution of sprinkler heads and include the effect of overlapping sprays on total heat transfer.

-
- Using the presence and effect of window breakage factor in existing zone model and accountability of the droplets trajectories, it is possible to estimate the spray cooling effect by knowing the fraction and distribution of water which may reach the glass from inside. More likely, the small-scale or large-scale fire experiments with glass protection by water cooling will be needed.

8.1.3 Use the existing combined model to study the effects of external factors

- To investigate the effectiveness of nozzle geometry and pressure, since their specifications: droplet size, diameter distribution, cone angle and velocity, are the sensitive parameters of the combined zone model.

8.1.4 Design and conduct the fire experiments using mists for extinguishment to verify the accuracy of gas cooling prediction and validity of the combined zone model

- There appears to be a serious lack of experimental data on mist nozzles. Both small scale (even non-fire) and large scale experiments can be valid.
- The mist nozzle characteristics should be known to extend to give a realistic spray parameters (droplet diameter distribution and flow rate). It would be good if a few different mist nozzles (even with the same nominal pressure) is studied to understand the sensitivity of fire suppression (or gas cooling) to droplet size distribution.
- To ensure that prediction of fire suppression is valid, the fire conditions (room size, ventilation, etc.) should be similar to those which were used to verify the fire zone model which is in use.
- The different stages of fire (at least one pre-flashover and one post-flashover) prior to nozzle activation should be studied in experiments.

8.2 NEW FIELD OF RESEARCH

There is considerable scope to carry out research on the radiation between droplets themselves [63] and droplets and gas. It may include radiation absorption, scattering, diffusion or attenuation by water sprays of different droplet sizes (from fine mists to large droplets) and densities, in a room fire environment. Precise experiments would be needed to estimate the contribution of radiation heat exchange in total gas cooling by water sprays. When the fraction of heat absorbed due to radiative exchange is understood better, it can be then used again in existing combined fire-droplet model, especially for prediction of extinguishment in post-flashover fires.

Radiation to wetted or coated by the water film solid surfaces (fuels or walls), which has been studied here theoretically could be studied experimentally to improve/extend the theory. The effect of surface quality and fuel type in this problem could be then understood better.

REFERENCES

- 1 Mawhinney, J.R., Dlugogorski, B.Z. and Kim, A.K., 1994, A closer look at the fire extinguishing properties of water mist, Proceedings of the 4th International Symposium on Fire Safety Science, July, pp.47-60.
- 2 Grant, G. and Drysdale, D., 1996, A study of the science of fire suppression and extinction, Interflam'96. 7th International Conference on Fire Science & Engineering, Edinburgh, pp.911-914
- 3 Sousa, A., An, M. and Venart, J.E., 1995, Numerical study of a waterfog fire suppression systems in a shipboard machinery room, 5th International Conference 'ASIAFLAM '95', March, pp. 243-254.
- 4 Hadjisophocleous, G.V., Shu Cao and Knill, K., 1995, Modelling of the suppression of liquid pool fires using fine watersprays, 1st International Conference 'ASIAFLAM '95', March, pp. 231-242.
- 5 Cote, A.E., 1993, Fire Protection Handbook, 18th Edition, NFPA, Boston, Mass., Chapter 6/Section 15.
- 6 Nash, P., Young R.A., 1991, Automatic sprinkler systems for fire protection, 2nd edition, Paramount, Borehamwood, England, p.288.
- 7 Bouchard, J.K., 1987, Automatic sprinkler systems handbook, Third edition, NFPA, p.614.
- 8 Solomon, R.E., (editor), 1994, Automatic sprinkler systems handbook, Fifth edition, p.710.
- 9 Bill, R.G and Ural, E.A., 1999, Water mist protection of combustion turbine enclosures, Proc. of the 6th International Symposium on Fire Safety Science, pp.457-468.
- 10 Kim, M. B., Jang, Y. J. and Kim, J. K., 1996, Burning rate of a pool fire with downward-directed sprays. Fire Safety Journal, Vol. 27, pp.370-48.
- 11 Thomas, R., 2000, Supplementary protection/ Concealed spaces. Sprinklers 2000 Seminar. FPA/ Standards Australia, 24 March, Melbourne, pp. 41-44.
- 12 Andersson, P. and Holmsted, G., 1999, Limitations of water mist as total flooding agent, Journal of Fire Protection Engineering, vol.9 (4), pp.31-50
- 13 Tuomissaari, M., 1993, Suppression of Compartment Fires with a Small Amount of Water. Proc. of International Conf. On Water Mist Fire Suppression, Sweden, November, pp. 10-13.
- 14 Galea, E., 1989, On the field modelling approach to the simulation on enclosure fires, J. of Fire Prot. Engr., vol.1(1), pp.11- 22.
- 15 Kanury, A.M., 1985, Scaling correlations of Flashover Experiments, Fire safety science and Engineering, Harmathy, pp.97 - 121.

-
-
- 16 Mawhinney, J.R., Hadjisophocleous, G.V., 1996, The role of fire dynamics in design of water mist fire suppression systems, Interflam'96. 7th International Conference on Fire Science & Engineering, Edinburgh, pp. 415-423
 - 17 Bishop, S.R., Holborn, P.G., Beard, A.N. and Drysdale, D., 1993, Dynamic modelling of building fires, *Appl. Math. Modelling*, vol.17 (April), pp.170-183.
 - 18 Cooper, L.Y., 1982, A Mathematical model for estimating available safe egress time in fires, *Fire and Materials*, vol.6 (3,4), pp.135-144.
 - 19 Wighus, R. 1999, Extinguishment limits of enclosed fires with water mist as the fire suppressant. Proc. of the 6th International Symposium on Fire Safety Science, p.1201.
 - 20 Hinkley, P.L., 1992, Sprinkler operation and the effect of venting: studies using a zone model, Building Research Establishment Report, Borehamwood, Colt International.
 - 21 Hill, G.R., Sarkos, C.P., Marker, T.R., 1991, Development and evaluation of an onboard aircraft cabin water spray system for postcrash fire protection, Society of Automotive Engineers (SAE), vol. 100, Sect.1, pt.2, pp.2784-92.
 - 22 Hoffman, N.A. and Galea, E.R., 1993, An extension of fire-field modelling technique to include fire-sprinkler interaction interaction, I. The mathematical basis, II. The simulations. *International Journal of Heat and Mass Transfer*, vol.36(6), pp.1435-1457.
 - 23 Jones, A., Nolan, P.F., 1995, Disscussions on the use of fine water sprays or mists for fire suppression, *Journal of Loss Prevention in the Process Industries (UK)*, vol.8(1), pp.17-22.
 - 24 Rasbash, D.J., Rogowsky, Z.W. and Stark,G.W.V., 1960, Mechanisms of extinction of liquid fires with water sprays, *Combustion and flame*, vol.4(3), pp.223 - 234.
 - 25 Kung, H.-Ch., 1977, Cooling of room fires by sprinklers sprays, *Journal of Heat Transfer*, vol.99,Aug., pp.353-359.
 - 26 McCaffrey, B.J., 1984, Jet diffusion flame suppression using water sprays - an interim report. *Combustion Science and Technology*, vol.40, pp.107-136.
 - 27 Yao, C., 1985, Applications of sprinkler technology - early suppression of high-challenge fires with fast-responce sprinklers, *Fire safety science and engineering*, Harmathy, pp.254 - 375.
 - 28 Yao,C., 1992, Overview of FMRC's sprinkler technology research, Proceedings of the 1st International Conference on Fire Suppression Research, pp.57 - 82, Brandforsk, Sweden.
 - 29 Yang, J.C.. Boyer, C.I., Grosshandler, W.L., 1996, Small-scale extinguishments using water droplets, not-published.
 - 30 Downie, B. and Gogos, G., 1995, Interaction of a water mist with a buoyant methane diffusion flame, *Fire Safety Journal*, vol.24 (4), pp.359- 381.

-
-
- 31 Ingason, H. and Olsson, S., 1992, Interaction between sprinkler and fire vents, SP Report. 1992.11, Swedish National Testing and Research Institute, Sweden.
- 32 Chow,W.K., 1989, On the evaporation effect of a sprinkler water spray. Fire Technology. 1989, Nov., pp.364-373.
- 33 Stephenson, S. and Coward, M.J., 1986, Attenuation of radiant heat on LNG/LPG carriers with freestand water curtains, LNG/LPG Conference, November, pp.157 - 168.
- 34 Lage, P.L.C. and Rangel, R.H., 1993, Single droplet vaporization including thermal radiation absorption, Journal of Thermophysics and Heat Transfer, vol.7 (3), pp.502-508.
- 35 Log, T., 1996, Radiant heat attenuation in fine water sprays, The 7th International Conference in Interflam-96, UK, pp.425 - 434
- 36 Morgan, H.P., 1979, Heat transfer from a buoyant smoke layer beneath a ceiling to a sprinkler spray. 1-A Tentative Theory, Fire and materials.,vol.3(1), pp.27-33.
- 37 Mawhinney, R.N., Galea, E.R. and Patel, M.K., 1996, Fire - sprinkler spray interaction modelling using an Euler - Lagrange approach., Seventh International Fire Science and Engineering Conference "Interflam-96", pp. 841 - 845.
- 38 Chow, W.K. and Fong, N.K., 1990, Numerical studies on the interaction between a sprinkler water spray and a natural venting inside a building, Heat and Mass Transfer in Fires. AIAA/ASME Thermophysics and Heat Transfer Conference, pp.93-100.
- 39 Chow, W.K., 1994, Simulation of sprinkler hot layer interaction using a field model, Fire and Materials (London), vol.18(6), pp.359-379.
- 40 Yao,C.and Kalelkar. A.S., 1980, Effect of drop size on sprinkler performance, Fire Technology, vol.6, p.p.254-268.
- 41 Gardiner, A.J., 1988, The mathematical modelling of the interaction between sprinklers and the thermally buoyant layers of gases from fires, PhD Thesis, South Bank Polytechnic, London.
- 42 Wighus,R., 1991, Extinguishment of enclosed Gas Fires with water spray, Proceedings of the 3rd International Symposium on Fire Safety Science, July, pp.997- 1006.
- 43 Novozhilov, V., Moghtaderi, B, Fletcher, D.F. and Kent, J.H., 1995, Numerical simulation of enclosed gas fire extinguishment with water spray, Australian Symposium on Combustion. "The Fourth Australian Flame Days", C5 pp.1 - 6.
- 44 Pietrzak, L.M., Ball, J.A., 1977/78, Investigation to improve the effectiveness of water in the suppression of compartment fires, Fire Research, no.1, pp.291-300.

-
-
- 45 Harvie, D.J.E., Novozhilov, V. and Kent, J.H., 1995, Heat loss to water spray during surface combustion: Experimental results, 1995, Australian Symposium on Combustion, "The Fourth Australian Flame Days", C6, pp.13 - 18.
- 46 Nam, S., 1996, Development of a computational model simulating the interaction between a fire plume and a sprinkler spray. Fire Safety Journal, vol.26, pp. 1-33.
- 47 Lawrence, M., Piterzak, L.M., 1979, Effect of Nozzles on Fire Studies in terms of Flow Rate. Droplet Size, Fire Engineering, vol 132, No. 12, pp. 26-33.
- 48 Piterzak, L.M. and Johanson, G.A., 1985, Analysis of fire suppression effectiveness using a physical based computer simulation, Proceedings of the 1st International Symp. on Fire Safety Science, pp.1207 -1216.
- 49 Salzberg F., Vovarka F.J., Maatman G.L., 1970, Minimum water requirements for suppression of room fires, Fire Technology, vol.6 (Feb.), pp. 22 - 28.
- 50 Paji, D.G., Galustov, V.S., 1984, Osnovi techniki raspilivaniya jzidkosteiy. (The basis of liquid dispersion technique). Moscow, "Chimiya", p.254.
- 51 Chow ,W.K. and Shek, L.C., 1993, Physical properties of a sprinkler water spray, Fire and Materials (London), vol.17(6), pp. 279-292.
- 52 Nyankina K., Michailenko,G.G., Shklyaruk,E.V., 1990, "Evaluation of the spraying characteristics in a pressure atomizers on applying Monte-Carlo method", J. 'Izvestiya Vuzov. Chimiya i Chim. Technologiya', No. 2, 101-103.
- 53 Nyankina, K, Yatskar, I.Y., Michailenko, G.G., 1993, "Modelling of the absorbtion of fluorine contaminated gases in the hollow spraying apparatus". J. 'Teor.Osnovi Chim.Technologii' (Theoretical base of Chemical Technology), v.27, No 4, pp 442-444.
- 54 Ravigururajan, T.S. and Beltran, M.R., 1989, A model for attenuation of fire radiation through water droplets, Fire Safety Journal, Vol.15, pp.171-181.
- 55 Chen, K.H. and Trezek, G.J., 1977, The effect of heat transfer coefficient, local wet bulb temperature and droplet size distribution function on the thermal performance of sprays, Journal of Heat Transfer, ASME, Vol.99 (August), pp.381-385.
- 56 Novozhilov, V., Harvie, D. J. E. & Kent, J. H., Apte, V.B., Pearson, D. A., 1997, Computational fluid dynamics study of wood fire extinguishment by water sprinkler. Fire Safety Journal, Vol. 29, pp.258 – 281,
- 57 Pepi, J.S., 1997, Water Mist Fire Protection – When Less is Better, PM Engineer, December, 11 pp.3-12
- 58 Drysdale, D., 1987, An introduction to fire dynamics, Third edition, John Wiley and Sons, Ch.2: Heat transfer and aerodynamics, pp.34 - 57; Ch.4.: Diffusion flames and fire plumes. pp.114-143; Ch.5: Steady burning of liquid and solid fuels, pp.152-164.

-
-
- 59 Crowe, C.T., Sharma, M.P. and Stock, D.E., 1977, The Particle-Source-In Cell (PSI-CELL) Modell for Gas-Droplet Flows, *Journal of Fluids Engineering*. June, pp.325-332.
- 60 Novozhilov, V. and Kent, J.H., Flashover Control with water based fire suppression systems. The Fourth Asia-Oceania Symposium on Fire Science and Technology, Tokyo, May 2000 (pre-print).
- 61 Chow, W.K. and Fong, N.K., 1992, Numerical Simulation on cooling of the fire induced air flow by sprinkler water sprays, *Fire Safety Journal*. vol.17, pp.263-290.
- 62 Luo M., 1993, Combustion of bagasse in a sugar mill boiler, PhD Thesis, University of Queensland, St. Lucia, Australia.
- 63 Sirignano, W. A., 1993, Fluid dynamics by sprays – 1992 freeman scholar lecture. ASME Trans., *Journal of Fluid Engineering*, September 1993, Vol. 115, pp.345-378
- 64 Gosman, A.D., Ioannides, E., 1981, Aspects of computer simulation of liquid-fuelled combustors, AIAA 19th, Aerospace Sciences Meeting, January 12-15, St.Louis. Missouri, pp.25-32
- 65 Ranz, W.E. and Marshall, W.R., 1952, Evaporation from drops (Parts 1 and 2), *Chemical Engineering Progress*, vol.48 (3), pp. 141 - 146. 173 - 180
- 66 Lockwood, F.C. and Shan, N.G., 1981, A new radiation solution method for incorporation in general combustion prediction procedures, 1981, Eighteenth Symposium (International) on Combustion, The Combustion Institute, pp.1405-1414.
- 67 Siegel, R., and Howell, J.R., 1992, Thermal radiation heat transfer. 3rd edition, Hemisphere Publishing Co., p.1061.
- 68 Peacock, R.D., Fomey, G.P., Reneke, P., Portier, R. and Jones, W.W., 1993, CFAST - The consolidate model of fire growth and smoke transport. NIST (National Institute of Standards and Technology) Technical Note 1299., U.S. Department of Commerce.
- 69 Motevalli, V. and Marks, C.H., 1990, Transient and steady state study of small-scale, fire induced unconfined ceiling jets, *Heat and Mass Transfer in Fires*, AIAA/ASME Thermophysical and Heat Transfer Conference, pp.49-62.
- 70 Unoki, S., 1985, Fire extinguishing time by sprinkler, *Proceedings of the 1st International Symp. on Fire Safety Science*, Oct., pp.1187 -1196.
- 71 Chow,W.K., 1995, Use of computational fluid dynamics for simulating enclosure fires, *Journal of Fire Sciences*, vol.12 (July-Aug.), pp.300 - 333.
- 72 Chukkapalli, G., and Turan, O.F., 1995, Structural parameters and prediction of adverse pressure gradient turbulent flows: An improved $\kappa-\epsilon$ model, *ASME Fluids Engineering*, vol. 117, pp. 424-432.

-
-
- 73 Forney, G. P. and McGrattam, K. B., 1999, Computing the Effect of Sprinkler Sprays on Fire Induced Gas Flow, Proceedings of the Sixth International Symposium on Fire Safety Science. France, 1999, pre-print.
- 74 Lesier, M. and Metais, O., 1996, New trends in large-eddy simulations of turbulence, Annu. Rev. Fluid. Mech., vol.28, pp. 45-82.
- 75 Cox, G., 1995, Combustion Fundamentals of Fire. Academic Press, Chapter 6., Compartment Fire Modelling. pp. 332-407.
- 76 Vervish, L. and Poinsot, T., 1998, Direct numerical simulation of non-premixed turbulent flames, Annu. Rev. Fluid. Mech., vol. 30, pp. 665-691.
- 77 Bilger, R.W., 1994, Computational Field Models in Fire Research and Engineering. Proceedings of the Fourth International Symposium on Fire Safety Science, pp. 95-112.
- 78 Boyd, R.K. and Kent, J.H., 1986, Three-dimensional furnace computer modelling. 21st Symposium (International) on Combustion. The Combustion Institute, p. 256.
- 79 Turokoglu, H., Farouk, B. and Yang, L., 1996, Modelling of interfacial transport processes in direct contact condenser. HTD-Vol.326, National Heat Transfer Conference, Vol. 4, ASME 1996 , pp.47-61
- 80 Fthenakis, V.M., Schatz, K.W., Rohatgi, U.S. and Zakkay, V., 1993, Computation of flow fields induced by water spraying of an unconfined gaseous plume. Journal of Fluids Engineering, Trans. ASME, Vol.115, pp.742-749
- 81 Chigier, N., 1995, Spray combustion, HTD-Vol. 321FED-Vol. 233, 1995 IMEC, Proceedings of the ASME Heat Transfer and Fluids Engineering Division, ASME, pp. 3- 29.
- 82 Young, J.B., 1995, The fundamental equations of gas-droplet multiphase flow, Int. J. Multiphase Flow, vol. 21(2), pp. 175-191.
- 83 Yao, S.-C. and Schrock, V.E., 1976, Heat and mass transfer from freely falling drops, ASME Trans. Journal of Heat Transfer, February, pp. 120-128
- 84 Galustov, V.S., 1989, Pryamotochnie Raspilitel'nie Apparati v Teploenergetike (Co-Current Sprayers in Energetics). Moscow, Energoatomizdat, p.239.
- 85 Levich, V., 1962, Physicochemical Hydrodynamics, Prentice-Hall, p. 406.
- 86 Chan, T.S., 1994, Measurements of water density and drop size distributions of selected ESFR sprinklers. J. Fire Protec. Engng. vol.6(2), pp. 385-404.
- 87 Hadjisophocleous, G., Cao, S. and Kim, A. 1996, Modelling the interaction between fire watersprays and fire plume. Procedings of the 4th International Conference on Advanced Computational Methods in Heat Transfer. Italy, July, pp.239-249.

-
-
- 88 Heskestad, G., 1988, Fire plumes. The SFPE Handbook of Fire Protection Engineering E.K. Budnick, Section 1/Chapter 6, pp.1/107-1/115, 1st edition, NFPA, MA.
- 89 Fire Engineering Guidelines, 1996, Fire Code Reform Centre Ltd., Claude Eaton, Business Manager (12 Chapters), 1st Edition.
- 90 Beyler, C.L., 1986, Fire plume and ceiling jets. *Fire Safety Journal*, vol. 11, pp. 53-75.
- 91 Budnick, E.K., Evans D.,D., Nelson H.,E., 1997, Simplified fire growth calculations, in Cote, A.E., "Fire Protection Handbook", Section 11/Chapter 10, 18th Edition, J.L.Linville.
- 92 Cox, G., 1995, Combustion Fundamentals of Fire. Academic Press.
a) Chapter 6. Cox, G., Compartment fire modelling.
b) Chapter 3. Zukoski, E.E., Properties of fire plumes.
- 93 CFX-F3D. 1995, Version 4.1: User Manual. CFD Services, Harwell Laboratory, UK.
- 94 Friedman, R., 1997, Theory of Fire Extinguishment in *Fire Protection Handbook* (ed. A.E. Cote) Section 1/Chapter 8: 1-92 – 1-102, NFPA MA 18th edition.
- 95 Kumar, S., Heywood, G.M. and Liew, S.K., 1997, Superdrop Modelling of a Sprinkler Spray in a Two-phase CFD-particle Tracking model. Proceedings of the Fifth International Symposium on Fire Safety Science. pp. 889-900.
- 96 Hershey, D., 1974, Transport Analysis, Ch. 1. Introduction. Plenum Press. New York.
- 97 Wallace, F.J. and Lanning, W. A., 1970, Basic Engineering Thermodynamics, Pitman Paperbacks, 532 pp.
- 98 Kreith, F. and Bohn, M.S., 1993, Principles of Heat Transfer, West Publishing Company, 5th Edition.
- 99 Jones, W.P., 1980, Air Conditioning Engineering, Edward Arnold, Great Britain.
- 100 Cheung L.Y., 1997, A critical evaluation on the study of sprinkler and hot-air layer interaction with computational fluid dynamics, PhD Thesis, Hong Kong.
- 101 Yuen, M.C. and Chen, L.W., 1978, Heat-Transfer Measurements of Evaporating Liquid Droplets. *Int. J. Heat Mass Transfer*, vol.21, pp.537-542.
- 102 Lee, S.K., and Cheung, T.J., 1989, Axisymmetric Unsteady Droplet Vaporization and Gas Temperature Distribution, *Journal of Heat Transfer*, ASME. Vol.111, pp. 487 - 493.
- 103 Cooper, L.Y., 1995, The interaction of an isolated sprinkler spray and a two-layer compartment fire environment, *Int. Journal of Heat Mass Transfer*, Vol.18, No.4, pp.679-690.
- 104 Lapple, S.E., Shepherd, C.B., 1940, Calculation of particle trajectories, *Industrial and Engineering Chemistry*, May, Vol. 12, No. 5, pp.605-617.

-
-
- 105 Novozhilov V., Moghtaderi, D., Fletcher, D.F. and Kent, J.H., 1995, merical simulation of enclosed gas fire extinguishment by a water spray. *Journal of Applied Fire Science*; vol. 5(2), pp 135-146.
- 106 Bullen, M.L., 1974, The effect of a sprinkler on the stability of a smoke layer beneath a ceiling, Fire Research Note No 1016, Fire Research Station, Borehamwood.
- 107 Herterich O., 1960. Water as an extinguishing agent, Heidelberg: Alfred Hüthling Publishing Company.
- 108 Alessandri, E., Mawhinney, R. N., Patel, M.K., and Galea E., 1996. Revisiting the carrier-phase source-term formulation in mixed Lagrangian-Eulerian particle models, Numerical Heat Transfer, Part B, v.30, pp.111-116.
- 109 Nyankina, K., Turan Ö. F, 1997, Thermally driven negative buoyancy within hot gas layer due to sprinkler operation. The Proceedings of the International Symposium on Fire Science and Technology. Korea, Seoul, Nov.12-13, pp.627-632.
- 110 Alam, T. and Beever, P., 1996, "An Experimental Program Funded by FCRC", Flashover Fires. Project 4, Report Number 96-002, CESARE, Center for Environmental Safety and Risk Engineering, Victoria University of Technology, VIC, AU.
- 111 Lefebvre, A.H., 1989, Atomization and Sprays, Hemisphere Publishing, London, Chapter 8, Drop Evaporation, pp.309-366.
- 112 Thomas, R, 1997, Low Pressure water mist performance in open area protection, Fire Australia, pp.1-10. Melbourne.
- 113 Morita, M., Kikkawa, A. and Watanabe, Y., 1999, Oil fire extinguishment by using water mist, 6th International Symposium on Fire Safety Science, France, July.
- 114 Evans, D.D., Ceiling Jet Flows. 1988, The SFPE Handbook of Fire Protection Engineering, NFPA, SFPE, MA, 1st Edition, Section 1/Chapter 9: pp.1.138-1.145.
- 115 Takashi, S., 1985, Experiments and Theory in the extinction of wood crib. Proceedings of the First International Symposium on Fire Safety Science, pp.1197 – 1206.
- 116 Kim, M.B., Jang, Y.J. and Yoon, M.O., 1996, Extinction limit of a pool fire with a water mist. Fire Safety Journal, vol. 28, pp. 295-306.
- 117 Novozhilov, V., Harvie, D.J.E., Green, A.R. and Kent, J.H., 1997, A computational fluid dynamic model of fire burning rate and extinction by water sprinkler. Combustion Science and Technology, No.123, pp.227-245.
- 118 Rhodes, T.R., Bell, K.J., 1976, Film boiling of freon-114 drops at pressures up to critical, All Union Conference in Heat-Mass Transfer, Minsk, USSR, pp. 148-153.

-
-
- 119 Makino, K., Michiyoshi, I., 1997, Effect of the initial size of water droplet on its evaporation on heated surfaces, International Journal of Heat and Mass Transfer, Vol.22, pp.979 – 981.
- 120 Novozhilov, V., Moghtaderi, B., Fletcher, D.F. and Kent, J.H., 1996, Computational fluid dynamics modelling of wood combustion. Fire Safety Journal, vol.27, No.1, pp.69-84.
- 121 Novozhilov, V., Moghtaderi, B., Kent, J.H., and Fletcher D.F., 1999, Solid fire extinguishment by a water spray. Fire Safety Journal, vol.32, No2, pp.119-135.
- 122 Kutateladze, S.S., 1963, Fundamentals of Heat Transfer. Edward Arnold Ltd., pp. 350-380.
- 123 Butterworth, D. and Hewitt, G.F., 1977, Two-phase Flow and Heat Transfer. Oxford University Press
- 124 Buyevich, Y.A., 1995, Modeling of spray cooling of superheated surfaces, Proceedings of ASME Heat Transfer and Engineering Divisions, pp.65-72, HTD.Vol.321/FED.Vol.233, ASME.
- 125 Harvie, D.J.E. and Fletcher, D.F., 1998, Numerical simulation of droplet impact on a high temperature solid surface, 13th Australian Fluid Mechanics Conference, pp. 953-956, December.
- 126 Chaves, H., Kubitzek, A.M. and Obermeier, F., 1999, Dynamic processes occurring during the spreading of thin liquid films produced by drop impact on hot walls, International Journal of Heat and Fluid Flow, v. 20, pp. 470-476.
- 127 Makino, K., Michiyoshi, I., 1984, Technical Notes. The behaviour of a water droplet on heated surfaces, International Journal of Heat and Mass Transfer, Vol. 27 (8), pp.781-790.
- 128 Michiyoshi, I., Makino, K., 1978, Heat transfer characteristics of evaporation of a liquid droplet on heated surfaces. International Journal of Heat and Mass Transfer, Vol. 21, pp.605-613.
- 129 Di Marzo, M. and Evans, D.D., Evaporation of a Water Droplet Deposited on a Hot High Thermal Conductivity Surface. ASME Journal of Heat Transfer, Vol.111, pp.210-213.
- 130 Hahne, E, Feurstein, G., 1992, Maximum and minimum heat flux in near critical pool boiling. All Union Conference in Heat-Mass Transfer, Minsk, USSR, pp. 159-170.
- 131 Tio, K. K. and Sadhal, S.S., 1992, Thermal analysis of droplet spray evaporation from a heated surface, ASME Trans., Journal of Heat Transfer, v.114, pp.219 – 227.
- 132 Isachenko, V.P., Osipova, V.A. and Sukomel, A.S., 1970, Translation, Moscow, Energoizdat.
- 133 DiNenno, P.J., Ed., 1988, 'The SFPE Handbook of Fire Protection Engineering', 1st Edition, National Fire Protection Association, USA, Chapter 1.9.

-
-
- 134 Cooper, J. and Yung, D., 1997, NRC-CNRC Fire Growth Model for Apartment Buildings. Internal Report No.734, NRCC, Institute for Research in Construction (IRC), Canada.
- 135 H.-Z., Yu, J. L. Lee and H.-Ch. Kung, 1994, Suppression of Rack-Storage Fires by Water. The 4th International Symposium on Fire Safety Science, Ottawa, Canada, pp.901-912.
- 136 Fleming, R.P., 1988, Automatic Sprinkler System Calculation The SFPE Handbook of Fire Protection Engineering, NFPA, SFPE, MA, 1st Edition.. Section 3/Chapter 2: pp.3.22-3.34
- 137 Portier, R.W., Peacock, R. D., and Reneke, P.A., FASTLite: Engineering Tools For Estimating Fire Growth and Smoke Transport, Building and fire Research Laboratory. NIST. The software is available in Internet:
<http://www.branz.org.nz/Branz/PandS/FireResearch/software.html>
- 138 Evans, D., 1993, Sprinkler Fire Suppression Algorithm for HAZARD, Building and Fire Research Laboratory, NISTIR 5254, U.S. Department of Commerce.
- 139 Nyankina, K. and Turan, Ö. F. 2001, "Sprinkler performance in zone-type fire environment. Part I: Droplet dynamics", submitted to International Journal on Engineering Performance-Based Fire Codes.
- 140 Nyankina, K. and Turan, Ö. F. 2001, "Sprinkler performance in zone-type fire environment, Part II: Heat and mass transfer", submitted to International Journal on Engineering Performance-Based Fire Codes.
- 141 Nyankina K. and Turan Ö. F 1999, Determining an optimal diameter in fire-sprinkler interaction in terms of relative sprinkler location, 6th International Symposium in Fire Safety Science, Poitiers, France, pp. 421-432, 3-4 July.
- 142 Nyankina, K. and Turan, Ö. F., He, Y., Britton, M., 1999, One-layer zone modelling of fire suppression: gas cooling and blockage of flame spread by water sprinklers, Interflam'99, 8th International Conference on Fire Science & Engineering. Edinburgh, pp.1081-1092, June-July.
- 143 Beever, P. and Britton, M., 1999, Research into Cost-Effective Fire Safety Measures for Residential Buildings, Report, Building Control Commission, Australia, February.
- 144 Takeda, H. and Yung, D., 1992, Simplified fire growth models for risk-cost assessment in apartment buildings. Journal of Fire Protection Engineering. Vol. 4, No. 2, pp.53-65
- 145 He, Y., 1996, Further Development and Modification of the NRCC Fire Growth Model, CESARE Report IR96-002, Centre for Environmental Safety and Risk Engineering, Victoria University of Technology, Australia, May.
- 146 He, Y., 1998. CESARE-RISK: Fire Growth and Smoke Spread Models - Further development and experimental validation. CESARE Technical Report for FCRC Project 4, Centre for Environmental Safety and Risk Engineering, Victoria University of Technology, VIC, AU, April.

-
-
- 147 Klopovic, S. 1998, Experimental and Computational Study of Flames Venting Externally During Full Scale Flashover Fires. PhD Thesis, Victoria University of Technology, Australia, p. 285.
- 148 Luo, M. and He, Y., 1998, Verification of Fire Models for Fire Safety System Design. Journal of Fire Protection Engineering. Vol. 9, No. 2, pp.1-13.
- 149 Clarke, F.B., 1985, On Oxygen Depletion in Large Fires, Fire Technology, Vol.21, No1. pp.66-68.

APPENDIX A

Five basic zone models are compared in tabular form in Table 1 for enclosure fire on the basis of their:

- (a) applicability (number of enclosures, openings, etc.)
- (b) required inputs, and
- (c) outputs.

Generally, zone models estimate changes to a building or space and its environment as the results of a fire in that structure. These models range from prediction of upper layer gas temperature in compartment fire to human response to the heat and toxic species produced. Many of models have been assembled into larger consolidated models and hazard assessment tools (for example, into HAZARD, ASET, etc.) [1]. Thus, all models can be conditionally divided to basic models which predict the time histories of the main fire parameters: burning rate, hot layer and wall temperatures, gas concentrations, etc; and extended basic models, which are based on one or another basic models and include various subroutines with the detectors activation times, untenable conditions' times, and as a result actual evacuation times (ASET).

Table 1. Comparative table of 6 base zone models.

Zone Model	Applicability	Input Parameters	Outputs
I	II	III	IV
FIRECALC	<p>One-Room Hot Layer Model</p> <p>Opening into unconstrained outer space (ceiling ventilation, for example)</p>	<p>Ceiling height</p> <p>Room area</p> <p>Height and width of room opening</p> <p>Height of the opening above the floor level</p> <p>Height of the fire source above the floor</p> <p>Flame temperature</p> <p>Ambient temperature</p> <p>Optical density of smoke at the source</p> <p>Ventilation at the ceiling level of the room</p> <p>Delay to ventilation start-up</p> <p>Number of independent fire sources</p> <p>Design the parameters</p>	<p><u>History of fire.</u></p> <p>Time dependent:</p> <p>Hot layer height</p> <p>Hot layer temperature</p> <p>Flow of hot gases through opening</p> <p>Height of the neutral plane</p>

I	II	III	IV
CFAST [2] (NIST, USA)	Multi-room (up to 15 enclosures) Hot Layer Model Openings into unconstrained outer space (ceiling vents) and adjacent compartments (doors)	<p><u>Geometrical data:</u> Total number of compartments Width, depth, height (volume and area) for each compartment</p> <p><u>Connection between compartments:</u> Total number of openings Geometry of openings</p> <p><u>Mechanical ventilation:</u> Number, geometry and discharge characteristics</p> <p><u>Thermophysical properties:</u> of the ceiling, floor, and wall</p> <p><u>Other objects:</u> general information about being burned objects (minimum ignition flux and ignition and volatilization temperatures, total mass, molecular weight, initial pyrolysis rate, area of fire (zero at the beginning), etc.)</p> <p><u>The fire specification:</u> number of the compartment of fire origin; fire location in RFO; initial relative humidity; the total time over which the results are printed; fire type; lower oxygen limit, heat of combustion ...)</p> <p><u>Initial conditions:</u> Walls' temperatures, pressure</p>	<p><u>3-D Time histories of:</u></p> <p>Hot layer height Hot layer temperature Ceiling and walls' temperatures Mass burning rate and heat release rate Gas (O₂, CO, CO₂) concentrations HCL concentration Smoke density Flow of hot gases through openings Height of the neutral plane</p>
FIRST *) (direct descendant of the HARVARD V program of H. Emmons and H. Mitler)	Room-of-Fire Origin Zone Model with the heating and possible ignition up-to- three targets (total 4 compartments); with specified openings	<p><u>Geometrical data describing:</u> Rooms and Openings</p> <p><u>Thermophysical properties of the:</u> ceiling, walls burning fuel, and targets</p> <p><u>Rate of soot generation and other species generation rate as a rate of pyrolysis rate</u></p> <p><u>The original fire and targets specification</u></p>	<p><u>Time Histories of:</u></p> <p>Hot upper layer and lower cooler layer temperature and thickness; species concentration; O₂ concentration; heat transfer rate; mass burning rate; wall surface temperatures</p>
NRCC APARTMENT FIRE GROWTH MODEL [3] (Canada)	One-Room Zone Model with Door Openings	<p>Fire type (smouldering or flaming)</p> <p>Room geometry (height, depth, width)</p> <p>Thermal properties and thickness of wall materials</p> <p>Door size and state (opened or closed)</p> <p>Fuel load (kg/m²)</p> <p>Total simulation time (total time from the moment of ignition over which the results are printed)</p>	<p><u>Time history of:</u></p> <p>Burning Rate (kg/s)</p> <p>O₂, CO, CO₂ Concentrations (% by weight)</p> <p>Room Temperature (°C)</p> <p>Wall Temperature (°C)</p>

CCFM *) (Consolidated Compartment Fire Model version VVENT) [L.Y.Cooper and G.P. Fomey]	Two-layer zone-type compartment fire model in multi-room (up to 9 rooms), multi-level facility <u>Openings:</u> Vents can be simple openings between adjacent spaces (natural vents) or fan/duct forced ventilation systems between arbitrary pairs of spaces (forced vents).	<p>The required inputs are a description of room geometry and vent characteristics (up to 9 rooms, 20 vents), initial state of the inside and outside environment, and fire energy release rates as a functions of time (up to 20 fires).</p> <p>If simulation of concentrations of products of combustion is desired, then product release rates must also be specified (up to three products).</p> <p>For forced vents, flow rates and direction can be user-specified or included in the simulation by accounting for user-specified fan and duct characteristics. Wind and stack effects can be taken into account.</p>	<p>The program outputs for each room are:</p> <p>pressure at the floor, layer interface height, upper/lower layer temperature and (optionally) product concentrations.</p>
--	---	---	--

*) Note: Description is taken from Internet (NIST website: <http://www.nist.gov>).

References

1. Cote A., Ed. (1986), 'Fire Protection Handbook', 18th Edition, NFPA, USA.
2. Portier R.W. et al., 'A User's Guide for CFAST Version 1.6', NIST.
3. Gaskin, J and Takeda, H., 1993, 'The NRCC Apartment Fire Growth Manual', NRCC, Ottawa, Canada.

APPENDIX B

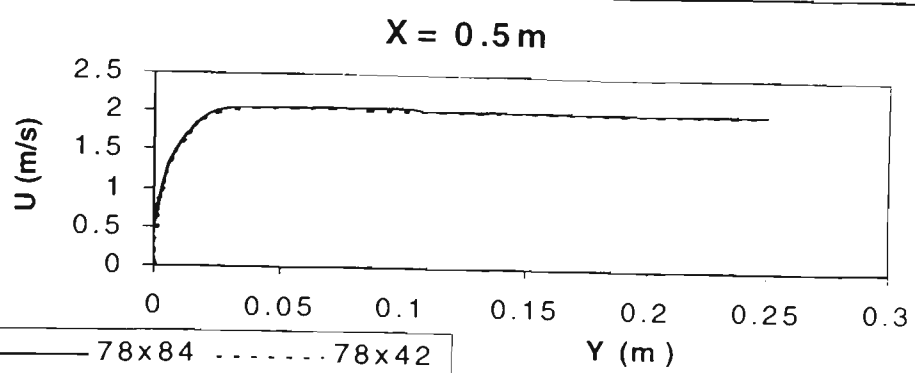
The Figure B-1 and Figure B-2 reflect the results of CFD simulations of channel flow with different grid sizes. Two grids with 78x42x1 and 78 x84x1 rectangular cells were chosen for comparison . In Figure B-1 (a to h), the horizontal velocity (U) profile is plotted across the channel width at different distances (X) from the inlet. The velocity profiles are plotted only for the upper half of the channel since the problem is symmetrical. The distances from inlet are shown at each plot's title. Similar to U-velocity, the V-velocity profile is also plotted in Figure B-2 (a to h) across the channel at different distances from inlet. The flow calculation showed that the finer grid, 78 x84x1, woul lead to practically negligible variations in gas flow in comparison with a coarser grid

The development of boundary layer from entrance ($X=0$) to the exit ($X=8m$) can be also observed in Figures 1a to 1h by comparing the distances at which profile becomes stable. In Table 1, the values of boundary layer thickness determined on the base of 99.95% approximation, i.e. the values of distance where the change in U-velocity does not prevail 0.05%, are given for two grids. The value calculated using empirical formula for fully developed turbulent flow [1] is also given for comparison in the last column. The deviation of the results can be explained by the range of Re number belonging to transition regime, rather than to turbulent.

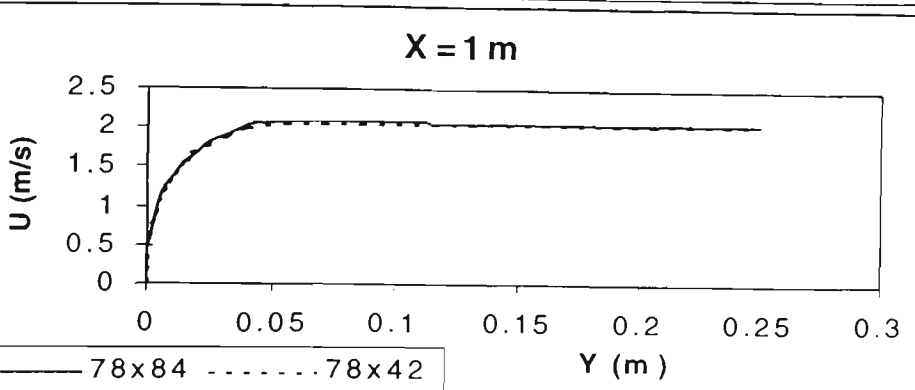
The development of boundary layer from entrance ($X=0$) to the exit ($X=8m$) can be observed in Figure B-1 (a to h) by looking at the development of distances at which profile becomes stable. The value calculated using empirical formula for fully developed turbulent flow [1] is also given for comparison in the last column. The deviation of the results can be explained by the range of Re number belonging to transition regime, rather than to turbulent.

Table 1: Comparison between simulated using different grids and empirical values of non-dimensionalised boundary layer depth.

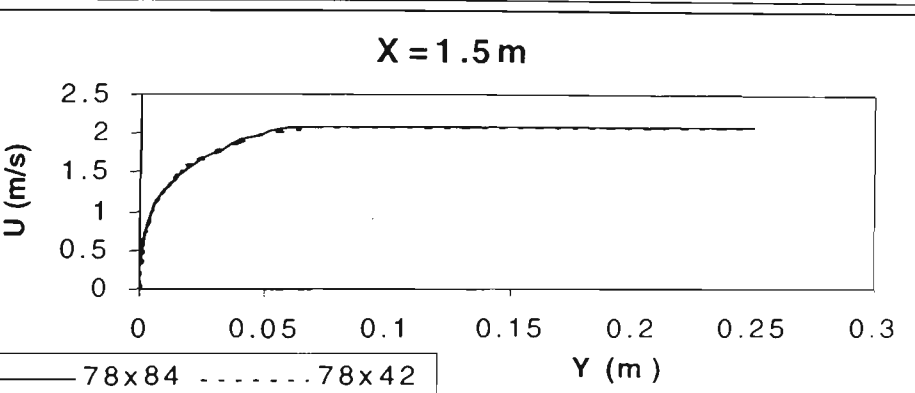
$\delta/X(G78x84)$	$\delta/X(G78x42)$	Re_x	$0.16/Re_x^{1/7}$
0.02875	0.0275	$1.07E+06$	0.022028



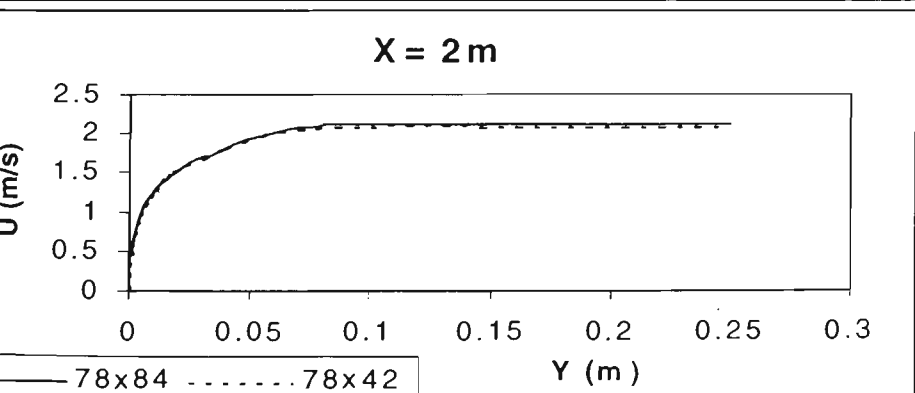
a



b



c



d

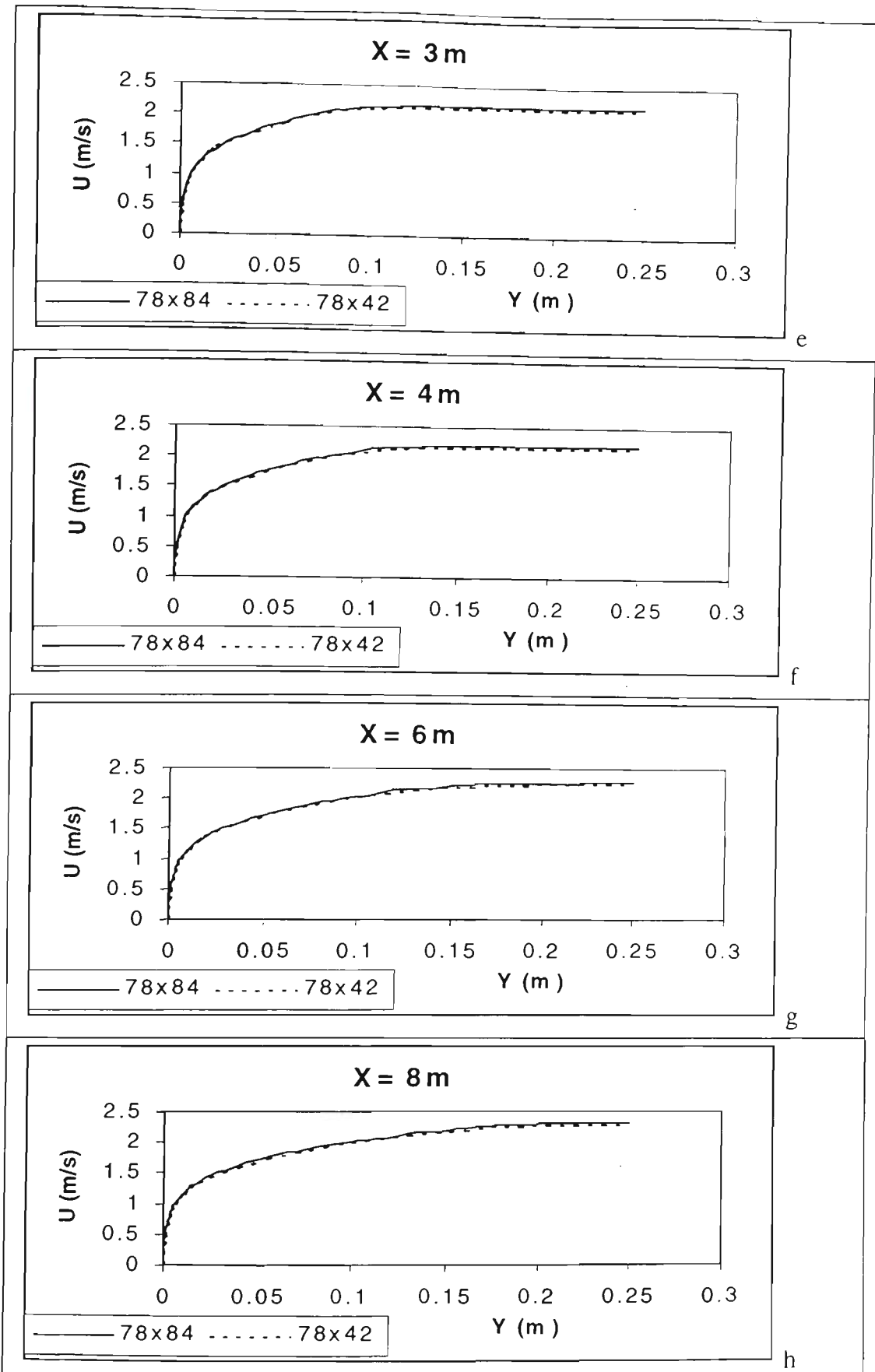
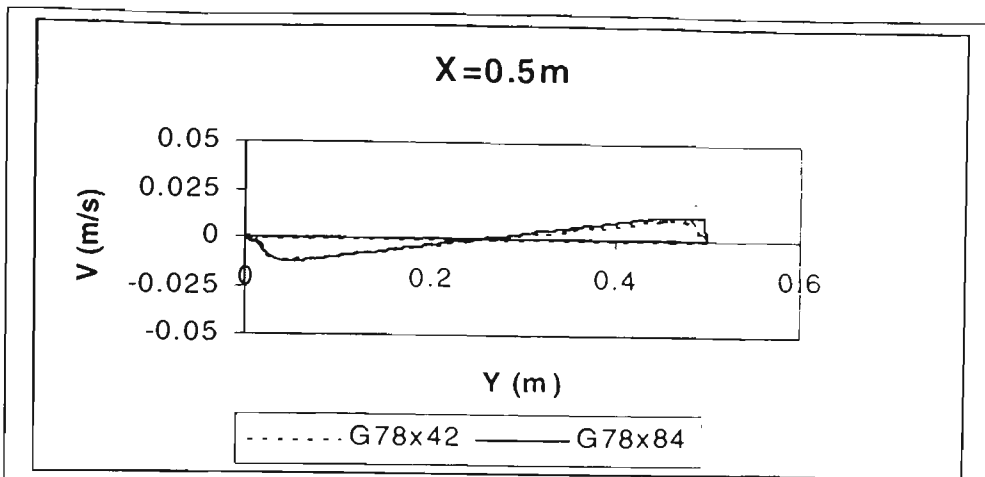
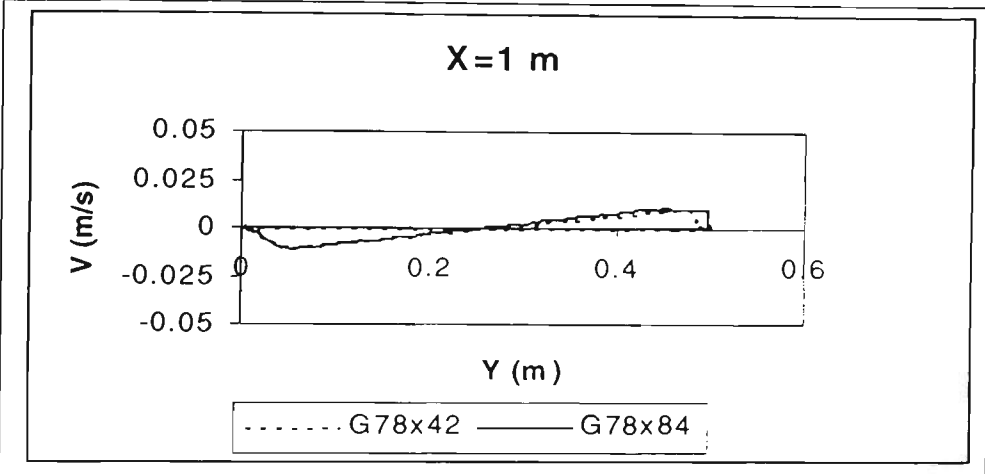


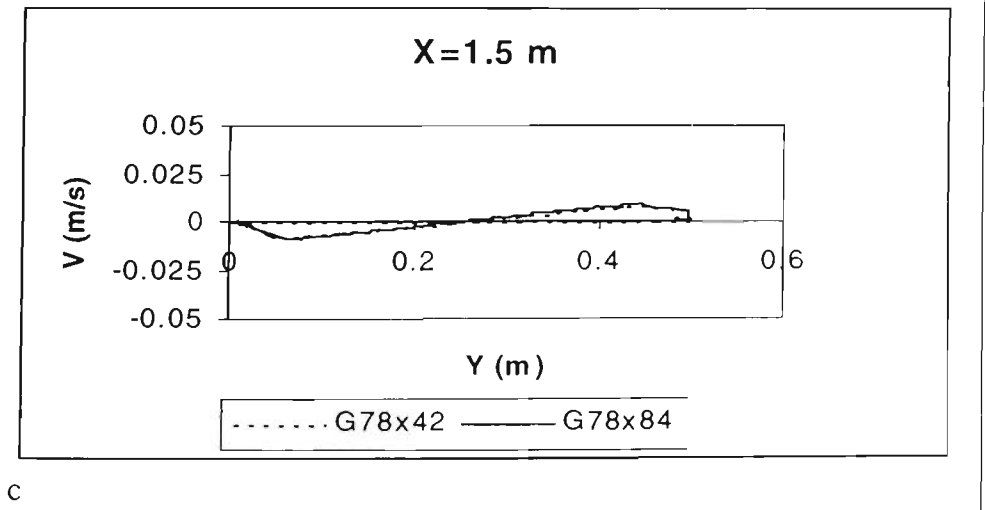
Figure B-1 Comparison of the U-velocity profiles at different distances from the channel inlet calculated using two grid sizes.



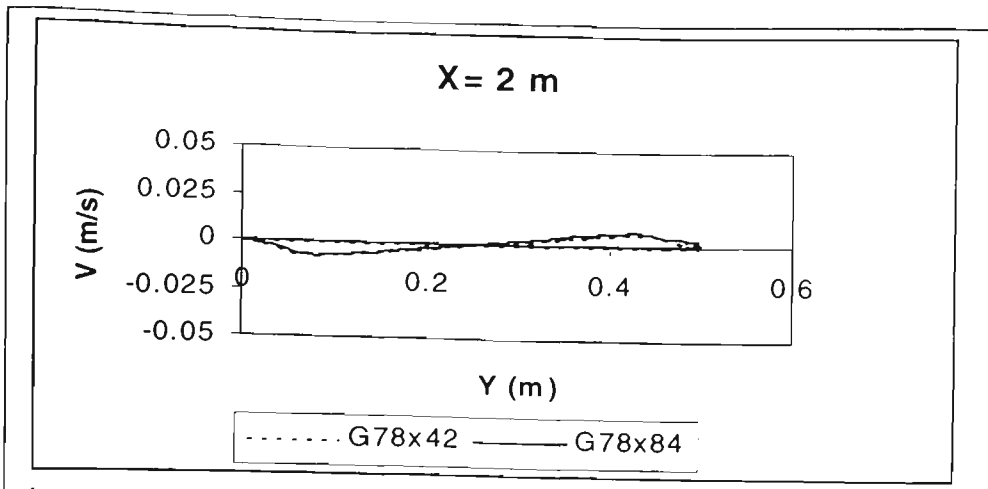
a



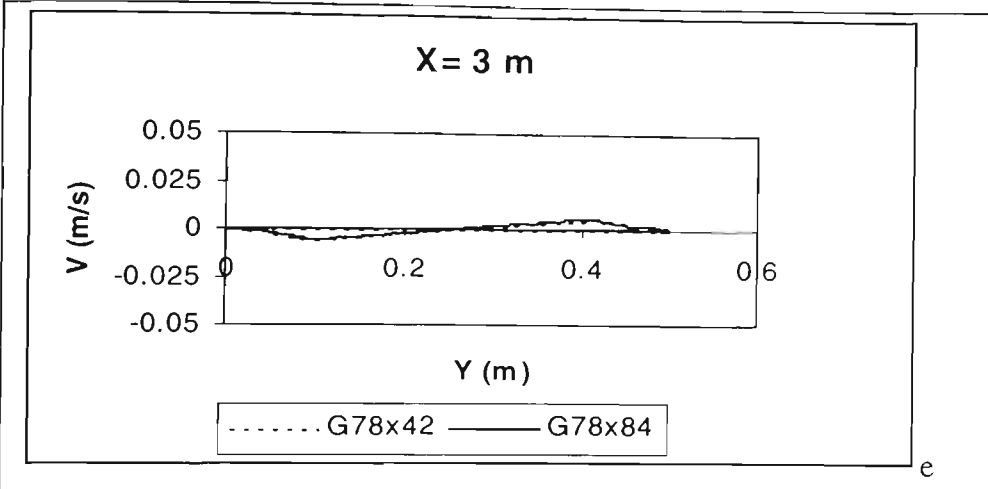
b



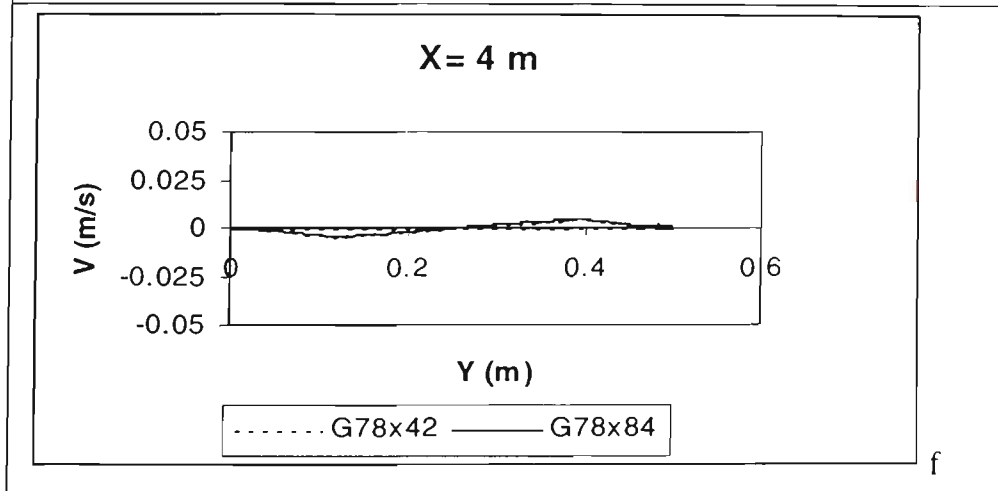
c



d



e



f

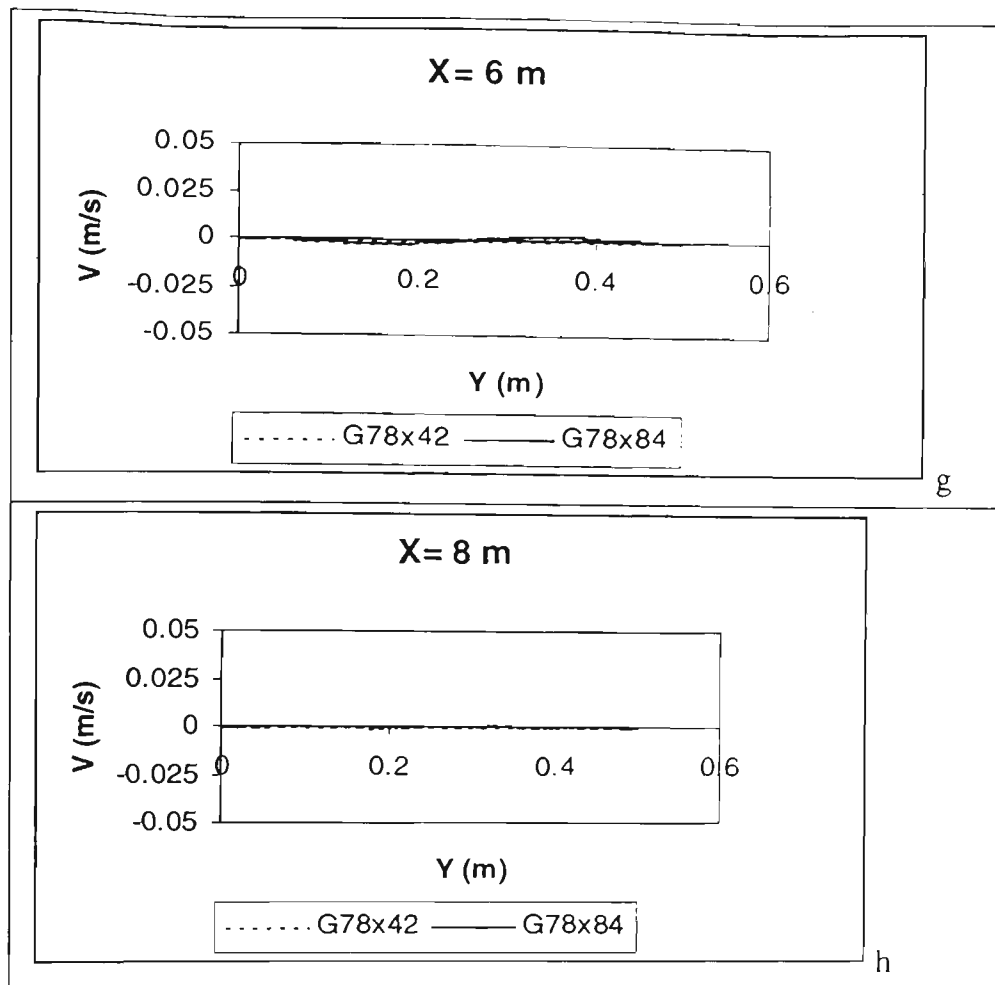


Figure B-2: Comparison of the V-velocity profiles at different distances from the channel inlet calculated using two grid sizes.

Based on the presented results it was concluded, that the CFD code successfully produces prediction of gas flow.

References:

1. White, F.M., Fluid Mechanics, McGRAW-HILL, INC, 3rd edition, 1994, 736pp.

APPENDIX C

Sample Input Data File #1 for Flaming Fire with Sprinkler

FO#				
1	Fire Type -- FLAMING			
2	Door -- Open			
3	Window Break Temperature = 300.00 C			
4	Room Height = 2.40 m			
5	Room Depth = 2.40 m			
6	Room Width = 3.50 m			
7	Wall Thermal Conductivity = 0.069 cal/cm min K			
8	Wall Density = 1.440 g/cm3			
9	Wall Thickness = 16.20 cm			
10	Door Height = 2.00 m			
11	Door Width = 0.80 m			
12	Fuel Thickness = 30.00 cm			
13	Fuel Size (radius) = 100.00 cm			
14	Fuel Mass = 117.00 kg			
15	Fire Simulation Time = 30.00 min			
16	Air Condition Air Supply = 0.00 litre/sec			
17	Air Condition Air Return = 0.00 litre/sec			
18	Number of element slabs = 300			
19	Flame spread adjustment = 1.00			
20	Initial burningradius = 1.50 cm			
21	WINDOW HEIGHT = 1.50 m			
22	WINDOW WIDTH = 2.40 m			
23	Acti. Extinction Coeff. = 0.05 l/m			
24	K = 50.0			
25	Critical Heat Flux = 420.0 kW/m**2			
26	Thermal Response Param. = 100.0 kW-s**0.5/m**2			
27	Adjacent room volume = 40.0 m**3			
28	Adjacent room surface = 46.0 m**2			
29	Fuel surface in adj room = 5.0 m**2			
30	Fuel mass in adj room = 100.0 kg			
31	Distance from the door = 0.0 m			
32	Crit. Temp. Wall Lining = 300.0 C			
33	Equiv. Fuel Area Lining = 0.0 m**2			
34	Equiv. Fuel Mass Lining = 0.0 kg			
35	Conductivity of Lining = 0.15 W/m K			
36	Density of Lining = 640.0 kg/m**3			
37	Specific Heat of Lining = 2.8 kJ/kg K			
38	Thickness of Lining = 1.0 cm			
39	Window glass thickness = 4.0 mm			
40	Glass density = 2700.0 kg/m**3			
41	Glass conductivity = 0.78 W/m deg			
42	Glass specific heat = 0.84 kJ/kg deg			
43	Glass breaking temp. dif.= 800.0 deg			
44	Sprinkler rti = 30.0 m^1/2s^1/2			
45	Sprinkler dis. from fire = 2.0 m			
46	Sprinkler Acti. Temp. = 68.1 C			
47	Window Lowering Time = 10000.0 sec			
48	Distance from the door = 1.0 m			
49	Sprinkler discharge rate = 1.35 kg/s			
50	Mean Droplet Diameter = 0.3 mm			

Sample Input Data File #2 for Flaming Fire

Sample Input Data File #2 for Flaming Fire with Sprinkler				
6973.0	498.0	0.550	9.85	0.0155
423.0	0.008	0.0255	11.0	0.005
0.02	1.8	9.2	0.045	1.0
H_c	H_v			
PU	6973.0	292.0 (Drysdale) or 498.0 (NRCC)		
Wood	4712.0	435.0		
Fiskville 5628.0	(Assuming total consumption)			
Fiskville 7440.0	(Assuming 300kg cellulosics remain)			
Stoichiometric ratio: 9.85 PU default				

Sample Input Data File #1 for Flaming Fire without Sprinkler

Original NRCC-VUT Fire Growth Model (no Sprinkler sub-model)

FO4

```

1      Fire Type -- FLAMING
2          Door -- Open
3  Window Break Temperature =    300.00 C
4          Room Height =        2.40 m
5          Room Depth =        3.60 m
6          Room Width =        5.40 m
7  Wall Thermal Conductivity = 0.069 cal/cm min K
8          Wall Density =     1.440 g/cm3
9          Wall Thickness =   16.20 cm
10         Door Height =      2.00 m
11         Door Width =       0.80 m
12         Fuel Thickness =   30.00 cm
13         Fuel Size (radius) = 140.00 cm
14         Fuel Mass =        232.00 kg
15         Fire Simulation Time = 40.00 min
16 Air Condition Air Supply = 0.00 litre/sec
17 Air Condition Air Return = 0.00 litre/sec
18 Number of element slabs = 350
19 Flame spread adjustment = 0.56
20 INITIAL BURNING RADIUS = 1.50 cm
21         WINDOW HEIGHT = 1.50 m
22         WINDOW WIDTH = 2.40 m
23 Acti. Extinction Coeff. = 0.05 1/m
24         K = 50.0
25 Critical Heat Flux = 20.0 kW/m**2
26 Thermal Response Param. = 100.0 kW-s**0.5/m**2
27 Adjacent room volume = 40.0 m**3
28 Adjacent room surface = 46.0 m**2
29 Fuel surface in adj room = 5.0 m**2
30 Fuel mass in adj room = 100.0 kg
31 Distance from the door = 0.0 m
32 Crit. Temp. Wall Lining = 300.0 C
33 Equiv. Fuel Area Lining = 0.0 m**2
34 Equiv. Fuel Mass Lining = 0.0 kg
35 Conductivity of Lining = 0.15 W/m K
36 Density of Lining = 640.0 kg/m**3
37 Specific Heat of Lining = 2.8 kJ/kg K
38 Thickness of Lining = 1.0 cm
39 Window glass thickness = 4.0 mm
40 Glass density = 2700.0 kg/m**3
41 Glass conductivity = 0.78 W/m deg
42 Glass specific heat = 0.84 kJ/kg deg
43 Glass breaking temp. dif.= 80.0 deg

```